Study of Disordered Biopolymer Gels: From Statistical Mechanics to Network Models

by

Seyedhashem Moosavian

A thesis submitted in partial fulfillment of the requirements for the degree of

Doctor of Philosophy

Department of Mechanical Engineering
University of Alberta

Abstract

Disordered biopolymer gels, such as those synthesized from polysaccharide and gelatin, play a crucial role in biomedical applications, particularly in tissue engineering. During the gelation process of these gels, polymer chains associate in the presence of gelling agents, forming physical cross-links known as the junction zones. In contrast to rubber-like networks, the resulting network comprises two main regions: the ordered region due to the junction zones and the amorphous region due to the unassociated chains. Under thermal fluctuations and/or external loading, the number and locations of junction zones can change leading to "zipping" (lengthening, i.e., expansion of the junction zones) and "unzipping" (shortening, i.e., shrinkage of the junction zones). This gives rise to intriguing features in biopolymer gels such as healing and damage-like energy dissipation. Despite the recognition of zipping and unzipping in such gels, the development of mathematical models that incorporate the microscopic mechanisms into the material's macroscopic mechanical properties is still in its early stages. The current study is devoted to providing a systematic framework that describes the overall behaviour of the biopolymer gels with zipping/unzipping under mechanical loading. The entire polymer network can be envisaged as a collection of coil-rod structures serving as the building blocks, where the coil and rod are representative of the disordered and ordered zones, respectively. The coil-rod structure is modelled by a rod attached to a freely jointed chain, where the length of the rod and the number of segments in the freely jointed chain are variable. During the zipping/unzipping process, segments can be exchanged between the coil and the rod, and the extent of exchange is governed by the binding energy of segments to form the

junction zone.

Prior to identifying coil-rod structures, an in-depth study of the statistical mechanics of the freely-jointed chain model is conducted. The analysis reveals that the conventional approach to deriving the canonical ensemble of this structure relies on the condition of "fixed displacement" rather than the desirable "fixed end-to-end distance". This nuanced distinction becomes negligible as the number of constituent segments increases. However, for coil-rod structures, this distinction between ensembles must be carefully taken into account, as the predictions from each ensemble result in markedly different force-extension relationships. The precise treatment of coil-rod structures establishes the foundation for the subsequent construction of a grand-canonical ensemble with a fixed end-to-end distance but a variable number of segments. The latter ensemble can appropriately formulate the zipping/unzipping when the individual chain, such as DNA is subjected to mechanical force. The proposed force-extension relationship for a single coil-rod can be integrated to generate stress-stretch relations for the collection of coil-rod structures forming a network. However, the presence of solvent and its interaction with the coil-rod structures lead to phenomena such as network swelling, thereby complicating the overall response. Another critical aspect pertains to the identification of a state devoid of residual stress, commonly known as the stress-free state. These concepts will be rigorously examined from the perspective of micro-scale network models. Experimental evidence demonstrates that the disordered biopolymer gel exhibits dissipation under cyclic loading. Furthermore, upon complete removal of the load, the sample experiences residual strain, commonly referred to as permanent set. These phenomena can be captured by the zipping/unzipping within the coil-rod structures in the proposed network model. Despite this model's ability to predict material response, it lacks explicit interactions between coils and rods. For this reason, the canonical ensemble of the more explicit network, where two coils share the same rod as a junction zone, is also elaborated upon. It is demonstrated that if the constituent freely-jointed

chains follow a Gaussian distribution, this system can be equivalently described as a collection of coil-rod structures.

The proposed multiscale formulation not only advances understanding of disordered biopolymer gels and underlying mechanism but also lays the groundwork for modeling hybrid gels that include coil-rod structures as a component.

Preface

All chapters in this thesis are my original work. Certain chapters have been submitted to, or published in, peer-reviewed journals and preprints as detailed below. Consequently, some chapters include their own introduction, methodology, results, discussions, and references, with supporting information appended in the Appendices. The abbreviations employed in this thesis are listed in the list of abbreviations and are defined in the chapters upon their first use. Specific symbols and terminology have been adjusted from the published articles to ensure consistency throughout the thesis. Acknowledgments specific to each chapter are provided prior to the chapter's references.

A version of Chapter 2 has been published as Moosavian, H., and Tang, T. "A critical examination of force–extension relationship for freely jointed chain model," *Extreme Mechanics Letters* 60 (2023): 101987. https://doi.org/10.1016/j.eml.2023.101987. A version of Chapter 3 has been published as Moosavian, H., and Tang, T. "Statistical mechanics of coil–rod structure in biopolymer gels," *Journal of the Mechanics and Physics of Solids* 175 (2023): 105272. https://doi.org/10.1016/j.jmps.2023.105272. A version of Chapter 4 has been published as Moosavian, H., and Tang, T. "A multiscale mechanics model for disordered biopolymer gels containing junction zones with variable length," *Journal of the Mechanics and Physics of Solids* (2024): 105792. https://doi.org/10.1016/j.jmps.2024.105792. For all three articles, I was responsible for formulating the research, performing derivations, verifying and analyzing results, generating figures, and drafting and revising the manuscripts. Dr. Tian Tang contributed to the analysis of simulation results, validation of findings, and re-

vision of the manuscripts. Furthermore, Dr. Tang was responsible for conceptualizing the research questions, securing financial support, and providing computational resources.

Acknowledgements

First, I would like to thank my supervisor, Dr. Tian Tang, for her expert advice and fruitful discussions on the research subjects. I also acknowledge the financial support from NSERC Canada, facilitated through my supervisor, as well as the scholarship support from Alberta Innovates, which made my Ph.D. program possible.
I would also like to express my deepest gratitude to my parents and my brother, Naser, for their unwavering support, endless encouragement, and unconditional love throughout this journey.

Table of Contents

List of Figures

List of Symbols

Constants

$[\mathbf{0}]_{3\times3}$	The 3×3 zero matrix	
$[\mathbf{I}]_{3\times3}$	The 3×3 identity matrix	
h	Planck's constant	$6.62607015 \times 10^{-34}\mathrm{m^2kg/s}$
$\boldsymbol{i}$	The imaginary unit number	$\sqrt{-1}$
$\mathbf{I}$	Identity tensor	
k_B	The Boltzmann constant	$1.380649 \times 10^{-23}\mathrm{J/K}$

Latin symbols

a	Unstretched length of the rod
$\mathbf{A}$	Matrix defined in Equations (5.28) and (D.39)
A_0	Normalization factor in the probability distribution (3.33) and (2.35)
b	Kuhn length of the coil
c_0	The factor dependent on the rod mass distribution in Equation (B.5)
C_n	Normalization factor, as a function of n and b in Equation (4.1)
$\mathbf{D}$	Matrix defined in Equation (D.9)
$\hat{\mathbf{e}}_x$, $\hat{\mathbf{e}}_y$, $\hat{\mathbf{e}}_z$	Unit vectors of the Cartesian coordinate system in Fourier space
E_0	Intrinsic energy within the rod structure
$\mathbf{F}$	Deformation gradient tensor
$\mathbf{f}$	External force vector applied at the end of the chain while the other end is fixed
$\mathbf{F}^e$	Elastic deformation gradient tensor
$\mathbf{F}^p$	Plastic deformation gradient tensor
$\langle f_r \rangle$	Average force required to maintain the structure at fixed end-to-end distance r

$\langle f_x \rangle$ Average force required to maintain the structure at fixed end-to-end distance along $x-$direction

$\langle f_x \rangle_r$ Average force required to maintain the structure at fixed end-to-end vector $\mathbf{r} = x\mathbf{i}$

$\langle f_r^{\mathrm{G}} \rangle$ Average force required to maintain the structure at fixed end-to-end distance r with activated zipping/unzipping

f_x Components of the force vector applied on the chain end along x direction while the other end is fixed

f_1, f_2 Labels of nodes at the rod ends in the general network with one rod

G Modulus

$\mathscr{G}$ Gibbs free energy

$\mathscr{H}$ The governing Hamiltonian of the system

$\hat{\mathbf{i}}$, $\hat{\mathbf{j}}$, $\hat{\mathbf{k}}$ Unit vectors of the Cartesian coordinate system in real space

$\mathscr{I}$ Variable defined in Equation (C.20)

$\mathscr{I}_1, \mathscr{I}_2$ Variables defined respectively in Equations (C.15a) and (C.15b)

I^* The moment of inertia of the rod around the x axis

I_0 Expression defined in Equation (D.20)

J Volume ratio

$(k_{ij})_x$, $(k_{ij})_y$, $(k_{ij})_z$ Components of $\mathbf{k}_{ij}$ in Cartesian coordinates

$\mathbf{K}$ Matrix defined in Equations (5.21a) and (D.36a)

$\mathbf{k}$ Position vector in the Fourier space corresponding to $\mathbf{r}$

$\mathbf{K}_a$, $\mathbf{K}_b$ Block matrices defined in (D.13) with dimensions $3p\times 1$ and 3×1, respectively

$\mathbf{k}_{ij}$ Position vector in the Fourier space corresponding to $\mathbf{R}_{ij}$

$\mathbf{L}$ Matrix defined in Equations (D.17) and (D.27)

Δl An arbitrary factor of length dimension for normalization purpose

$\widetilde{\mathbf{L}}$ Matrix defined in Equation (D.45)

l_1, l_2 Dimensions of the two-dimensional rectangle cell along horizontal and vertical directions in the stress-free state

L_θ Generalized momentum of the rod, Figure B.1

L_φ Generalized momentum of the rod, Figure B.1

l_{xj} The projected length of the jth group of chain segments on the x axis

M Number of solvent molecules per unit unswollen volume

m Mass of the end points in the rod model

$\mathbf{M}$ Orthogonal matrix for diagonalizing $\mathbf{\Gamma}$

m^* Extra number of segments 46 and 63 compared to 15 and 52

N Number of Kuhn segments in the fully unwound coil-rod structure

n Number of Kuhn segments in the coil

$\bar{n}_i$ The number of Kuhn segments of the ith chain in the equivalent affine network

$\mathbf{N}$ The unit vector along the line element in the reference configuration

$\tilde{n}_j$ The number of the jth group of the chain segments having a projection length between l_{xj} and $l_{xj} + \delta l_{xj}$ on the x axis

n_0 Number of Kuhn segments with maximum contribution to the summation (3.43)

n_f Count of free nodes

n_r Number of rods

N_t Total number of segments in the structure

$n_{\max}$ Maximum number of Kuhn segments in the coil during zipping/unzipping

$n_{\min}$ Minimum number of Kuhn segments in the coil during zipping/unzipping

n_{ij} Number of Kuhn segments of a coil between nodes i and j

$p(x)$ The probability that the two ends of the structure are separated by x in the x direction at constant temperature

p Number of independent end-to-end vectors of the p-node structure

$\mathbf{P}$ First Piola-Kirchhoff stress tensor

$P(\mathbf{x}_1, \cdots, \mathbf{x}_{t-1})$ Probability that the vectors in a t-node structure are $\mathbf{x}_1, \cdots, \mathbf{x}_{t-1}$, with fixed temperature and number of Kuhn segments n

p^* The additional parameter in the micro-sphere network model appeared in Equation (2.46)

p_0 Unknown pressure in Equation (3.49)

$p_n^{\mathbf{f}}(x)$ The probability that the two ends of the coil-rod structure are separated by x in the x direction at constant temperature under the force $\mathbf{f}$

$p_n^{\mathrm{CR}}(x)$ The probability that the two ends of the free coil-rod structure are separated by x in the x direction at constant temperature

$p_n^{\mathrm{C}}(x)$ The probability that the two ends of the free coil structure are separated by x in the x direction at constant temperature

p_x, p_y, p_z Components of the momentum vector of the rod end along x, y and z direction

P_1, P_2, P_3 Principal components of first Piola-Kirchhoff stress tensor

$Q(f_x, T, N_t)$ Isothermal-isotension partition function with fixed applied force f_x in x direction, temperature, and number of segments

$Q^{\mathrm{R}}(f_x, T)$ Isothermal-isotension partition function of the rod with fixed applied force f_x in x direction and temperature

$Q^{\mathrm{W}}(f_x, T)$ Isothermal-isotension partition function of the Weiner's rigid model for the rod structure with fixed applied force f_x in x direction and temperature

q_x, q_y, q_z Components of the position vector of the rod end along x, y and z direction

r End-to-end distance of the chain structure in the current state

r End-to-end position vector of the coil-rod structure

$\bar{\mathbf{R}}$ Matrix defined in Equation (D.10)

$\mathbf{R}$ Matrix defined in Equations (5.21b) and (D.36b)

$\mathbf{R}_a$, $\mathbf{R}_b$ Block matrices defined in (D.14) with dimensions $3p\times 1$ and 3×1, respectively

$\mathbf{R}_{ij}$ Chain vector from node i to node j

$\mathbf{R}_i$ Position vector of node i

$\langle \mathbf{r} \rangle$ Average end-to-end vector in arbitrary direction due to the application of a fixed force $\mathbf{f}$ on the ends

$\left(\overline{R}_i\right)_x$, $\left(\overline{R}_i\right)_y$, $\left(\overline{R}_i\right)_z$ Components of $\overline{\mathbf{R}}_i$ in Cartesian coordinates

$(R_{ij})_x$, $(R_{ij})_y$, $(R_{ij})_z$ Components of $\mathbf{R}_{ij}$ in Cartesian coordinates

$\mathrm{d}\mathbf{r}$ An arbitrary volume element in the space

$\overline{\mathbf{R}}_i$ The end-to-end vector of the ith chain in the equivalent affine network

$\tilde{\mathbf{R}}$ Matrix defined in Equation (D.42)

$\tilde{\mathbf{R}}_a$, $\tilde{\mathbf{R}}_b$ Block matrices defined similarly to (D.14) with a tilde, dimensions $3p\times 1$ and 3×1, respectively

r^* The end-to-end distance with maximum probability

r_0 End-to-end distance of the chain in the reference configuration

S Entropy of the body per unit reference volume

s Entropy of an individual chain with an end-to-end distance r

ΔS^{d} Entropy change of the body per unit reference volume due to deformation

ΔS^{m} Entropy change of the body per unit reference volume due to mixing

s_0 Entropy of an individual chain with an end-to-end distance r_0

$s_1,\ s_2, \cdots, s_{p+1}$ Label of fixed node i in the general network with p fixed nodes

T Temperature

t Number of nodes on one side of the general network with one rod

$\mathbf{u}$ Variable vector defined in Equation (5.9b)

$u_x,\ u_y,\ u_z$ Components of $\mathbf{u}$ in Cartesian coordinates

$\mathbf{v}$ Variable vector defined in Equation (5.9a)

V_0 Volume of the unswollen body

V_p Occupied volume by the polymer chains

V_s Occupied volume by the solvent

$W(\mathbf{r})$ The probability that the end-to-end vector of the free structure is $\mathbf{r}$, at fixed temperature and number of segments

$\mathbf{w}$ Variable vector defined in Equation (5.27)

$\overline{W}\,(\mathbf{k})$ Fourier transform of the probability distribution $W\,(\mathbf{r})$

$W_n^{\mathrm{C}*}(r)$ The traditional distribution function of Kuhn and Grün based on Equation (2.31)

$W^{\mathrm{R}}\,(\mathbf{r})$ The probability that the end-to-end vector of the free rod is $\mathbf{r}$, at fixed temperature

$W_n^{\mathbf{f}}(\mathbf{r})$ The probability that the end-to-end vector of the structure is $\mathbf{r}$ under the chain force $\mathbf{f}$, with fixed temperature and number of Kuhn segments n

$W_n^{\mathrm{CR}}(\mathbf{r})$ The probability that the end-to-end vector of the free coil-rod structure is $\mathbf{r}$, with fixed temperature and number of Kuhn segments n in the coil

$W_n^{\mathrm{C}}(\mathbf{r})$ The probability that the end-to-end vector of the free coil structure is $\mathbf{r}$, with fixed temperature and number of Kuhn segments n

$w_x,\ w_y,\ w_z$ Components of $\mathbf{w}$ in Cartesian coordinates based on (5.27)

$\mathbf{X}$ Vector defined in Equation (D.5)

$\langle x \rangle$ Average end-to-end distance in $x-$direction due to the application of a fixed force f_x on the ends

X_1, X_2, X_3 The material coordinates

x_1, x_2, x_3 The spatial coordinates

X_i The ith element of vector $\mathbf{X}$

$\mathbf{Y}$ Matrix defined in Equations (5.26), (D.37), and (D.38)

$Z(\mathbf{r}, T, N_t)$ The canonical partition function with fixed end-to-end position vector, temperature, and number of segments

$Z^{\mathrm{R}}(x, T)$ The canonical partition function of the rod with fixed end-to-end projection in x direction and temperature

$Z^{\mathrm{W}}(x, T)$ The canonical partition function of the Weiner's rigid model for the rod with fixed end-to-end projection in x direction and temperature

Z_0 The integration of canonical partition function over the entire space, Equation (3.6)

Greek symbols

α Ratio of the length of one unit in the rod to the Kuhn length (see Figure 3.6)

β A dimensionless parameter defined in Equations (2.31) and (5.46)

ε Required energy for liberation of one Kuhn segment in the rod

η A dimensionless parameter defined in Equation (2.49)

η_i The ith eigenvalue of matrix $\mathbf{\Gamma}$

γ The shear strain in pure shear test as shown in 2.4

$\mathbf{\Gamma}$ Matrix defined in Equations (5.23), (D.15), and (D.34)

$\mathbf{\Gamma}_{\mathrm{aa}}$, $\mathbf{\Gamma}_{\mathrm{ab}}$, $\mathbf{\Gamma}_{\mathrm{bb}}$ Block matrices defined in Equation (D.21)

$\tilde{\mathbf{\Gamma}}$ Matrix defined in Equations (D.41) and (5.30)

$\tilde{\mathbf{\Gamma}}_{\mathrm{aa}}$, $\tilde{\mathbf{\Gamma}}_{\mathrm{ab}}$, $\tilde{\mathbf{\Gamma}}_{\mathrm{bb}}$ Block matrices defined in Equation (D.44)

γ_{ij} Element ij in matrix $\mathbf{\Gamma}$ defined in Equation (D.15)

κ Stiffness in the flexible rod model

$\bar{\lambda}^{\mathbf{N}}$ The macro-stretch of the line element located along direction $\mathbf{N}$ in the reference configuration

$\mathbf{\Lambda}$ Matrix defined in Equations (5.24) and (D.35)

λ^* The stretch of the volume element averaged over different directions as defined in Equation (2.46)

$\lambda^{\mathbf{N}}$ The micro-stretch of the chain located along direction $\mathbf{N}$ in the reference configuration

λ_p The residual stretch after unloading

λ_s The stretch of the swollen stress-free state due to the solvent introduction

λ_v The stretch due to the solvent introduction

λ_1, λ_2, λ_3 Principal stretches

λ_{chain} The chain stretch in the eight-chain network model

μ The swelling parameter in Equation (4.22)

ν Total number of Gaussian chains in the general network with $p+1$ nodes

$\Omega(\mathbf{r}, T, \varepsilon)$ The grand canonical partition function with fixed end-to-end position vector, temperature, and chemical potential

ω The spherical surface with unit radius in the reference configuration

$\bar{\Omega}$ The total number of conformations of a free chain with fixed end-to-end distance x

ϕ and θ Spherical coordinate variables

Φ Grand canonical potential energy

φ Generalized coordinate of the rod, Figure B.1

$\Pi(x, f_y, f_z, T, n)$ The semi-canonical partition function under fixed applied forces f_y and f_z, fixed distance along x, fixed number of Kuhn segments n, and fixed temperature as introduced in Equation (2.25)

$\Pi(x, T, N_t)$ The partition function with fixed end-to-end distance in x direction, temperature, and number of segments

Ψ Helmholtz free energy per unit reference volume

ψ Helmholtz free energy of the individual chain

Ψ_0 Helmholtz free energy of the unswollen state per unit reference volume

ψ_i Helmholtz free energy of the ith chain per unit reference volume

$\boldsymbol{\sigma}$ Cauchy stress tensor

σ_1, σ_2, σ_3 Principal Cauchy stresses

τ The volume ratio of occupying one coil-rod structure to one solvent molecule

ϑ A dimensionless parameter introduced in Equation (3.38)

ϱ Number of chains per unit reference volume

ξ A dimensionless parameter defined in Equation (3.34)

ξ_1, ξ_2 Dimensionless parameters defined in Equations (3.36a) and (3.36b)

ζ The ratio of a to the Kuhn length b

$\tilde{\zeta}_{ij}$ Element ij in matrix $\widetilde{\mathbf{\Gamma}}^{-1}$

ζ_{ij} Element ij in matrix $\mathbf{\Gamma}^{-1}$ defined in Equation (D.19)

Operators and functions

$\dot{\square}$ The material time derivative of $\square$

$\mathbf{A}^{-1}$ The inverse of a matrix or tensor $\mathbf{A}$

$\mathbf{A}^{-\mathrm{T}}$ The inverse transpose of a matrix or tensor $\mathbf{A}$

$\mathbf{A}^{\mathrm{T}}$ The transpose of a matrix or tensor $\mathbf{A}$

$|\,\mathbf{A}\,|$ The norm of $\mathbf{A}$

$\delta\,(\mathbf{x})$ Three-dimensional Dirac delta function

$\delta\,(x)$ One-dimensional Dirac delta function

$\det(\mathbf{A})$ The determinant of a matrix or tensor $\mathbf{A}$

$\mathrm{erfc}\,(\cdots)$ The complementary error function

$\mathrm{erf}\,(\cdots)$ The error function

$\mathscr{F}(\cdots,\cdots)$ A function defined in Equation (B.17)

$H\,(\cdots)$ The Heaviside step function

$K_i(\cdots)$ The ith order modified Bessel function of the second kind

$\mathscr{L}\,(\cdots)$ Langevin function

$\mathrm{tr}(\mathbf{A})$ The trace of a matrix or tensor $\mathbf{A}$

Abbreviations

AFM Atomic force microscopy.

DNA Deoxyribonucleic acid.

FJC Freely-jointed chain model.

Chapter 1

Introduction

1.1 Background

Owing to the extensive commercial utilization of polymers in both natural and synthetic materials, recent decades have seen substantial research into the design and synthesis of polymer-based structures, such as elastomers and gels. Since the 1950s, biopolymers, with their unique biocompatibility, have emerged as ideal candidates for a wide range of applications across various fields, including biomedical applications [1–4], the food industry [5, 6], cosmetics [7, 8], environmental applications [9], and industrial applications [10].

Biopolymer chains are long sequences of biological macromolecules synthesized by living organisms and are primarily categorized into three distinct groups [11]: (i) Polynucleotides, such as DNA, (ii) Polypeptides or polyamino acids, (iii) Polysaccharides. Many biopolymer chains such as polysaccharides naturally form gels due to their inherent properties [12]. Gels are generally defined as three-dimensional hydrophilic polymer networks swollen by a solvent. Due to the diverse types of biopolymer chains, biopolymer gels are classified into two main categories [13]: (i) rod-like ordered biopolymer gels, such as globular protein gels with branched networks; and (ii) disordered biopolymer gels, such as polysaccharide gels, where individual chains associate laterally through physical interactions (such as hydrogen bonding, ionic interactions, and van der Waals forces) to form the so-called "junction zones". As

shown in Fig. 1.1, macromolecules connect through these junction zones to form a coherent network capable of resisting mechanical loadings. Depending on the type of biopolymer gel, the junction zones can take various forms, such as egg-box structures in alginate, double helices in agar, associations of double helices with intermediate cations in carrageenan, and triple helices in gelatin.

Disordered biopolymer gels differ from rubber-like materials in many aspects such as cross-linking mechanisms, and synthesis processes. In addition to the vast application of disordrered biopolymer gels, there is growing research interest in hybrid gels, such as polyacrylamide-alginate gels, where disordered biopolymers play a vital role as one of the components [14]. The structure of biopolymer gels is highly dependent on synthesis processes such as temperature and solution concentration [15]. At the microscale, the lengths of junction zones can be comparable to those of the coil regions, playing a significant role in the gel's load-bearing mechanism. Due to the weak physical interactions therein, these junction zones exhibit a temporary nature, allowing them to dissociate in some locations and re-associate in others under external stimuli. This mechanism, termed zipping/unzipping, is the basis for novel properties such as self-healing. Such behaviour along with the complex interaction between the network and solution [16] makes the mathematical modeling of gels more challenging compared to rubber-like materials.

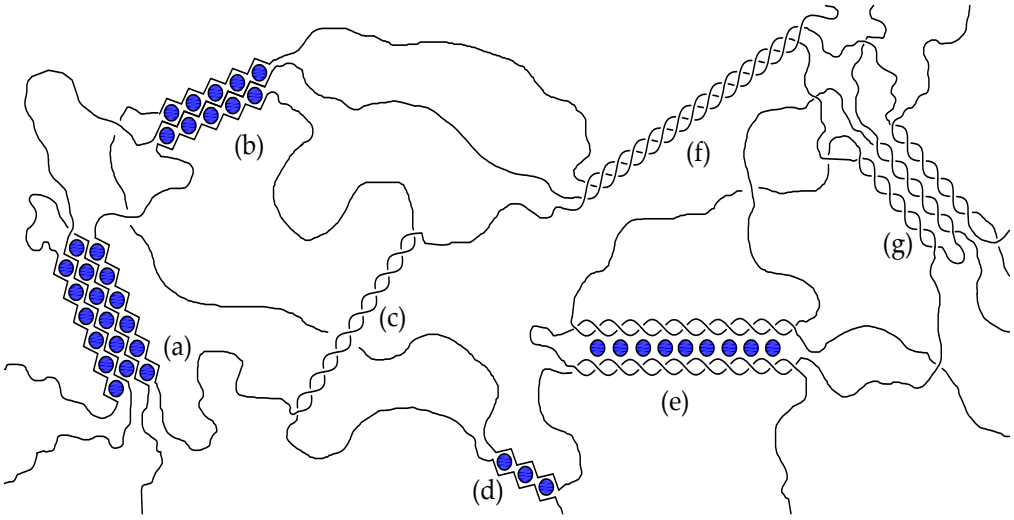

Figure 1.1: Examples of conformation and aggregation of junction zones in disordered biopolymer gel networks: (a)-(b) egg-box multimer (alginate), (c) double helix (agar), (d) egg-box dimer, (e) association of double helices with intermediate cations (carrageenan), (f) triple helix (gelatin), (g) association of double helices without intermediate cations (agarose gels). Each junction zone can be considered as a rod while the remaining disordered region can be considered as coils.

1.2 Motivation and objective

Given the wide range of applications of disordered biopolymer gels such as polysaccharide gels, understanding their mechanical properties is both intriguing and crucial. There are two main approaches to study the mechanical properties of gels. The first involves phenomenological models that describe the Helmholtz free energy in terms of *a priori* mathematical function of principal stretches or stretch invariants, capturing material behavior through fitting various experimental tests [17]. Originally developed for rubber-like materials, this approach has also been extensively applied to biopolymer gels [18–25]. In contrast, constitutive models in the second paradigm are formulated based on the statistical mechanics of polymer chains and associated conformations. This approach involves more complex calculations, such as the inverse Langevin functions. Parameters in these constitutive relations reflect the fundamental physical characteristics of polymer networks, distinguishing it from the phenomeno-

logical approach. Compared to the significant advancement in multiscale modelling of rubber-like materials containing mostly chemical crosslinks, the modelling of biopolymer gels with physical junction zones is still in its infancy. In this study, by adopting the second approach, the objective is to establish a framework that bridges micromechanics of disordered biopolymer gels with the corresponding constitutive relations at the macroscopic scale through statistical mechanics. Establishing an accurate model enables precise material design without the necessity for time-consuming experimental trials involving exhaustive parametric studies.

1.3 Thesis Outline

In Chapter 2, the conventional treatment of the canonical partition function for the freely-jointed chain model is challenged. It is shown that, although the erroneous treatment in the literature does not affect the coil partition function considerably, a careful remedy is crucial for the coil-rod structure. In Chapter 3, the disordered biopolymer gel is envisioned as a collection of coil-rod structures, where the coil represents the disordered (amorphous) region, and the rod represents the junction zone. At the chain scale, the coil-rod structure is studied under different ensembles, and the force-extension relationship for each case is derived. To account for zipping/unzipping, the grand canonical ensemble is introduced, allowing for the exchange of segments between the rod and coil. The precise recognition of the force-extension relationship for coil-rod structure enables us to develop network model of biopolymer gels in Chapter 4. The Helmholtz free energy of the coil-rod structure within the eight-chain network with and without swelling is extracted. Subsequently the zipping/unzipping present in the coil-rod model is reflected in the governing stress-stretch relations of the gel. Although the coil-rod structure is a simple and effective microscopic element that allows for a systematic framework for biopolymer gel modelling, a more realistic network model should include the explicit interaction of different coils through a common junction zone. For this purpose, in Chapter 5, a more advanced

network model is introduced in which two coils share the same junction zone through one rod. It is shown that it is possible to find convergence of the two approaches (coil-rod as elements vs. coils sharing rod as elements) when the coils are represented by Gaussian statistics. This further confirms the applicability of considering the coil-rod structure as the building blocks for the biopolymer gel network. The study concludes in Chapter 5 with recommendations for potential expansions of the proposed model and an acknowledgment of its current limitations.

References

[1] J. L. Drury and D. J. Mooney, "Hydrogels for tissue engineering: Scaffold design variables and applications," *Biomaterials*, vol. 24, no. 24, pp. 4337–4351, 2003, Synthesis of Biomimetic Polymers, ISSN: 0142-9612. DOI: https://doi.org/10.1016/S0142-9612(03)00340-5.

[2] N. Peppas, P. Bures, W. Leobandung, and H. Ichikawa, "Hydrogels in pharmaceutical formulations," *European Journal of Pharmaceutics and Biopharmaceutics*, vol. 50, no. 1, pp. 27–46, 2000, ISSN: 0939-6411. DOI: https://doi.org/10.1016/S0939-6411(00)00090-4.

[3] J. S. Boateng, K. H. Matthews, H. N. Stevens, and G. M. Eccleston, "Wound healing dressings and drug delivery systems: A review," *Journal of Pharmaceutical Sciences*, vol. 97, no. 8, pp. 2892–2923, 2008, ISSN: 0022-3549. DOI: https://doi.org/10.1002/jps.21210.

[4] N. A. Ibrahim, A. A. Nada, and B. M. Eid, "Polysaccharide-based polymer gels and their potential applications," in *Polymer Gels: Synthesis and Characterization*, V. K. Thakur and M. K. Thakur, Eds. Singapore: Springer Singapore, 2018, pp. 97–126.

[5] A. Imeson, *Food stabilisers, thickeners and gelling agents*. John Wiley & Sons, 2011.

[6] T. Bourtoom, "Edible films and coatings: Characteristics and properties," *International food research journal*, vol. 15, no. 3, pp. 237–248, 2008.

[7] R. K. Sivamani, J. Goodman, N. V. Gitis, and H. I. Maibach, "Coefficient of friction: Tribological studies in man – an overview," *Skin Research and Technology*, vol. 9, no. 3, pp. 227–234, 2003. DOI: https://doi.org/10.1034/j.1600-0846.2003.02366.x. eprint: https://onlinelibrary.wiley.com/doi/pdf/10.1034/j.1600-0846.2003.02366.x.

[8] J. Koehler, F. P. Brandl, and A. M. Goepferich, "Hydrogel wound dressings for bioactive treatment of acute and chronic wounds," *European Polymer Journal*, vol. 100, pp. 1–11, 2018, ISSN: 0014-3057. DOI: https://doi.org/10.1016/j.eurpolymj.2017.12.046.

[9] K. Kabiri, H. Omidian, M. J. Zohuriaan-Mehr, and S. Doroudiani, "Superabsorbent hydrogel composites and nanocomposites: A review," *Polymer Composites*, vol. 32, no. 2, pp. 277–289, 2011. DOI: https://doi.org/10.1002/pc.21046. eprint: https://4spepublications.onlinelibrary.wiley.com/doi/pdf/10.1002/pc.21046.

[10] T. Someya, Z. Bao, and G. G. Malliaras, "The rise of plastic bioelectronics," *Nature*, vol. 540, no. 7633, pp. 379–385, 2016.

[11] R. S. Dassanayake, S. Acharya, and N. Abidi, "Biopolymer-based materials from polysaccharides: Properties, processing, characterization and sorption applications," in *Advanced Sorption Process Applications*, S. Edebali, Ed., Rijeka: IntechOpen, 2019, ch. 1. DOI: 10.5772/intechopen.80898.

[12] J. OLIVEIRA and R. REIS, "18 - hydrogels from polysaccharide-based materials: Fundamentals and applications in regenerative medicine," in *Natural-Based Polymers for Biomedical Applications*, ser. Woodhead Publishing Series in Biomaterials, R. L. Reis, N. M. Neves, J. F. Mano, M. E. Gomes, A. P. Marques, and H. S. Azevedo, Eds., Woodhead Publishing, 2008, pp. 485–514, ISBN: 978-1-84569-264-3. DOI: https://doi.org/10.1533/9781845694814.4.485.

[13] A. H. Clark and S. B. Ross-Murphy, "Structural and mechanical properties of biopolymer gels," in *Biopolymers*, Berlin, Heidelberg: Springer Berlin Heidelberg, 1987, pp. 57–192, ISBN: 978-3-540-47827-0.

[14] J.-Y. Sun *et al.*, "Highly stretchable and tough hydrogels," *Nature*, vol. 489, no. 7414, pp. 133–136, 2012.

[15] A. Clark, "Structural and mechanical properties of biopolymer gels," in *Food Polymers, Gels and Colloids*, E. Dickinson, Ed., Woodhead Publishing, 1991, pp. 322–338, ISBN: 978-1-85573-787-7. DOI: https://doi.org/10.1533/9781845698331.322.

[16] S. Kasapis, I. Norton, and U. Johan B, *Modern Biopolymer Science: Bridging the Divide between Fundamental Treatise and Industrial Application*. Elsevier Science, 2009, ISBN: 9780080921143.

[17] R. W. Ogden, G. Saccomandi, and I. Sgura, "Fitting hyperelastic models to experimental data," *Computational Mechanics*, vol. 34, pp. 484–502, 2004.

[18] H. McEvoy, S. Ross-Murphy, and A. Clark, "Large deformation and ultimate properties of biopolymer gels: 1. single biopolymer component systems," *Polymer*, vol. 26, no. 10, pp. 1483–1492, 1985, ISSN: 0032-3861. DOI: https://doi.org/10.1016/0032-3861(85)90081-3.

[19] J. Tang, M. A. Tung, J. Lelievre, and Y. Zeng, "Stress-strain relationships for gellan gels in tension, compression and torsion," *Journal of Food Engineering*, vol. 31, no. 4, pp. 511–529, 1997, ISSN: 0260-8774. DOI: https://doi.org/10.1016/S0260-8774(96)00087-8.

[20] J. Zhang, C. R. Daubert, and E. Allen Foegeding, "A proposed strain-hardening mechanism for alginate gels," *Journal of Food Engineering*, vol. 80, no. 1, pp. 157–165, 2007, ISSN: 0260-8774. DOI: https://doi.org/10.1016/j.jfoodeng.2006.04.057.

[21] V. Magnenet, J. Schiavi-Tritz, C. Huselstein, and R. Rahouadj, "Constitutive equations for Ca2+ -alginate gels," *Journal of the Mechanical Behavior of Biomedical Materials*, vol. 5, no. 1, pp. 90–98, 2012, ISSN: 1751-6161. DOI: https://doi.org/10.1016/j.jmbbm.2011.08.009.

[22] X. Xu and S. A. Safran, "Nonlinearities of biopolymer gels increase the range of force transmission," *Phys. Rev. E*, vol. 92, p. 032 728, 3 2015. DOI: 10.1103/PhysRevE.92.032728.

[23] C. Wex, S. Arndt, A. Stoll, C. Bruns, and Y. Kupriyanova, "Isotropic incompressible hyperelastic models for modelling the mechanical behaviour of biological tissues: A review," *Biomedical Engineering / Biomedizinische Technik*, vol. 60, no. 6, pp. 577–592, 2015. DOI: doi:10.1515/bmt-2014-0146.

[24] H. Wang and X. Xu, "Continuum elastic models for force transmission in biopolymer gels," *Soft Matter*, vol. 16, pp. 10 781–10 808, 48 2020. DOI: 10.1039/D0SM01451F.

[25] K. Upadhyay, G. Subhash, and D. Spearot, "Hyperelastic constitutive modeling of hydrogels based on primary deformation modes and validation under 3d stress states," *International Journal of Engineering Science*, vol. 154, p. 103 314, 2020, ISSN: 0020-7225. DOI: https://doi.org/10.1016/j.ijengsci.2020.103314.

Chapter 2

A Critical Examination of Force-extension Relationship for Freely-jointed Chain Model

A version of this chapter has been published. Reprinted with permission from Moosavian, H., and Tang, T. "A critical examination of force–extension relationship for freely jointed chain model," *Extreme Mechanics Letters* 60 (2023): 101987. https://doi.org/10.1016/j.eml.2023.101987

2.1 Introduction

The statistical mechanics of the freely-jointed chain (FJC) model has a profound influence on the development of micromechanical insight into the macroscopic properties of polymers. Owing to its simplicity, the model has been widely applied in various branches of polymer science [1]. A FJC is assumed to consist of n consecutive rigid segments with identical length b (the Kuhn length) such that each segment is free to rotate in any direction. To determine the entropic elasticity of the chain, the primary objective of the FJC model is to evaluate the entropy of the system or equivalently the number of available conformations of the chain at any given end-to-end vector $\mathbf{r}$. Alternatively, the relative number of chain conformations can be related to the probability distribution of a "free" chain (not subjected to any forces) as a

function of $\mathbf{r}$, i.e., $W_n(\mathbf{r})$. More precisely, $W_n(\mathbf{r})\mathrm{d}\mathbf{r}$ denotes the probability of finding one end of the free chain at volume element $\mathrm{d}\mathbf{r}$, while the other end is fixated at the origin. The simplest possible treatment is to postulate the Gaussian distribution for $W_n(\mathbf{r})$ [2]. However, studies show that this distribution becomes increasingly inadequate as the end-to-end distance of the chain $|\mathbf{r}|$ approaches the fully extended length nb, especially with unrealistic nonzero values in the impermissible range $|\mathbf{r}| \geq nb$.

To overcome this difficulty, Kuhn and Grün [3] propounded a more elaborate theory for the probability distribution of FJC with large n in the entire range of extension. Their proposed non-Gaussian formulation led to a probability distribution involving the inverse Langevin function (Hereafter referred to as the inverse Langevin distribution), which recovers the Gaussian distribution for small end-to-end distance ($|\mathbf{r}| \to 0$). The pertinent force-extension relationship was also derived based on this probability distribution. Later, Treloar [4] provided an exact form of the probability distribution for arbitrary values of n and end-to-end vector $\mathbf{r}$, at the cost of considerable sacrifice of simplicity. Accordingly, for practical purposes, the inverse Langevin distribution and the resulting force-extension relation are still in the spotlight of abundant research studies. They have contributed to different fields including the modelling of single chain behaviour [1, 5–8], its augmented versions accounting for extensibility [9–11] and coil-rod structure [12], the development of macroscopic constitutive equations for single polymer networks [13–22], filled elastomers [23], double networks [24–26], nanocomposite hydrogels [27] and mechanochemically responsive polymers [28], as well as the study of photoelasticity [14, 29], damage and fracture phenomena [30–35], to name but a few.

In contrast to the wide application of the model by Kuhn and Grün [3], a noteworthy correction model by Flory [36] has received scant attention. Specifically, Flory pointed out that the proposed probability by Kuhn and Grün [3] is established on the premise that the chain conformations have a given end-to-end displacement along an arbitrarily chosen direction rather than having a specific end-to-end vector $\mathbf{r}$. Subse-

quently, a modified version of the probability distribution $W_n(\mathbf{r})$ was provided. How should one understand the source of deviation between the original work by Kuhn and Grün and the modified version? What is the implication of this modification to the force-extension relationship for a single chain? How much will it impact the micromechanics-based constitutive models for polymer networks? The present study aims at answering these questions through a critical examination on the derivation of $W_n(\mathbf{r})$ and its influence on several network models.

For this purpose, in Section 2.2, different statistical ensembles are introduced to expound the difference between their associated probability distributions and clarify the force-extension relationship that can be derived from each ensemble. It is emphasized that both "force" and "extension" can have different meanings in different ensembles. Next, in Section 2.3, Flory's modification is implemented to the probability by Kuhn and Grün to determine the corrected force-extension relationship which is given by

$$\langle f_x \rangle_r = k_B T \frac{\xi}{b} + k_B T \left(\frac{1}{x} - \frac{\xi}{nb\left(1 - \xi^2 \mathrm{csch}^2 \xi\right)} \right). \tag{2.1}$$

In this equation, $\langle f_x \rangle_r$ is the average force applied at the ends of an FJC with a fixed end-to-end vector $\mathbf{r} = x\hat{\mathbf{i}}$, k_B is the Boltzmann constant, and T is temperature. ξ is defined as

$$\xi = \mathscr{L}^{-1}\left(\frac{x}{nb}\right), \tag{2.2}$$

where $\mathscr{L}^{-1}(\cdots)$ is the inverse of the Langevin function $\mathscr{L}(\cdots)$ and $\mathscr{L}(s) = \coth(s) - 1/s$. In comparison, the original force-extension relationship derived by Kuhn and Grün is

$$\langle f_x \rangle = \frac{k_B T}{b} \xi. \tag{2.3}$$

It will be shown that Equation (2.3) predicts the average force on an FJC when its end-to-end displacement in x direction is fixed while the displacements along y

and z directions can change freely. Fundamentally, $\langle f_x \rangle$ and $\langle f_x \rangle_r$ are different, but the former has been commonly used in the place of the latter. In Section 2.4, the preceding results are utilized to extract the stress-stretch curves for several network models under different loading conditions. Although results in Section 2.4 show that for large n the correction alters the results only slightly, Section 2.5 demonstrates that misuse of the probability distribution can cause large discrepancies, for instance, in the development of a force-extension relationship for a coil-rod structure.

2.2 FJC in different ensembles

In order to understand the nature of Flory's correction, it is beneficial to study several pertinent ensembles. In this section, different ensembles are described in detail, all with fixed temperature T and fixed number of Kuhn segment n.

2.2.1 Isothermal-isotension ensemble

Suppose that a chain is fixed at one end, while the other end is subjected to a force $\mathbf{f}$. The corresponding partition function is dependent on $\mathbf{f}$, temperature T, and n. For FJC, the exact form of the isothermal-isotension partition function is given by [36]

$$Q(\mathbf{f}, T, n) = Z_0 \left\{ \frac{\sinh\left[(k_B T)^{-1} b|\mathbf{f}|\right]}{(k_B T)^{-1} b|\mathbf{f}|} \right\}^n, \tag{2.4}$$

where $|\mathbf{f}|$ denotes the magnitude of vector $\mathbf{f}$. Z_0 refers to the same partition function in the absence of any external force $\mathbf{f}$ (i.e., for a free chain). The Gibbs free energy is calculated from $Q(\mathbf{f}, T, n)$ by

$$\mathscr{G}(\mathbf{f}, T, n) = -k_B T \ln Q(\mathbf{f}, T, n). \tag{2.5}$$

Thus, the average of the chain's end-to-end vector is

$$\langle \mathbf{r} \rangle = -\frac{\partial \mathscr{G}}{\partial \mathbf{f}} = k_B T \frac{\partial Q / \partial \mathbf{f}}{Q}. \tag{2.6}$$

Now, if the coordinate system is set up such that the x axis is aligned with the force direction (see Figure 2.1a), then

$$|\mathbf{f}| = f_x, \tag{2.7}$$

$$f_y = f_z = 0. \tag{2.8}$$

The isothermal-isotension partition function (2.4) is rephrased as

$$Q(f_x, f_y = 0, f_z = 0, T, n) = Z_0 \left\{ \frac{\sinh\left[(k_B T)^{-1} b f_x\right]}{(k_B T)^{-1} b f_x} \right\}^n. \tag{2.9}$$

Substitution of Equation (2.9) into (2.6) leads to

$$\langle x \rangle = nb\mathscr{L}\left(\frac{f_x b}{k_B T}\right), \tag{2.10}$$

and

$$\langle y \rangle = \langle z \rangle = 0, \tag{2.11}$$

since the partition function (2.9) is independent of f_y and f_z.

2.2.2 Canonical ensemble

Suppose that the chain ends are fixed at two points separated by the end-to-end vector $\mathbf{r}$. Different conformations of the chain constitute the canonical ensemble with fixed $\mathbf{r}$, T, and n. The Helmholtz free energy is related to the canonical partition function $Z(\mathbf{r}, T, n)$ by

$$\psi(\mathbf{r}, T, n) = -k_B T \ln Z(\mathbf{r}, T, n). \tag{2.12}$$

The average force exerting on the chain ends is

$$\langle \mathbf{f} \rangle = \frac{\partial \psi}{\partial \mathbf{r}} = -k_B T \frac{\partial Z / \partial \mathbf{r}}{Z}. \tag{2.13}$$

If the coordinate system is chosen such that the x axis is along the end-to-end vector (see Figure 2.1b), then

$$|\mathbf{r}| = x, \tag{2.14}$$

$$y = z = 0. \tag{2.15}$$

Herein, the canonical partition function is written as $Z(x, y = 0, z = 0, T, n)$, and Equation (2.13) is simplified to

$$\langle f_x \rangle_r = -k_B T \frac{\partial Z / \partial x}{Z}, \tag{2.16}$$

where $\langle f_x \rangle_r$ denotes the component of the average force along x direction. Since $Z(x, y = 0, z = 0, T, n)$ is independent of y and z,

$$\langle f_y \rangle_r = \langle f_z \rangle_r = 0, \tag{2.17}$$

and $\langle f_x \rangle_r$ is equal to the magnitude of $\langle \mathbf{f} \rangle$. The subscript r emphasizes this is the average force along the end-to-end vector of the chain.

To compute the canonical partition function, we note that $Z(\mathbf{r}, T, n)$ and $Q(\mathbf{f}, T, n)$ are related via the Laplace transform [36]

$$Q(\mathbf{f}, T, n) = \iiint Z(\mathbf{r}, T, n) \exp\left[(k_B T)^{-1} \mathbf{f} \cdot \mathbf{r} \right] \, \mathrm{d}\mathbf{r}. \tag{2.18}$$

In essence, $Q(\mathbf{f}, T, n)$ is determined by summing all possible $Z(\mathbf{r}, T, n)$ over different $\mathbf{r}$, weighted by the Boltzmann factor $\exp\left[(k_B T)^{-1} \mathbf{f} \cdot \mathbf{r} \right]$. By substituting Equation (2.18) into Equation (2.6), we obtain

$$\langle \mathbf{r} \rangle = \iiint \mathbf{r} W_n^{\mathbf{f}}(\mathbf{r}) \, \mathrm{d}\mathbf{r}, \tag{2.19}$$

where $W_n^{\mathbf{f}}(\mathbf{r})$ is the distribution function defined as

$$W_n^{\mathbf{f}}(\mathbf{r}) = \frac{Z(\mathbf{r}, T, n) \exp\left[(k_B T)^{-1} \mathbf{f} \cdot \mathbf{r} \right]}{\iiint Z(\mathbf{r}, T, n) \exp\left[(k_B T)^{-1} \mathbf{f} \cdot \mathbf{r} \right] \, \mathrm{d}\mathbf{r}}. \tag{2.20}$$

$W_n^{\mathbf{f}}(\mathbf{r})\mathrm{d}\mathbf{r}$ can be identified as the probability that, under the force $\mathbf{f}$, one end of the chain is at $\mathrm{d}\mathbf{r}$ while the other end is fixed at the origin. By setting $\mathbf{f} = \mathbf{0}$, one can obtain the probability density for one chain end to be at $\mathbf{r}$ in the absence of applied force, while the other end is fixed at the origin:

$$W_n(\mathbf{r}) = \frac{Z(\mathbf{r}, T, n)}{\iiint Z(\mathbf{r}, T, n) \, \mathrm{d}\mathbf{r}}. \tag{2.21}$$

For a chain subjected to zero force the probability $W_n(\mathbf{r})$ merely depends on the end-to-end distance r and not direction of $\mathbf{r}$; hence the vector $\mathbf{r}$ can be replaced by r in $W_n(\mathbf{r})$ and $Z(\mathbf{r}, T, n)$. Since $W_n(r)$ is proportional to $Z(r, T, n)$, it can replace $Z(r, T, n)$ in the calculation of $\langle f_x \rangle_r$ in Equation (2.16), i.e.,

$$\langle f_x \rangle_r = -k_B T \, \frac{\partial W_n(x, y = 0, z = 0)/\partial x}{W_n(x, y = 0, z = 0)}. \tag{2.22}$$

Now we define another probability distribution as follows. Let $p_n^{\mathbf{f}}(x)\mathrm{d}x$ be the probability of finding one end of a chain under applied force $\mathbf{f}$ located in $\mathrm{d}x$ along $x-$direction, while the other end is fixed at the origin. Apparently,

$$p_n^{\mathbf{f}}(x) = \int_{y=-\infty}^{+\infty} \int_{z=-\infty}^{+\infty} W_n^{\mathbf{f}}(\mathbf{r}) \, \mathrm{d}y\mathrm{d}z. \tag{2.23}$$

Substitution of (2.20) into (2.23) yields

$$p_n^{\mathbf{f}}(x) = \frac{\Pi(x, f_y, f_z, T, n)\exp\left[(k_B T)^{-1} f_x x\right]}{\int \Pi(x, f_y, f_z, T, n)\exp\left[(k_B T)^{-1} f_x x\right] \, \mathrm{d}x}, \tag{2.24}$$

where

$$\Pi(x, f_y, f_z, T, n) = \int_{y=-\infty}^{+\infty} \int_{z=-\infty}^{+\infty} Z(\mathbf{r}, T, n)\exp\left[(k_B T)^{-1} (f_y y + f_z z)\right] \mathrm{d}y\mathrm{d}z. \tag{2.25}$$

In the absence of applied force, the corresponding probability simplifies to

$$p_n(x) = \frac{\Pi(x, f_y = 0, f_z = 0, T, n)}{\int \Pi(x, f_y = 0, f_z = 0, T, n) \, \mathrm{d}x}. \tag{2.26}$$

Through analogy of the above result with (2.21), one can introduce a new ensemble which has $\Pi(x, f_y = 0, f_z = 0, T, n)$ as its partition function. We name this ensemble "semi-canonical ensemble" and explain it in detail below.

2.2.3 Semi-canonical ensemble

Consider an ensemble of chains with one end fixed at the origin. The other end is fixed along an arbitrarily chosen x axis, while its y and z positions are free to move.

Moreover, the force applied at this end is zero along y and z directions. Evidently, this is neither the isothermal-isotension nor the canonical ensemble. The only difference between this new ensemble and the isothermal-isotension ensemble is the specification of x rather than f_x (see Figure 2.1c). It can be seen that

$$\langle y \rangle = \langle z \rangle = 0. \tag{2.27}$$

Similar to Equation (2.16), the average of the applied force is given by

$$\langle f_x \rangle = -k_B T \, \frac{\partial \Pi(x, f_y = 0, f_z = 0, T, n)/\partial x}{\Pi(x, f_y = 0, f_z = 0, T, n)}. \tag{2.28}$$

By using Equation (2.26), the average force can also be calculated from $p_n(x)$:

$$\langle f_x \rangle = -k_B T \, \frac{\partial p_n(x)/\partial x}{p_n(x)}. \tag{2.29}$$

2.3 FJC model of Kuhn and Grün

Kuhn and Grün [3] determined the probability that the end-to-end vector of a FJC under no external force has a projection of x along an arbitrarily chosen x axis without constraints on y or z. This is precisely $p_n(x)\mathrm{d}x$ discussed in Section 2.2.3. The expression derived by Kuhn and Grün is

$$p_n^{\mathrm{C}}(x) = \frac{A_0}{\sqrt{n}} \left(\frac{\sinh \xi}{\xi} \right)^n \exp\left[-\frac{\xi x}{b} \right], \tag{2.30}$$

where A_0 is the normalization factor and ξ is defined in Equation (2.2). The detailed proof of Equation (2.30) was provided in Kuhn and Grün [3] as well as in Flory [36]. However, for the sake of self-containment, the derivation is given in Appendix A.1. With the aid of (2.29), the associated force-extension relationship is obtained as given in Equation (2.3). It should be emphasized that x here does not denote the end-to-end distance, instead it is the end-to-end displacement of the chain along x direction. Therefore, $\langle f_x \rangle$ represents the average force applied along the x axis in order to fix the end-to-end displacement along x while allowing the displacements along y and z

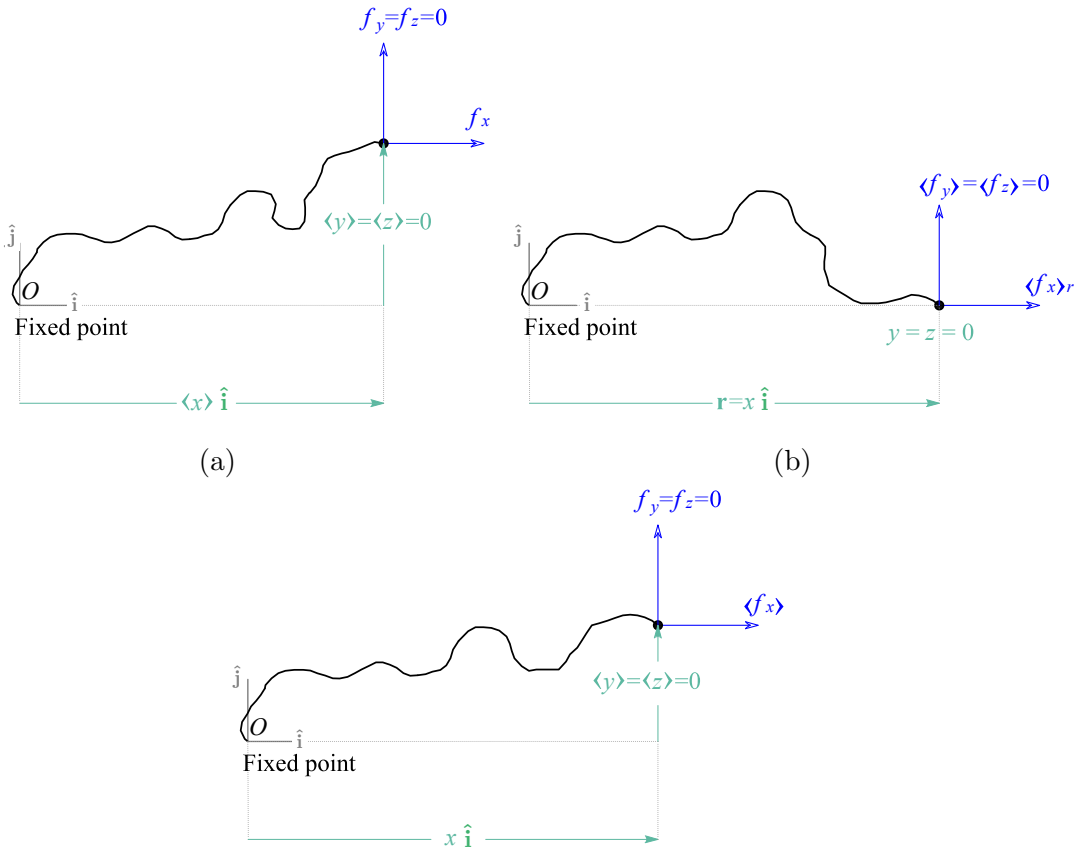

Figure 2.1: Different ensembles for a FJC with fixed number of Kuhn segments under constant temperature: (a) the isothermal-isotension ensemble in which the applied force is specified such that $f_y = f_z = 0$; (b) the canonical ensemble in which the components x, y, and z are fixed such that $y = z = 0$; (c) the semi-canonical ensemble in which different conformations occur with fixed x and fixed $f_y = f_z = 0$.

directions to freely change. This average force is described in the framework of the partition function $\Pi(x, f_y = 0, f_z = 0, T, n)$ rather than $Z(x, y, z, T, n)$. However, in Kuhn and Grün [3] an erroneous distribution $W^*(r)$ is derived by simply replacing x with r,

$$W_n^{\mathrm{C}*}(r) = \frac{A_0}{\sqrt{n}} \left(\frac{\sinh\beta}{\beta} \right)^n \exp\left[-\frac{\beta r}{b} \right], \tag{2.31}$$

where $\beta = \mathscr{L}^{-1}\left(\frac{r}{nb}\right)$.

When the FJC model is applied to evaluate the entropy of a polymer network, the probability relevant to the chains is $W_n^{\mathrm{C}}(\mathbf{r}) = W_n^{\mathrm{C}}(x = r, y = 0, z = 0)$ discussed in Section 2.2.2, and the relevant force-extension relationship is given by Equation (2.22). However, (2.3) and the probability distribution (2.31) are used by many researchers unwittingly. $W_n^{\mathrm{C}}(r)$ can be determined from $p_n^{\mathrm{C}}(x)$ using the following relation [4]

$$-\left(\frac{\mathrm{d}p_n^{\mathrm{C}}(x)}{\mathrm{d}x} \right)_{x=r} = 2\pi r W_n^{\mathrm{C}}(r). \tag{2.32}$$

The proof of the above relation is deferred to Appendix A.2. By adopting the chain rule, the left-hand side of the above relation is rephrased as

$$\frac{\mathrm{d}p_n^{\mathrm{C}}(x)}{\mathrm{d}x} = \left(\frac{\partial p_n^{\mathrm{C}}(x)}{\partial \xi} \right)_x \frac{\mathrm{d}\xi}{\mathrm{d}x} + \left(\frac{\partial p_n^{\mathrm{C}}(x)}{\partial x} \right)_\xi. \tag{2.33}$$

On the other hand the following identity holds for Equation (2.30):

$$\left(\frac{\partial p_n^{\mathrm{C}}(x)}{\partial \xi} \right)_x = A_0\sqrt{n}\,(\xi\sinh\xi)^n \exp\left[-\frac{\xi x}{b} \right] \left(\coth\xi - \frac{1}{\xi} - \frac{x}{nb} \right) = 0. \tag{2.34}$$

Now applying Equations (2.33) and (2.34) in Equation (2.32) yields

$$W_n^{\mathrm{C}}(r) = \frac{A_0\beta}{2\pi\sqrt{n}br} \left(\frac{\sinh\beta}{\beta} \right)^n \exp\left[\frac{-\beta r}{b} \right], \tag{2.35}$$

which was mentioned in Flory [36]. Finally, substitution of Equation (2.35) in (2.22) leads to Equation (2.1). It should be noted that in Equation (2.1) the second term is not singular as $x \to 0$, since $1 - \xi^2\mathrm{csch}^2\xi \sim \xi^2/3$ for small ξ and thus the second term converges to 0. The vast majority of the works using force-extension relationship

of FJC have adopted $\langle f_x \rangle$ in (2.3) rather than $\langle f_x \rangle_r$ in (2.1). Unlike (2.3), $\langle f_x \rangle_r$ is not merely a function of x/nb, but also depends on n separately. Figure 2.2 depicts the relative difference $\left| \dfrac{\langle f_x \rangle_r - \langle f_x \rangle}{\langle f_x \rangle_r} \right|$ vs. x/nb. Decreasing n as well as increasing x/nb give rise to larger discrepancies between the two formulations. On the other hand, for $n \geq 50$ the relative difference is less than 2%. The inset also compares the normalized forces $\langle f_x \rangle_r b/k_B T$ with $\langle f_x \rangle b/k_B T$ against x/nb for $n = 5$. Clearly, $\langle f_x \rangle b/k_B T$ overestimates the stiffness of the chain, especially near the fully extended state.

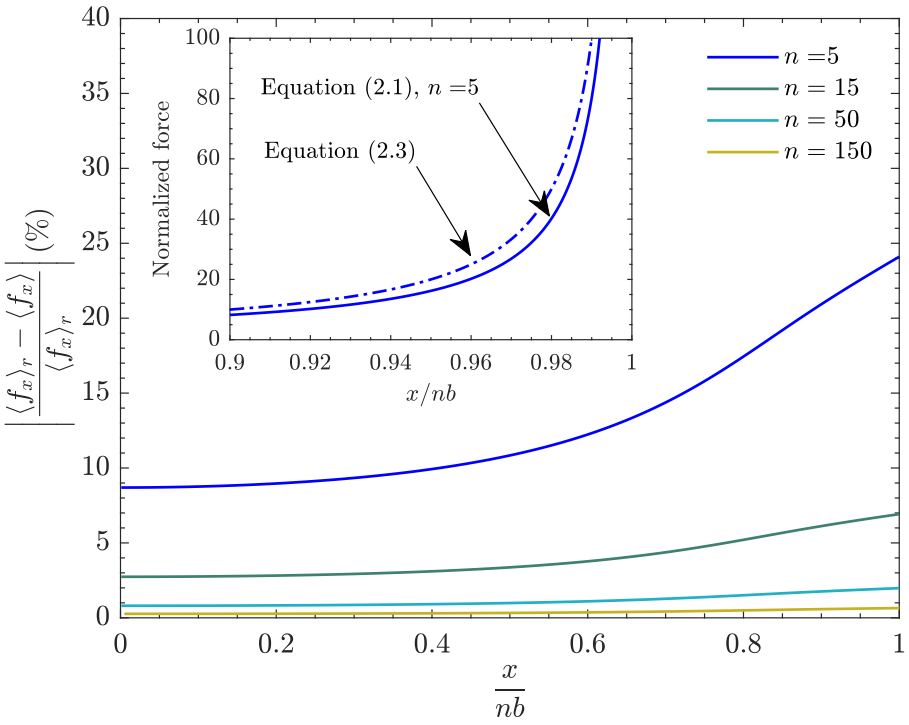

Figure 2.2: The relative difference between the average forces predicted by Equations (2.3) and (2.1) vs. the normalized end-to-end distance, for $n = 5$, 15, 50, and 150. The inset shows the normalized force vs. x/nb obtained from (2.3) and (2.1) for $n = 5$.

The above results show that increasing n causes the force-extension curves predicted from Equations (2.3) and (2.1) to converge. As $n \to \infty$, the statistical average of each property can be replaced by its thermodynamic value. In other words,

the three pictures in Figure 2.1 all correspond to the scenario where $y = z = 0$, $f_y = f_z = 0$, and f_x is applied to obtain x. Hence, the different ensembles can be employed interchangeably in the thermodynamic limit. Experimentally, single molecule stretching has been achieved by techniques such as atomic force microscopy (AFM). In the majority of the cases, the force-extension relationship given by Equation (2.3) or similar entropic elasticity based models is able to fit the experimental data up to a certain extension [7, 37], beyond which entropic elasticity is insufficient and enthalpic elasticity needs to be considered. The good agreement with experimental data is due to the large length of the chain (i.e., large n), despite the application of erroneous Equation (2.3). We should also point out that the corrected Equation (2.1) suffers from the same limitation as Equation (2.3) in the high-stretch regime, where adding extensibility is necessary to match experimentally measured force-extension relationship.

2.4 Implementation in macroscopic constitutive models

In the construction of macroscopic network models two factors are of cardinal importance: (a) the arrangement of the chains constituting the whole network structure; (b) the relation between force and end-to-end distance of the individual chains. For those models that use the FJC to account for entropic elasticity, the force-extension relationship of the chain plays an important role in the subsequent stress-stretch relation for the network. In accordance with the wide usage of the original inverse Langevin statistics, well-known models such as the three chain model [13], eight chain model [16], full network model [17] and micro-sphere model [20] utilized the $\langle f_x \rangle$-x relation in (2.3). In the current study, it is of interest to probe into the influence of using the $\langle f_x \rangle_r$-x relation (2.1) for deriving the macroscopic stress-stretch relation rather than Equation (2.3). Herein, the full network and micro-sphere models (without any inclusion of tube-like constraints) are revisited with both (2.3) and (2.1); subsequently

the pertinent results are compared for the equi-biaxial, uniaxial, and pure shear tests.

From macroscopic viewpoint, the Helmholtz free energy density (energy per unit reference volume) Ψ is defined as a function of deformation gradient $\mathbf{F}$ and temperature T:

$$\Psi = \Psi_0 + \Psi(\mathbf{F}, T), \tag{2.36}$$

where Ψ_0 is the Helmholtz free energy density of the reference configuration. For incompressible materials, the Cauchy stress tensor is defined as

$$\boldsymbol{\sigma} = \frac{\partial \Psi}{\partial \mathbf{F}} \mathbf{F}^{\mathrm{T}} - p_0 \mathbf{I}, \tag{2.37}$$

where $\mathbf{I}$ and p_0 are the identity tensor and unknown hydro-static pressure, respectively. For the collection of chains forming a network, Ψ can be written as the summation of the Helmholtz free energy of the individual chains in a unit reference volume. Thus,

$$\Psi(\mathbf{F}, T) = \sum_{i=1}^{\varrho} \psi_i(\lambda^{\mathbf{N}}), \tag{2.38}$$

where ϱ is the number of chains in the unit reference volume, and $\lambda^{\mathbf{N}}$ refers to the micro-stretch of the chain initially oriented along unit vector $\mathbf{N}$. The micro-stretch is defined as the ratio of the current chain end-to-end distance to the corresponding value in the reference configuration, r_0. ψ_i is the Helmholtz free energy of the ith chain and can be related to $\langle f_x \rangle_r$ by

$$\psi_i(\lambda^{\mathbf{N}}) = \int_{r_0}^{r_0 \lambda^{\mathbf{N}}} \langle f_x \rangle_r \, \mathrm{d}x. \tag{2.39}$$

For the full network model [17] the chains are assumed to be uniformly distributed in all directions in the reference configuration. Hence

$$\Psi(\mathbf{F}) = \frac{1}{4\pi} \iint_{\omega} \varrho \psi(\lambda^{\mathbf{N}}) \mathrm{d}\omega, \tag{2.40}$$

where ω denotes a spherical surface with unit radius in the reference configuration and $\psi = \psi_i$ given in (2.39). Insertion of the above relation in Equation (2.37) yields

$$\boldsymbol{\sigma} + p_0 \mathbf{I} = \frac{1}{4\pi} \iint_{\omega} \varrho \frac{\partial \psi(\lambda^{\mathbf{N}})}{\partial \lambda^{\mathbf{N}}} \frac{\partial \lambda^{\mathbf{N}}}{\partial \mathbf{F}} \mathbf{F}^{\mathrm{T}} \mathrm{d}\omega. \tag{2.41}$$

By taking $r_0 = \sqrt{n}b$ as the end-to-end distance of the chain in the reference configuration, one can deduce that

$$\boldsymbol{\sigma} + p_0\mathbf{I} = \frac{1}{4\pi}\iint_{\omega} \varrho\sqrt{n}b\langle f_x\rangle_r\Big|_{x=\sqrt{n}b\lambda^{\mathbf{N}}} \left(\frac{\partial\lambda^{\mathbf{N}}}{\partial\mathbf{F}}\mathbf{F}^{\mathrm{T}}\right) \mathrm{d}\omega. \tag{2.42}$$

To construct a proper relationship between the macroscopic deformation and micro-stretch, let us define the macro-stretch of a line element located along direction $\mathbf{N}$ in the reference configuration:

$$\bar{\lambda}^{\mathbf{N}} = \sqrt{\mathbf{N}\cdot\mathbf{F}^{\mathrm{T}}\mathbf{F}\mathbf{N}}. \tag{2.43}$$

For the affine network models, it is assumed that the micro-stretch of the chain is identical to the macro-stretch along the same direction $\mathbf{N}$, i.e.,

$$\lambda^{\mathbf{N}} = \bar{\lambda}^{\mathbf{N}}. \tag{2.44}$$

Figure 2.3(a) and 2.3(b) illustrate this relationship. Now, applying Equations (2.43) and (2.44) in Equation (2.42) leads to

$$\boldsymbol{\sigma} + p_0\mathbf{I} = \frac{1}{4\pi}\iint_{\omega} \varrho\sqrt{n}b\langle f_x\rangle_r\Big|_{x=\sqrt{n}b\lambda^{\mathbf{N}}} \left(\bar{\lambda}^{\mathbf{N}}\right)^{-1} (\mathbf{F}\mathbf{N})\,(\mathbf{F}\mathbf{N})\,\mathrm{d}\omega, \tag{2.45}$$

which completes the constitutive relation for the full network model.

Analogous to the previous treatment, a non-affine micro-sphere model can be developed in which (2.44) is no longer assumed. Instead, the following relation

$$\lambda^* = \left(\frac{1}{4\pi}\iint_{\omega} \left(\bar{\lambda}^{\mathbf{N}}\right)^{p^*} \mathrm{d}\omega\right)^{1/p^*} \tag{2.46}$$

is introduced to replace $\lambda^{\mathbf{N}}$, where p^* is an additional material parameter of the model. λ^* is essentially the stretch of the volume element averaged over different directions, as illustrated by Figure 2.3(a) and 2.3(c). The free energy density of the network, $\Psi(\mathbf{F})$, can now be simplified to $\varrho\psi(\lambda^*)$, where $\psi(\lambda^*) = \displaystyle\int_{r_0}^{r_0\lambda^*} \langle f_x\rangle_r \mathrm{d}x$. The Cauchy stress tensor is then given by

$$\boldsymbol{\sigma} + p_0\mathbf{I} = \varrho\frac{\partial\psi(\lambda^*)}{\partial\lambda^*}\frac{\partial\lambda^*}{\partial\mathbf{F}}\mathbf{F}^{\mathrm{T}}. \tag{2.47}$$

Applying (2.46) in the above relation and assuming the end-to-end distance of $\sqrt{n}b$ in the reference configuration results in

$$\boldsymbol{\sigma} + p_0\mathbf{I} = \frac{1}{4\pi}\,(\lambda^*)^{1-p^*}\,\varrho\sqrt{n}b\langle f_x\rangle_r\Big|_{x=\sqrt{n}b\lambda^*}\iint_\omega \left(\bar{\lambda}^{\mathbf{N}}\right)^{p^*-2}(\mathbf{FN})\,(\mathbf{FN})\,\mathrm{d}\omega. \qquad (2.48)$$

It should be emphasized that in the present formulation, the tube-like constraints on the individual chains are excluded for the sake of simplicity. In this case, the non-affine micro-sphere model with $p^* = 2$ collapses to the eight-chain model [20].

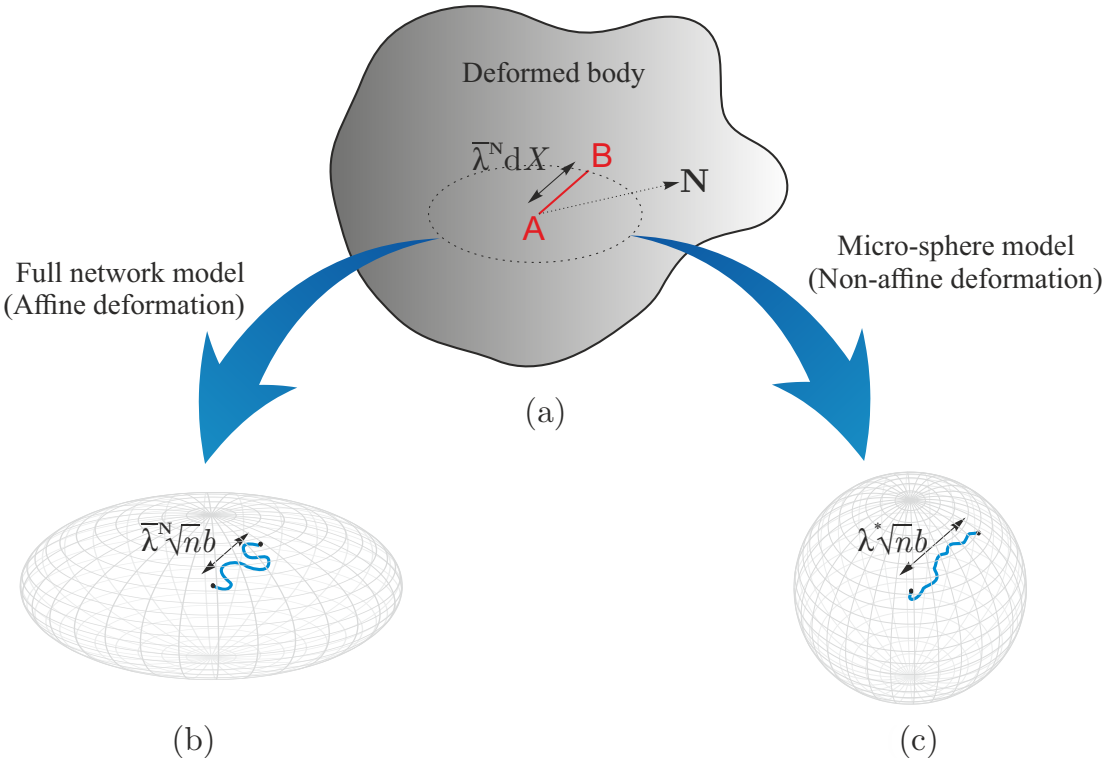

Figure 2.3: Schematic illustrations for the relationship between macroscopic stretch and microscopic chain extension in the full network and micro-sphere models. (a) Macroscopic deformation where a line element AB, originally oriented along $\mathbf{N}$ with length $\mathrm{d}X$, is deformed into $\bar{\lambda}^{\mathbf{N}}\mathrm{d}X$. (b) The full network model with affine deformation where the micro-stretch of the chain $\lambda^{\mathbf{N}}$ is assumed equal to the macro-stretch $\bar{\lambda}^{\mathbf{N}}$. The ellipsoid drawn indicates the dependence of $\lambda^{\mathbf{N}}$ on $\mathbf{N}$. (c) The micro-sphere model with non-affine deformation where the micro-stretch of the chain λ^* is obtained by an averaging process over different directions (indicated by the sphere drawn). In both (b) and (c) the initial end-to-end distance of the chain is considered as $\sqrt{n}b$.

Equations (2.45) and (2.48) connect the deformation gradient $\mathbf{F}$ to the Cauchy stress $\boldsymbol{\sigma}$; however, the selection of proper force-extension relation of the individual

chains is a key factor in the constitutive equations. By applying different relations such as those given in Equation (2.3) or (2.1), different stress states in the macroscopic sample can be obtained for the same deformation. Figure 2.4 displays the normalized Cauchy stress σ_1/G vs. the principal stretch λ_1 in equi-biaxial test, uniaxial test, and pure shear test for both affine (Equation (2.45)) and non-affine models (Equation (2.48)). $G = \varrho k_B T$ is a modulus. In the non-affine model, the parameter p^* is set to 2 to recover the eight-chain model. The results are provided with different force-extension relationships (2.3) and (2.1) for $n = 10$ in order to depict the impact of Flory's correction at the macroscopic level. All integrations over the unit sphere were calculated numerically through the 21-point integration scheme of Bažant and Oh [38].

By introducing the following dimensionless quantity as a measure of deviation

$$\eta = \frac{1}{\sqrt{G}(\hat{\lambda} - 1)} \int_1^{\hat{\lambda}} \sqrt{\left|\sigma_1^{(1)}(\lambda_1) - \sigma_1^{(2)}(\lambda_1)\right|} \mathrm{d}\lambda_1 \tag{2.49}$$

the total difference between the stress components $\sigma_1^{(1)}$ and $\sigma_1^{(2)}$ can be evaluated from the two different methods (superscripts (1) and (2) represent the use of Equations (2.3) and (2.1), respectively). The variable $\hat{\lambda}$ denotes the stretch at which the sample encounters chain locking without any further extension. All figures are drawn for extension λ_1 between 1 and $\hat{\lambda}$. Since the stress components are proportional to λ_1^{-1} as $\lambda_1 \to \hat{\lambda}$, the square root function is introduced to the integrand to ensure convergent integration for η. Based on η reported in the plots, for the full network model (Figures 2.4a, 2.4c, 2.4e) the normalized stress in the equi-biaxial test possesses the maximum difference, while the differences for uniaxial and pure shear tests are smaller and approximately the same. In the eight-chain model (Figures 2.4b, 2.4d, 2.4f), the equi-biaxial test has the minimum departure between the curves, while the uniaxial and pure shear tests exhibit larger deviations. Furthermore, comparison between the full network and eight-chain models shows larger η for the latter. Hence, the eight-chain model is more sensitive to the correction of the force-extension

relationship.

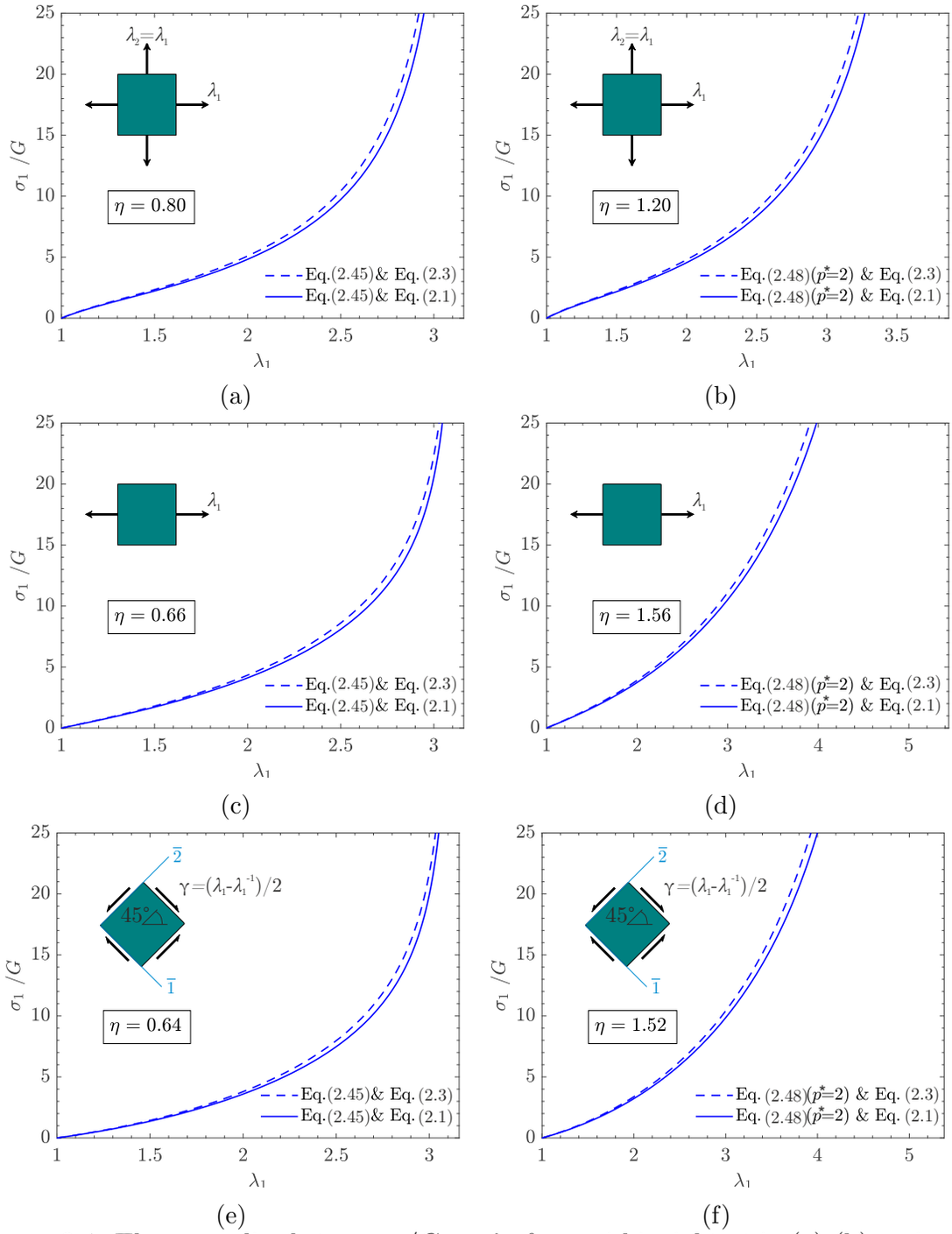

Figure 2.4: The normalized stress σ_1/G vs. λ_1 for equi-biaxial test in (a)-(b), uniaxial test in (c)-(d), and pure shear test in (e)-(f). (a), (c), (e) represent the affine (full network) model, while (b), (d), (f) display the non-affine micro-sphere model with $p^* = 2$. In all plots, λ_1 is the principal stretch in direction 1 (horizontal), and the other two principal directions are vertical, 2, and perpendicular to the page, 3. σ_1 is the normal stress in direction 1. In pure shear, the deformation is given by $x_{\bar{1}} = \sqrt{1+\gamma^2}X_{\bar{1}} + \gamma X_{\bar{2}}$, $x_{\bar{2}} = \gamma X_{\bar{1}} + \sqrt{1+\gamma^2}X_{\bar{2}}$, and $x_{\bar{3}} = X_{\bar{3}}$ where x_i and X_i, $i = \bar{1}, \bar{2}, \bar{3}$ respectively denote the spatial and material coordinates. Directions $\bar{1}$ and $\bar{2}$ are shown in the insets of (e) and (f).

2.5 Impact of misusing the probability

While Figure 2.2 shows that for large number of Kuhn segments n, the difference caused by using $\langle f_x \rangle$ in (2.3) as opposed to $\langle f_x \rangle_r$ in (2.1) is small, this section demonstrates an example where the difference caused by misusing the probability is significant. The example considered is a coil-rod structure, which contains a FJC with n Kuhn segments connected to a rigid rod with length a. Such a structure has been studied as a building block for some biopolymer gels [39]. Based on the work by Higgs and Ball [12], if the coil part obeys the Gaussian statistics, then

$$W_n^{\mathrm{CR}}(r) = \sqrt{\frac{3}{8n\pi^3 a^2 b^2}}\,\frac{1}{r}\exp\left[-\frac{3}{2nb^2}(r^2+a^2)\right]\sinh\left[\frac{3}{nb^2}ar\right]. \tag{2.50}$$

By using Equation (2.50) in Equation (2.22), the following relation is obtained

$$\langle f_x \rangle_r = \frac{3ak_BT}{nb^2}\left(\frac{x}{a} - \mathscr{L}\left[\frac{3ax}{nb^2}\right]\right). \tag{2.51}$$

We now show that using the probability $p_n(x)$ and Equation (2.29) results in a significantly different outcome for the $\langle f_x \rangle$-x relationship. By using $W_n^{\mathrm{CR}}(r)$ in Eq (2.50) and the relation in Equation (2.32) which is equivalent to $p_n^{\mathrm{CR}}(x) = \displaystyle\int_{|x|}^{+\infty} 2\pi r W_n^{\mathrm{CR}}(r)\mathrm{d}r$, one can calculate $p_n(x)$ as:

$$p_n^{\mathrm{CR}}(x) = \frac{1}{2}\left(\mathrm{erf}\left[\sqrt{\frac{3}{2nb^2}}\,(x+a)\right] - \mathrm{erf}\left[\sqrt{\frac{3}{2nb^2}}\,(x-a)\right]\right), \tag{2.52}$$

where $\mathrm{erf}(\cdots)$ denotes the error function. Substitution of Equation (2.52) in Equation (2.29) gives rise to

$$\langle f_x \rangle = k_BT\sqrt{\frac{6}{\pi nb^2}}\,\frac{\exp\left[\dfrac{-3}{2nb^2}\,(x-a)^2\right] - \exp\left[\dfrac{-3}{2nb^2}\,(x+a)^2\right]}{\mathrm{erf}\left[\sqrt{\dfrac{3}{2nb^2}}\,(x+a)\right] - \mathrm{erf}\left[\sqrt{\dfrac{3}{2nb^2}}\,(x-a)\right]}. \tag{2.53}$$

Figure 2.5 compares the results of Equations (2.51) and (2.53) for $a/b = 5$. Recognizing that Gaussian statistics is inaccurate for large extension, the comparison is made for x/a up to 1.75. When $n = 10$, $\langle f_x \rangle_r$ shows compressive force at small

x/nb, while such phenomenon is absent for $\langle f_x \rangle$. Physically, this can be understood by recognizing that $\langle f_x \rangle_r$ is the force evaluated in the canonical ensemble where y and z are fixed at zero (Figure 2.5, inset (II)), while $\langle f_x \rangle$ is the force calculated in the semi-canonical ensemble where y and z are free to change (Figure 2.5, inset (I)). Due to the presence of the rigid rod, for sufficiently small x, conformations in inset (II) of Figure 2.5 can only be accommodated by a compressive force. In inset (I) of Figure 2.5, however, conformations with large y and z can form, which removes the requirement of a compressive force. $\langle f_x \rangle_r$ and $\langle f_x \rangle$ therefore exhibit qualitatively different behaviours. By increasing the number of Kuhn segments to $n = 30$, the differences between the curves become negligible. However, it is important to recognize that $\langle f_x \rangle_r$ and $\langle f_x \rangle$ are fundamentally different, and cannot be used interchangeably without caution. In disordered biopolymer gels, the rigid rod models the junction zone formed by association of chains and the length of the coil trapped between the junction zones can be much smaller than that of the coiled chain in rubber-like materials [40]. In fact, the length of the junction zone (a) can be comparable to the length of coil (nb), and misusing the probability can lead to physically incorrect predictions.

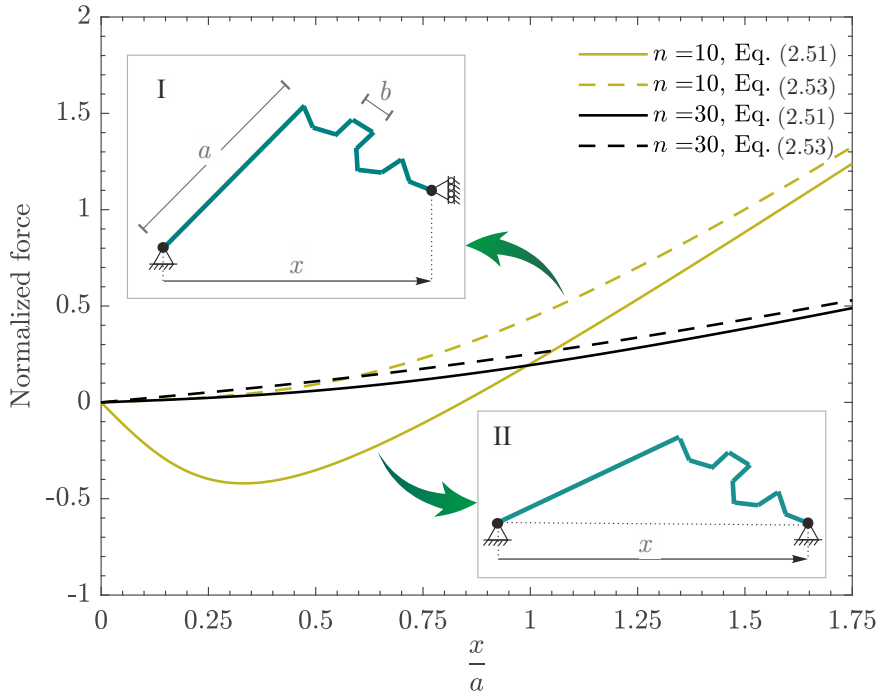

Figure 2.5: The comparison of normalized average force vs. x/a predicted from Equations (2.51) and (2.53) for $a/b = 5$, and $n = 10$ and 30. Both $\langle f_x \rangle_r$ (Equation (2.51)) and $\langle f_x \rangle$ (Equation (2.53)) are normalized by $k_B T/b$. Insets I and II show the schematics of the coil-rod structure with $n = 10$ for semi-canonical and canonical ensembles, respectively.

2.6 Conclusion

The current study provides a critical examination on the different probability distributions for an FJC, which leads to different force-extension relationships. We demonstrate that such difference arises from different statistical ensembles used to investigate the FJC: 1) the canonical ensemble where the end-to-end distance is fixed vs. 2) an ensemble where the projection of the end-to-end vector is fixed along an arbitrary direction (which we referred to as the semi-canonical ensemble in this work). The seminal work by Kuhn and Grün [3] did not make such a distinction; the reported force-extension relationship should have been for the semi-canonical ensemble and not for the canonical ensemble. Flory [36] pointed out this difference but to the best of the authors' knowledge, almost all works in the literature still use the original

result of Kuhn and Grün [3] to relate the force acting on the chain ends to the chain's end-to-end distance. Recognizing this misconception, a correction is introduced to the model of Kuhn and Grün [3], and this modified force-extension relationship is applied to macroscopic constitutive models (full network model, non-affine microsphere model) to examine its impact. While results from both ensembles converge in the thermodynamic limit (when the number of Kuhn segments n approaches infinity), they are distinguishable for smaller n. We further demonstrate that the misuse of the probability distributions can lead to large and even qualitative differences for a coil-rod structure consisting an FJC connected to a rigid rod, often considered as a building element for biopolymer gels. Care therefore should be exercised when using the probability distributions to study FJC-based mechanics models.

Acknowledgements

TT acknowledges financial support from the Natural Sciences and Engineering Research Council of Canada (NSERC; Grant numbers: RGPIN-2018-04281, RGPAS-2018-522655) and Canada Research Chairs Program (Grant number: TIER1 2021-00023). HM acknowledges scholarship support from Alberta Innovates.

References

[1] M. Rubinstein and R. Colby, *Polymer Physics*. OUP Oxford, 2003, ISBN: 9780198520597.

[2] W. Kuhn, "Beziehungen zwischen Molekülgröße, statistischer Molekülgestalt und elastischen Eigenschaften hochpolymerer Stoffe," *Kolloid-Zeitschrift*, vol. 76, no. 3, pp. 258–271, 1936.

[3] W. Kuhn and F. Grün, "Beziehungen zwischen elastischen Konstanten und Dehnungsdoppelbrechung hochelastischer Stoffe," *Kolloid-Zeitschrift*, vol. 101, no. 3, pp. 248–271, 1942.

[4] L. R. G. Treloar, "The statistical length of long-chain molecules," *Trans. Faraday Soc.*, vol. 42, pp. 77–82, 0 1946. DOI: 10.1039/TF9464200077.

[5] M. Volkenshteĭn, S. Timasheff, and M. Timasheff, *Configurational Statistics of Polymeric Chains* (High polymers). Interscience Publishers, 1963.

[6] L. Treloar, *The Physics of Rubber Elasticity* (Oxford Classic Texts in the Physical Sciences). Oxford University Press, USA, 1975, ISBN: 9780191523304.

[7] S. B. Smith, L. Finzi, and C. Bustamante, "Direct mechanical measurements of the elasticity of single dna molecules by using magnetic beads," *Science*, vol. 258, no. 5085, pp. 1122–1126, 1992. DOI: 10.1126/science.1439819. eprint: https://www.science.org/doi/pdf/10.1126/science.1439819.

[8] J. Weiner, *Statistical Mechanics of Elasticity* (Dover Books on Physics). Dover Publications, 2002, ISBN: 9780486422602.

[9] S. B. Smith, Y. Cui, and C. Bustamante, "Overstretching b-dna: The elastic response of individual double-stranded and single-stranded dna molecules," *Science*, vol. 271, no. 5250, pp. 795–799, 1996. DOI: 10.1126/science.271.5250.795. eprint: https://www.science.org/doi/pdf/10.1126/science.271.5250.795.

[10] A. Fiasconaro and F. Falo, "Analytical results of the extensible freely jointed chain model," *Physica A: Statistical Mechanics and its Applications*, vol. 532, p. 121 929, 2019, ISSN: 0378-4371. DOI: https://doi.org/10.1016/j.physa.2019.121929.

[11] M. R. Buche, M. N. Silberstein, and S. J. Grutzik, "Freely jointed chain models with extensible links," *Phys. Rev. E*, vol. 106, p. 024 502, 2 2022. DOI: 10.1103/PhysRevE.106.024502.

[12] P. G. Higgs and R. C. Ball, "Some ideas concerning the elasticity of biopolymer networks," *Macromolecules*, vol. 22, no. 5, pp. 2432–2437, 1989. DOI: 10.1021/ma00195a073. eprint: https://doi.org/10.1021/ma00195a073.

[13] M. C. Wang and E. Guth, "Statistical theory of networks of non-gaussian flexible chains," *The Journal of Chemical Physics*, vol. 20, no. 7, pp. 1144–1157, 1952. DOI: 10.1063/1.1700682. eprint: https://doi.org/10.1063/1.1700682.

[14] L. R. G. Treloar, "The photoelastic properties of short-chain molecular networks," *Trans. Faraday Soc.*, vol. 50, pp. 881–896, 0 1954. DOI: 10.1039/TF9545000881.

[15] L. R. G. Treloar, G. Riding, and G. Gee, "A non-gaussian theory for rubber in biaxial strain. i. mechanical properties," *Proceedings of the Royal Society of London. A. Mathematical and Physical Sciences*, vol. 369, no. 1737, pp. 261–280, 1979. DOI: 10.1098/rspa.1979.0163. eprint: https://royalsocietypublishing.org/doi/pdf/10.1098/rspa.1979.0163.

[16] E. M. Arruda and M. C. Boyce, "A three-dimensional constitutive model for the large stretch behavior of rubber elastic materials," *Journal of the Mechanics and Physics of Solids*, vol. 41, no. 2, pp. 389–412, 1993, ISSN: 0022-5096. DOI: https://doi.org/10.1016/0022-5096(93)90013-6.

[17] P. Wu and E. Van Der Giessen, "On improved network models for rubber elasticity and their applications to orientation hardening in glassy polymers," *Journal of the Mechanics and Physics of Solids*, vol. 41, no. 3, pp. 427–456, 1993, ISSN: 0022-5096. DOI: https://doi.org/10.1016/0022-5096(93)90043-F.

[18] M. C. Boyce and E. M. Arruda, "Constitutive models of rubber elasticity: A review," *Rubber chemistry and technology*, vol. 73, no. 3, pp. 504–523, 2000.

[19] C. O. Horgan and G. Saccomandi, "A molecular-statistical basis for the gent constitutive model of rubber elasticity," *Journal of Elasticity*, vol. 68, no. 1, pp. 167–176, 2002.

[20] C. Miehe, S. Göktepe, and F. Lulei, "A micro-macro approach to rubber-like materials—part I: The non-affine micro-sphere model of rubber elasticity," *Journal of the Mechanics and Physics of Solids*, vol. 52, no. 11, pp. 2617–2660, 2004, ISSN: 0022-5096. DOI: https://doi.org/10.1016/j.jmps.2004.03.011.

[21] A. Bahrololoumi, V. Morovati, E. A. Poshtan, and R. Dargazany, "A multi-physics constitutive model to predict hydrolytic aging in quasi-static behaviour of thin cross-linked polymers," *International Journal of Plasticity*, vol. 130, p. 102 676, 2020, ISSN: 0749-6419. DOI: https://doi.org/10.1016/j.ijplas.2020.102676.

[22] T. Zhao, J. Cao, X. Li, M. Xia, B. Xue, and H. Yuan, "A network-based visco-hyperelastic constitutive model for optically clear adhesives," *Extreme Mechanics Letters*, vol. 51, p. 101 594, 2022, ISSN: 2352-4316. DOI: https://doi.org/10.1016/j.eml.2021.101594.

[23] R. Dargazany, V. N. Khiêm, and M. Itskov, "A generalized network decomposition model for the quasi-static inelastic behavior of filled elastomers," *International Journal of Plasticity*, vol. 63, pp. 94–109, 2014, Deformation Tensors in Material Modeling in Honor of Prof. Otto T. Bruhns, ISSN: 0749-6419. DOI: https://doi.org/10.1016/j.ijplas.2013.12.004.

[24] X. Zhao, "A theory for large deformation and damage of interpenetrating polymer networks," *Journal of the Mechanics and Physics of Solids*, vol. 60, no. 2, pp. 319–332, 2012, ISSN: 0022-5096. DOI: https://doi.org/10.1016/j.jmps.2011.10.005.

[25] Y. Liu, H. Zhang, and Y. Zheng, "A Micromechanically Based Constitutive Model for the Inelastic and Swelling Behaviors in Double Network Hydrogels," *Journal of Applied Mechanics*, vol. 83, no. 2, Nov. 2015, 021008, ISSN: 0021-8936. DOI: 10.1115/1.4031897.

[26] D. Zhong *et al.*, "A constitutive model for multi network elastomers pre-stretched by swelling," *Extreme Mechanics Letters*, vol. 40, p. 100 926, 2020, ISSN: 2352-4316. DOI: https://doi.org/10.1016/j.eml.2020.100926.

[27] Q. Wang and Z. Gao, "A constitutive model of nanocomposite hydrogels with nanoparticle crosslinkers," *Journal of the Mechanics and Physics of Solids*, vol. 94, pp. 127–147, 2016, ISSN: 0022-5096. DOI: https://doi.org/10.1016/j.jmps.2016.04.011.

[28] Q. Wang, G. R. Gossweiler, S. L. Craig, and X. Zhao, "Mechanics of mechanochemically responsive elastomers," *Journal of the Mechanics and Physics of Solids*, vol. 82, pp. 320–344, 2015, ISSN: 0022-5096. DOI: https://doi.org/10.1016/j.jmps.2015.05.007.

[29] D. Sun, T. Lu, and T. Wang, "Nonlinear photoelasticity of rubber-like soft materials: Comparison between theory and experiment," *Soft Matter*, vol. 17, pp. 4998–5005, 19 2021. DOI: 10.1039/D1SM00267H.

[30] S. R. Lavoie, R. Long, and T. Tang, "A rate-dependent damage model for elastomers at large strain," *Extreme Mechanics Letters*, vol. 8, pp. 114–124, 2016, Nanomechanics: Bridging Spatial and Temporal Scales, ISSN: 2352-4316. DOI: https://doi.org/10.1016/j.eml.2016.05.016.

[31] Y. Mao, B. Talamini, and L. Anand, "Rupture of polymers by chain scission," *Extreme Mechanics Letters*, vol. 13, pp. 17–24, 2017, ISSN: 2352-4316. DOI: https://doi.org/10.1016/j.eml.2017.01.003.

[32] F. J. Vernerey, R. Brighenti, R. Long, and T. Shen, "Statistical damage mechanics of polymer networks," *Macromolecules*, vol. 51, no. 17, pp. 6609–6622, 2018. DOI: 10.1021/acs.macromol.8b01052. eprint: https://doi.org/10.1021/acs.macromol.8b01052.

[33] S. C. Lamont, J. Mulderrig, N. Bouklas, and F. J. Vernerey, "Rate-dependent damage mechanics of polymer networks with reversible bonds," *Macromolecules*, vol. 54, no. 23, pp. 10 801–10 813, 2021. DOI: 10.1021/acs.macromol.1c01943. eprint: https://doi.org/10.1021/acs.macromol.1c01943.

[34] J. Lei, Z. Li, S. Xu, and Z. Liu, "A mesoscopic network mechanics method to reproduce the large deformation and fracture process of cross-linked elastomers," *Journal of the Mechanics and Physics of Solids*, vol. 156, p. 104 599, 2021, ISSN: 0022-5096. DOI: https://doi.org/10.1016/j.jmps.2021.104599.

[35] P. K. Arunachala, R. Rastak, and C. Linder, "Energy based fracture initiation criterion for strain-crystallizing rubber-like materials with pre-existing cracks," *Journal of the Mechanics and Physics of Solids*, vol. 157, p. 104 617, 2021, ISSN: 0022-5096. DOI: https://doi.org/10.1016/j.jmps.2021.104617.

[36] P. Flory, *Statistical Mechanics of Chain Molecules*. Interscience Publishers, 1969.

[37] A. Ghatak, K. Vorvolakos, H. She, D. L. Malotky, and M. K. Chaudhury, "Interfacial rate processes in adhesion and friction," *The Journal of Physical Chemistry B*, vol. 104, no. 17, pp. 4018–4030, 2000. DOI: 10.1021/jp9942973. eprint: https://doi.org/10.1021/jp9942973.

[38] P. Bažant and B. H. Oh, "Efficient numerical integration on the surface of a sphere," *ZAMM - Journal of Applied Mathematics and Mechanics / Zeitschrift für Angewandte Mathematik und Mechanik*, vol. 66, no. 1, pp. 37–49, 1986. DOI: https://doi.org/10.1002/zamm.19860660108. eprint: https://onlinelibrary.wiley.com/doi/pdf/10.1002/zamm.19860660108.

[39] K. Nishinari, S. Koide, and K. Ogino, "On the temperature dependence of elasticity of thermo-reversible gels," *Journal de Physique*, vol. 46, no. 5, pp. 793–797, 1985. DOI: 10.1051/jphys:01985004605079300.

[40] H. McEvoy, S. Ross-Murphy, and A. Clark, "Large deformation and ultimate properties of biopolymer gels: 1. single biopolymer component systems," *Polymer*, vol. 26, no. 10, pp. 1483–1492, 1985, ISSN: 0032-3861. DOI: https://doi.org/10.1016/0032-3861(85)90081-3.

Chapter 3

Statistical Mechanics of Coil-rod Structure in Biopolymer Gels

A version of this chapter has been published. Reprinted with permission from Moosavian, H., and Tang, T."Statistical mechanics of coil–rod structure in biopolymer gels," *Journal of the Mechanics and Physics of Solids* 175 (2023): 105272. https://doi.org/10.1016/j.jmps.2023.105272

3.1 Introduction

To describe the mechanical properties of a wide range of synthetic polymers, such as rubber-like materials, it is conventional to model a uniform network containing the macromolecules as flexible chains connected together through covalent cross-linking [1]. However, studies reveal that the proposed strategy is inadequate for identifying the physical properties of many biopolymer gels [2]. In contrast to rubber-like materials, the constituting chains in many biopolymer gels randomly interlock with neighboring chains by means of physical rather than covalent cross-linking. The significance of such physical cross-linkages has been widely reported, for example in high strength hydrogels [3]. As a result, models describing rubber elasticity encounter difficulties for capturing mechanical response of biopolymer gels. For example, the unorthodox relationship between the elastic moduli of Na- and Ca-alginate gels and

the temperature cannot be justified through a linear relationship predicted from the traditional rubber elasticity model [4]. In addition, studies on biopolymer gels show that the thermal, mechanical, and chemical history of synthesis, including the type of polymer precursors, swelling/de-swelling, or heating/cooling gelation process, significantly affect the final properties of such gels. For instance, the mechanical features of Ca-alginate gels depend on the type of alginate and the preparation method [5].

Based on Clark and Ross-Murphy [6], biopolymer gels are divided into two main groups: (i) rod-like ordered biopolymer gels such as globular proteins with branched networks where the pertinent networks are formed by junction points resembling synthetic polymers; (ii) disordered biopolymer gels such as polysaccharide gels in which the individual chains associate together laterally, forming helical junction zones and/or ion-mediated aggregation zones (egg-box structures) with length comparable to that of the coil parts of the chain. Compared with covalent bonds, the non-covalent links within the junction zones can more easily dissociate and re-associate. Consequently, when an external loading is applied, the junction zones can shrink by unwinding or expand by zipping, allowing the exchange of segments between the junction zone and coil region of the network. The rate of zipping/unzipping of the junction zones can be governed by several factors, including the concentration of cations or the temperature [7]. Polymer networks such as gelatin or polysaccharide gels can therefore be envisaged as a collection of coil-rod structures serving as building blocks, where the rod and coil respectively represent the ordered junction zone and the remaining disordered region. For this reason, the elucidation of the mechanics of the coil-rod structure is of cardinal importance to gain insight into the properties of disordered biopolymer networks.

In the literature, there have been abundant studies that develop phenomenological models for the description of constitutive relations of biopolymer gels [8–12]. Readers are referred to the comprehensive review of the continuum elastic models for biopolymer gels by Wang and Xu [13]. On the contrary, micro-mechanical studies

accounting for behaviours at the molecular level are fairly limited. Some research focused on the constitutive relations of ordered biopolymer networks consisting of rod-like macromolecules. For example, Doi and Kuzuu [14] attempted to capture the energetic contribution of entanglements in such networks. Dobrynin and Carrillo [15] proposed a micromechanical-based constitutive model capable of predicting the strain-hardening of synthetic polymer networks as well as ordered biopolymer gels such as actin. De Tommasi *et al.* [16] adopted a multi-scale approach to derive a constitutive relationship for polymeric networks containing macromolecules with unfolding domains. Likewise, there is scant information on the micro-scale modelling of disordered biopolymer networks. Nishinari *et al.* [17] proposed a reel model for the zipping/unzipping mechanism to explain the nonlinear effect of the temperature on the elastic modulus in thermoreversible gels. In their treatment, the junction zones served as a reservoir capable of changing the number of the Kuhn segments in the coils, although the junction zone itself was not explicitly incorporated in the formulation. Mechanics of the coil was described by the inverse Langevin model, with energy levels assigned to each conformation proportional to the number of Kuhn segments in the coil. This model was verified for different types of biopolymer gels [18]. Inspired by this study, Higgs and Ball [19] simplified the reel model using Gaussian approximation and obtained the partition function of a reel structure attached to a rigid rod with a fixed length. Subsequently, they studied the effects of the zipping mechanism by comparing the properties of the reel structure with the conventional coil structure. In their zipping/unzipping treatment, the total number of segments is not conserved as the length of the rod remains fixed while the number of Kuhn segments in the coil is allowed to change. In addition, a number of assumptions were made which led to some unphysical features such as discontinuity in the force-extension curve.

The main goal of this study is to provide a comprehensive statistical mechanics framework for modelling the coil-rod structure considering the exchange of segments between the disordered region (the coil) and the junction zone (the rod). Since the

choice of ensemble depends on the question to be addressed and it can impact the results of the analysis, in Section 3.2, the fundamental concepts behind different ensembles are clarified. Subsequently, in Section 3.3, the statistical mechanics analysis of a rod structure is carried out with different ensembles. The formulation is extended to the coil-rod structure with fixed rod length in Section 3.4, to derive the relationship between the force applied at the ends of the structure and the end-to-end separation. In Section 3.5 the treatment of coil-rod structure is cast in a more general form to incorporate zipping and unzipping behaviour. Finally, as examples of its applications, in Section 3.6 the model is implemented into the eight-chain model to describe the macroscopic mechanical response of a network, as well as used to predict the unwinding of a double-stranded DNA under a tensile force.

3.2 Statistical mechanics considerations of a macromolecule

The main focus of this work, which is a general interest for the study of macromolecules, is the relationship between the force applied at the two ends of the structure and the end-to-end extension. The theoretical assessment of this mechanical property necessitates the formulation of a partition function via statistical mechanics. Since the temperature, extension, applied force and number of units in the molecule are convenient measurable properties, we generally deal with three ensembles: Canonical ensemble, isothermal-isotension ensemble, and grand canonical ensemble.

3.2.1 Canonical ensemble

In the canonical ensemble, two possible scenarios can be considered:

(i) The structure is maintained at a fixed end-to-end position vector $\mathbf{r}$, fixed temperature T and fixed number of segments N_t. An average force $\langle \mathbf{f}_r \rangle$ is required to maintain the structure with fixed end-to-end distance $|\mathbf{r}| = r$ along the direction $\frac{1}{r}\mathbf{r}$. If the canonical partition function $Z(\mathbf{r}, T, N_t)$ is at hand, one can

derive a relationship between the $\langle \mathbf{f}_r \rangle$ and $\mathbf{r}$. For a single molecular structure, the direction of $\mathbf{r}$ is immaterial to the partition function $Z(\mathbf{r}, T, N_t)$. Thus, with no loss of generality, the end-to-end vector $\mathbf{r}$ can be replaced by "end-to-end distance r". The Helmholtz free energy ψ is calculated from

$$\psi(r, T, N_t) = -k_B T \ln \left[Z(r, T, N_t) \right], \tag{3.1}$$

in which k_B is the Boltzmann constant. The average force is colinear with the fixed end-to-end vector $\mathbf{r}$ and its magnitude $\langle f_r \rangle$ is calculated by

$$\langle f_r \rangle = \frac{\partial \psi(r, T, N_t)}{\partial r}. \tag{3.2}$$

This ensemble has been in the spotlight of abundant research due to its significance in incorporating the chain properties into a network. For instance, Higgs and Ball [19] merely focused on canonical ensemble for the coil-rod structure.

(ii) The structure is kept at a fixed end-to-end "displacement", fixed temperature T and fixed number of segments N_t. The displacement can be imposed in any arbitrary direction, while the other components of the end-to-end vector are free to move. Without loss of generality, we will call this arbitrary direction x in this work. The average force $\langle f_x \rangle$ required to keep the structure with fixed x can be determined with the aid of this canonical ensemble, by recognizing that it is the work conjugate of x and its direction is along the x axis. Once the partition function $\Pi(x, T, N_t)$ is available, the Helmholtz free energy is obtained as

$$\psi(x, T, N_t) = -k_B T \ln \left[\Pi(x, T, N_t) \right]. \tag{3.3}$$

Now, by taking its derivative with respect to x, one can obtain the average force as

$$\langle f_x \rangle = \frac{\partial \psi(x, T, N_t)}{\partial x}. \tag{3.4}$$

Evidently, the number of conformations with fixed displacement is much larger than the previous ensemble. This stems from the fact that in the previous scenario, all displacement components x, y, and z are fixed. Although studying scenario (i) is of more practical relevance, there is an interesting relationship between the two scenarios which facilitates the derivation of the partition function with fixed end-to-end distance. This relationship is established below.

Consider a chain with one end fixed at the origin and without any applied external forces. The probability that the other end of the chain is located in a volume element $\mathrm{d}\mathbf{r}$ is given by [20]

$$W(\mathbf{r})\mathrm{d}\mathbf{r} = \frac{Z\left(\mathbf{r}, T, N_t\right)\mathrm{d}\mathbf{r}}{Z_0}, \tag{3.5}$$

where

$$Z_0 = \iiint Z\left(\mathbf{r}, T, N_t\right)\mathrm{d}\mathbf{r}, \tag{3.6}$$

and $W(\mathbf{r})$ denotes the probability distribution as a function of $\mathbf{r}$, commonly referred to simply as the "distribution function". The volume element $\mathrm{d}\mathbf{r}$ in (3.5) is located at the end of the position vector $\mathbf{r}$ with Cartesian coordinates (x, y, z). Similar to $Z(\mathbf{r}, T, N_t)$, $W(\mathbf{r})$ depends on the end-to-end distance r rather than end-to-end vector $\mathbf{r}$. Now, Equation (3.1) is rewritten as

$$\psi(r, T, N_t) = -k_B T \ln\left[W(r)\right] + \mathrm{cte}. \tag{3.7}$$

This alternative formulation enables us to use $W(r)$ to determine $\langle f_r \rangle$ vs. r for the coil-rod structure. Likewise, if $p(x)\mathrm{d}x$ is the probability that one end of a structure, free of any external forces, is located between x and $x + \mathrm{d}x$, while the other end is fixed at the origin, then:

$$p(x)\mathrm{d}x = \frac{Z\left(x, T, N_t\right)\mathrm{d}x}{\displaystyle\int_{x=-\infty}^{+\infty} Z\left(x, T, N_t\right)\mathrm{d}x}. \tag{3.8}$$

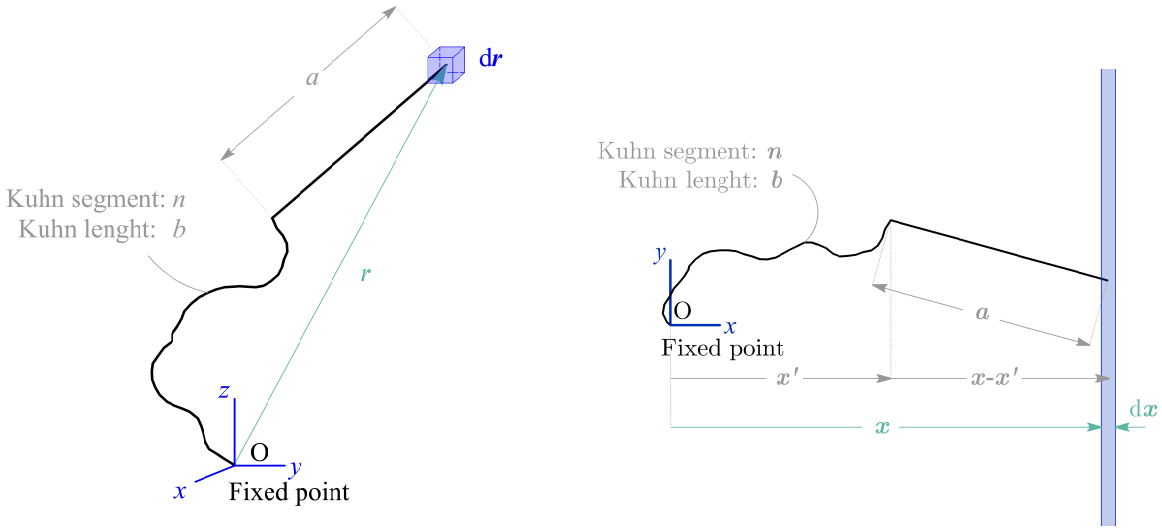

(a) Probability distribution $W_n^{\mathrm{CR}}(\mathbf{r})$ (b) Probability distribution $p_n^{\mathrm{CR}}(x)$

Figure 3.1: Schematics of the coil-rod structure and the two different probabilities. The superscript CR denotes the coil-rod structure, and the subscript n indicates the number of Kuhn segments in the coil.

Figure 3.1 depicts the aforementioned probabilities for the coil-rod structure with number of Kuhn segments n, Kuhn length b, and rod-length a. It can be readily shown that $W(r)$ and $p(x)$ satisfy the following equation:

$$-\left(\frac{\mathrm{d}p(x)}{\mathrm{d}x}\right)_{x=r} = 2\pi r W(r). \tag{3.9}$$

The detailed derivation of (3.9) is provided in Appendix B.1. To emphasize that $W(r)$ and $p(x)$ are obtained in the absence of external forces, they are termed as the probability distribution of the "free" chains hereafter.

3.2.2 Isothermal-isotension ensemble

In this case, the structure with one fixed end is acted upon by a fixed force $\mathbf{f}$ at the other end under fixed temperature T and a fixed number of segments N_t [20][1]. With no loss of generality, the coordinate system is set up such that x axis is in the direction of the applied force and the magnitude of the force is designated by

[1]This is analogous to the isothermal-isobaric ensemble for ideal gas with a fixed number of particles, fixed temperature T, and fixed applied pressure.

f_x. In this sense, different conformations with different x can be established as a concomitant of the applied force. The average $\langle x \rangle$ is the work conjugate of the force f_x and can be determined in the isothermal-isotension ensemble. Specifically, the isothermal-isotension partition function $Q(f_x, T, N_t)$ can be related to the partition function $\Pi(x, T, N_t)$ by [21]

$$Q(f_x, T, N_t) = \frac{1}{\Delta l} \int_{-\infty}^{+\infty} \Pi(x, T, N_t) \exp\left[\frac{f_x x}{k_B T}\right] \mathrm{d}x, \tag{3.10}$$

where Δl is a quantity with a dimension of length to ensure the dimensionless nature of the partition function. Because the derivation of the force-extension relationship involves differentiating the logarithm of the partition function, it is not influenced by the actual value of Δl. Alternatively, the isothermal-isotension partition function can be written in terms of $Z(r, T, N_t)$ by using spherical coordinates as below [20]

$$Q(f_x, T, N_t) = \frac{1}{\Delta l^3} \int_{\theta=0}^{2\pi} \int_{\phi=0}^{\pi} \int_{r=0}^{+\infty} Z(r, T, N_t) \exp\left[\frac{f_x r \cos\phi}{k_B T}\right] r^2 \sin\phi \, \mathrm{d}r \, \mathrm{d}\phi \, \mathrm{d}\theta. \tag{3.11}$$

After specification of $Q(f_x, T, N_t)$, the Gibbs free energy $\mathscr{G}$ is derived as

$$\mathscr{G}(f_x, T, N_t) = -k_B T \ln Q(f_x, T, N_t). \tag{3.12}$$

Subsequently,

$$\langle x \rangle = -\frac{\partial \mathscr{G}(f_x, T, N_t)}{\partial f_x} \tag{3.13}$$

is utilized to obtain a relation between $\langle x \rangle$ and f_x.

3.2.3 Grand canonical ensemble

In the ensembles discussed above, the length of the rod is considered fixed, which becomes inadequate if phenomena such as zipping and unzipping are to be accounted for. To allow for variable rod length and exchange of segments between the rod and coil portions of the structure, the grand canonical ensemble will be employed such that the structure is maintained at a fixed end-to-end position vector $\mathbf{r}$, fixed

temperature T and fixed chemical potential. This ensemble samples, according to the appropriate probability distribution, all possible conformations with different rod length or equivalently different number of Kuhn segments in the coil. The formulation in the grand canonical ensemble will be presented in Section 3.5.

It should be acknowledged that there have been many discussions on the equivalence of ensembles in the thermodynamic limit which, in the context of chain mechanics, refers to $N_t \to \infty$. For the standard coil structure, different ensembles can lead to different results for small or moderate N_t [22], while convergence of different ensembles has been demonstrated for large N_t [23]. The equivalence is no longer valid for certain polymer lattice models involving two equilibrium states for each segment. In this case, the force-extension relationships predicted from canonical and isothermal-isotension ensembles can be qualitatively different even for large N_t [24]. The equivalence of these two ensembles will be examined below for a single rod as well as for the coil-rod structure.

3.3 Analysis of a single rod

In this work, the junction zone is modeled as a single rigid rod. Different treatments are available in the literature. For example, in ordered biopolymer gels such as actin and collagen, the rod structures have been modeled using a semi-flexible chain with bending and axial stiffnesses [25]. The worm-like chain model [26] is another popular model often adopted for semi-flexible rod-like structures. The use of a non-deformable rod to represent the junction zone is a further simplification from the worm-like chain model, which is a reasonable assumption when the length of the rod is small compared to the persistence length of the worm-like chain [27]. According to Weiner [28], there are two distinct paths for the extraction of the partition function for a single rigid rod: (1) The rigid model in which the Hamiltonian of the rod is established based on the existing kinematic constraint. Hereafter, this model is referred to as Weiner's rigid model. (2) The flexible model in which the rod is first assumed to be flexible

with a finite axial stiffness κ. Then, the result of a stiff rod is achieved by setting κ to infinity. It should be noted that the term "flexible" for infinite κ may be misleading as it represents the rigid rod structure *per se*; nevertheless, the results may be different from Weiner's rigid model. In the current section, the flexible model is examined in detail and the results from the canonical and isothermal-isotension ensembles are compared. The description of Weiner's rigid model is deferred to Appendix B.2 where the differences between the approaches are clarified.

Consider a segment AB placed between two fixed walls with distance x at fixed temperature T (see Figure 3.2). The segment is modelled by a Hookean spring with stiffness κ and unstretched length a. Furthermore, the mass m of the segment is lumped at point B. Point A is affixed at the origin, while B is allowed to occupy any points on the right wall. Hence, the Hamiltonian of the segment is determined as

$$\mathscr{H} = \frac{1}{2m}(p_y^2 + p_z^2) + \frac{1}{2}\kappa\left(\sqrt{q_y^2 + q_z^2 + x^2} - a\right)^2. \tag{3.14}$$

In the above relation, p_y and p_z denote the components of the linear momentum of the concentrated mass m. q_y and q_z are the $y-$ and $z-$ components of the position vector of point B, respectively. Since the concentrated mass at B is confined to move in the yz plane, the system has two degrees of freedom and the corresponding canonical ensemble partition function is

$$\begin{aligned} Z^{\mathrm{R}}(x,T) =& \frac{1}{h^2}\int_{p_y=-\infty}^{+\infty}\int_{p_z=-\infty}^{+\infty} \exp\left[-\frac{p_y^2+p_z^2}{2mk_BT}\right] \mathrm{d}p_y\mathrm{d}p_z \\ &\times \int_{q_y=-\infty}^{+\infty}\int_{q_z=-\infty}^{+\infty} \exp\left[-\frac{\kappa}{2k_BT}\left(\sqrt{q_y^2+q_z^2+x^2}-a\right)^2\right] \mathrm{d}q_y\mathrm{d}q_z, \end{aligned} \tag{3.15}$$

in which the Planck's constant h is introduced to preserve the partition function dimensionless. In the above relation, superscript R is utilized to indicate the rod structure. After some mathematical manipulations, the above partition function is

expressed as below:

$$Z^{\mathrm{R}}(x,T) = \frac{4\pi^2 m k_B T a^2}{h^2} \times \left\{ \frac{k_B T}{\kappa a^2} \exp\left[\frac{-\kappa a^2}{2k_B T} \left(\frac{|x|}{a} - 1 \right)^2 \right] + \sqrt{\frac{\pi k_B T}{2\kappa a^2}} \operatorname{erfc}\left[\sqrt{\frac{\kappa a^2}{2k_B T}} \left(\frac{|x|}{a} - 1 \right) \right] \right\}, \tag{3.16}$$

in which $\operatorname{erfc}(\cdots)$ signifies the complementary error function. In the limit of very large κ, one can obtain

$$Z^{\mathrm{R}}(x,T) = \sqrt{\frac{32\pi^5 m^2 k_B^3 T^3 a^2}{h^4}} \frac{H(x+a) - H(x-a)}{\sqrt{\kappa}}, \tag{3.17}$$

where $H(\cdots)$ is the Heaviside step function. By employing Equation (3.17) in (3.8) it is found that

$$p^{\mathrm{R}}(x)\mathrm{d}x = \frac{\mathrm{d}x}{2a} \left(H(x+a) - H(x-a) \right). \tag{3.18}$$

which agrees with Treloar [29] for a single rigid rod. Finally, by substituting Equation (3.16) in (3.10), one can obtain the isothermal-isotension partition function as

$$\begin{aligned} Q^{\mathrm{R}}(f_x,T) = {} & \frac{1}{\Delta l} \sqrt{\frac{8\pi^5 m^2 k_B^5 T^5}{\kappa^3 h^4}} \frac{k_B T}{f_x a} \\ & \times \left\{ \exp\left[-\frac{f_x a}{k_B T} \left(1 - \frac{f_x}{2\kappa a} \right) \right] \left(\frac{f_x a}{k_B T} - \frac{\kappa a^2}{k_B T} \right) \left(1 + \operatorname{erf}\left[\frac{\kappa a^2 - f_x a}{\sqrt{2k_B T \kappa a^2}} \right] \right) \right. \\ & \left. + \exp\left[\frac{f_x a}{k_B T} \left(1 + \frac{f_x}{2\kappa a} \right) \right] \left(\frac{f_x a}{k_B T} + \frac{\kappa a^2}{k_B T} \right) \left(1 + \operatorname{erf}\left[\frac{\kappa a^2 + f_x a}{\sqrt{2k_B T \kappa a^2}} \right] \right) \right\}, \end{aligned} \tag{3.19}$$

in which $\operatorname{erf}(\cdots)$ represents the error function. For very large values of κ,

$$Q^{\mathrm{R}}(f_x,T) = \frac{1}{\Delta l} \sqrt{\frac{128\pi^5 m^2 a^4 k_B^3 T^3}{\kappa h^4}} \frac{k_B T}{f_x a} \sinh\left(\frac{f_x a}{k_B T} \right), \tag{3.20}$$

which is equivalent to the well-known result of the partition function for a single segment of a freely jointed chain [30].

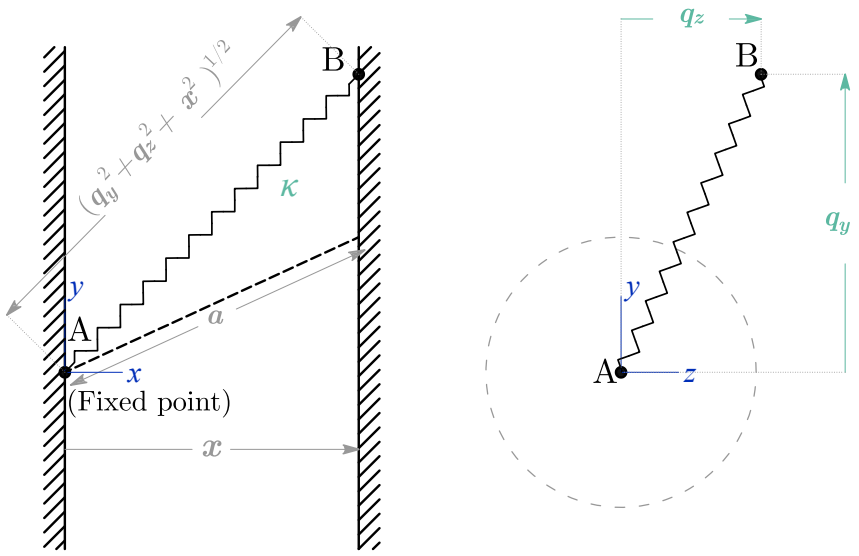

Figure 3.2: The single segment modelled by a Hookean spring is constrained between two fixed walls with a distance of x. Since the B end is allowed to occupy any position on the right wall, there are two degrees of freedom. The spring stiffness is κ and the unstretched length of the segment is a.

After calculation of partition functions (3.16), the average applied force $\langle f_x \rangle$ can be obtained using Equations (3.3) and (3.4). In the normalized form,

$$\begin{aligned}\frac{\langle f_x \rangle a}{k_B T} &= \frac{2\left(k_B T\right)^{-1} \kappa a x}{2+\sqrt{\frac{2\pi\kappa a^2}{k_B T}} \exp\left[\frac{\kappa a^2}{2k_B T}\left(\frac{|x|}{a}-1\right)^2\right] \operatorname{erfc}\left[\sqrt{\frac{\kappa a^2}{2k_B T}\left(\frac{|x|}{a}-1\right)}\right]} \\ &= \frac{2\left(k_B T\right)^{-1} \kappa a x}{2+\sqrt{\frac{2\pi\kappa a^2}{k_B T}} \exp\left[\frac{\kappa a^2}{2k_B T}\right]\left(1+\operatorname{erf}\left[\sqrt{\frac{\kappa a^2}{2k_B T}}\right]\right)} + \mathcal{O}\left(\left(\frac{x}{a}\right)^2\right). \end{aligned} \tag{3.21}$$

The second step in Equation (3.21) is obtained as a result of the Taylor expansion of the function about $x/a = 0$. Similarly, the average displacement $\langle x \rangle$ can be obtained in the isothermal-isotension ensemble by substituting (3.19) in Equations (3.12) and

(3.13), which in the normalized form is given by

$$\begin{aligned}\frac{\langle x\rangle}{a} = &-\frac{k_BT}{f_xa}+\frac{k_BT}{\kappa a^2}\Bigg\{\sqrt{\frac{8\kappa^3a^6}{\pi k_B^3T^3}}\exp\left[-\frac{\kappa a^2}{2k_BT}\right]\\
&+\exp\left[-\frac{f_xa}{k_BT}\left(1-\frac{f_xa}{2\kappa a^2}\right)\right]\left[\frac{\kappa a^2}{k_BT}+\left(\frac{f_xa}{k_BT}-\frac{\kappa a^2}{k_BT}\right)^2\right]\left(1+\operatorname{erf}\left[\frac{\kappa a^2-f_xa}{\sqrt{2k_BT\kappa a^2}}\right]\right)\\
&+\exp\left[\frac{f_xa}{k_BT}\left(1+\frac{f_xa}{2\kappa a^2}\right)\right]\left[\frac{\kappa a^2}{k_BT}+\left(\frac{f_xa}{k_BT}+\frac{\kappa a^2}{k_BT}\right)^2\right]\left(1+\operatorname{erf}\left[\frac{\kappa a^2+f_xa}{\sqrt{2k_BT\kappa a^2}}\right]\right)\Bigg\}\\
&\times\Bigg\{\exp\left[-\frac{f_xa}{k_BT}\left(1-\frac{f_xa}{2\kappa a^2}\right)\right]\left(\frac{f_xa}{k_BT}-\frac{\kappa a^2}{k_BT}\right)\left(1+\operatorname{erf}\left[\frac{\kappa a^2-f_xa}{\sqrt{2k_BT\kappa a^2}}\right]\right)\\
&+\exp\left[\frac{f_xa}{k_BT}\left(1+\frac{f_xa}{2\kappa a^2}\right)\right]\left(\frac{f_xa}{k_BT}+\frac{\kappa a^2}{k_BT}\right)\left(1+\operatorname{erf}\left[\frac{\kappa a^2+f_xa}{\sqrt{2k_BT\kappa a^2}}\right]\right)\Bigg\}^{-1}.\end{aligned} \tag{3.22}$$

For very large κ the leading order term is

$$\frac{\langle x\rangle}{a}=\mathscr{L}\left(\frac{f_xa}{k_BT}\right)=\frac{1}{3}\frac{f_xa}{k_BT}f_x+\mathscr{O}\left(\left(\frac{f_xa}{k_BT}\right)^3\right), \tag{3.23}$$

where $\mathscr{L}(\cdots)$ represents the Langevin function.

Figure 3.3 shows the normalized force $\langle f_x\rangle a/k_BT$ versus x/a obtained from the canonical ensemble for different values of κa^2. By increasing $\kappa a^2/k_BT$ the curves tend to level off for sufficiently small x/a with a sharper increase toward infinity as x approaches a. Figure 3.3 also depicts the normalized applied force f_xa/k_BT versus normalized average displacement $\langle x\rangle/a$ obtained from the isothermal-isotension ensemble for different values of κa^2. Clearly, for a given $\kappa a^2/k_BT$ this ensemble predicts stiffer behaviour compared to the canonical ensemble. The discrepancies between the two ensembles are negligible for $\kappa a^2 = k_BT$, while larger differences between the ensembles are detected as κa^2 increases to $10000\,k_BT$. This feature confirms that the rod structure cannot be considered as a macroscopic thermodynamic system.

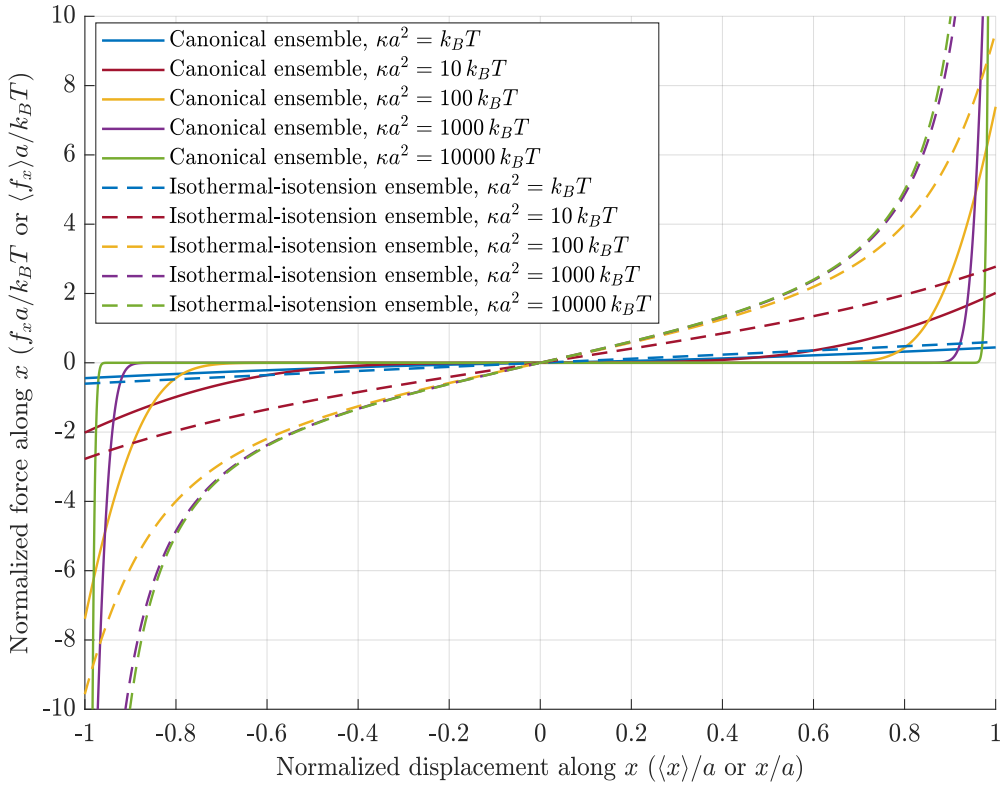

Figure 3.3: Normalized force vs. normalized displacement along the $x-$axis for different values of κa^2. For the isothermal-isotension ensemble $f_x a/k_BT$ is plotted against $\langle x\rangle/a$, while for the canonical ensemble $\langle f_x\rangle a/k_BT$ is plotted against x/a.

3.4 Coil-rod structure with fixed rod length

In this section, we will present the formulation for the determination of the force versus end-to-end distance (or x displacement) of the coil-rod structure in the canonical and isothermal-isotension ensembles.

To calculate the probability distribution of the coil-rod structure $W_n^{\mathrm{CR}}(r)$, it is preferable to obtain the probability distribution along x direction $p_n^{\mathrm{CR}}(x)$ in advance. Hereafter, the superscript CR indicates the coil-rod structure. For this purpose, it is convenient to employ the convolution property to relate $p_n^{\mathrm{CR}}(x)$ to $p^{\mathrm{R}}(x)$ for the rod

(Equation (3.18)) and $p_n^{\mathrm{C}}(x)$ for the coil (see Figure 3.1b):

$$p_n^{\mathrm{CR}}(x) = \int_{-\infty}^{+\infty} p_n^{\mathrm{C}}(x')p^{\mathrm{R}}(x-x')\mathrm{d}x' = \frac{1}{2a}\int_{x-a}^{x+a} p_n^{\mathrm{C}}(x')\mathrm{d}x'. \tag{3.24}$$

The latter identity is achieved through the use of Equation (3.18). For the coil the superscript C has been added and the subscript n is the number of Kuhn segments it contains. Carrying the above result into Equation (3.9) and applying Leibniz integral rule yield

$$W_n^{\mathrm{CR}}(r) = \frac{1}{4\pi a r}\left[p_n^{\mathrm{C}}(r-a) - p_n^{\mathrm{C}}(r+a)\right]. \tag{3.25}$$

Herein, without the explicit calculation of $W_n^{\mathrm{C}}(r)$ and $W^{\mathrm{R}}(r)$, the distribution function of the coil-rod structure $W_n^{\mathrm{CR}}(r)$ is achieved in terms of the probability distribution of the coil along x direction, i.e., $p_n^{\mathrm{C}}(x)$.

3.4.1 Gaussian approximation

Let us first approximate the coil structure by a Gaussian chain with Kuhn length b and the number of Kuhn segment n. The probability $p_n^{\mathrm{C}}(x)$ of such structure is given by [1]

$$p_n^{\mathrm{C}}(x) = \sqrt{\frac{3}{2\pi n b^2}}\exp\left[-\frac{3x^2}{2nb^2}\right]. \tag{3.26}$$

Combining Equations (3.25) and (3.26) leads to

$$W_n^{\mathrm{CR}}(r) = \sqrt{\frac{3}{8n\pi^3 a^2 b^2}}\,\frac{1}{r}\exp\left[-\frac{3}{2nb^2}(r^2+a^2)\right]\sinh\left(\frac{3}{nb^2}ar\right), \tag{3.27}$$

which is equivalent to the model of Higgs and Ball [19]. It is important to note that the term "Gaussian distribution" only applies to the coiled part of the coil-rod structure, while the coil-rod does not exhibit the Gaussian behaviour. By differentiating the Helmholtz free energy (3.7) with respect to r, the average external force $\langle f_r\rangle$ is derived as

$$\frac{\langle f_r\rangle a}{k_B T} = -\frac{3\zeta^2}{n}\mathscr{L}\left(\frac{3\zeta^2}{n}\,\frac{r}{a}\right) + \frac{3\zeta^2}{n}\left(\frac{r}{a}\right), \tag{3.28}$$

where $\zeta = a/b$. For small extension r/a, it can be readily shown that

$$\frac{\langle f_r \rangle a}{k_B T} = \frac{3\zeta^2}{n}\left(1 - \frac{\zeta^2}{n}\right)\frac{r}{a} + \mathscr{O}\left(\left(\frac{r}{a}\right)^2\right). \tag{3.29}$$

The above relation shows that the initial slope of the $\langle f_r \rangle - r$ curve is negative when $\zeta > \sqrt{n}$. This feature stems from the fact that under zero external force the coil structure has a maximum probability at zero end-to-end distance (see (3.26)), but the presence of the rod shifts the maximum of the probability (3.27) toward a non-zero end-to-end distance. Hereafter this distance will be denoted by r^*. It is worthwhile to mention that the above result is valid only if the number of Kuhn segments is large and the end-to-end distance of the coil is very small. In other words, the Gaussian description of the coil-rod structure is legitimate when $r \to a$ and $n \gg 1$. Performing Taylor series expansion of Equation (3.28) about $r = a$, one can obtain an estimation of r^* at which the average force $\langle f_r \rangle$ vanishes:

$$\frac{r^*}{a} \approx \frac{\mathscr{L}\left(\frac{3\zeta^2}{n}\right) - \frac{3\zeta^2}{n}\mathscr{L}'\left(\frac{3\zeta^2}{n}\right)}{1 - \frac{3\zeta^2}{n}\mathscr{L}'\left(\frac{3\zeta^2}{n}\right)}, \tag{3.30}$$

where $\mathscr{L}'(\cdots)$ is the first derivative of the Langevin function.

In the following, we provide a more rigorous calculation and the validity of the Gaussian approximation is inspected through comparison with the exact result.

3.4.2 Exact treatment

Compared to the coiled chain in rubber-like materials, the length of the coil between junction zones in biopolymers is not necessarily large. Therefore, the Gaussian distribution assumption for the coil may be invalid, and it is necessary to account for the finite number of segments in the coil [8].

Consider a freely jointed chain with an arbitrary number of Kuhn segment n subjected to no external force. If one end of this coil is located at the origin, the probability that the other end is located between x and $x + \mathrm{d}x$, along an arbitrary direction

x, is given by [29]

$$p_n^{\mathrm{C}}(x)\mathrm{d}x = \\ \frac{1}{2b}\sum_{s=0}^{k}\frac{n(-1)^s}{s!(n-s)!}\left[\frac{1}{2}\left(n-\frac{x}{b}\right)-s\right]^{n-1}\mathrm{d}x \quad \text{if } -(2k+2-n)b \le x \le (n-2k)b, \tag{3.31}$$

and zero for $|x| \geq nb$. In the above relation, $k = 0, 1, \cdots, n-1$. The substitution of Equation (3.31) in Equation (3.25) results in the exact form of $W_n^{\mathrm{CR}}(r)$, from which the average force can be determined:

$$\frac{\langle f_r \rangle a}{k_B T} = \frac{a}{r} - a\left(\frac{\mathrm{d}p_n^{\mathrm{C}}(r-a)}{\mathrm{d}r} - \frac{\mathrm{d}p_n^{\mathrm{C}}(r+a)}{\mathrm{d}r}\right)\left(p_n^{\mathrm{C}}(r-a) - p_n^{\mathrm{C}}(r+a)\right)^{-1}. \tag{3.32}$$

As a side note, in Appendix B.3, the closed-form expression of the probability distribution $p_n^{\mathrm{CR}}(x)$ is derived from (3.24) and (3.31).

3.4.3 Approximation for a large number of Kuhn segments

As x approaches $-nb$, the numerical calculation of summation in (3.31) for large n encounters fluctuations. To circumvent this issue, we will devise an alternative remedy for large n. It should be emphasized that the Gaussian approximation in 3.4.1 is only valid if the end-to-end distance $r/b \ll 1$ and $n \gg 1$, while the current treatment is applicable for $n \gg 1$ irrespective of r values.

The probability distribution of a freely jointed coil along x direction can be expressed in a single term under certain conditions [20][2],

$$p_n^{\mathrm{C}}(x) = \frac{A_0}{\sqrt{n}}\left[\frac{\sinh\xi}{\xi}\right]^n \exp\left[-\frac{\xi x}{b}\right], \tag{3.33}$$

in which

$$\xi = \mathscr{L}^{-1}\left(\frac{x}{nb}\right), \tag{3.34}$$

[2]These conditions are thoroughly discussed in Flory's book. During the derivation, the summation of probabilities in (3.31) is replaced by an approximate expression, and then the factorial functions are estimated with Stirling's approximation.

and A_0 is a normalization factor and a function of b. Substituting (3.33) into Equation (3.25) yields

$$W_n^{\mathrm{CR}}(r) = \frac{A_0}{4\pi a r\sqrt{n}}\left\{\left[\frac{\sinh\xi_1}{\xi_1}\right]^n \exp\left[-\xi_1\zeta\left(\frac{r}{a}-1\right)\right] - \left[\frac{\sinh\xi_2}{\xi_2}\right]^n \exp\left[-\xi_2\zeta\left(\frac{r}{a}+1\right)\right]\right\}, \tag{3.35}$$

in which

$$\xi_1 = \mathscr{L}^{-1}\left[\frac{\zeta}{n}\left(\frac{r}{a}-1\right)\right], \tag{3.36a}$$

$$\xi_2 = \mathscr{L}^{-1}\left[\frac{\zeta}{n}\left(\frac{r}{a}+1\right)\right]. \tag{3.36b}$$

The average force applied at the ends of the coil-rod structure can therefore be calculated from the Helmholtz free energy,

$$\frac{\langle f_r\rangle a}{k_BT} = \frac{a}{r} + \zeta\frac{\xi_1\left[\frac{\sinh\xi_1}{\xi_1}\right]^n \exp\left[-\xi_1\zeta\left(\frac{r}{a}-1\right)\right] - \xi_2\left[\frac{\sinh\xi_2}{\xi_2}\right]^n \exp\left[-\xi_2\zeta\left(\frac{r}{a}+1\right)\right]}{\left[\frac{\sinh\xi_1}{\xi_1}\right]^n \exp\left[-\xi_1\zeta\left(\frac{r}{a}-1\right)\right] - \left[\frac{\sinh\xi_2}{\xi_2}\right]^n \exp\left[-\xi_2\zeta\left(\frac{r}{a}+1\right)\right]}. \tag{3.37}$$

For small values of r/a, and $a < nb$ ($\zeta < n$) it can be shown that

$$\frac{\langle f_r\rangle a}{k_BT} = \zeta^2\frac{3-n\vartheta^2\mathscr{L}'(\vartheta)}{3n\mathscr{L}'(\vartheta)}\frac{r}{a} + \mathscr{O}\left(\left(\frac{r}{a}\right)^2\right), \tag{3.38}$$

where $\vartheta = \mathscr{L}^{-1}\left(\frac{\zeta}{n}\right)$. For large n the result of the Gaussian approximation (3.29) can be recovered from Equation (3.38).

3.4.4 Comparison of different results in the canonical ensemble

The normalized average force $\langle f_r\rangle a/k_BT$ is plotted against the normalized end-to-end distance r/a for fixed $\zeta = 5$ and $n = 5$, 10, 25 in Figure 3.4. Three cases are considered below and the results are provided for the exact model (3.32), Gaussian approximation (3.28), and large n approximation (3.37).

Case 1: $\zeta^2 \leq n$

Demonstrated by the curves with $n = 25$ in Figure 3.4, the coil component in this case is dominant, and hence the behaviour of the curves resembles that of coiled chains without a rod component. The average force monotonically increases as the structure extends. The Gaussian and large n approximations both have reasonable agreement with the exact model for small r/a. For $r/a > 2.5$ the large n approximation still agrees well with the exact model, while there is a substantial deviation from the Gaussian approximation. This is due to the assumption of small end-to-end distance for the coiled structure inherited from the Gaussian approximation.

Case 2: $\zeta < n < \zeta^2$

As shown in Figure 3.4, for $n = 10$ there are two states with zero force, at $r = 0$ and $r^* = 0.83a$. Recall that r^* represents the end-to-end distance with maximum probability. In this case, the curves behave completely differently from the conventional force-extension curves in that a convexity appears in the plots. The convex behaviour reflects the fact that the maximum probability of the free coil-rod structure occurs at a non-zero end-to-end distance (r^*) as opposed to zero in the pure free coil chain model. For this reason, such a structure can sustain compressive forces if $r < r^*$. Physically, the phenomenon is caused by the presence of the rod, which has a rigid structure and when its length is comparable to the contour length of the coil, a compressive force is required to reach sufficiently small end-to-end distance for the coil-rod structure. The zero end-to-end distance $r = 0$ still represents an equilibrium state, albeit unstable. Similar to the previous case, the large n approximation agrees with the exact model for the entire range of r, while the Gaussian approximation departs from the exact model significantly as the end-to-end distance increases. In particular, under the Gaussian approximation, the coil-rod structure is permitted to be stretched more than its contour length, i.e., $r/a = 3$, which is not realistic within the framework of entropic elasticity.

Case 3: $\zeta \geq n$

For this case, the length of the rod is greater than the contour length of the coil, i.e., $nb < a$, and it is impossible to reach zero end-to-end distance. This feature can be captured by the curves in Figure 3.4 with $n = 5$ (exact result and large n approximation) in which infinite compressive force is required to push the two ends toward each other. Zero force is found to occur at $r^* = 0.92a$ which is the end-to-end distance with the highest probability of the free coil-rod structure. Clearly, the curve predicted from the Gaussian approximation differs drastically from the other two curves not only for large extension $r/a > 1.5$ but also for small extension $r/a < 0.5$. Such a poor performance of the Gaussian approximation is expected and necessitates the application of the non-Gaussian model for smaller n or large a.

It is worthwhile to mention that in all cases, the average force predicted from the exact model goes to infinity as the end-to-end distance approach the fully stretched state, i.e., $r \to a + nb$. Moreover, as r/a approaches 1, the accuracy of the Gaussian approximation increases because of the small extension of the coil.

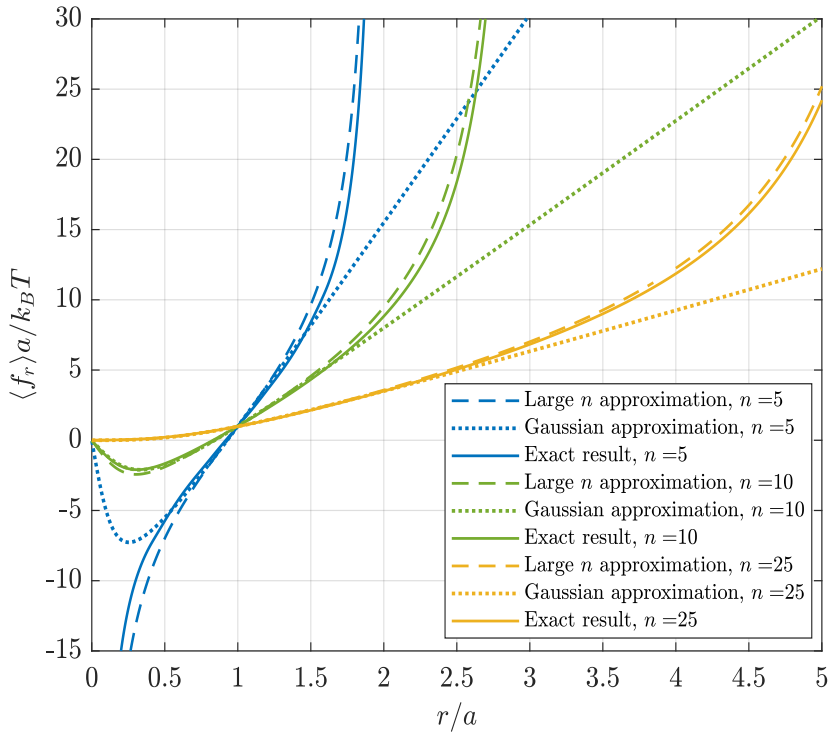

Figure 3.4: Normalized force $\langle f_r \rangle a/k_B T$ vs. normalized end-to-end distance r/a of the coil-rod structure with fixed $\zeta = 5$ and Kuhn segments $n = 5$, 10, 25 in the coil.

3.4.5 Comparison between canonical and isothermal-isotension ensembles

When an applied force is prescribed in $x-$direction, the coil-rod structure can take different conformations with various end-to-end vectors $\mathbf{r}$. The exact canonical partition function has been obtained via Equations (3.25), (3.31), and (3.5). By substituting the result in (3.11) it can be shown that

$$Q(f_x, T, n+1) = Z_0 \sinh\left(\frac{f_x a}{k_B T}\right) \frac{4\pi k_B T}{f_x a} \left(\sinh\left(\frac{f_x b}{k_B T}\right) \frac{4\pi k_B T}{f_x b}\right)^n . \tag{3.39}$$

Now, by utilizing Equation (3.13), we have

$$\frac{\langle x \rangle}{a} = \mathscr{L}\left(\frac{f_x a}{k_B T}\right) + \frac{nb}{a}\mathscr{L}\left(\frac{f_x b}{k_B T}\right) = \frac{a f_x}{3 k_B T}\left[1 + \frac{n}{\zeta^2}\right] + \mathscr{O}\left(\left(\frac{f_x a}{k_B T}\right)^2\right). \tag{3.40}$$

The second step of the above equation shows the asymptotic behaviour of the function near the origin. The normalized value of $f_x a/k_B T$ is depicted versus $\langle x \rangle/a$ in

Figure 3.5 for $\zeta = 5$ and different $n = 5,\ 10,\ 15$. By increasing n the curves tend to behave more linearly, and the Gaussian characteristics of the coil-rod structure are more pronounced. Figure 3.5 also shows the results from the canonical ensemble in dashed lines, which are obtained by applying Equations (S19) and (3.8) in (3.3) and (3.4). Although one ensemble measures the average of the displacement $\langle x \rangle$ and the other measures the average of the applied force $\langle f_x \rangle$, good agreement between the two ensembles is observed. The results at small x are still distinguishable due to the presence of the rod structure mentioned in Section 3.3, but the discrepancies fade away as x increases. One feature of the f_x (or $\langle f_x \rangle$) vs. $\langle x \rangle$ (or x) is that the initial slope is always positive, which is different from the $\langle f_r \rangle$ vs. r result derived from the canonical ensemble (Figure 3.4). In fact, for canonical ensemble with prescribed displacement x, even for very small x, the coil-rod structure can still access conformations with large end-to-end distance r due to the displacements along y and z directions. Consequently, a compressive force is not required to maintain a small displacement x as opposed to the case with a small end-to-end distance r.

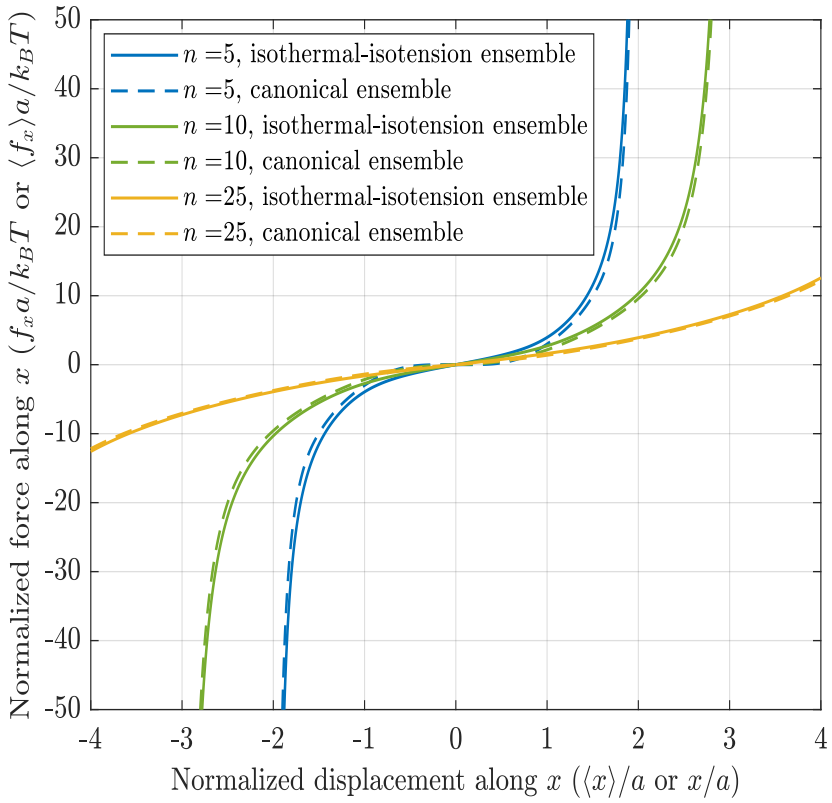

Figure 3.5: Normalized force vs. normalized displacement along x direction for $\zeta = 5$ and $n = 5,\ 10,\ 25$. For the isothermal-isotension ensemble $f_x a/k_BT$ is plotted against $\langle x\rangle/a$, while for the canonical ensemble $\langle f_x\rangle a/k_BT$ is plotted against x/a.

3.5 Coil-rod structure with zipping/unzipping mechanism

As it was alluded to, external mechanical loading may cause the unzipping of the segments contributing to the junction zones. For example, in ion-mediated biopolymers, the trapped cations are set free from the junction zones under the external loading, and the length of the associated junction zones is reduced accordingly. To incorporate the zipping/unzipping mechanism, the Boltzmann average of statistical mechanics will be used. This treatment considers each coil-rod conformation with a different rod length as an equilibrium point in the phase space. The energy of each conformation is ascertained based on the binding energy of the constituent units of

the rod. As the number of these units increases, the total energy of the coil-rod structure decreases and the structure tends to be more stable. The number of Kuhn segments in the coil is reduced during the formation of new units in the rod. If we suppose that N is the number of Kuhn segments in the completely unwound system (purely coiled structure), then the number of Kuhn segments participating in the rod is $N - n$. Without loss of generality, we define an effective unit in the rod such that it is formed from one Kuhn segment from the coil. The number of effective units in the rod is therefore $N - n$. The length of each effective unit is denoted by αb with α being the ratio between the length of one unit in the rod and the Kuhn length. Accordingly, the length of the rod a is dependent on n as below

$$a = (N - n)\alpha b. \tag{3.41}$$

We denote the energy required to liberate one effective unit from the rod by ε. Figure 3.6 illustrates the energy landscape of the rod, using the egg-box model as an example. As n increases and the effective units are released from the rod, the energy of the rod increases, reaching different equilibrium states (energy wells) separated by multiple of ε. The length αb is also shown in the rod structure.

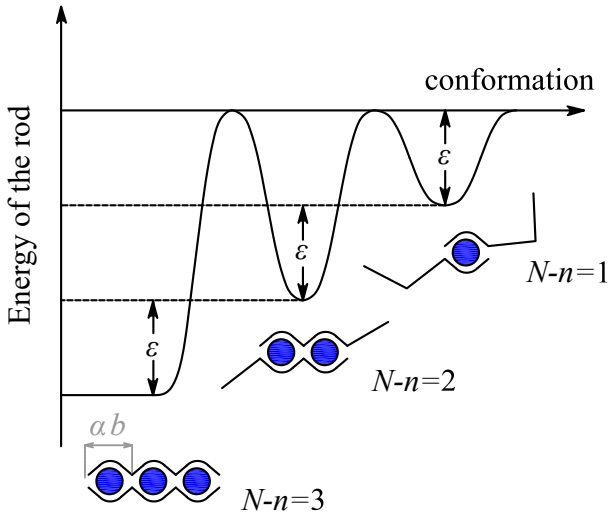

Figure 3.6: Schematics representation of the energy landscape for the rod, using egg-box model for illustration.

By applying the Boltzmann average and Equation (3.5), one can write the partition function for a coil-rod with prescribed end-to-end vector $\mathbf{r}$ but variable n,

$$\Omega(\mathbf{r},T,\varepsilon)=Z_0\exp\left[\frac{N\varepsilon}{k_BT}\right]\sum_{n=n_{\min}}^{n_{\max}}W_n^{\mathrm{CR}}(\mathbf{r})\exp\left[-\frac{n\varepsilon}{k_BT}\right], \tag{3.42}$$

where $n_{\min}$ and $n_{\max}$ are respectively the minimum and maximum allowable numbers of Kuhn segments in the coil during zipping/unzipping. This form is equivalent to the grand canonical partition function with fixed chemical potential ε. Let us rewrite Equation(3.42) as

$$\Omega(r,T,\varepsilon)=Z_0\exp\left[\frac{N\varepsilon}{k_BT}\right]\sum_{n=n_{\min}}^{n_{\max}}\exp\left\{\ln\left[W_n^{\mathrm{CR}}(r)\right]-\frac{n\varepsilon}{k_BT}\right\}, \tag{3.43}$$

where the vector $\mathbf{r}$ has been replaced by r due to the dependence of $W_n^{\mathrm{CR}}(\mathbf{r})$ through r. At fixed r, by increasing n the probability distribution $W_n^{\mathrm{CR}}(r)$ increases as a result of having more conformations. On the other hand, the energy level goes up due to the liberation of the units from the rod. These two competing effects can yield a specific value of $n_0(r)$ for which the argument of the exponential function in (3.43) is maximum. This term makes the most contribution to the sum in (3.43), and examination of the variation of n_0 with respect to r allows us to detect the occurrence of zipping/unzipping. Specifically, a flat region of n_0 vs. r indicates the tendency of the structure to have a fixed number of Kuhn segments in the coil, while a region of varying n_0 vs. r shows the tendency of the structure to update the number of Kuhn segments through zipping or unzipping processes. After the calculation of $\Omega(r,T,\varepsilon)$ in Equation (3.43), the grand canonical potential can be determined as

$$\Phi(r,T,\varepsilon)=-k_BT\ln\left[\Omega(r,T,\varepsilon)\right], \tag{3.44}$$

from which the average force is evaluated by

$$\langle f_r^{\mathrm{G}}\rangle=\frac{\partial\Phi(r,T,\varepsilon)}{\partial r}. \tag{3.45}$$

Figure 3.7a shows the normalized force $\langle f_r^{\mathrm{G}}\rangle b/k_BT$ vs. the normalized end-to-end distance r/b for $N=20$, $n_{\min}=5$, $n_{\max}=19$, $\alpha=0.8$ and $\varepsilon=0.1k_BT$. Here the large

n approximation for $W_n^{\mathrm{CR}}(\mathbf{r})$ (Equation (3.35)) has been used to ensure numerical stability. Results for fixed n at $n_{\min}$ and at $n_{\max}$ are also plotted for comparison. The inset shows the variation of n_0 with r/b. A qualitative comparison of the main plot with the inset identifies five different regimes. For $r/b \leq 2$, the structure has a fixed number of Kuhn segments, n_0 is constant and the force-extension curve converges to that of the coil-rod structure with fixed $n = 19$. For $2 \leq r/b \leq 11.7$, n_0 decreases with r/b suggesting the occurrence of zipping. The force-extension relationship starts deviating from the curve that corresponds to $n = 19$ and moving towards the curve that corresponds to $n = 5$. Meanwhile the plot exhibits negligible average force and hence stiffness. In other words, when the applied force is small, the coil-rod structure is able to achieve different end-to-end distances by varying the number of units in the rod. For $11.7 \leq r/b \leq 16.7$, n_0 is constant again, and the force-extension curve almost overlaps with the curve corresponding to fixed $n = 5$. With this maximum rod length, the structure can bear the normalized tensile force up to 17. In the regime of $16.7 \leq r/b \leq 18.4$, n_0 increases with r/b indicating the unwinding of the coil-rod structure and its transition towards $n = 19$. The unwinding alleviates the loading on the structure and a slightly decreasing trend is observed in the force-extension curve. It should be noted that some small fluctuations exist in the curve in this regime, which is not due to the numerical issues. Rather, this is caused by the discrete nature of n in the summation (3.43). In other words, each oscillation in the curve corresponds to, on average, the liberation of one unit from the rod. Finally, when $r/b \geq 18.4$, n_0 stays at 19 and the load-bearing nature of the structure is activated, with sharp increase in the normalized force at the minimum rod length.

To demonstrate the effects of binding energy, Figure 3.7b shows the results under the same condition as in Figure 3.7a except for a larger binding energy of $\varepsilon = 5k_BT$. A close examination of the main curve with the inset shows the presence of four regimes. When $r/b \leq 8.3$, n_0 decreases with r/b and zipping occurs. Unlike in Figure 3.7a, at $r/b = 0$, $n_0 = 10$ instead of $n_{\max} = 19$ and its decreasing trend starts

immediately after r/b deviates from zero. This distinct feature is caused by the larger binding energy, which drives the units to zip and form the rod. The force-extension curve is substantially different from both reference curves (corresponding to $n = 19$ and 5) in this regime. Notably, the force is compressive, this can be explained by the lengthening of the rod and shortening of the coil part which tend to generate a bulkier structure. A similar observation is made in Figure 3.4 where short coil require compressive force to achieve a small end-to-end distance. For $8.3 \leq r/b \leq 16.9$, n_0 is at $n_{\min} = 5$ and the force-extension curve also agrees with the one at maximum rod length. In addition, the force transitions from compression to tension at $r/b = 11.8$. Further extension causes unzipping in the range of $16.9 \leq r/b \leq 19.4$. Similar to Figure 3.7a, upon unzipping the force shows an overall decreasing trend, but the oscillations in the curve are much more pronounced because the liberation of one unit from the rod is associated with more substantial change in the energy. Beyond $r/b \geq 19.4$, the rod reaches its minimum length and the force on the structure increases significantly with the end-to-end distance. It is worth pointing out that in the formulation of zipping/unzipping, $(k_BT)^{-1}$ and ε always appear together as the product $\dfrac{\varepsilon}{k_BT}$. Therefore, increasing the binding energy ε is equivalent to increasing $(k_BT)^{-1}$ or decreasing the temperature. The comparison between Figure 3.7a and Figure 3.7b hence also demonstrates the change in the behaviour of the coil-rod structure caused by decreasing the temperature. Figures 3.7a and 3.7b also remove the discontinuity that appeared in the force vs. extension curve obtained by Higgs and Ball [19]. The discontinuity was caused by a number of assumptions in their partition function calculation which are avoided in the current work.

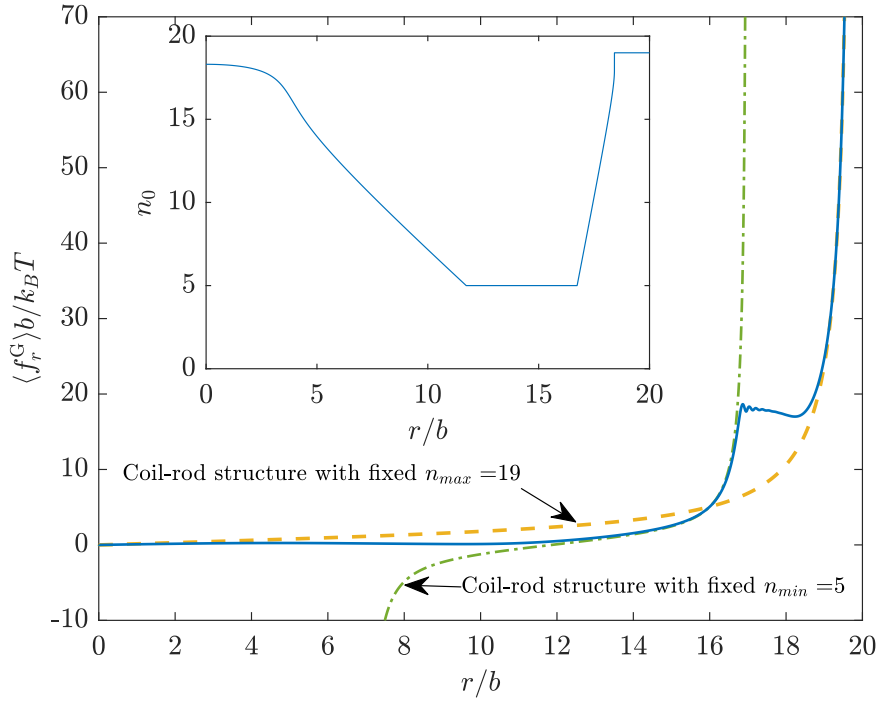

(a)

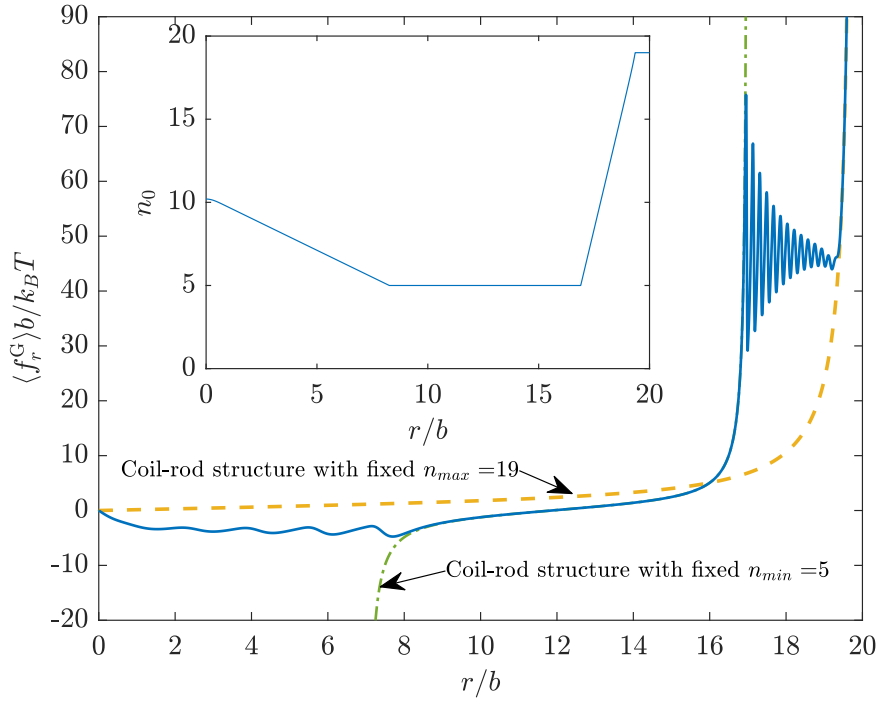

(b)

Figure 3.7: Normalized force $\langle f_r^{\mathrm{G}} \rangle b/k_BT$ vs. normalized end-to-end displacement r/b of the coil-rod structure for $\varepsilon/k_BT = 0.1$ in (a) and 5 in (b). The insets show the associated value of n_0 against r/b. The results are produced with $N = 20$, $n_{\max} = 19$, $n_{\min} = 5$, and $\alpha = 0.8$.

3.6 Demonstration of model application

3.6.1 Implementation in eight-chain model

In this section, the force-extension relationship developed in this work is implemented into the macroscopic eight-chain model of Arruda and Boyce [31] to predict the mechanical response of a network containing coil-rod structures. Following the idea of Arruda and Boyce [31], eight coil-rod structures are placed in a cube such that for each structure, one of its ends is fixed at the center while the other is tethered at a corner of the cube. The Helmholtz free energy per unit reference volume can be written in terms of the end-to-end distance of the chain r in the current configuration

$$\Psi = \sum_{i=1}^{\varrho} \psi_i(r), \tag{3.46}$$

where ϱ refers to the number of chains per unit reference volume. ψ_i is the energy stored in the ith chain

$$\psi_i(r) = \int_{r_0}^{r} \langle f_r \rangle \, \mathrm{d}r, \tag{3.47}$$

where r_0 is the end-to-end distance of the chain in the reference configuration. If the cube edges are parallel to the principal stretches λ_1, λ_2, and λ_3, it can be shown that the stretch of each chain in the current configuration λ_{chain} is given as [31]:

$$\lambda_{\text{chain}} = \frac{r}{r_0} = \frac{1}{\sqrt{3}} \left(\lambda_1^2 + \lambda_2^2 + \lambda_3^2\right)^{1/2}. \tag{3.48}$$

Differentiating (3.46) while assuming all chains to be identical and imposing incompressibility $\lambda_1\lambda_2\lambda_3 = 1$, the principal Cauchy stresses (σ_i, $i = 1, 2, 3$) can be obtained

$$\sigma_i = \lambda_i \frac{\mathrm{d}\Psi}{\mathrm{d}\lambda_i} - p_0 = \frac{\varrho r_0 \lambda_i^2}{\sqrt{3}\left(\lambda_1^2 + \lambda_2^2 + \lambda_3^2\right)^{1/2}} \langle f_r \rangle \Big|_{r_0 \lambda_{\text{chain}}} - p_0, \tag{3.49}$$

where p_0 is the unknown pressure to be determined from the boundary conditions. Clearly, the stress-stretch relations directly depend on the force-extension behaviour of the constituent chains, i.e., $\langle f_r \rangle$-r . For coil-rod structures with fixed rod and coil lengths, $\langle f_r \rangle$ can be obtained via Equations (3.28), (3.32), or (3.37) for various

approximations. It should be noted that the end-to-end distance r_0 in the reference configuration is taken to be $\sqrt{n}b$ for a freely jointed chain [1], which is not applicable for the coil-rod structure. Instead, we determine r_0 from

$$r_0 = \int_0^\infty r W_n^{\mathrm{CR}}(r)\mathrm{d}r, \tag{3.50}$$

which is the average end-to-end distance of a coil-rod structure subjected to zero force. Figure 3.8 shows the normalized principal stress σ_1/G ($G = \varrho k_B T$) vs. the principal stretch λ_1 for three different loading conditions: biaxial (with equal stretches in directions 1 and 2), uniaxial (stretch in direction 1) and pure shear (in the 1-2 plane). $\langle f_r \rangle$-r relation in Equation (3.37) is used for $n = 25$ and different $\zeta = 0$, 5, 25. $\zeta = 0$ corresponds to the case where the rod is absent and the coil-rod structure reduces to a freely jointed chain. For any given loading condition, as the length of the rod increases, the network becomes stiffer and the difference can be significant. For instance, by introducing a rod with the length equal to 5 Kuhn segments, σ_1 is doubled at $\lambda_1 = 3$ for uniaxial tension and pure shear, and more than doubled for biaxial loading. This signifies the importance of considering the rod element in macroscopic modeling of biopolymer gel networks.

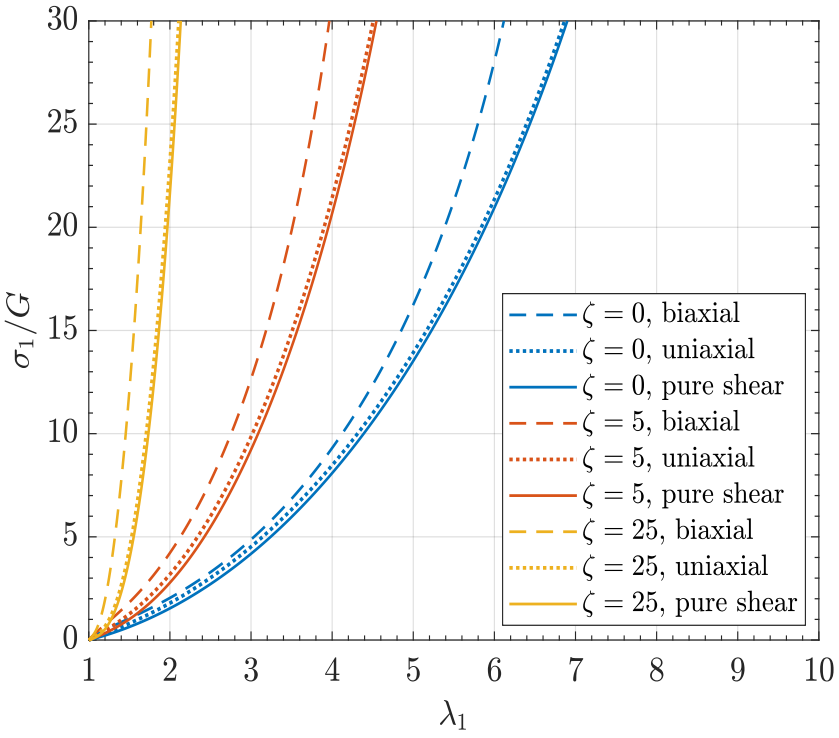

Figure 3.8: Normalized Cauchy stress σ_1/G vs. the principal stretch λ_1 for biaxial, uniaxial and pure shear loadings of a biopolymer gel network modeled by implementing Equation (3.37) into the eight-chain model of Arruda and Boyce [31]. The coil has a fixed number of Kuhn segments $n = 25$, while different rod lengths are considered, $\zeta = 0$, 5, 25.

3.6.2 Prediction of DNA unwinding

In this section, we test the validity of the proposed zipping/unzipping mechanism against existing experimental data. For this purpose, the experiments performed by Clausen-Schaumann *et al.* [32] are considered, which involve the unwinding of a double-stranded DNA. The exploration of DNA unwinding is crucial as it occurs extensively in biological processes, including replication, transcription and DNA-protein interaction [33]. Clausen-Schaumann *et al.* [32] reported the stretching of a 1.5 μm-long segment of double-stranded λ-BstE II digest DNA at $T = 20°$C using atomic force microscopy (AFM). They observed that after a highly cooperative mechanism,

a conformational transition occurred at force 65 pN. At this point, the DNA double helix started to shrink, and only one of the two strands remained attached to the AFM tip and to the substrate. Below we show that the current model is capable of capturing the unwinding process and the conversion of the double-stranded DNA to single-stranded ones. Here, the double-stranded DNA is modelled as the rigid rod, while the single-stranded DNA is treated as a freely jointed coil structure. Under applied loading, the double-stranded DNA unwinds completely so that $N = n_{\max}$, and the number of unknown parameters in the model reduces to $n_{\min}$, $n_{\max}$, b, α and ε. Figure 3.9 shows the original experimental data and the model prediction using the following parameter values:

$$n_{\min} = 600, \quad n_{\max} = 12000, \qquad b = 3\,\text{Å}, \quad \alpha = 0.46, \quad \varepsilon = 0.1\,k_B T. \tag{3.51}$$

Due to the large values of $n \in [n_{\min}, n_{\max}]$ and exponential decay in (3.43), it is sufficient to approximate the sum in (3.43) by considering only the term n_0 with maximum contribution. Good agreement is found between the model and experiments. In particular, the model suggests four regimes: $0 \leq r \leq 1.56\,\mu$m at which the system demonstrates negligible stiffness, $1.56\,\mu\text{m} \leq r \leq 1.71\,\mu$m where the system can endure limited tensile force up to 65 pN with fixed $n = 600$, $1.71\,\mu\text{m} \leq r \leq 2.71\,\mu$m where the double helix unwinds and the force plateus, and $r \geq 2.71\,\mu$m where the force-bearing mechanism is reactivated at fixed $n = 12000$. It is of interest to note that the binding energy per unit length is given by $\varepsilon/\alpha b \approx 0.04\,\text{kcal mol}^{-1}\,\text{Å}^{-1}$. Taking the binding energy of a base pair to be $2k_BT$ [33] and considering the base pair step length as 36 Å [34], the binding energy per unit length for the DNA is estimated to be $0.03\,\text{kcal mol}^{-1}\,\text{Å}^{-1}$. In Clausen-Schaumann *et al.* [32], the data corresponding to single-stranded DNA were fitted using a modified freely-jointed chain model [35] with stretchable Kuhn segments of length 15 Å. Admittedly, the Kuhn length for the coil used in the present work is smaller, but considering the correct order of magnitude and the simplicity of our model, the parameters in (3.51) are deemed physically

reasonable. The model is therefore able to capture the entire force-extension curve of the DNA which underwent conformation transition through unwinding of the double helix. It should be pointed out that in Figure 3.9 the negative force in the experimental data near zero extension originates from the contact between the substrate and the AFM tip [36], not from the elasticity of the DNA chain. This part of the data is therefore not considered when comparison is made with the model. Also, while the stiffness of the AFM tip can play a significant role in the measurement [37, 38], its stiffness is likely large enough to allow the end-to-end distance to be prescribed (Equation (3.42)) when empolying the grand canonical ensemble [39].

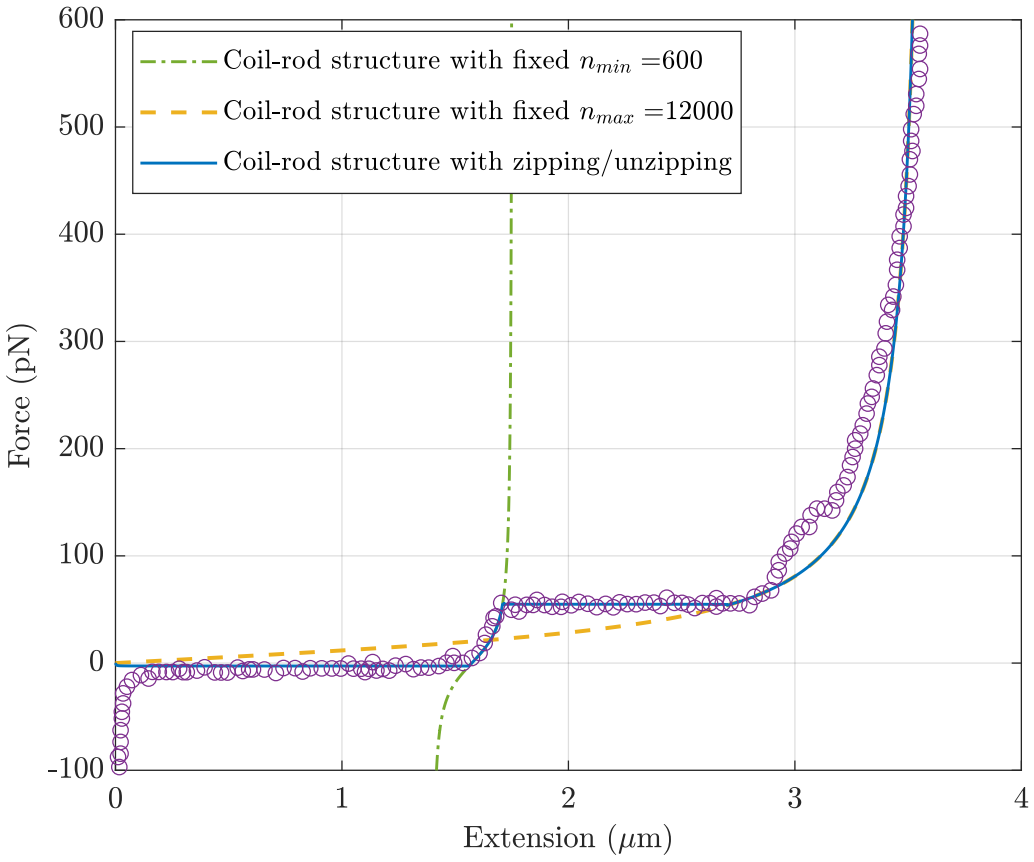

Figure 3.9: Force-extension curve of the double-stranded DNA in Clausen-Schaumann *et al.* [32] (purple points). The solid curve is the prediction from the current model with the parameters in (3.51). The dashed lines represent results with fixed n at $n_{\min} = 600$ and $n_{\max} = 12000$.

Some discussions are warranted on the modeling of unwinding/unfolding of biomacromolecules. It is acknowledged that there are other works that study the unwinding of double-stranded DNA via more elaborated description of intramolecular interactions. For example, in the model of denaturation by Theodorakopoulos *et al.* [40], the interaction between a base pair is modelled via the Morse potential [41] and the DNA unzipping is explained through the formation of domain walls in the one-dimensional lattice model. In comparison, in the present work the strength of interaction between the two DNA strands is represented by a single quantity, namely the binding energy ε. Despite the simplicity, it is encouraging to see that the model is capable of predicting the DNA unzipping phenomenon with physically reasonable parameter values. Although absent in Figure 3.9, Figure 3.7 shows the potential existence of sawtooth-like behaviour in the force-extension curve caused by unzipping. This type of phenomenon has been reported in the unfolding of proteins such as titin [42]. A number of attempts have been made to model this phenomenon by considering folded and unfolded domains of a polymer structure. For example, Qi *et al.* [43] investigated the effect of folded domains on the mechanics of biomacromolecules and their networks. The molecule is represented by a freely jointed chain or a worm-like chain while the Eyring model is used to capture the kinetics of unfolding. The model is able to achieve good fitting with the experimental data on the stretching of spectrin which exhibit sawtooth patterns. Based on the extensible freely jointed chain model [44], Manca *et al.* [39] represented a polymer chain by connected domains each having a potential energy with two local minima. These two minima corresponds to two stable equilibrium states, one folded and the other unfolded. Monte-Carlo simulations using this model show sawtooth behaviour in the force-extension curves. Inspired by this work, Cannizzo *et al.* [45] analyzed a discrete chain containing bistable units using three different models (Ising scheme, zipper model, and the stationary phase approximation) and studied the temperature effect on the force-extension response. De Tommasi *et al.* [46] proposed a microstructure-based continuum model for the

mechanics of spider silks, based on the original idea of De Tommasi *et al.* [47]. The material is assumed to consists of hard (folded) and soft (unfolded) domains, which can transition between them. The total bearing force is taken to be the summation of the forces associated with the soft and hard domains. Via energy minimization of a two-state system, the same group [48] also proposed a model for macromolecule unfolding and demonstrated its ability to match experimental data on the stretching of titin protein. These previous studies are valuable and provides different perspectives on how unwinding/unfolding may be modeled. Compared with these works, our approach to modeling unfolding is different in that: 1) we explicitly consider the rod element and its associated probability distribution; and 2) we employ the grand-canonical ensemble to statistically sample all the conformations corresponding to different number of segments in the coil. Since all the models are capable of reproducing experimental observations (with certain fitting parameters), it is of interest to conduct more examination in the future to compare their advantages and limitations.

3.7 Conclusion

Macroscopic responses of disordered biopolymer gels to external mechanical loading originate from the interaction between constituting macromolecules inside the network. To capture the presence of junction zones in disordered biopolymer gels, a coil-rod structure can be considered as a building block which consists of a freely jointed chain and a rigid rod segment. In this study, the force-extension relations of the coil-rod structure are explored via a statistical mechanics formulation. The proposed formulation not only improves previous models in the literature but also unveils new features such as the requirement of compressive force to reach small end-to-end distance when the rod length is sufficiently large relative to the coil. When allowing the exchange between units in the rod and Kuhn segments in the coil, the model is capable of capturing zipping/unzipping in the junction zone and the associated changes in the force-extension curve. The application of the current model is not

merely limited to zipping/unzipping in the junction zones of biopolymer networks. It can also serve as a tool that provides a perspicuous explanation for the unwinding of interlocked strands, such as double helix structures. As an example of the application and based on availability of data, the coil-rod model is used to simulate the unwinding of double-stranded DNA subjected to external loading. The model is shown to be able to predict the transition of the double helical structure to single strands with satisfactory accuracy. An attempt is also made to implement the coil-rod model into the eight-chain model to predict the mechanical response of a coil-rod network under different loading conditions.

Acknowledgements

TT acknowledges financial support from the Natural Sciences and Engineering Research Council of Canada (NSERC; Grant numbers: RGPIN-2018-04281, RGPAS-2018-522655) and Canada Research Chairs Program (Grant number: TIER1 2021-00023). HM acknowledges scholarship support from Alberta Innovates.

References

[1] L. Treloar, *The Physics of Rubber Elasticity* (Oxford Classic Texts in the Physical Sciences). Oxford University Press, USA, 1975, ISBN: 9780191523304.

[2] A. H. Clark and S. B. Ross-Murphy, "The concentration dependence of biopolymer gel modulus," *British Polymer Journal*, vol. 17, no. 2, pp. 164–168, 1985. DOI: https://doi.org/10.1002/pi.4980170214. eprint: https://onlinelibrary.wiley.com/doi/pdf/10.1002/pi.4980170214.

[3] W. Wang, Y. Zhang, and W. Liu, "Bioinspired fabrication of high strength hydrogels from non-covalent interactions," *Progress in Polymer Science*, vol. 71, pp. 1–25, 2017, ISSN: 00796700. DOI: 10.1016/j.progpolymsci.2017.04.001.

[4] S. T. Moe, K. I. Draget, G. Skjåk-Bræk, and O. Simdsrød, "Temperature dependence of the elastic modulus of alginate gels," *Carbohydrate Polymers*, vol. 19, no. 4, pp. 279–284, 1992, ISSN: 0144-8617. DOI: https://doi.org/10.1016/0144-8617(92)90081-Z.

[5] M. Moresi and M. Bruno, "Characterisation of alginate gels using quasi-static and dynamic methods," *Journal of Food Engineering*, vol. 82, no. 3, pp. 298–309, 2007, ISSN: 0260-8774. DOI: https://doi.org/10.1016/j.jfoodeng.2007.02.040.

[6] A. H. Clark and S. B. Ross-Murphy, "Structural and mechanical properties of biopolymer gels," in *Biopolymers*, Berlin, Heidelberg: Springer Berlin Heidelberg, 1987, pp. 57–192, ISBN: 978-3-540-47827-0.

[7] A. Clark, "Structural and mechanical properties of biopolymer gels," in *Food Polymers, Gels and Colloids*, E. Dickinson, Ed., Woodhead Publishing, 1991, pp. 322–338, ISBN: 978-1-85573-787-7. DOI: https://doi.org/10.1533/9781845698331.322.

[8] H. McEvoy, S. Ross-Murphy, and A. Clark, "Large deformation and ultimate properties of biopolymer gels: 1. single biopolymer component systems," *Polymer*, vol. 26, no. 10, pp. 1483–1492, 1985, ISSN: 0032-3861. DOI: https://doi.org/10.1016/0032-3861(85)90081-3.

[9] J. Zhang, C. R. Daubert, and E. Allen Foegeding, "A proposed strain-hardening mechanism for alginate gels," *Journal of Food Engineering*, vol. 80, no. 1, pp. 157–165, 2007, ISSN: 0260-8774. DOI: https://doi.org/10.1016/j.jfoodeng.2006.04.057.

[10] A. H. Clark and S. B. Ross-Murphy, "Chapter 1 - biopolymer network assembly: Measurement and theory," in *Modern Biopolymer Science*, S. Kasapis, I. T. Norton, and J. B. Ubbink, Eds., San Diego: Academic Press, 2009, pp. 1–27, ISBN: 978-0-12-374195-0. DOI: https://doi.org/10.1016/B978-0-12-374195-0.00001-X.

[11] V. Magnenet, J. Schiavi-Tritz, C. Huselstein, and R. Rahouadj, "Constitutive equations for Ca2+ -alginate gels," *Journal of the Mechanical Behavior of Biomedical Materials*, vol. 5, no. 1, pp. 90–98, 2012, ISSN: 1751-6161. DOI: https://doi.org/10.1016/j.jmbbm.2011.08.009.

[12] X. Xu and S. A. Safran, "Nonlinearities of biopolymer gels increase the range of force transmission," *Phys. Rev. E*, vol. 92, p. 032 728, 3 2015. DOI: 10.1103/PhysRevE.92.032728.

[13] H. Wang and X. Xu, "Continuum elastic models for force transmission in biopolymer gels," *Soft Matter*, vol. 16, pp. 10 781–10 808, 48 2020. DOI: 10.1039/D0SM01451F.

[14] M. Doi and N. Y. Kuzuu, "Nonlinear elasticity of rodlike macromolecules in condensed state," *Journal of Polymer Science: Polymer Physics Edition*, vol. 18, no. 3, pp. 409–419, 1980. DOI: https://doi.org/10.1002/pol.1980.180180301. eprint: https://onlinelibrary.wiley.com/doi/pdf/10.1002/pol.1980.180180301.

[15] A. V. Dobrynin and J. M. Y. Carrillo, "Universality in nonlinear elasticity of biological and polymeric networks and gels," *Macromolecules*, vol. 44, no. 1, pp. 140–146, 2011, ISSN: 00249297. DOI: 10.1021/ma102154u.

[16] D. De Tommasi, G. Puglisi, and G. Saccomandi, "Multiscale mechanics of macromolecular materials with unfolding domains," *Journal of the Mechanics and Physics of Solids*, vol. 78, pp. 154–172, 2015, ISSN: 0022-5096. DOI: https://doi.org/10.1016/j.jmps.2015.02.002.

[17] K. Nishinari, S. Koide, and K. Ogino, "On the temperature dependence of elasticity of thermo-reversible gels," *Journal de Physique*, vol. 46, no. 5, pp. 793–797, 1985. DOI: 10.1051/jphys:01985004605079300.

[18] K. Nishinari, "Rheological and related studies on industrially important polysaccharides and proteins," *Journal of Central South University of Technology*, vol. 14, no. 1, pp. 498–504, 2007.

[19] P. G. Higgs and R. C. Ball, "Some ideas concerning the elasticity of biopolymer networks," *Macromolecules*, vol. 22, no. 5, pp. 2432–2437, 1989. DOI: 10.1021/ma00195a073. eprint: https://doi.org/10.1021/ma00195a073.

[20] P. Flory, *Statistical Mechanics of Chain Molecules*. Interscience Publishers, 1969.

[21] T. Hill, *An Introduction to Statistical Thermodynamics* (Addison-Wesley series in chemistry). Dover Publications, 1986, ISBN: 9780486652429.

[22] J. T. Titantah, C. Pierleoni, and J.-P. Ryckaert, "Different statistical mechanical ensembles for a stretched polymer," *Phys. Rev. E*, vol. 60, pp. 7010–7021, 6 1999. DOI: 10.1103/PhysRevE.60.7010.

[23] R. G. Winkler, "Equivalence of statistical ensembles in stretching single flexible polymers," *Soft Matter*, vol. 6, pp. 6183–6191, 24 2010. DOI: 10.1039/C0SM00488J.

[24] S. Giordano, "Helmholtz and Gibbs ensembles, thermodynamic limit and bistability in polymer lattice models," *Continuum Mechanics and Thermodynamics*, vol. 30, no. 3, pp. 459–483, 2018, ISSN: 09351175. DOI: 10.1007/s00161-017-0615-5.

[25] J. M. Y. Carrillo, F. C. MacKintosh, and A. V. Dobrynin, "Nonlinear elasticity: From single chain to networks and gels," *Macromolecules*, vol. 46, no. 9, pp. 3679–3692, 2013, ISSN: 00249297. DOI: 10.1021/ma400478f.

[26] J. F. Marko and E. D. Siggia, "Stretching dna," *Macromolecules*, vol. 28, no. 26, pp. 8759–8770, 1995. DOI: 10.1021/ma00130a008. eprint: https://doi.org/10.1021/ma00130a008.

[27] A. Buhot and A. Halperin, "Extension behavior of helicogenic polypeptides," *Macromolecules*, vol. 35, no. 8, pp. 3238–3252, 2002, ISSN: 00249297. DOI: 10.1021/ma011631w.

[28] J. H. Weiner, "Use of s = k log p for stretched polymers," *Macromolecules*, vol. 15, no. 2, pp. 542–544, 1982. DOI: 10.1021/ma00230a064. eprint: https://doi.org/10.1021/ma00230a064.

[29] L. R. G. Treloar, "The statistical length of long-chain molecules," *Trans. Faraday Soc.*, vol. 42, pp. 77–82, 0 1946. DOI: 10.1039/TF9464200077.

[30] H. Yamakawa, *Modern theory of polymer solutions*. Harper & Row, 1971.

[31] E. M. Arruda and M. C. Boyce, "A three-dimensional constitutive model for the large stretch behavior of rubber elastic materials," *Journal of the Mechanics and Physics of Solids*, vol. 41, no. 2, pp. 389–412, 1993, ISSN: 0022-5096. DOI: https://doi.org/10.1016/0022-5096(93)90013-6.

[32] H. Clausen-Schaumann, M. Rief, C. Tolksdorf, and H. E. Gaub, "Mechanical stability of single dna molecules," *Biophysical journal*, vol. 78, no. 4, pp. 1997–2007, 2000.

[33] K. Liebl and M. Zacharias, "Unwinding induced melting of double-stranded dna studied by free energy simulations," *The Journal of Physical Chemistry B*, vol. 121, no. 49, pp. 11 019–11 030, 2017, PMID: 29064703. DOI: 10.1021/acs.jpcb.7b07701. eprint: https://doi.org/10.1021/acs.jpcb.7b07701.

[34] C. Dong, N. Zahir, and K. Konstantopoulos, *Biomechanics in Oncology* (Advances in Experimental Medicine and Biology). Springer International Publishing, 2018, ISBN: 9783319952949.

[35] S. B. Smith, Y. Cui, and C. Bustamante, "Overstretching B-DNA: the elastic response of individual double-stranded and single-stranded DNA molecules," *Science*, vol. 271, no. 5250, pp. 795–799, 1996.

[36] W. Zhang and X. Zhang, "Single molecule mechanochemistry of macromolecules," *Progress in Polymer Science (Oxford)*, vol. 28, no. 8, pp. 1271–1295, 2003, ISSN: 00796700. DOI: 10.1016/S0079-6700(03)00046-7.

[37] G. Florio and G. Puglisi, "Unveiling the influence of device stiffness in single macromolecule unfolding," *Scientific Reports*, vol. 9, no. 1, pp. 1–11, 2019, ISSN: 20452322. DOI: 10.1038/s41598-019-41330-x.

[38] L. Bellino, G. Florio, and G. Puglisi, "The influence of device handles in single-molecule experiments," *Soft Matter*, vol. 15, no. 43, pp. 8680–8690, 2019, ISSN: 17446848. DOI: 10.1039/c9sm01376h.

[39] F. Manca, S. Giordano, P. L. Palla, F. Cleri, and L. Colombo, "Two-state theory of single-molecule stretching experiments," *Physical Review E - Statistical, Nonlinear, and Soft Matter Physics*, vol. 87, no. 3, pp. 1–6, 2013, ISSN: 15393755. DOI: 10.1103/PhysRevE.87.032705.

[40] N. Theodorakopoulos, M. Peyrard, and R. S. MacKay, "Nonlinear structures and thermodynamic instabilities in a one-dimensional lattice system," *Physical Review Letters*, vol. 93, no. 25, pp. 1–4, 2004, ISSN: 00319007. DOI: 10.1103/PhysRevLett.93.258101.

[41] M. Peyrard, "Nonlinear dynamics and statistical physics of DNA," *Nonlinearity*, vol. 17, no. 2, 2004, ISSN: 09517715. DOI: 10.1088/0951-7715/17/2/R01.

[42] M. Rief, M. Gautel, F. Oesterhelt, J. M. Fernandez, and H. E. Gaub, "Reversible unfolding of individual titin immunoglobulin domains by AFM," *Science*, vol. 276, no. 5315, pp. 1109–1112, 1997, ISSN: 00368075. DOI: 10.1126/science.276.5315.1109.

[43] H. J. Qi, C. Ortiz, and M. C. Boyce, "Mechanics of biomacromolecular networks containing folded domains," *Journal of Engineering Materials and Technology*, vol. 128, no. 4, pp. 509–518, 2006, ISSN: 00944289. DOI: 10.1115/1.2345442.

[44] F. Manca, S. Giordano, P. L. Palla, R. Zucca, F. Cleri, and L. Colombo, "Elasticity of flexible and semiflexible polymers with extensible bonds in the Gibbs and Helmholtz ensembles," *Journal of Chemical Physics*, vol. 136, no. 15, p. 154 906, 2012, ISSN: 00219606. DOI: 10.1063/1.4801656.

[45] A. Cannizzo, L. Bellino, G. Florio, G. Puglisi, and S. Giordano, "Thermal control of nucleation and propagation transition stresses in discrete lattices with non-local interactions and non-convex energy," *European Physical Journal Plus*, vol. 137, no. 5, 2022, ISSN: 21905444. DOI: 10.1140/epjp/s13360-022-02790-9.

[46] D. De Tommasi, G. Puglisi, and G. Saccomandi, "Damage, self-healing, and hysteresis in spider silks," *Biophysical Journal*, vol. 98, no. 9, pp. 1941–1948, 2010, ISSN: 15420086. DOI: 10.1016/j.bpj.2010.01.021.

[47] D. De Tommasi, G. Puglisi, and G. Saccomandi, "Localized versus diffuse damage in amorphous materials," *Physical Review Letters*, vol. 100, no. 8, pp. 1–4, 2008, ISSN: 00319007. DOI: 10.1103/PhysRevLett.100.085502.

[48] D. De Tommasi, N. Millardi, G. Puglisi, and G. Saccomandi, "An energetic model for macromolecules unfolding in stretching experiments," *Journal of the Royal Society Interface*, vol. 10, no. 88, 2013, ISSN: 17425662. DOI: 10.1098/rsif.2013.0651.

Chapter 4

A Multiscale Mechanics Model for Disordered Biopolymer Gels Containing Junction Zones with Variable Length

A version of this chapter has been published. Reprinted with permission from Moosavian, H., and Tang, T. "A Multiscale Mechanics Model for Disordered Biopolymer Gels Containing Junction Zones with Variable Length," *Journal of the Mechanics and Physics of Solids* 192 (2023): 105792. https://doi.org/10.1016/j.jmps.2024.105792

4.1 Introduction

Biopolymer gels have found ubiquitous applications in various aspects of our daily life, including the food industry, biomedicine, and tissue engineering, owing to their abundance, cost-effectiveness, biocompatibility, and biodegradability [1–3]. For instance, polysaccharides gels can emulate extracellular scaffolds, making them suitable candidates for *in vivo* tissue replacement, as seen in applications like artificial cartilage [4]. Recently, there has been a growing interest in applying biopolymer gels as an interpenetrating network with other networks to tailor advanced hydrogels with su-

perior properties such as extra toughness, strength, or self-healing capabilities [5–8]. To enable effective strategies for designing and fabricating hydrogels with the aforementioned properties, it is essential to develop mathematical models predicting the mechanical behavior of biopolymer gels under external loading.

Among biopolymer gels, of particular interest is disordered biopolymer gels where the network consists of disordered domains of unassociated polymer chains as well as quasi-crystalline junction zones formed from chain association in the presence of an electrolyte or a change in temperature. Depending on the type of biopolymers, these junction zones may take on different forms, examples including double helices in agar, triple helices in gelatin, and cation-bridged chains in alginate gels [9]. Compared to the significant advancement in multiscale modeling for rubber-like materials with chemical cross-links, the modeling of biopolymer gels with junction zones is still in its infancy. The mechanical properties of biopolymer gels are affected by many factors such as the chain's sequence, polydispersity, and the type of ions involved [10, 11]. Even the statistical mechanics of two polymer chains sharing a junction zone has been shown to be quite involved [12]. Understanding the network with junction zones is more complex since the number of junction zones and their positions fluctuate with time [13]. More importantly, under mechanical loading, the size of the junction zones can undergo substantial changes, referred to as unzipping (shortening or shrinkage of a junction zone) or zipping (lengthening or expansion of a junction zone), which plays a crucial role in the overall response of the gel network [14]. Nishinari *et al.* [15] pioneered the statistical mechanics analysis of disordered biopolymer gels. In their work, the unassociated polymer chains (coils) in the disordered regions were represented by the freely-jointed chain model but the number of Kuhn segments in each coil was permitted to alter to account for zipping/unzipping. A partition function was introduced by averaging possible configurations of coils with different numbers of Kuhn segments. Inspired by this work, Higgs and Ball [16] attempted to model the junction zones in addition to the coils. They proposed a structure where a coil

is attached to a rigid rod representing the junction zone, albeit with a fixed length. Chapter 3 extended the analysis of the coil-rod structure, allowing changes in the rod length to capture zipping/unzipping.

Compared with the above chain-level studies and other modeling work on zipping/unzipping of individual chains such as unwinding of DNA helices [17, 18], the literature on zipping/unzipping inside a network is more limited. Kutter and Terentjev [19] and Courty *et al.* [20] calculated the content of helical junction zones in a network when subjected to external strain. The model by Nishinari *et al.* [15], allowing the Kuhn segments in the coils to change but without explicit consideration of junction zones, was applied to a network and shown to capture the temperature-dependence of the elastic modulus. Zhang *et al.* [21] proposed a stress-stretch relation that considers the contributions from unassociated coils and the junction zones. While their model captured strain hardening observed during the torsion and compression of alginate gels, the coil and the junction zone do not interact, hence the lack of exchange between them via zipping/unzipping. Studies such as Magnenet *et al.* [22] have merely focused on the chemical and mechanical properties of junction zones of alginate gels and their effects on the constitutive equations through irreversible thermodynamics. Chapter 3 demonstrated the application of the micromechanical coil-rod model in a network by implementing it into the eight-chain model [23], but with a fixed rod length. Accordingly, there is a lack of multiscale formulation that links zipping/unzipping at the chain scale to mechanical responses observed for the network at macroscopic scale.

In fact, some intriguing phenomena observed experimentally were hypothesized to be related to zipping/unzipping. For instance, after one complete cycle of loading and unloading, a gel sample can be left with a "permanent set" – a new stress-free configuration with an isotropic volume change compared with the sample before the loading [5, 22, 24, 25]. This suggests the occurrence of some irreversible processes potentially caused by zipping/unzipping of the junction zones. Can we establish

a multiscale framework that integrates force-extension relationship of the building blocks (i.e., coil-rod structures) of disordered biopolymer gels, the variable junction zones due to zipping/unzipping, and the collective contribution of the building blocks to the network? And can this framework provide rational explanations to the experimental observations? This study aims at addressing these questions and by doing so, we contribute novel insights into the behavior of disordered biopolymer gels under mechanical loading, which is crucial for advancements in their design and engineering.

The rest of the context is organized as follows. Section 4.2 outlines the statistical mechanics of coil-rod structure and associated zipping/unzipping behavior. The micromechanics model is integrated with the well-known eight-chain model [23] in Section 4.3, but with a critical examination on the end-to-end distance of the coil-rod structure in a stress-free network. This end-to-end distance depends on the length of the rod, and must be determined from a model that accounts for finite compressibility. In Section 4.4, the effect of solvent introduction during the gelation process is included. Finally, the proposed model is compared with experimental data on an alginate gel in Section 4.5, followed by a discussion on the limitations of the model and its prospects for future enhancements.

4.2 Micromechanics of coil-rod structure

The formulation of a single coil-rod structure has been previously established within the framework of statistical mechanics in Chapter 3. Herein, those results necessary for constructing the multiscale model are briefly summarized.

Consider an ideal coil-rod structure consisting of a single rigid rod with length a, attached to a non-Gaussian freely-jointed chain with Kuhn length of b and number of Kuhn segments n. Excluded volume effect is not considered in the ideal coil-rod model such that long-range energetic interactions between the constituent segments are neglected. If one end of the coil-rod structure (hereafter interchangeably referred to as the "chain") is anchored at the origin, the probability $W_n^{\mathrm{CR}}(r)\,\mathrm{d}V$ of finding the

other end inside the volume element $\mathrm{d}V$ at a position vector $\mathbf{r}$ depends solely on the distance from the origin r. For $n > 10$, $W_n^{\mathrm{CR}}(r)$ is accurately captured in Chapter 3:

$$W_n^{\mathrm{CR}}(r) = \frac{C_n}{4\pi a r}\left\{\left[\frac{\sinh\xi_1}{\xi_1}\right]^n \exp\left[-\xi_1\left(\frac{r-a}{b}\right)\right] - \left[\frac{\sinh\xi_2}{\xi_2}\right]^n \exp\left[-\xi_2\left(\frac{r+a}{b}\right)\right]\right\}, \tag{4.1}$$

in which

$$\xi_1 = \mathscr{L}^{-1}\left[\frac{r-a}{nb}\right], \tag{4.2a}$$

$$\xi_2 = \mathscr{L}^{-1}\left[\frac{r+a}{nb}\right], \tag{4.2b}$$

and C_n is a normalization factor, as a function of n and b, and independent of the end-to-end distance r. The analytical expression for C_n is given in Appendix C.1. In Equations (4.2a) and (4.2b), $\mathscr{L}^{-1}(x)$ denotes the inverse Langevin function and $\mathscr{L}(x) = \coth x - 1/x$. The Helmholtz free energy of an individual chain in the canonical ensemble $\psi = -k_B T \ln\left[W_n^{\mathrm{CR}}(r)\right]$, where k_B and T are respectively the Boltzmann constant and the absolute temperature. Given a specified end-to-end vector $\mathbf{r}$, the magnitude of the average force applied on the chain in the direction of $\mathbf{r}$ is:

$$\langle f_r \rangle = \frac{\partial \psi(r,T,n)}{\partial r} = -k_B T \frac{\partial \ln\left[W_n^{\mathrm{CR}}(r)\right]}{\partial r}. \tag{4.3}$$

The substitution of (4.1) into (4.3) results in the following normalized form:

$$\frac{b\langle f_r\rangle}{k_B T} = \frac{b}{r} + \frac{\xi_1\left[\frac{\sinh\xi_1}{\xi_1}\right]^n \exp\left[-\xi_1\left(\frac{r-a}{b}\right)\right] - \xi_2\left[\frac{\sinh\xi_2}{\xi_2}\right]^n \exp\left[-\xi_2\left(\frac{r+a}{b}\right)\right]}{\left[\frac{\sinh\xi_1}{\xi_1}\right]^n \exp\left[-\xi_1\left(\frac{r-a}{b}\right)\right] - \left[\frac{\sinh\xi_2}{\xi_2}\right]^n \exp\left[-\xi_2\left(\frac{r+a}{b}\right)\right]}. \tag{4.4}$$

The limiting case of $a \to 0$ is attainable from Equation (4.4), and demonstrated in Appendix C.2 to be in accordance with previous findings for a coil structure without rod.

Based on the above formulation which assumes the rod length a to be constant, the shrinkage or expansion of junction zones during mechanical loading or unloading

can be captured by considering zipping/unzipping modeled in the grand canonical ensemble. In essence, the chain's overall behavior arises from a trade-off between two mechanisms: achieving lower energy with increased association of coil segments, which tends to lengthen the rod; and maximizing entropy through more liberated segments which tends to shorten the rod. If the number of Kuhn segments in the fully unwound coil is N, then for the coil-rod structure with n Kuhn segments in the coil there are $N - n$ segments in the rod. Assuming that the length of each Kuhn segment, being b in the coil, is changed to αb when confined in the rod, the length of the rod is therefore $\alpha b(N - n)$. The length αb is typically less than b as it represents the projected length of a Kuhn segment onto the rod. By performing Boltzmann averaging of different configurations, and denoting the required energy for the liberation of one Kuhn segment from the rod as ε, one can arrive at the grand canonical partition function $\Omega(r, T, \varepsilon)$ under fixed temperature, end-to-end vector and binding energy

$$\Omega(r, T, \varepsilon) \propto \sum_{n=n_{\min}}^{n_{\max}} \exp\left\{\ln\left[W_n^{\mathrm{CR}}(r)\right] - \frac{n\varepsilon}{k_B T}\right\}, \tag{4.5}$$

where $n_{\min}$ and $n_{\max}$ respectively specify the minimum and maximum allowable number of Kuhn segments in the coil. Due to the heterogeneous nature of real networks, it is unlikely to observe extreme cases where there are only coils with no rods or only rods with no coils. Therefore, the two parameters $n_{\min}$ and $n_{\max}$ are introduced to avoid such extreme situations. The average force $\langle f_r^{\mathrm{G}} \rangle$ required to maintain r is obtained as

$$\langle f_r^{\mathrm{G}} \rangle = -k_B T \frac{\partial \ln \Omega(r, T, \varepsilon)}{\partial r}, \tag{4.6}$$

where the superscript G signifies the grand canonical ensemble. It should be noted that any proportionality constant in (4.5) is immaterial in Equation (4.6), due to the differentiation with respect to r.

It is of interest to determine the term ($n = n_0$) with the maximum contribution to the sum in (4.5), as an indicator for the degree of zipping/unzipping. Applying the

condition for an extermum

$$\left.\frac{\partial W_n^{\mathrm{CR}}(r)}{\partial n}\right|_{n=n_0} = \frac{\varepsilon W_{n_0}^{\mathrm{CR}}(r)}{k_B T} \tag{4.7}$$

along with Equation (4.1) leads to

$$\frac{\varepsilon}{k_B T} = -\frac{1}{2n_0} + \frac{1}{N-n_0} + \left.\frac{\ln\left[\frac{\sinh\,\xi_1}{\xi_1}\right]\left[\frac{\sinh\xi_1}{\xi_1}\right]^n \exp\left[-\xi_1\left(\frac{r-a}{b}\right)\right] - \ln\left[\frac{\sinh\,\xi_2}{\xi_2}\right]\left[\frac{\sinh\xi_2}{\xi_2}\right]^n \exp\left[-\xi_2\left(\frac{r+a}{b}\right)\right]}{\left[\frac{\sinh\xi_1}{\xi_1}\right]^n \exp\left[-\xi_1\left(\frac{r-a}{b}\right)\right] - \left[\frac{\sinh\xi_2}{\xi_2}\right]^n \exp\left[-\xi_2\left(\frac{r+a}{b}\right)\right]}\right|_{n=n_0}. \tag{4.8}$$

Appendix C.3 provides the detailed derivation of Equation (4.8) as well as the simplification for pure coil with $a = 0$. Upon solving the aforementioned equation, n_0 is determined as a function of r, subjected to the constraint $n_{\min} \leq n_0 \leq n_{\max}$. The proposed force-extension relationships (3.2) and (4.6) can be incorporated into the macroscopic constitutive equations of the network containing coil-rod structures, as elucidated in the next section.

4.3 Implementation into a network model

Due to its simplicity and efficiency, the eight-chain model, proposed by Arruda and Boyce [23], serves as the foundation network model and is extended such that the coils in the original model are replaced by coil-rod structures (see Figure 4.1). To formulate the stress-stretch relation accurately, several considerations must be taken into account. Of particular importance is the status of the coil-rod structures when the bulk network is in its reference, typically chosen to be stress-free state. For an affine network encompassing Gaussian coil structures, the end-to-end distance of the coils in the stress-free network is taken to be $\sqrt{n}b$, which is the square-root of the mean-square end-to-end distance of a corresponding set of free chains [26]. However, this assumption was rarely justified and may not be valid for more complex models

such as non-Gaussian chains[1]. As pointed out by Cioroianu *et al.* [28], the coils with end-to-end distance of $\sqrt{n}b$ are in fact subjected to a pre-stress, which can influence the constitutive relations. Nonetheless, it is perpetuated in other works and has led many researchers to unwittingly consider this value for coils in a stress-free network. When the coils are replaced by coil-rod structures, the less flexible rod part likely will lead to an end-to-end distance that is different from $\sqrt{n}b$. It is important to determine this end-to-end distance from a rational approach, which requires the relaxation of the incompressibility constraint in the original eight-chain model. In addition, the incorporation of zipping/unzipping modifies the original eight-chain model, designed for capturing entropic elasticity, to include the consideration of binding energy in the junction zone. Finally, as zipping/unzipping occurs, the length of the rod changes, which in turn alters the end-to-end distance of the chain in a stress-free network and the stress-stretch relation. These considerations are discussed in detail in the formulations below.

[1]Herein, the term 'non-Gaussian' is tacitly used to emphasize the finite extensibility of the individual 'ideal' chains beyond the Gaussian limit, as per the terminology of Treloar [26]. It is acknowledged that non-ideal chains, such as those with excluded volume effects, can also be referred to as non-Gaussian [27]. Such considerations, however, fall outside the scope of the current study.

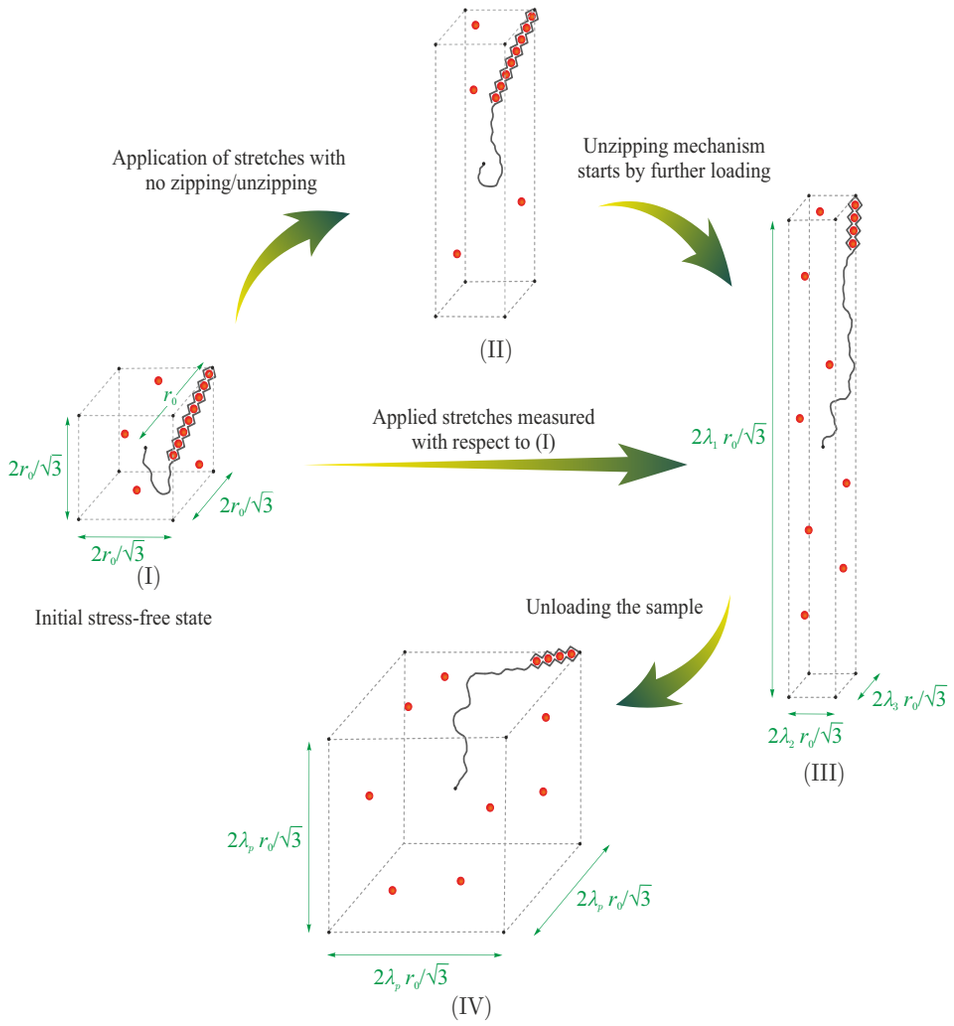

Figure 4.1: Different states of the gel containing coil-rod structures within the eight-chain network model. To prevent visual clutter, only one chain is shown inside each cube. The red spheres represent gelation agents and can associate the Kuhn segments forming a rod. During unzipping, the gelation agents are released. (I) The reference state which is also a stress-free state with n_1 Kuhn segments in the coil. The length of the cube associated with the eight-chain model is $2r_0/\sqrt{3}$ where r_0 is the end-to-end distance of the chain. (II) A deformed state in which the polymer chains are extended but the number of Kuhn segment in coils remains fixed as n_1. (III) Further deformation triggers unzipping such that the number of Kuhn segments in the coil increases to $n_3 > n_1$. The principal stretches λ_1, λ_2, and λ_3 are measured with respect to state (I). (IV) A new stress-free state with n_4 Kuhn segments in the coils. Compared to state (I), the dimensions of the cube cell is modified by a factor of λ_p.

In the current framework, it is postulated that all coil-rod structures have the same total number of Kuhn segments N, number of Kuhn segments n in the coil, Kuhn length b, and rod length a. In accordance with the original model, the sides of the cube undergo principal stretches λ_1, λ_2, and λ_3 in the deformed state. Hence, all the chains situated along the diagonals experience the same stretch λ_{chain} as:

$$\lambda_{\text{chain}} = \sqrt{\frac{\lambda_1^2 + \lambda_2^2 + \lambda_3^2}{3}}. \tag{4.9}$$

4.3.1 Identification of the stress-free state

Let r_0 denote the end-to-end distance of the constituting chains of a stress-free network. To precisely determine r_0, we begin with a formulation that allows volume change in the network [29]. This technique is not applicable to incompressible materials, where the unknown hydrostatic pressure is responsible for maintaining the reference state free of stress. Let us define the reference state with volume V_0, and all subsequent applied stretches are measured with respect to this state. The entropy of an individual coil-rod structure with an end-to-end distance r_0, where one end is fixed and the other end occupies the volume $\mathrm{d}V_0$, is given by $s_0 = c + k_B \ln\left[W_n^{\text{CR}}(r_0)\mathrm{d}V_0\right]$, c being a constant. Similarly, the entropy of this coil-rod structure with a different end-to-end distance r in the deformed state with volume V is $s = c + k_B \ln\left[W_n^{\text{CR}}(r)\mathrm{d}V\right]$. Therefore, the change of entropy of the chain from the reference state to the deformed state is written as

$$\Delta s = k_B \ln\left[\frac{W_n^{\text{CR}}(r)}{W_n^{\text{CR}}(r_0)}\right] + k_B \ln J, \tag{4.10}$$

with $J = \mathrm{d}V/\mathrm{d}V_0$ being the volume ratio.

In the eight-chain model, the macroscopic stretches are related to microscopic chain extension via

$$r = \lambda_{\text{chain}} r_0. \tag{4.11}$$

Additionally, the volume ratio on the micro-scale is linked to the principal stretches by $J = \lambda_1\lambda_2\lambda_3$. The change in entropy ΔS of the network per unit reference volume

V_0 is equal to the sum of entropy change of all constituent individual chains expressed as follows:

$$\Delta S = \varrho k_B \ln \left[\frac{W_n^{\mathrm{CR}}(\lambda_{\mathrm{chain}} r_0)}{W_n^{\mathrm{CR}}(r_0)} \right] + \varrho k_B \ln J, \tag{4.12}$$

in which ϱ denotes the number of chains per unit reference volume V_0. Hence the Helmholtz free energy of the deformed state is

$$\Psi = \Psi_0 - T\Delta S = \Psi_0 - \varrho k_B T \ln \left[\frac{W_n^{\mathrm{CR}}(\lambda_{\mathrm{chain}} r_0)}{W_n^{\mathrm{CR}}(r_0)} \right] - \varrho k_B T \ln J, \tag{4.13}$$

where Ψ_0 denotes the Helmholtz free energy in the reference state. The principal Cauchy stresses for compressible material is calculated by [30]

$$\sigma_i = \frac{\lambda_i}{J} \frac{\partial \Psi}{\partial \lambda_i}, \qquad i = 1, 2, 3, \quad \text{(no sum on } i\text{)}. \tag{4.14}$$

Based on Equation (4.13), (4.14), as well as (3.2), (4.9), and (4.11) one can conclude that

$$\sigma_i = \frac{G\lambda_i^2}{3J\lambda_{\mathrm{chain}}} \frac{r_0}{b} \frac{b\langle f_r \rangle \Big|_{r_0 \lambda_{\mathrm{chain}}}}{k_B T} - \frac{G}{J}, \qquad i = 1, 2, 3, \tag{4.15}$$

where

$$G = \varrho k_B T \tag{4.16}$$

represents a modulus of the network. The normalized form (4.4) can be directly applied in (4.15) to represent the stress components in terms of G, without k_B and T. Alternatively, the principal values of first Piola-Kirchhoff (or nominal) stress tensor are given in terms of principal stretches as follows:

$$P_i = \frac{G\lambda_i}{3\lambda_{\mathrm{chain}}} \frac{r_0}{b} \frac{b\langle f_r \rangle \Big|_{r_0 \lambda_{\mathrm{chain}}}}{k_B T} - \frac{G}{\lambda_i}, \qquad i = 1, 2, 3. \tag{4.17}$$

Evidently, the calculation of stress components necessitates knowledge of r_0. To evaluate r_0, the condition of stress-free state $\sigma_1 = \sigma_2 = \sigma_3 = 0$ when $\lambda_1 = \lambda_2 = \lambda_3 = 1$ is adopted. Hence, Equation (4.15) is simplified to

$$\frac{r_0}{b} \frac{b\langle f_r \rangle \Big|_{r_0}}{k_B T} = 3. \tag{4.18}$$

The above equation determines r_0/b for coil-rod structures in a network under zero stress, and it is a function of n and a. In the limiting case of very small rod length a, and very large number of Kuhn segments n, $\langle f_r \rangle\Big|_{r_0} = \dfrac{k_B T}{b}\mathscr{L}^{-1}\left[\dfrac{r_0}{nb}\right]$ (see Equation (C.25) in Appendix C.2). With further assumption of Gaussian behaviour $\mathscr{L}^{-1}\left[\dfrac{r_0}{nb}\right] \to \dfrac{3r_0}{nb}$ as $n \to +\infty$, one can conclude that $r_0 = \sqrt{n}b$. This result is the prevailing assumption in the majority of works in the literature for the end-to-end distance of pure coils in a stress-free eight-chain network.

According to Equation (4.18), r_0 depends on the number of Kuhn segments n in the coil. If a coil-rod structure undergoes zipping or unzipping, n changes which subsequently modifies r_0, i.e., the state of the chain in a stress-free network. Let us consider a coil-rod structure with fixed N but varying Kuhn segments n in the coil and rod length $a = \alpha b(N - n)$. Physically, the determination of r_0 prevails through two competing mechanisms. The formation of longer rod imparts greater rigidity to the structure, to the extent that in the extreme case of pure rod with no coil, the structure assumes only one conformation with a length of $Nb\alpha$. On the other hand, the presence of more segments in the coil leads to a longer structure (since $b > \alpha b$), even though the end-to-end distance can be much less than the contour length. For example, in the extreme case of no rod, for large n, $r_0 = \sqrt{n}b \ll nb$. Figures 4.2(a)-(c) illustrate the variations of r_0/b with n for different values of N and α. For $\alpha = 0.5$ (Figure 4.2(a)), at any given N an increase in n results in a decrease in r_0 due to shrinkage of the rod. However, when n is sufficiently close to N, the rod length becomes negligible, and r_0 undergoes minimal change with respect to n. In this case, the $r_0 = \sqrt{n}b$ curve (dash-dotted) serves as the minimum envelope for the sets of curves. It is also clear that at a given n (or fixed coil), larger N leads to a larger r_0 due to the longer rod. As α decreases to 0.1 (Figure 4.2(b)), the conversion from rod to coil is accompanied by significant lengthening of the chain's contour length (from $0.1b$ in the rod to b in the coil for each Kuhn segment), and the monotonic decreasing behavior observed in Figure 4.2(a) disappears. In fact, for $N \leq 60$, r_0 increases

with n, while for $N > 60$, there is a convex trend in r_0 vs. n. For instance, for $N = 100$, r_0 is the same for both $n = 0$ and $n = 100$. Consequently, in the presence of zipping/unzipping, different coil-rod configurations can have the same end-to-end distance when subjected to zero external stress. For $\alpha = 0.01$ (Figure 4.2(c)), the contribution of rod length is almost negligible. Consequently, r_0 increases with n and essentially follows $r_0 = \sqrt{n}b$.

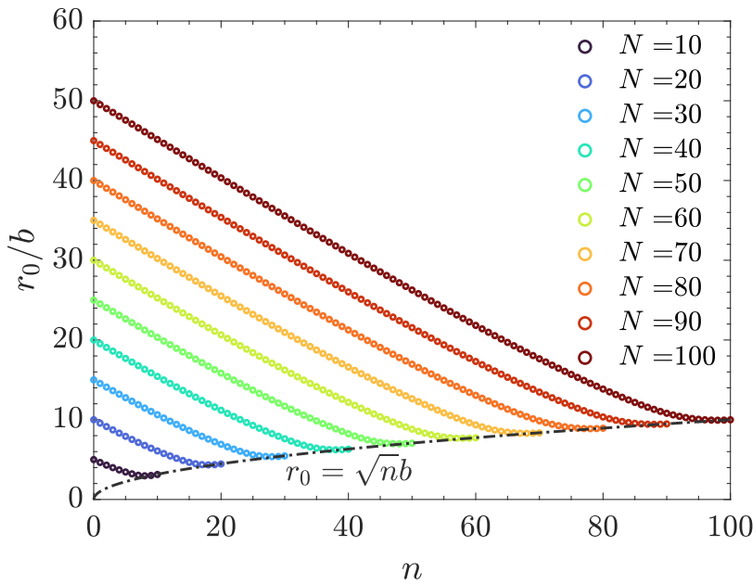

(a)

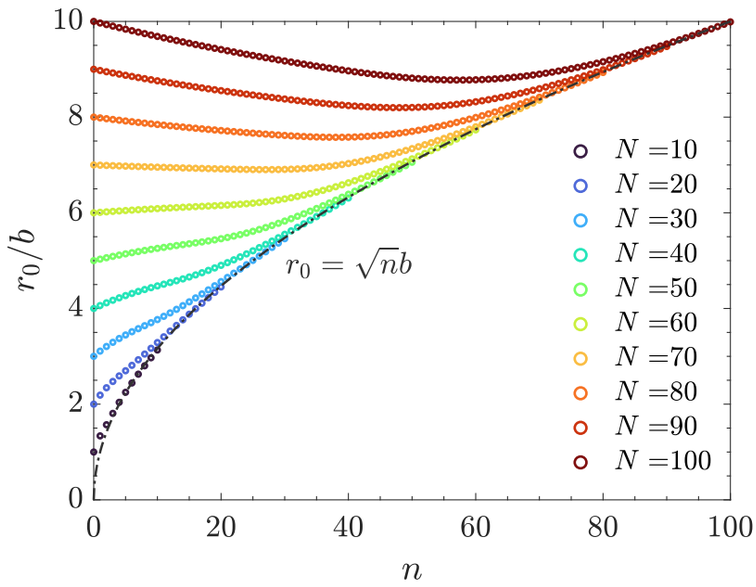

(b)

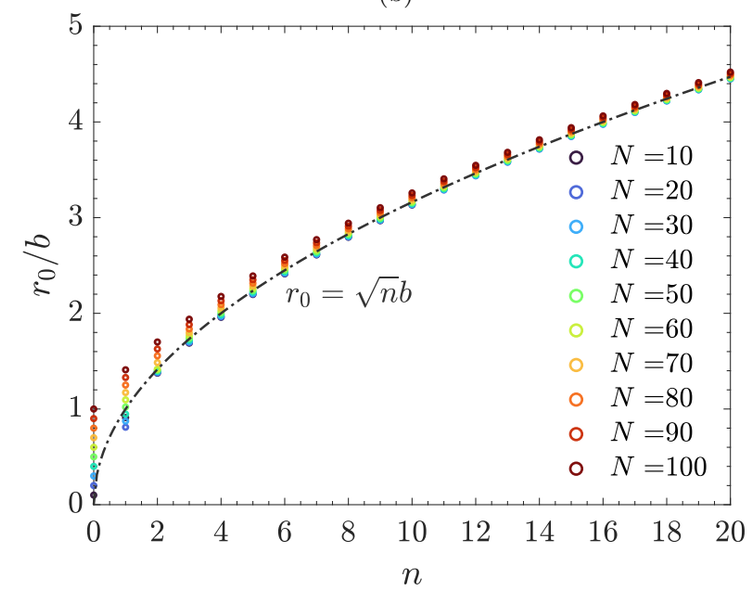

(c)

Figure 4.2: Normalized end-to-end distance r_0/b in a stress-free eight-chain network vs. n for different values of $N = 10$ to 100. $\alpha = 0.5, 0.1, 0.01$ respectively for (a), (b), and (c). Dash-dotted curve in each subfigure corresponds to $r_0 = \sqrt{n}b$.

Different r_0 associated with different n has an impact on the stress-stretch relation. To demonstrate this, Figure 4.3 shows the normalized first Piola-Kirchhoff stress, P_1/G, against the stretch λ_1 during the uniaxial tensile test along direction 1. For a given λ_1, Equation (4.17) is used in junction with the condition $P_2 = P_3 = 0$ to determine P_1, as well as λ_2 and λ_3 (equal in uniaxial tension). All curves correspond to the same N and α, but have different n and r_0. According to Figure 4.2(b), for a gel network under zero stress, the end-to-end distance of the chain is respectively $r_0 = 5.26\,b$ and $7.10\,b$ for $n = 10$ and 50. The blue curve in Figure 4.3 is generated for $n = 10$ with $r_0 = 5.26\,b$, resulting in the expected stress vanishing at $\lambda_1 = 1$. Similar behavior is observed for the dashed black curve, produced for $n = 50$ and $r_0 = 7.10\,b$. The solid black curve, however, corresponds to $n = 50$ (no rod in the chains) and $r_0 = 5.26\,b$, the stress-free state for a network containing chains with a finite rod ($n = 10$, $N - n = 40$). The inset shows that at zero stress, $\lambda_1 = 1.35$ ($= \lambda_2 = \lambda_3$), which corresponds to the stress-free state of the network with $n = 50$ measured with respect to $r_0 = 5.26\,b$. (1.35=7.10/5.26 is the ratio of r_0 between $n = 50$ and $n = 10$).

Imagine that during a uniaxial tensile test of a sample that begins with $n = 10$, unzipping occurs increasing n to 50. If at this point, the sample is unloaded but the coil-rod structure does not have time to recover (i.e., through zipping) to the original n, then one would expect that loading would follow the blue curve in Figure 4.3 upwards while unloading would follow the solid black curve downwards, since the macroscopic stretch in this test is measured with respect to the original sample. This would then lead to an isotropic deformation (relative to the original sample, 1.35 in Figure 4.3) when the stress is reduced to zero, which has been reported as a "permanent set" in the literature [31, 32]. In the next section, we present a formulation that can capture the length change in the rod during loading and unloading of the network, i.e., transition between stress-stretch curves such as the blue and solid black ones in Figure 4.3.

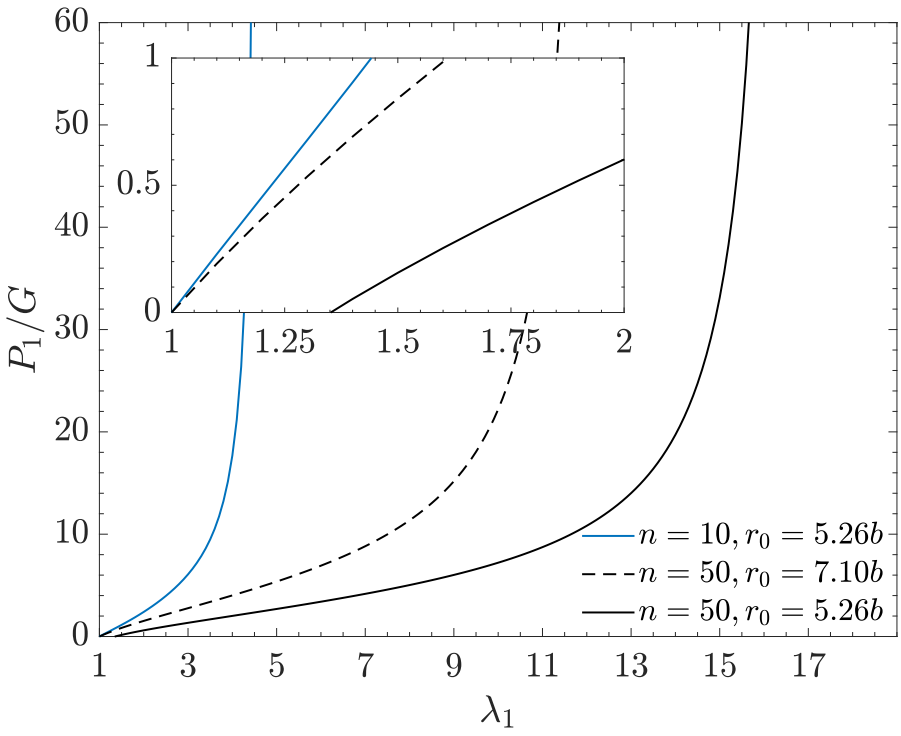

Figure 4.3: Normalized first Piola-Kirchhoff stress P_1/G vs. stretch λ_1 for uniaxial tension of a eight-chain network containing coil-rod structures, $N = 50$, $\alpha = 0.1$ while different n and r_0 are used as shown in the legend.

4.3.2 Mechanics of the network with zipping/unzipping

The stress-stretch relations (4.15) and (4.17) were formulated based upon coil-rod structures with a fixed rod length. By replacing $\langle f_r \rangle$ in these equations with $\langle f_r^{\mathrm{G}} \rangle$ from (4.6), the constitutive relation is extended to incorporate zipping/unzipping:

$$\sigma_i = \frac{G\lambda_i^2}{3J\lambda_{\mathrm{chain}}} \frac{r_0}{b} \frac{b\langle f_r^{\mathrm{G}} \rangle\Big|_{r_0\lambda_{\mathrm{chain}}}}{k_B T} - \frac{G}{J}, \qquad i = 1, 2, 3, \tag{4.19a}$$

$$P_i = \frac{G\lambda_i}{3\lambda_{\mathrm{chain}}} \frac{r_0}{b} \frac{b\langle f_r^{\mathrm{G}} \rangle\Big|_{r_0\lambda_{\mathrm{chain}}}}{k_B T} - \frac{G}{\lambda_i}, \qquad i = 1, 2, 3. \tag{4.19b}$$

From this point onward, the value of $n_{\max}$ in Equation (4.5) is taken as N unless otherwise specified.

The terminology of λ_i and r_0 will now be clarified in the presence of zipping/unzipping. As shown in Figure 4.1, suppose that there is a stress-free state (I) for the network, where the coil-rod structures in the network have n_1 Kuhn segments in the

coil and the end-to-end distance of r_0. In this case, the cube with a diagonal of $2r_0$ has an edge length of $2r_0/\sqrt{3}$. This state is considered as the reference state and all deformations are measured with respect to this one. Next, under external loading the cube is deformed from its original state to state (II) where the chains are on the threshold of unzipping. By applying further deformation, the rod part of each chain begins to shrink, while the coil part expands. This causes the number of Kuhn segments in the coil to become larger than n_1. If the principal stretches are designated by λ_i, the lengths of the cube edges are given by $2\lambda_i r_0/\sqrt{3}$, as shown in (III). The entire process of loading from (I) to (III) can be formulated by applying Equations (4.5), (4.6), (4.19), with $n_{\min} = n_1$. Next the loads are gradually removed from the sample. If the process is entirely reversible, zipping would occur and the sample would trace back from (III) to (II) and from (II) to (I) without any changes in the initial undeformed state. However, given that the rate of chain association is different from dissociation [33], removal of the external loads from state (III) results in a new stress-free state (IV) where the coil-rod structures have an end-to-end distance of $\lambda_p r_0$ rather than r_0. Here the chains have n_4 Kuhn segments in the coil and the condition of $n_1 < n_4 < n_3$ leads to partial zipping during unloading. The transition from states (III) to (IV) can be mathematically modelled by using Equations (4.5), (4.6), and (4.19), with $n_{\min} = n_4$. Since $n_3 > n_1$, as illustrated in Figure 4.2(c), if α is sufficiently small, it can be confidently asserted that $\lambda_p > 1$. Thus, state (IV) experiences an expansion λ_p with respect to state (I) and can capture the permanent set at the end of the unloading.

Figure 4.4(a) depicts the variation of the normalized first Piola-Kirchhoff stress, P_1/G in terms of the principal stretch λ_1 during a uniaxial loading-unloading cycle along direction 1. The parameters $N = 150$, $\alpha = 0.05$, $\varepsilon = 1.5\, k_B T$. The reference state (I) ($\lambda_1 = \lambda_2 = \lambda_3 = 1$) is chosen for coil-rod structures with $n_{\min} = 10$, resulting in $r_0 = 7.85\, b$. As λ_1 increases from 1, the values of P_1 and $\lambda_2 = \lambda_3$ are computed from (4.19b) such that the condition $P_2 = P_3 = 0$ holds. The blue curve exhibits

an increasing trend that precisely tracks the dashed yellow curve which corresponds to a fixed $n = 10$, until reaching $\lambda_1 = 2.25$ (state II), where unzipping is triggered. Afterwards, P_1 transitions from the dashed yellow curve towards the dash-dotted purple curve which corresponds to a fixed $n = 15$. After stretching the sample to $\lambda_1 = 4.32$ and $P_1 = 16.39\,G$ (state (III)), the load is gradually removed. At this stage the formulation (4.19b) is updated with $n_{\min} = 15$ instead of 10. Evidently, after λ_1 is reduced to below 2.82 the unloading (red) curve follows the dash-dotted purple curve with fixed $n = 15$. Complete removal of the load leads to a new stress-free state (IV) at $\lambda_1 = 1.02$ (as shown in the inset of Figure 4.4(a)).

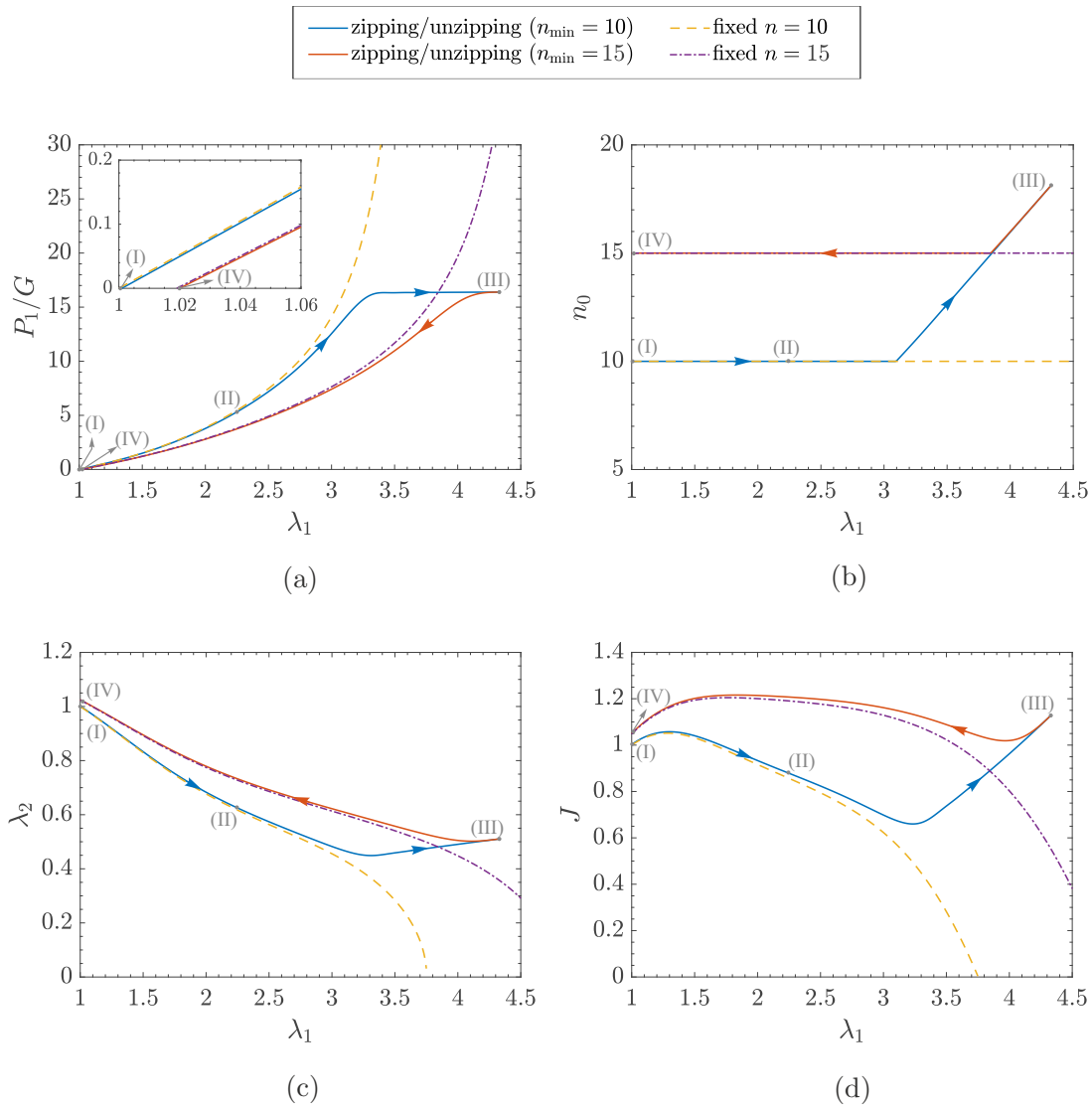

Figure 4.4: Different parameters vs. stretch λ_1 for a uniaxial loading-unloading cycle along direction 1; $N = 150$, $\alpha = 0.05$, $\varepsilon = 1.5k_BT$. Dashed yellow and dash-dotted purple curves assume fixed $n = 10$ and 15, respectively. Blue and red curves depict the presence of zipping/unzipping with $n_{\min} = 10$ and 15, respectively. (a) Normalized Piola-Kirchhoff stress P_1, (b) Number of Kuhn segments n_0 in the coil with maximum contribution to the grand canonical partition function, (c) Stretch ratio λ_2, (d) Volume ratio J.

Figure 4.4(b) illustrates the variation of n_0, as introduced in Equation (4.8), against λ_1. The horizontal line between states (I) and (II) represents the behavior with a fixed $n_0 = 10$. The increase in n_0 from 10 is initiated at $\lambda_1 = 3.09$ and continues till state (III) where $n_0 = 18$. During unloading, n_0 decreases to 15 at $\lambda_1 = 3.86$

through zipping, and subsequently remains constant until reaching state (IV). It can be observed that the initiation of unzipping at state (II) does not necessarily cause a simultaneous change in n_0. To explain this, the contribution of different n to the grand canonical partition function, in a normalized form, is illustrated in Figure 4.5 for $\lambda_1 = 2$, 3, 3.5. The curve for $\lambda_1 = 2$ shows the significant contribution of $n_0 = 10$ before state (II). The curve for $\lambda_1 = 3$ shows that shortly after state (II) while $n_0 = 10$ still contributes the most, other configurations also begin to play a more important role. This justifies why the loading curve (Figure 4.4(a)) diverges from the fixed $n = 10$ curve prior to the deviation of n_0 from 10 in Figure 4.4(b). Finally, for $\lambda_1 = 3.5$, n_0 shifts to 13, consistent with the increasing trend in Figure 4.4(b) observed for $\lambda_1 > 3.09$.

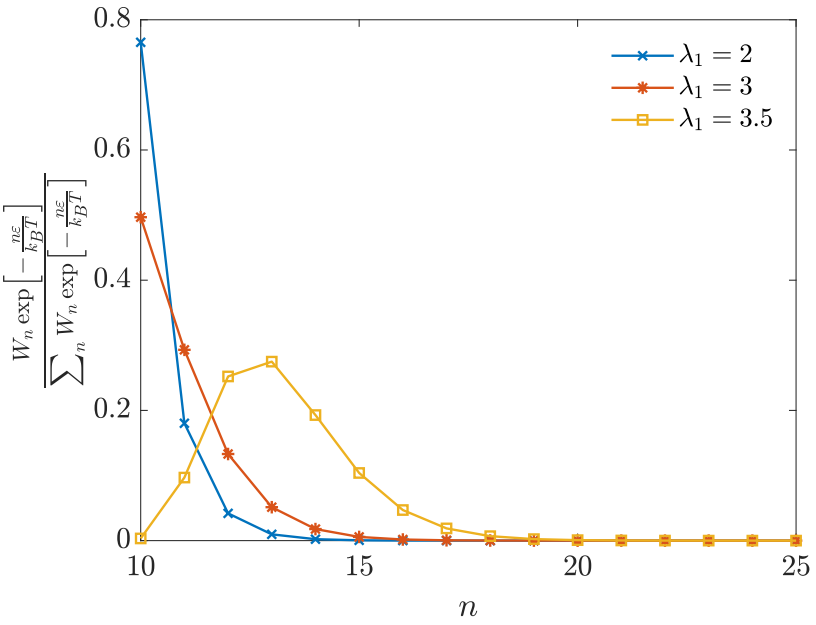

Figure 4.5: The contribution of different n to the grand canonical partition function in Equation (4.5) under the stretches of $\lambda_1 = 2$, 3, and 3.5. The terms in Equation (4.5) are normalized by the grand canonical partition function Ω. The parameters are $N = 150$, $\alpha = 0.05$, $\varepsilon = 1.5\, k_B T$, $n_{\min} = 10$.

Figure 4.4(c) illustrates the calculated principal stretch λ_2 (equal to λ_3) as a func-

tion of λ_1 by solving $P_2 = P_3 = 0$ in Equation (4.19b). λ_2 starts from 1 in state (I) and decreases to 0.62 in state (II) where $\lambda_1 = 2.25$. If unzipping is deactivated, the curve would follow the dashed yellow curve, with λ_2 ultimately approaching 0 at $\lambda_1 = 3.76$. With the activation of unzipping, further stretching from state (II) causes λ_2 to decrease to 0.42 and subsequently increase, transitioning from state (II) to state (III). During unloading, λ_2 gradually increases and converges to the result with a fixed $n = 15$, as indicated by the dash-dotted purple curve. It eventually reaches $\lambda_2 = \lambda_3 = 1.02$ at $\lambda_1 = 1.02$ in state (IV). The variation of the volume ratio J, measured with respect to state (I), is plotted against λ_1 in Figure 4.4(d). As depicted by the blue curve, the sample exhibits a slight expansion, returns to the initial volume, and subsequently contracts upon reaching state (II). Afterwards, the sample starts unzipping, and further stretching gives rise to contraction and then expansion of the sample until state (III). The changes in the volume ratio are less pronounced during unloading for larger $n_{\min}$, as shown by the red curve. In Appendix C.4, another example is given with a different set of parameters, which shows more drastic unzipping during loading, accompanied by a larger change in J.

Since biopolymer networks only exist as solvated medium, the analysis of such networks highly depends on the thermodynamics of aqueous polymer solutions, and the role of solvation forces [9]. More specifically, the introduction of diluents can lead to considerable changes in the stress-stretch curves of gels due to swelling [34, 35]. Consistent with traditional constitutive modeling of gel network in the literature, the above formulation does not explicitly consider swelling. To include the effect of swelling, a typical approach is to scale r_0 to $\lambda_v r_0$ and replace G with $G\lambda_v^{-3}$, where λ_v represents the isotropic expansion due to swelling, regardless of whether the reference state is stress-free or not [26]. Since the stress-free state is demonstrated to be crucial for the constitutive relation, below we carry out a rigorous formulation to consider swelling, which incorporates the entropy of mixing alongside the expansion due to swelling and acknowledges the delicate issue of stress-free state.

4.4 Consideration of swelling

Figure 4.6 illustrates the schematics of different states during swelling and additional deformation. The unswollen state (0), characterized by a cube with edge length $2r_0/\sqrt{3}$ contains coil-rod structures with n_1 Kuhn segments in the coil. This state is expanded isotropically by a ratio of λ_s due to the introduction of solvents, resulting in state (I). Throughout this process, it is assumed that the number of Kuhn segments in the coil remains fixed at n_1. Similar to Figure 4.1, state (II) represents the threshold of the deformed state before which no unzipping occurs. With further deformation, unzipping takes place, leading to the new configuration (III) with larger number of Kuhn segments in the coil. Since experimentally the reference state (I) serves as the basis for measuring stretches λ_1, λ_2, and λ_3, the dimensions of the deformed cell in state (III) are $2\lambda_s\lambda_i r_0/\sqrt{3}$, where $i = 1, 2, 3$. Finally, upon releasing of the load, the system reaches state (IV) where all chains are extended by $\lambda_s\lambda_p r_0$, due to the presence of some irrecoverable unzipping. The mathematical analysis of theses states is provided in the following.

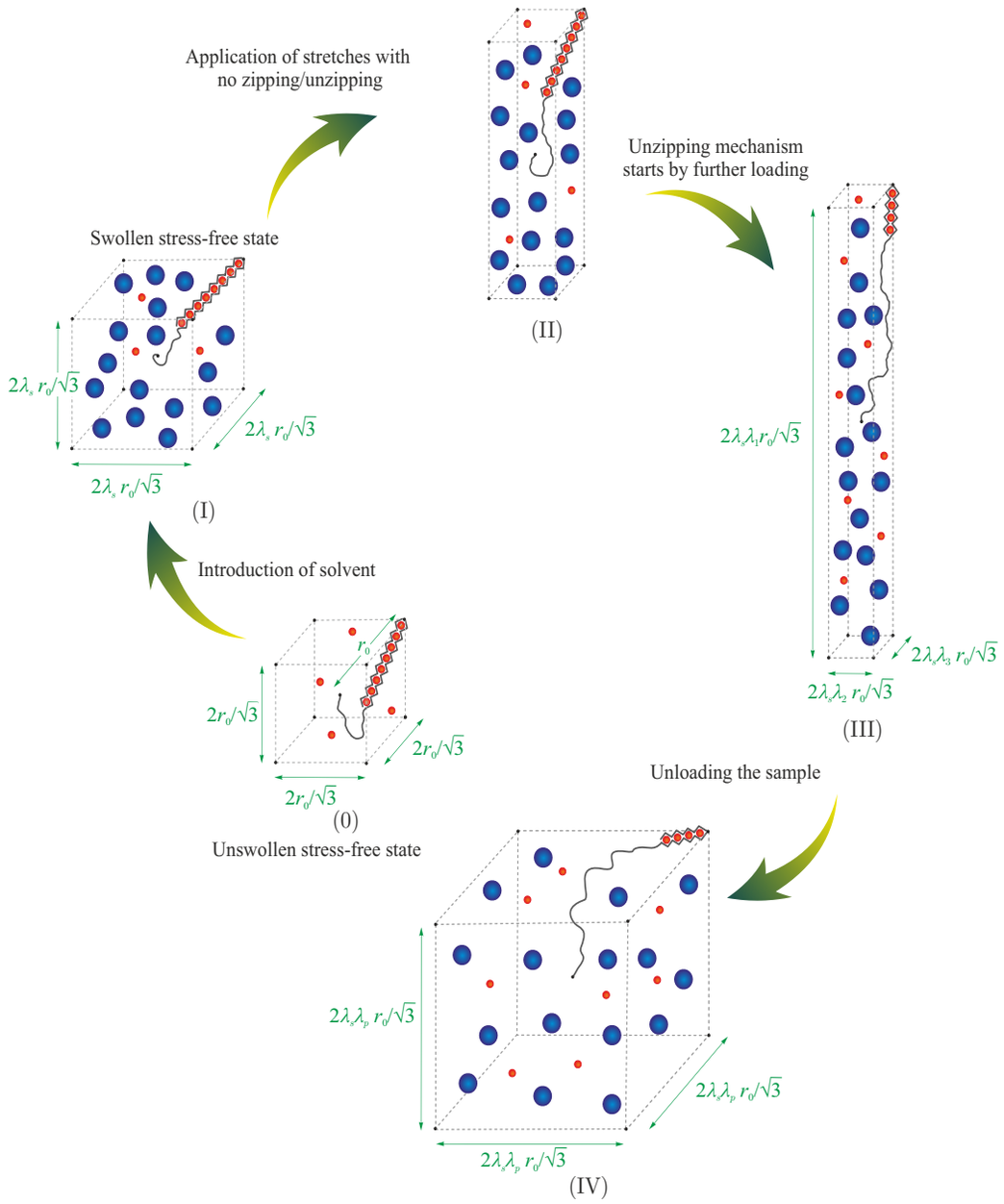

Figure 4.6: Different states of the gel containing coil-rod structure within an eight-chain network model in the presence of solvent. For visual clarity, only one chain is shown inside each cube. The red spheres represent the gelation agents and can associate the Kuhn segments forming a rod, while the large blue spheres represent the solvent molecules. (0) The unswollen state has no solvents, and the constituting coil-rod structures with n_1 Kuhn segments in the coil have an end-to-end distance of r_0 to ensure a stress-free state. (I) The swollen stress-free state in which the solvents expand the cell isotropically by stretch λ_s while maintaining the number of Kuhn segments in the coil. (II) The deformed state in which the polymer chains are further extended, but the number of Kuhn segment in coils remained fixed at n_1. (III) Further deformation triggers unzipping, changing the number of Kuhn segments in the coil to a larger value. The stretches λ_1, λ_2, and λ_3 are measured with respect to state (I). (IV) Stress-free state after complete unloading from state (III). During this process the minimum allowable number of Kuhn segments in the coil is set as $n_4 > n_1$. Compared to state (I), the dimensions of the cube are enlarged by λ_p.

Starting from the unswollen state (0) in which the end-to-end distance of the constituent chains has been calculated via Equation (4.18). Next, M solvent molecules per unit unswollen volume are added such that the sample is expanded isotropically by a stretch λ_v and converted to a swollen state. Assuming no zipping/unzipping during swelling, according to Equation (4.12), the entropy change per unit unswollen volume due to the volume expansion is given by

$$\Delta S^{\mathrm{d}} = \varrho k_B \ln \left[\frac{W_n^{\mathrm{CR}}(\lambda_v r_0)}{W_n^{\mathrm{CR}}(r_0)} \right] + \varrho k_B \, \ln \lambda_v^3, \tag{4.20}$$

where the superscript "d" represents the entropy change due to deformation. Besides ΔS^{d}, there is additional entropy change due to mixing of solvent molecules with coil-rod structures. To compute this entropy, one can apply the Flory-Huggins theory [36, 37] to the network. The fundamental concept involves assigning a specific volume to each solvent molecule, while each coil-rod structure in the unswollen state (0) occupies τ times the volume of a solvent molecule. The entropy of mixing as the sample experiences stretching by λ_v is expressed as

$$\Delta S^{\mathrm{m}} = - M k_B \ln \left[\mu \tau^{-1} \lambda_v^{-3} \right] - \varrho k_B \, \ln \left[\frac{\lambda_v^3 - \mu \tau^{-1}}{\lambda_v^3} \right], \tag{4.21}$$

where the superscript "m" denotes the entropy change due to mixing and

$$\mu = M / \varrho. \tag{4.22}$$

The total entropy change per unit unswollen volume is obtained by adding Equations (4.20) and (4.21):

$$\Delta S = \Delta S^{\mathrm{d}} + \Delta S^{\mathrm{m}} = \varrho k_B \, \ln \left[\frac{W_n^{\mathrm{CR}}\left(\lambda_v r_0\right)}{W_n^{\mathrm{CR}}\left(r_0\right)} \right] - M k_B \ln \left[\mu \tau^{-1} \lambda_v^{-3} \right] - \varrho k_B \, \ln \left[\frac{\lambda_v^3 - \mu \tau^{-1}}{\lambda_v^6} \right]. \tag{4.23}$$

The detailed derivation of Equation (4.23) is deferred to Appendix C.5. The Helmholtz free energy of the swollen state, per unit unswollen volume, for an arbitrary stretch λ_v is given by

$$\Psi = \Psi_0 + G \left\{ -\ln \left[\frac{W_n^{\mathrm{CR}}(\lambda_v r_0)}{W_n^{\mathrm{CR}}(r_0)} \right] + \ln \left[\frac{\lambda_v^3 - \mu \tau^{-1}}{\lambda_v^6} \right] + \mu \ln \left[\mu \tau^{-1} \lambda_v^{-3} \right] \right\}, \tag{4.24}$$

where Ψ_0 represents the Helmholtz free energy of state (0). By utilizing Equation (4.14) one can obtain the Cauchy stress components of the swollen state as

$$\sigma_1 = \sigma_2 = \sigma_3 = G \left\{ \frac{1}{3\lambda_v^2} \frac{r_0}{b} \frac{b\langle f_r \rangle \Big|_{r_0 \lambda_v}}{k_B T} + \frac{1}{\lambda_v^3 - \mu\tau^{-1}} - \frac{2+\mu}{\lambda_v^3} \right\}. \tag{4.25}$$

In the above relation r_0 is determined based on Equation (4.18). For sufficiently large τ (generally true for biopolymer gels), Equation (4.25) is further simplified to

$$\sigma_1 = \sigma_2 = \sigma_3 = G \left\{ \frac{1}{3\lambda_v^2} \frac{r_0}{b} \frac{b\langle f_r \rangle \Big|_{r_0 \lambda_v}}{k_B T} - \frac{1+\mu}{\lambda_v^3} \right\}. \tag{4.26}$$

Figure 4.7 shows the normalized Cauchy stress vs. λ_v for n = 10, 15, 30, and 50. The stretch λ_v for each n is measured with respect to its own r_0 as calculated from Equation (4.18). The intercept of each curve with the horizontal axis corresponds to the swollen stress-free state (I) with stretch λ_s measured with respect to the unswollen state (0) (see Figure 4.6). For instance $\lambda_s = 1.13$ if $n = 10$ and $N = 150$, $\alpha = 0.05$, $\mu = 1$. At λ_s, the tensile stress given by the first term of Equation (4.26) is counterbalanced by the compressive stress of the second term, resulting in vanishing total stress.

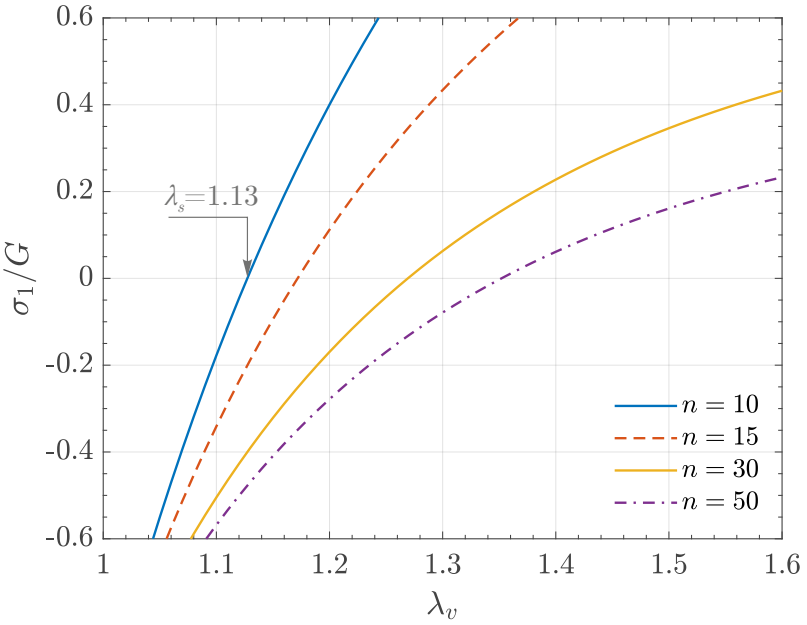

Figure 4.7: Normalized Cauchy stress σ_1/G ($\sigma_1 = \sigma_2 = \sigma_3$) vs. the stretch λ_v for $N = 150$, $\mu = 1$, $\alpha = 0.05$, and different number of Kuhn segments n in the coil. The intersection with the abscissa indicates the swollen stress-free state under the isotropic stretch of λ_s.

Once λ_s is at hand, one can study the application of additional mechanical deformation. Suppose that the swollen stress-free state (I) is subjected to principal stretches λ_1, λ_2, and λ_3 measured with respect to state (I), converting it to state (II) (see Figure 4.6). The associated entropy change per unit unswollen volume from state (0) to state (II) is given by

$$S_{\mathrm{II}} - S_0 = \varrho k_B \ln\left[\frac{W_n^{\mathrm{CR}}(\lambda_s \lambda_{\mathrm{chain}} r_0)}{W_n^{\mathrm{CR}}(r_0)}\right] - \varrho k_B \ln\left[\frac{\lambda_s^3 J - \mu\tau^{-1}}{J^2 \lambda_s^6}\right] - M k_B \ln\left[\mu\tau^{-1}\lambda_s^{-3} J^{-1}\right], \tag{4.27}$$

where the details of the derivation is provided in Appendix C.5. The Helmholtz free energy of the deformed state (II) per unit unswollen volume is therefore

$$\Psi_{\mathrm{II}} = \Psi_0 + G\left\{-\ln\left[\frac{W_n^{\mathrm{CR}}(\lambda_s \lambda_{\mathrm{chain}} r_0)}{W_n^{\mathrm{CR}}(r_0)}\right] + \ln\left[\frac{\lambda_s^3 J - \mu\tau^{-1}}{J^2 \lambda_s^6}\right] + \mu \ln\left[\mu\tau^{-1}\lambda_s^{-3} J^{-1}\right]\right\}. \tag{4.28}$$

For sufficiently large τ, applying Equation (4.14) leads to

$$\sigma_i = G\left\{\frac{\lambda_i^2}{3J\lambda_s^2\lambda_{\text{chain}}}\frac{r_0}{b}\frac{b\langle f_r\rangle\Big|_{\lambda_s\lambda_{\text{chain}}r_0}}{k_BT} - \frac{1+\mu}{J\lambda_s^3}\right\}, \quad i=1,2,3. \tag{4.29}$$

To account for unzipping in state (III), $\langle f_r\rangle$ is replaced by $\langle f_r^{\text{G}}\rangle$:

$$\sigma_i = G\left\{\frac{\lambda_i^2}{3J\lambda_s^2\lambda_{\text{chain}}}\frac{r_0}{b}\frac{b\langle f_r^{\text{G}}\rangle\Big|_{\lambda_s\lambda_{\text{chain}}r_0}}{k_BT} - \frac{1+\mu}{J\lambda_s^3}\right\}, \quad i=1,2,3, \tag{4.30}$$

which is the extension of Equation (4.19a) in the presence of swelling consideration. The above relation measures the applied force in state (III) per unit area of state (III). However, G and μ introduced respectively in (4.16) and (4.22) are parameters defined based on the unswollen state (0). For $\lambda_1 = \lambda_2 = \lambda_3 = 1$ ($J = 1$), Equation (4.30) converts to the special case of Equation (4.26) for $\lambda_v = \lambda_s$ and consequently the stress components vanish. The principal components of the first Piola-Kirchhoff stress, while allowing for zipping/unzipping, is given by

$$P_i = G\left\{\frac{\lambda_i}{3\lambda_s^2\lambda_{\text{chain}}}\frac{r_0}{b}\frac{b\langle f_r^{\text{G}}\rangle\Big|_{\lambda_s\lambda_{\text{chain}}r_0}}{k_BT} - \frac{1+\mu}{\lambda_s^3\lambda_i}\right\}, \quad i=1,2,3, \tag{4.31}$$

which measures the applied force in state (III) per unit area of the swollen stress-free state (I). In Appendix C.6, the second law of thermodynamics is examined with the above constitutive relation by decomposing the deformation gradient into its elastic and plastic components. It is shown that the second law of thermodynamics is satisfied by the multiscale framework presented here.

Figure 4.8(a) depicts the normalized first Piola-Kirchhoff stress P_1/G against the principal stretch λ_1 of the swollen network during a uniaxial loading-unloading test for $\mu = 1$, where N, α, and ε are set to the same values as those in Figure 4.4. For this case, the parameter $r_0 = 7.85\,b$ has been previously computed for the unswollen state, and $\lambda_s = 1.13$ has been determined from Figure 4.7. Two solid curves, blue and red, utilize Equation (4.31), in which $\langle f_r^{\text{G}}\rangle$ is computed for $n_{\min} = 10$ and 15, respectively.

The dashed yellow curve and the dash-dotted purple curve are obtained from the same equation but using $\langle f_r \rangle$ rather than $\langle f_r^{\mathrm{G}} \rangle$ with fixed $n = 10$ and 15, respectively. For clarification, different states (I) to (IV) explained in Figure 4.6 are also marked in Figure 4.8. The stress component P_1 has a similar behavior to Figure 4.4(a), but the threshold for unzipping is reduced from $P_1 = 5.47\,G$ at $\lambda_1 = 2.25$ to $P_1 = 5.11\,G$ at $\lambda_1 = 2.09$ for state (II). This reduction for triggering unzipping can be justified due to the presence of pre-stretch λ_s in the swollen state (I). The sample undergoes further extension up to $\lambda_1 = 3.82$ in state (III). After unloading from (III) to (IV), the permanent set of state (IV) is $\lambda_p = 1.06$ (as shown in the inset), larger than 1.02 observed in the inset of Figure 4.4(a). Figures 4.8(b), (c), and (d) respectively demonstrate n_0, λ_2 (or λ_3), and volume ratio J vs. λ_1 for the same uniaxial loading-unloading test. Although all states (I) to (IV) have changed due to swelling, the qualitative behavior is similar to their counterparts in Figure 4.4(b)-(d).

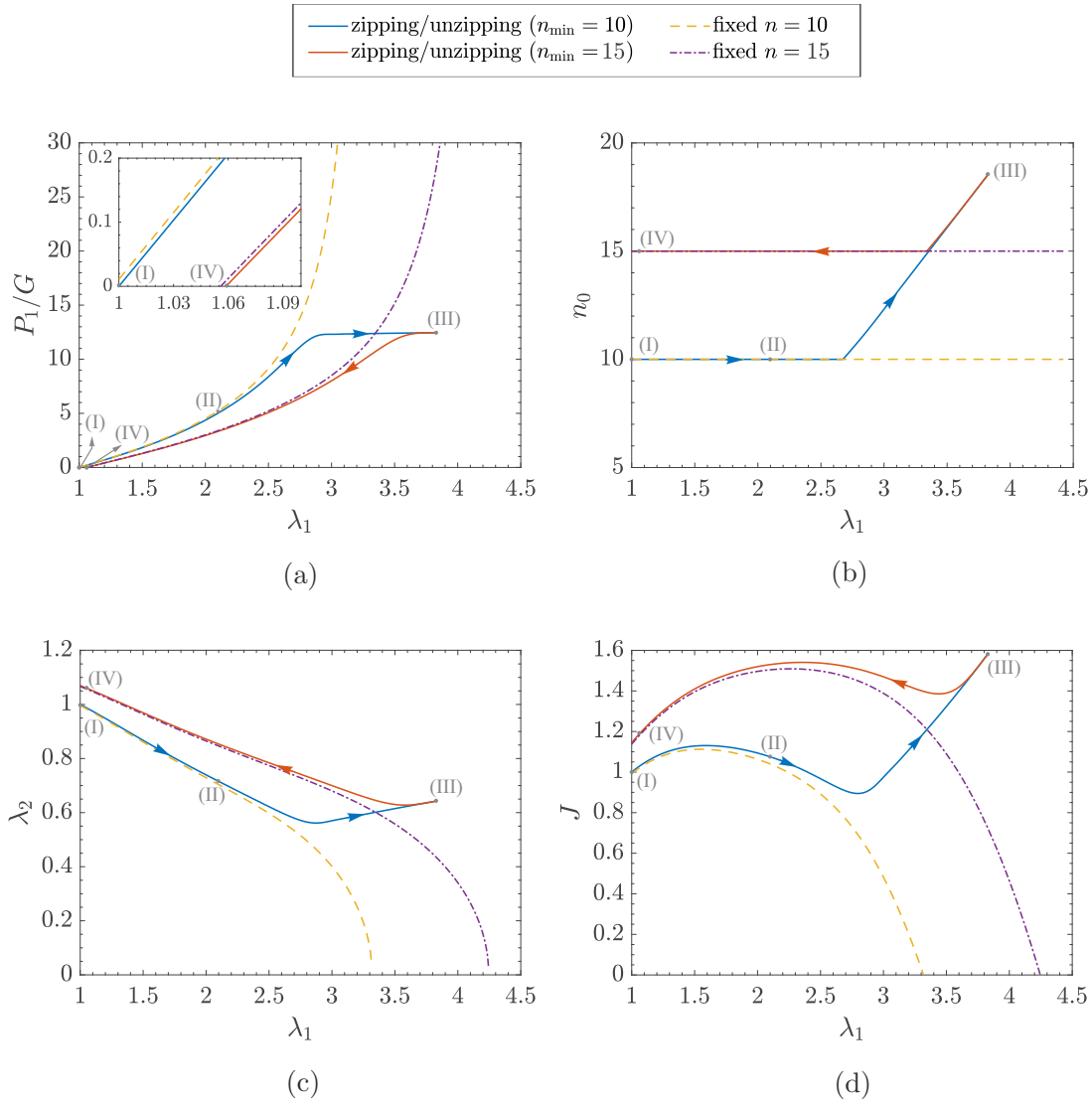

Figure 4.8: Different mechanical parameters in a uniaxial loading-unloading test vs. stretch ratio λ_1 for a gel network containing coil-rod structures and with swelling effects explicitly considered; $\mu = 1$, $N = 150$, $\alpha = 0.05$, $\varepsilon = 1.5k_BT$. Dashed yellow and dash-dotted purple curves assume fixed $n = 10$ and 15, respectively. Blue and red curves allow zipping/unzipping with $n_{\min} = 10$ and 15, respectively. (a) Normalized Piola-Kirchhoff stress P_1, (b) Number of Kuhn segments n_0 in the coil with maximum contribution to the grand canonical partition function, (c) Stretch ratio λ_2, (d) Volume ratio J.

4.5 Discussion

The proposed model is compared with experimental data from a uniaxial tensile test carried out on alginate gel, as reported by Sun *et al.* [5]. While their primary

interest is in alginate-polyacrylamide hybrid gels, the authors provided loading and unloading data for alginate gel separately, demonstrating that the hysteresis observed in the hybrid gel could be attributed to the inherent behavior of the parent alginate gel. Alginate, characterized as an ionic hydrophilic polysaccharide, is a copolymer consisting of two guluronic residues: β-D-mannuronic acid (M) and α-L-guluronic acid (G). According to the egg-box model [38], gelation takes place through the chelation of divalent cations, typically Ca^{2+}, between specific sites on the polyguluronic chains.

Figure 4.9(a) presents the experimental data of first Piola Kirchhoff stress (in kPa) against the principal stretch λ_1 from Sun *et al.* [5]. In the proposed model the egg-box structure is treated as the rod and the remaining parts of the network are considered as the coil. Based on Baumberger and Ronsin [39] and taking the Kuhn segment as two consecutive G units, the binding energy for one Kuhn segment in the rod is $\varepsilon = 12k_BT$. Applying the constitutive relation (4.31) for the swollen sample, all remaining five parameters in Equation (4.32) are determined through a fitting procedure using the loading branch of the experimental data, resulting in the blue curve:

$$G = 0.002\,\text{kPa}, \quad N = 495, \quad \mu = 7743, \quad \alpha = 0.739, \quad n_{\min} = 10. \tag{4.32}$$

Considering water content in the gel as 86 wt % [5], μ value in (4.32) corresponds to an estimated molar weight of 22 689 g/mol for the polymer chains, which falls within the range of 20 000 g/mol to 1 000 000 g/mol as reported by Vold *et al.* [40]. Moreover, the parameter α is close to the ratio between the length of one egg-box unit (9Å, [39]) and the length of two unassociated G units ($\simeq$ 11Å, [41]), which is 0.82. Corresponding to the parameters in Equation (4.32), the swelling stretch to reach a stress-free state is determined to be $\lambda_s = 1.03$, and the end-to-end chain distance in the unswollen stress-free state is calculated as $r_0 = 358.43\,b$. The same parameters with a different $n_{\min} = 138$ result in the unloading curve of the sample (red curve). Clearly, both curves properly capture the loading and unloading behaviour with physically realistic

parameters. The larger prediction of permanent set by the model (1.09) compared to 1.05 found in the experiment can possibly be attributed to the model's inability to capture chain entanglements [42]. Figure 4.9(b) shows the values of n_0 vs. λ_1. The sample begins with $n_0 = 10$ but undergoes immediate unzipping upon loading. The number of Kuhn segments in the coil increases up to $\lambda_1 = 1.22$. During unloading, the red curve shows partial zipping converging to the state with fixed $n_0 = 138$. Figure 4.9(c) illustrates the variation of J with respect to λ_1. Herein, the sample experiences a maximum J of 1.27 during loading and unloading.

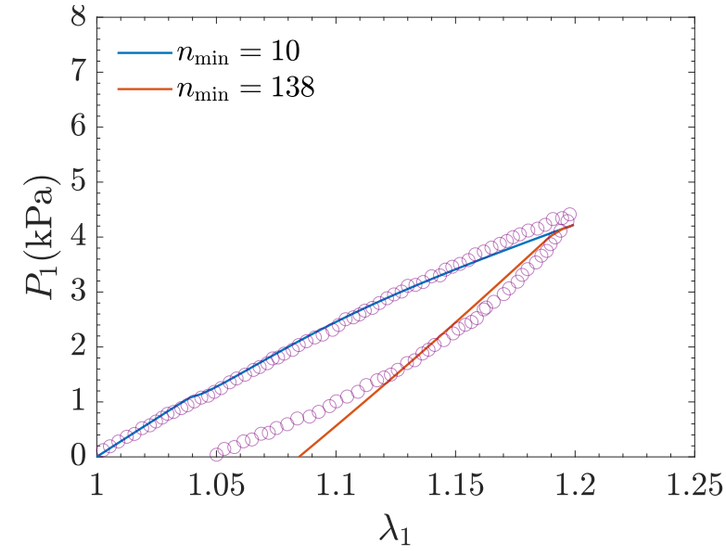

(a)

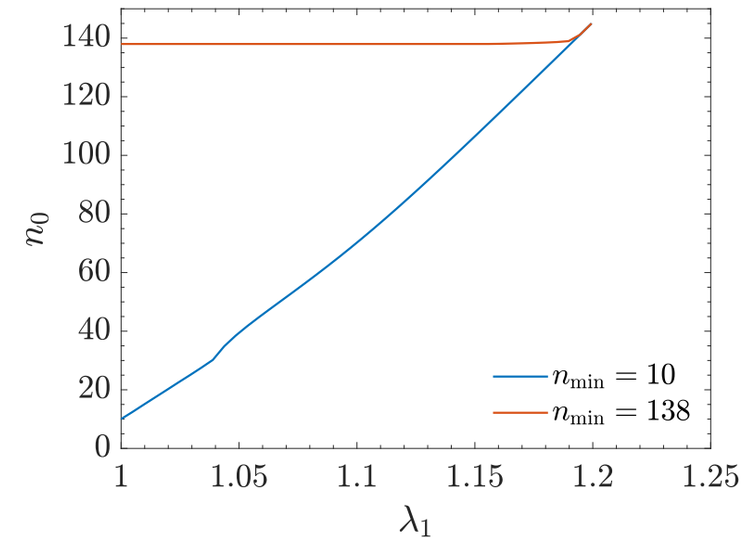

(b)

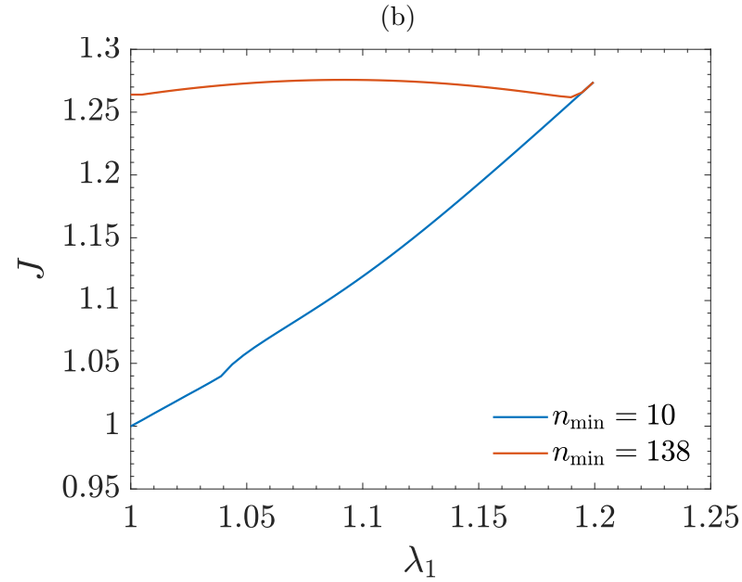

(c)

Figure 4.9: (a) The first Piola-Kirchhoff stress P_1 as a function of stretch λ_1 for a uniaxial loading-unloading test with parameters $N = 495$, $G = 0.002$ kPa, $\mu = 7743$, $\varepsilon = 12\,k_BT$, and $\alpha = 0.739$, along with experimental data from Sun *et al.* [5]. (b) The relationship between n_0 and λ_1. (c) The variation of J with λ_1.

Finite compressibility considered in the current treatment plays a pivotal role as it enables us to determine the unknown parameter r_0 from (4.18), instead of the conventionally approach of setting $r_0 = \sqrt{n}b$ for incompressible materials. Physically, it is also reasonable to expect certain degree of compressibility arising from zipping/unzipping and the dependence of r_0 on the length of the rod. When swelling is considered, the finite compressibility allows us to obtain λ_s from (4.26). If the material were treated as incompressible, one would not be able to uniquely determine λ_s since an arbitrary hydrostatic pressure can be imposed so that the reference state remains stress-free. Consequently, the recognition of stress-free states is obscured in incompressible formulations, and λ_s must be treated as an additional material parameter [34]. The importance of a rational relation between stress-free state and r_0 is also recognized by Trentadue *et al.* [43] and Fazio *et al.* [44]. However, their strategy differs from the one adopted here and in Bischoff *et al.* [29]. In their works [43, 44], the microscopic worm-like chain model is tailored to give $\langle f_r \rangle \Big|_{r_0} = 0$. Such models, when implemented macroscopically, automatically render a stress-free state under incompressible condition for a chain end-to-end distance of r_0. Other approaches to defining stress-free state also exist, notably the one pointed out by De Tommasi *et al.* [45]. In particular, the authors attempted to address the folding/unfolding phenomenon in biopolymers such as proteins using the affine network model. By neglecting the effects of folded domains it was assumed that chains with different number of Kuhn length n have different initial end-to-end distances $r_0 = \sqrt{n}b$. An extra internal variable was introduced in the constitutive relation that depends on the maximum stretch experienced by the sample in its loading history. This variable, conceptually analogous to $n_{\min}$ introduced here, is responsible for the observed permanent set as well as capturing the unfolding phenomenon.

While application of the model is demonstrated using an experiment involving homogeneous deformation, the model is able to handle inhomogeneous deformation where zipping/unzipping occurs locally in the material. It should also be recognized

that the rod in the model represents the junction zones in biopolymer gels, each shared by multiple coils attached to it. Therefore, although by using an affine network model it may appear that zipping/unzipping occurring in one chain is unaffected by the others, different coils in the network can be considered interacting through a common junction zone. Certainly, by relaxing the affine network assumption, which originates from the eight-chain model [23], different results may be observed, including the determination of r_0 (Equation (4.18), Figure 4.2).

In the present formulations, the swelling effects are established based upon the assumption that the number of Kuhn segments in the coil remains fixed during swelling. This assumption can be relaxed by replacing $\langle f_r \rangle$ in Equation (4.26) by $\langle f_r^{\mathrm{G}} \rangle$. In materials like alginate gels, the solvent contains ions such as Ca^{2+}, and they may become trapped or released during zipping or unzipping. While this phenomenon can modify the entropy of mixing, such an effect is neglected to avoid adding complexity to the model. More advanced models that incorporate this and other effects such as fluid diffusion [46] can be investigated in future studies.

While damage-based models in the literature can serve as an alternative for capturing unzipping-caused hysteresis, the current model is equipped with the ability to incorporate healing effects through partial zipping. A more comprehensive analysis for time-dependent healing requires modeling the kinetics of zipping/unzipping or viscoelasticity. The current model can be combined with damage mechanisms associated with chemical cross-links, such as chain scission, to predict fracture and failure. For instance, according to Sun *et al.* [5], the stress and stretch at rupture are 3.7 kPa and 1.2, respectively. However, in the current formulation, the chains can sustain higher forces and extensions. Another crucial aspect to consider is the incorporation of anisotropy during zipping/unzipping, a feature currently lacking in the formulation here. Research by Puglisi *et al.* [47] and Vitucci *et al.* [48] has demonstrated that accounting for anisotropic damage in different directions enhances the models' ability to capture the Mullins effect and permanent set not only in uniaxial experiments but

also in shear and equibiaxial deformation tests. The consideration of these factors will be of interest in future studies.

4.6 Conclusion

A multiscale mechanics model is developed for disordered biopolymer gels that contains coil-rod structures as their building blocks, where the coil represents the amorphous region of the gel and the rod represents the junction zone formed from physical crosslinking between coils. Under external loading, the junction zone can expand or contract, arising from increased ("zipping") or decreased ("unzipping") coil association. Built on the statistical mechanics model of a single coil-rod structure proposed in Chapter 3, a network model is developed for the constitutive relation of the gel, where zipping/unzipping is incorporated via the grand canonical ensemble allowing exchange of Kuhn segments between the coil and rod portions. While using the eight-chain model [23] as a starting point, it is demonstrated that finite compressibility must be enabled to determine the end-to-end distance of the coil-rod structures in a stress-free network. This delicate point, often neglected in the literature, is crucial in capturing the permanent set observed in loading-unloading experiments. Swelling effects during gelation, including volume change and the entropy of polymer/solvent mixing, are explicitly included in the formulation. Results from the model shows interesting behaviors such as unzipping-caused leveling off of the stress-stretch curve, partial zipping during unloading as a signature of healing, and the presence of hysteresis and a permanent set during a loading-unloading cycle as a result of irreversible unzipping. Finally, the model is applied to the uniaxial loading-unloading test for an alginate gel, with experimental data from Sun *et al.* [5]. The present model serves as a foundation for modeling more advanced biopolymer gels such as hybrid polyacrylamide-alginate gels [5] which have attracted significant attention in recent years.

Acknowledgements

TT acknowledges financial support from the Natural Sciences and Engineering Research Council of Canada (NSERC; Grant numbers: RGPIN-2018-04281, RGPAS-2018-522655) and Canada Research Chairs Program (Grant number: TIER1 2021-00023). HM acknowledges scholarship support from Alberta Innovates.

References

[1] K. Y. Lee and D. J. Mooney, "Hydrogels for tissue engineering," *Chemical Reviews*, vol. 101, no. 7, pp. 1869–1880, 2001, PMID: 11710233. DOI: 10.1021/cr000108x. eprint: https://doi.org/10.1021/cr000108x.

[2] A. S. Hoffman, "Hydrogels for biomedical applications," *Advanced Drug Delivery Reviews*, vol. 64, pp. 18–23, 2012, MOST CITED PAPERS IN THE HISTORY OF ADVANCED DRUG DELIVERY REVIEWS: A TRIBUTE TO THE 25TH ANNIVERSARY OF THE JOURNAL, ISSN: 0169-409X. DOI: https://doi.org/10.1016/j.addr.2012.09.010.

[3] S. Mohan, O. S. Oluwafemi, N. Kalarikkal, S. Thomas, and S. P. Songca, "Biopolymers – application in nanoscience and nanotechnology," in *Recent Advances in Biopolymers*, F. K. Perveen, Ed., Rijeka: IntechOpen, 2016, ch. 3. DOI: 10.5772/62225.

[4] J. L. Drury and D. J. Mooney, "Hydrogels for tissue engineering: Scaffold design variables and applications," *Biomaterials*, vol. 24, no. 24, pp. 4337–4351, 2003, Synthesis of Biomimetic Polymers, ISSN: 0142-9612. DOI: https://doi.org/10.1016/S0142-9612(03)00340-5.

[5] J.-Y. Sun *et al.*, "Highly stretchable and tough hydrogels," *Nature*, vol. 489, no. 7414, pp. 133–136, 2012.

[6] T. L. Sun *et al.*, "Physical hydrogels composed of polyampholytes demonstrate high toughness and viscoelasticity," *Nature materials*, vol. 12, no. 10, pp. 932–937, 2013.

[7] J. Wang, J. Wei, S. Su, J. Qiu, and S. Wang, "Ion-linked double-network hydrogel with high toughness and stiffness," *Journal of Materials Science*, vol. 50, pp. 5458–5465, 2015.

[8] A. B. Ihsan *et al.*, "Self-healing behaviors of tough polyampholyte hydrogels," *Macromolecules*, vol. 49, no. 11, pp. 4245–4252, 2016. DOI: 10.1021/acs.macromol.6b00437. eprint: https://doi.org/10.1021/acs.macromol.6b00437.

[9] A. H. Clark and S. B. Ross-Murphy, "Structural and mechanical properties of biopolymer gels," in *Biopolymers*, Berlin, Heidelberg: Springer Berlin Heidelberg, 1987, pp. 57–192, ISBN: 978-3-540-47827-0.

[10] C. Joly-Duhamel, D. Hellio, A. Ajdari, and M. Djabourov, "All gelatin networks: 2. the master curve for elasticity," *Langmuir*, vol. 18, no. 19, pp. 7158–7166, 2002. DOI: 10.1021/la020190m. eprint: https://doi.org/10.1021/la020190m.

[11] H. Hecht and S. Srebnik, "Structural characterization of sodium alginate and calcium alginate," *Biomacromolecules*, vol. 17, no. 6, pp. 2160–2167, 2016. DOI: 10.1021/acs.biomac.6b00378. eprint: https://doi.org/10.1021/acs.biomac.6b00378.

[12] D. Dhar and Y. Singh, "Linear and branched polymers on fractals," in *Statistics of Linear Polymers in Disordered Media*, B. K. Chakrabarti, Ed., Amsterdam: Elsevier Science, 2005, pp. 149–194, ISBN: 978-0-444-51709-8. DOI: https://doi.org/10.1016/B978-044451709-8/50005-0.

[13] S. B. Ross-Murphy, "Physical gelation of biopolymers," *Food Hydrocolloids*, vol. 1, no. 5, pp. 485–495, 1987, Special issue: 2nd International Workshop on Plant Polysaccharides, ISSN: 0268-005X. DOI: https://doi.org/10.1016/S0268-005X(87)80047-4.

[14] T. Baumberger and O. Ronsin, "Cooperative effect of stress and ion displacement on the dynamics of cross-link unzipping and rupture of alginate gels," *Biomacromolecules*, vol. 11, no. 6, pp. 1571–1578, 2010, PMID: 20499914. DOI: 10.1021/bm1002015. eprint: https://doi.org/10.1021/bm1002015.

[15] K. Nishinari, S. Koide, and K. Ogino, "On the temperature dependence of elasticity of thermo-reversible gels," *Journal de Physique*, vol. 46, no. 5, pp. 793–797, 1985. DOI: 10.1051/jphys:01985004605079300.

[16] P. G. Higgs and R. C. Ball, "Some ideas concerning the elasticity of biopolymer networks," *Macromolecules*, vol. 22, no. 5, pp. 2432–2437, 1989. DOI: 10.1021/ma00195a073. eprint: https://doi.org/10.1021/ma00195a073.

[17] S. Cocco, J. F. Marko, and R. Monasson, "Theoretical models for single-molecule DNA and RNA experiments: From elasticity to unzipping," *Comptes Rendus Physique*, vol. 3, no. 5, pp. 569–584, 2002, ISSN: 1631-0705. DOI: https://doi.org/10.1016/S1631-0705(02)01345-2.

[18] N. Singh and Y. Singh, "Statistical theory of force-induced unzipping of dna," *The European Physical Journal E*, vol. 17, no. 1, pp. 7–19, 2005.

[19] S. Kutter and E. M. Terentjev, "Networks of helix-forming polymers," *The European Physical Journal E*, vol. 8, pp. 539–547, 2002.

[20] S. Courty, J. L. Gornall, and E. M. Terentjev, "Mechanically induced helix-coil transition in biopolymer networks," *Biophysical Journal*, vol. 90, no. 3, pp. 1019–1027, 2006, ISSN: 0006-3495. DOI: https://doi.org/10.1529/biophysj.105.067090.

[21] J. Zhang, C. R. Daubert, and E. Allen Foegeding, "A proposed strain-hardening mechanism for alginate gels," *Journal of Food Engineering*, vol. 80, no. 1, pp. 157–165, 2007, ISSN: 0260-8774. DOI: https://doi.org/10.1016/j.jfoodeng.2006.04.057.

[22] V. Magnenet, J. Schiavi-Tritz, C. Huselstein, and R. Rahouadj, "Constitutive equations for Ca2+ -alginate gels," *Journal of the Mechanical Behavior of Biomedical Materials*, vol. 5, no. 1, pp. 90–98, 2012, ISSN: 1751-6161. DOI: https://doi.org/10.1016/j.jmbbm.2011.08.009.

[23] E. M. Arruda and M. C. Boyce, "A three-dimensional constitutive model for the large stretch behavior of rubber elastic materials," *Journal of the Mechanics and Physics of Solids*, vol. 41, no. 2, pp. 389–412, 1993, ISSN: 0022-5096. DOI: https://doi.org/10.1016/0022-5096(93)90013-6.

[24] T. Distler, E. Schaller, P. Steinmann, A. Boccaccini, and S. Budday, "Alginate-based hydrogels show the same complex mechanical behavior as brain tissue," *Journal of the Mechanical Behavior of Biomedical Materials*, vol. 111, p. 103 979, 2020, ISSN: 1751-6161. DOI: https://doi.org/10.1016/j.jmbbm.2020.103979.

[25] Z. Clapacs *et al.*, "Biocompatible and enzymatically degradable gels for 3d cellular encapsulation under extreme compressive strain," *Gels*, vol. 7, no. 3, 2021, ISSN: 2310-2861. DOI: 10.3390/gels7030101.

[26] L. Treloar, *The Physics of Rubber Elasticity* (Oxford Classic Texts in the Physical Sciences). Oxford University Press, USA, 1975, ISBN: 9780191523304.

[27] S. M. Bhattacharjee, A. Giacometti, and A. Maritan, "Flory theory for polymers," *Journal of Physics: Condensed Matter*, vol. 25, no. 50, p. 503 101, 2013. DOI: 10.1088/0953-8984/25/50/503101.

[28] A. R. Cioroianu, E. M. Spiesz, and C. Storm, "Disorder, pre-stress and non-affinity in polymer 8-chain models," *Journal of the Mechanics and Physics of Solids*, vol. 89, pp. 110–125, 2016, ISSN: 0022-5096. DOI: https://doi.org/10.1016/j.jmps.2016.01.014.

[29] J. E. Bischoff, E. M. Arruda, and K. Grosh, "A new constitutive model for the compressibility of elastomers at finite deformations," *Rubber chemistry and technology*, vol. 74, no. 4, pp. 541–559, 2001.

[30] R. Ogden, *Non-linear Elastic Deformations* (Dover Civil and Mechanical Engineering). Dover Publications, 1997, ISBN: 9780486696485.

[31] R. W. Ogden and D. G. Roxburgh, "A pseudo-elastic model for the Mullins effect in filled rubber," *Proceedings of the Royal Society of London. Series A: Mathematical, Physical and Engineering Sciences*, vol. 455, no. 1988, pp. 2861–2877, 1999. DOI: 10.1098/rspa.1999.0431.

[32] A. Dorfmann and R. Ogden, "A constitutive model for the mullins effect with permanent set in particle-reinforced rubber," *International Journal of Solids and Structures*, vol. 41, no. 7, pp. 1855–1878, 2004, ISSN: 0020-7683. DOI: https://doi.org/10.1016/j.ijsolstr.2003.11.014.

[33] H. Sund and K. Markau, "Association-dissociation phenomena in biopolymers," *International Journal of Polymeric Materials and Polymeric Biomaterials*, vol. 4, no. 3-4, pp. 251–292, 1976. DOI: 10.1080/00914037608072382. eprint: https://doi.org/10.1080/00914037608072382.

[34] M. C. Boyce and E. M. Arruda, "Swelling and mechanical stretching of elastomeric materials," *Mathematics and Mechanics of Solids*, vol. 6, no. 6, pp. 641–659, 2001. DOI: 10.1177/108128650100600605. eprint: https://doi.org/10.1177/108128650100600605.

[35] S. R. Lavoie, P. Millereau, C. Creton, R. Long, and T. Tang, "A continuum model for progressive damage in tough multinetwork elastomers," *Journal of the Mechanics and Physics of Solids*, vol. 125, pp. 523–549, 2019, ISSN: 0022-5096. DOI: https://doi.org/10.1016/j.jmps.2019.01.001.

[36] P. J. Flory, "Thermodynamics of high polymer solutions," *The Journal of Chemical Physics*, vol. 10, no. 1, pp. 51–61, 1942. DOI: 10.1063/1.1723621. eprint: https://doi.org/10.1063/1.1723621.

[37] M. L. Huggins, "Solutions of Long Chain Compounds," *The Journal of Chemical Physics*, vol. 9, no. 5, pp. 440–440, 1941, ISSN: 0021-9606. DOI: 10.1063/1.1750930. eprint: https://pubs.aip.org/aip/jcp/article-pdf/9/5/440/8138635/440_1_online.pdf.

[38] G. T. Grant, E. R. Morris, D. A. Rees, P. J. Smith, and D. Thom, "Biological interactions between polysaccharides and divalent cations: The egg-box model," *FEBS Letters*, vol. 32, no. 1, pp. 195–198, 1973, ISSN: 0014-5793. DOI: https://doi.org/10.1016/0014-5793(73)80770-7.

[39] T. Baumberger and O. Ronsin, "From thermally activated to viscosity controlled fracture of biopolymer hydrogels," *The Journal of Chemical Physics*, vol. 130, no. 6, p. 061 102, 2009. DOI: 10.1063/1.3078267. eprint: https://doi.org/10.1063/1.3078267.

[40] I. M. N. Vold, K. A. Kristiansen, and B. E. Christensen, "A study of the chain stiffness and extension of alginates, in vitro epimerized alginates, and periodate-oxidized alginates using size-exclusion chromatography combined with light scattering and viscosity detectors," *Biomacromolecules*, vol. 7, no. 7, pp. 2136–2146, 2006, PMID: 16827580. DOI: 10.1021/bm060099n. eprint: https://doi.org/10.1021/bm060099n.

[41] O. Smidsrød, R. Glover, and S. G. Whittington, "The relative extension of alginates having different chemical composition," *Carbohydrate Research*, vol. 27, no. 1, pp. 107–118, 1973, ISSN: 0008-6215. DOI: https://doi.org/10.1016/S0008-6215(00)82430-1.

[42] D. R. Rottach, J. G. Curro, J. Budzien, G. S. Grest, C. Svaneborg, and R. Everaers, "Permanent set of cross-linking networks: Comparison of theory with molecular dynamics simulations," *Macromolecules*, vol. 39, no. 16, pp. 5521–5530, 2006. DOI: 10.1021/ma060767x. eprint: https://doi.org/10.1021/ma060767x.

[43] F. Trentadue, D. De Tommasi, and G. Puglisi, "A predictive micromechanically-based model for damage and permanent deformations in copolymer sutures," *Journal of the Mechanical Behavior of Biomedical Materials*, vol. 115, p. 104 277, 2021, ISSN: 1751-6161. DOI: https://doi.org/10.1016/j.jmbbm.2020.104277.

[44] V. Fazio, D. De Tommasi, N. M. Pugno, and G. Puglisi, "Spider silks mechanics: Predicting humidity and temperature effects," *Journal of the Mechanics and Physics of Solids*, vol. 164, p. 104 857, 2022, ISSN: 0022-5096. DOI: https://doi.org/10.1016/j.jmps.2022.104857.

[45] D. De Tommasi, G. Puglisi, and G. Saccomandi, "Multiscale mechanics of macromolecular materials with unfolding domains," *Journal of the Mechanics and Physics of Solids*, vol. 78, pp. 154–172, 2015, ISSN: 0022-5096. DOI: https://doi.org/10.1016/j.jmps.2015.02.002.

[46] A. Hajikhani, P. Wriggers, and M. Marino, "Chemo-mechanical modelling of swelling and crosslinking reaction kinetics in alginate hydrogels: A novel theory and its numerical implementation," *Journal of the Mechanics and Physics of Solids*, vol. 153, p. 104 476, 2021, ISSN: 0022-5096. DOI: https://doi.org/10.1016/j.jmps.2021.104476.

[47] G. Puglisi, D. De Tommasi, M. F. Pantano, N. M. Pugno, and G. Saccomandi, "Micromechanical model for protein materials: From macromolecules to macroscopic fibers," *Phys. Rev. E*, vol. 96, p. 042 407, 4 2017. DOI: 10.1103/PhysRevE.96.042407.

[48] G. Vitucci, D. De Tommasi, G. Puglisi, and F. Trentadue, "A predictive microstructure inspired approach for anisotropic damage, residual stretches and hysteresis in biodegradable sutures," *International Journal of Solids and Structures*, vol. 270, p. 112 232, 2023, ISSN: 0020-7683. DOI: https://doi.org/10.1016/j.ijsolstr.2023.112232.

Chapter 5

Statistical Mechanics and Phantom Network Modelling of Disordered Biopolymer Gels

5.1 Introduction

Polymer networks are established through the copious interpenetration of chains. The complex interactions between them as well as network defects such as topological loops [1] make studying their statistical thermodynamics formidable. In the method proposed by James and Guth [2], known as the affine network model, the chain vectors are situated randomly within the network, and their extension is assumed to follow the macroscopic deformation controlled by external loading. In this framework, since the interaction of chains are only considered via cross-links, the partition function of each chain provides sufficient information to obtain the partition function of the entire network. Building upon this pioneering work, subsequent literature endeavors to develop more advanced models that describe observed phenomena in polymer networks while being numerically affordable. To name but a few, these includes the three-chain model [3], the full-network model [4, 5], the eight-chain model [6, 7], and the micro-sphere model [8]. In the method proposed by Flory [9], known as the phantom network model, the constraints of macroscopic deformation are relaxed, allowing the chains to maintain their topology while freely passing through each other. In

this framework, the network is treated as a collection of chains where only a subset of junctions is restricted by macroscopic deformation, while the remaining junction points fluctuate around their average positions.

In disordered biopolymer gels, amorphous regions known as coils are interconnected through ordered regions called junction zones [10, 11]. The process of junction zone formation varies depending on the specific biopolymers involved. For instance, in agar gels, the chains intertwine to create a double helix structure, while in alginate gels, the junction zone is formed through the mediation of external cation agents, resulting in egg-box structures. Disordered biopolymer gels can be decomposed into two fundamental building blocks: coils and junction zones. Coils are often modeled as freely-jointed chains, while junction zones are represented by rigid rods. Within affine network framework, the end-to-end extension of each component (coil or rod) is assumed to be proportional to the corresponding macroscopic displacement. Given the infinite stiffness of a rigid rod, it cannot undergo extension. This assumption implies that the macroscopic behavior encompassing the rod reflects an unrealistically high stiffness under affinity assumptions. To mitigate such unrealistic phenomenon, Higgs and Ball [12] considered the network as a collection of "coil-rod" structures, in each structure the freely-jointed chain is connected to a rigid rod. The associated end-to-end extension of this combined structure (rather than treating the coil and rod separately), still follows the macroscopic deformation akin to an affine network. However, the node connecting the coil and rod can freely move resembling the phantom network model.

Since this structure is defined by two nodes, hereafter it is referred to as "two-node coil-rod structure" and can be directly applied to the well-known affine network models in the literature (see Fig. 5.1a). Additionally, this model allows us to capture the phenomenon of zipping/unzipping, where junction zones in biopolymer gels expand or shrink due to applied loading. In Chapter 4, it has been demonstrated that combining the coil-rod structure with zipping/unzipping in the eight-chain network

effectively captures both the dissipation caused by unzipping and the phenomenon of permanent set observed during cyclic loading and unloading. Despite these advantages, the coil-rod structure in the aforementioned model is treated as a single entity. The decomposition of the complicated network, involving different regions of coils and rods, into a collection of coil-rod structures is a simplification worth further examination. This prompts us to advance the coil-rod structure model into a more explicit network where two or more coils are connected through a single junction zone in the middle (see Fig. 5.1b). By providing such a model, the ranges of applicability and limitations of the coil-rod structure can also be explored, addressing whether it can adequately model the complex interactions between coils and rods.

In Section 5.2, the model of the coil-rod structure is reviewed, and a new four-node coil-rod structure is formulated within the framework of statistical mechanics. Two formalisms for deriving the probability distribution are explained. Subsequently, the results are simplified by invoking Gaussian statistics for the coils. It is shown that under this assumption, the four-node coil-rod structure can be decomposed into a collection of one coil-rod structure and two pure coils. In Section 5.3, using the latter result, the properties of the four-node coil-rod structure are further inspected by confining the structure's nodes to an in-plane rectangular cell. The stress-free state of the proposed network model is obtained, and the constitutive relations are derived. Subsequently, the Gaussian approximation is compared with the exact result, and its applicability is discussed. The concept of unzipping and its underlying features are then integrated into the proposed network model. With the aid of the in-plane result, the four-node coil-rod structure is introduced in Section 5.4 for a three-dimensional rectangular prism network, and the results are compared with the coil-rod structure in the eight-chain network model.

5.2 Statistical mechanics of a four-node coil-rod structure

Prior to development of the four-node coil-rod structure, the formulation of a two-node coil-rod structure is reviewed. For the freely-jointed chain model with Kuhn length b and number of Kuhn segments n, if the end-to-end distance $|\mathbf{r}|$ is sufficiently small and n is sufficiently large, one can find the probability distribution $W_n^{\mathrm{C}}(|\mathbf{r}|)$ as

$$W_n^{\mathrm{C}}(|\mathbf{r}|) = \left(\frac{3}{2\pi n b^2}\right)^{3/2} \exp\left[-\frac{3\,|\mathbf{r}|^2}{2nb^2}\right], \tag{5.1}$$

where $\mathbf{r}$ represents the end-to-end vector of the coil and $|\cdots|$ denotes the norm of the vector. This probability is commonly referred to as Gaussian distribution. Additionally, for a single rigid rod with length a, the probability distribution can be described through

$$W^{\mathrm{R}}(|\mathbf{r}|) = \frac{1}{4\pi a^2}\delta(|\mathbf{r}| - a), \tag{5.2}$$

where $\delta(\cdots)$ denotes the one-dimensional Dirac delta function applied to a scalar argument. In the work in Chapter 4, it was shown that if the Gaussian coil is followed by a rigid rod (see Fig. 5.1a), the probability distribution of the resultant structure is modified to

$$W_n^{\mathrm{CR}}(|\mathbf{r}|) = \sqrt{\frac{3}{(2\pi)^3\, n a^2 b^2}}\,\frac{1}{|\mathbf{r}|}\exp\left[-\frac{3}{2nb^2}(|\mathbf{r}|^2 + a^2)\right]\sinh\left(\frac{3a\,|\mathbf{r}|}{nb^2}\right). \tag{5.3}$$

The superscripts C, R, and CR respectively signifies the coil, rod, and coil-rod structure. For $a \to 0$ the rod vanishes, and Equation (5.3) converts back to that of Gaussian coil (5.1). The result given by (5.3) is applicable to the affine network models by simply replacing the coils in the traditional models such as eight-chain network [6] with the coil-rod structures. As elaborated in the forthcoming sections, the information on the probability distribution and the geometry of network model is sufficient to derive the constitutive relations of the material. The entropy and Helmholtz free energy of each chain are obtained by taking the natural logarithm of

the probability distribution. Depending on construction of geometry that places the microstructure into the network, the end-to-end distance of the chains is related to the macroscopic deformation, and the Helmholtz free energy of the network is then given by the summation of the corresponding values of the chains in terms of the deformation gradient tensor. Once the Helmholtz free energy is available, the derivation of stress-stretch relations is straightforward.

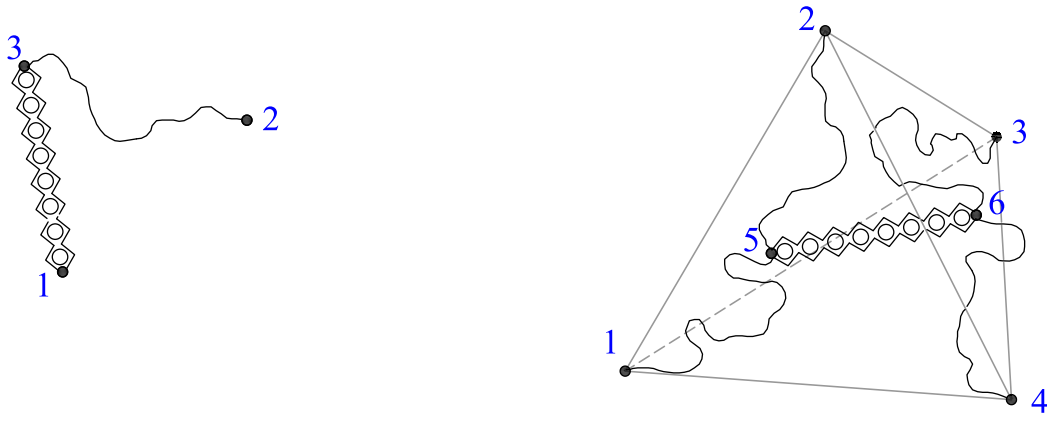

(a) (b)

Figure 5.1: (a) The two-node coil-rod structure with nodes 1 and 2 attached to the macroscopic element and fluctuating node 3. The zigzag structure represents the schematic of the egg-box structure, with hollow circles indicating the gelling agents. Segment between 1 and 3 is modelled by a rigid rod and coil 23 is modelled by freely-jointed chain. (b) The topology of the four-node coil-rod structure with nodes 1 to 4 attached to the macroscopic element and fluctuating nodes 5 and 6. The zigzag structure 56 represents the rigid rod and the remaining four coils follow the freely-jointed chain model.

5.2.1 Four-node coil-rod structure

The simplest scenario illustrating the explicit interaction of coils and rods involves two coils sharing a single junction zone between them. Let us consider two coils, labeled 13 and 24, which are laterally associated, thereby creating the junction zone 56 and regenerating four new coils 15, 25, 36, and 46. In three-dimensional space, the four nodes can form a cell as demonstrated by a tetrahedral in Fig. 5.1b. Hereafter, such a structure is referred to as the "four-node coil-rod structure".

By defining $\mathbf{R}_{ij} = \mathbf{R}_i - \mathbf{R}_j$, with $\mathbf{R}_i$ being the position vector of node i and setting node 1 fixed, the probability of locating node i within $\mathrm{d}\mathbf{R}_{1i}$ for $i = 2, \ldots, 6$ is expressed as $P\left(\mathbf{R}_{12}, \mathbf{R}_{13}, \mathbf{R}_{14}, \mathbf{R}_{15}, \mathbf{R}_{16}\right) \prod_{i=2}^{6} \mathrm{d}\mathbf{R}_{1i}$. To derive the probability distribution function of such system, all coils are represented by freely-jointed chain models, while the junction zone is envisioned as a rigid rod of length a. In the affine network model, all nodes 1 to 6 are tethered to the macroscopic element, ensuring that the extension of vectors $\mathbf{R}_{ij}$ follows the applied macroscopic deformation. Although deriving the probability distribution based on this viewpoint is relatively straightforward, the presence of a rigid rod imparts significant stiffness to the macroscopic element, rendering the overall response unrealistic. To circumvent this issue, the phantom network is adopted, enabling nodes 1 to 4 to undergo manipulation by macroscopic deformation, while nodes 5 and 6 are capable of fluctuating around their mean positions. The probability of finding the nodes i inside the volume element $\mathrm{d}\mathbf{R}_{1i}$ $(i = 2, 3, 4)$ is denoted by $P\left(\mathbf{R}_{12}, \mathbf{R}_{13}, \mathbf{R}_{14}\right)\, \mathrm{d}\mathbf{R}_{12}\, \mathrm{d}\mathbf{R}_{13}\, \mathrm{d}\mathbf{R}_{14}$. The repetition of such structures results in a network forming a body with volume V_0 in the undeformed state. Accordingly, the entropy of the deformed state per unit volume V_0 is presented by the Boltzmann equation:

$$S = c + \varrho k_B \ln \left[\, \mathrm{d}\mathbf{R}_{12}\, \mathrm{d}\mathbf{R}_{13}\, \mathrm{d}\mathbf{R}_{14}\right] + \varrho k_B \ln P(\mathbf{R}_{13}, \mathbf{R}_{13}, \mathbf{R}_{14}), \tag{5.4}$$

where ϱ is the chain density per unit volume V_0, k_B is the Boltzmann constant and c is an arbitrary constant. The entropy change from the undeformed to the deformed state is readily obtained by subtracting their respective values. Once ΔS is at hand, the Helmholtz free energy per unit reference volume V_0, Ψ is obtained as

$$\Psi = -T\Delta S, \tag{5.5}$$

where T is the absolute temperature. Depending on the geometry of four-node coil-rod structure the dimensions $\mathrm{d}\mathbf{R}_{1i}$ $(i = 2, 3, 4)$ should be related to the principal stretches of the bulk material, λ_1, λ_2, and λ_3. Consequently, for compressible material, the

principal components of First Piola-Kirchhoff stress P_1, P_2, and P_3 can be obtained as [13]

$$P_i = \frac{\partial \Psi}{\partial \lambda_i}, \qquad i = 1, 2, 3. \tag{5.6}$$

It can be seen that the constitutive equation directly depends on the probability distribution $P(\mathbf{R}_{13}, \mathbf{R}_{13}, \mathbf{R}_{14})$. In general, there are two approaches to find this probability: the real space method and the Fourier space method, which will be elaborated upon in the next sections.

5.2.2 Real space representation of the probability

Suppose the probability distribution for a coil with $n_{pq} = n_{qp}$ Kuhn segments trapped between nodes p and q is denoted as $W^{\mathrm{C}}_{n_{pq}}(|\mathbf{r}|)$. By setting node 1 fixed, the probability of locating node i within $\mathrm{d}\mathbf{R}_{1i}$ for $i = 2, \ldots, 6$ is expressed as:

$$\begin{aligned} &P\left(\mathbf{R}_{12}, \mathbf{R}_{13}, \mathbf{R}_{14}, \mathbf{R}_{15}, \mathbf{R}_{16}\right) \prod_{i=2}^{6} \mathrm{d}\mathbf{R}_{1i} \\ &= W^{\mathrm{C}}_{n_{15}}\left(|\mathbf{R}_{15}|\right) W^{\mathrm{C}}_{n_{52}}\left(|\mathbf{R}_{52}|\right) W^{\mathrm{C}}_{n_{63}}\left(|\mathbf{R}_{63}|\right) W^{\mathrm{C}}_{n_{46}}\left(|\mathbf{R}_{46}|\right) W^{\mathrm{R}}\left(|\mathbf{R}_{56}|\right) \prod_{i=2}^{6} \mathrm{d}\mathbf{R}_{1i}. \end{aligned} \tag{5.7}$$

Now, the probability of finding nodes 1 to 4 within their own volume elements $\mathrm{d}\mathbf{R}_i$ is given by integration of the aforementioned probability over all possible locations of nodes 5 and 6, i.e.,

$$\begin{aligned} &P\left(\mathbf{R}_{12}, \mathbf{R}_{13}, \mathbf{R}_{14}\right) \prod_{i=2}^{4} \mathrm{d}\mathbf{R}_{1i} = \prod_{i=2}^{4} \mathrm{d}\mathbf{R}_{1i} \times \\ &\int\int W^{\mathrm{C}}_{n_{15}}\left(|\mathbf{R}_{15}|\right) W^{\mathrm{C}}_{n_{52}}\left(|\mathbf{R}_{52}|\right) W^{\mathrm{C}}_{n_{63}}\left(|\mathbf{R}_{63}|\right) W^{\mathrm{C}}_{n_{46}}\left(|\mathbf{R}_{46}|\right) \frac{1}{4\pi a^2} \delta(|\mathbf{R}_{56}| - a) \mathrm{d}\mathbf{R}_{15} \mathrm{d}\mathbf{R}_{16}. \end{aligned} \tag{5.8}$$

By employing the following change of variables

$$\mathbf{v} = \frac{1}{2}\left(\mathbf{R}_{15} - \mathbf{R}_{16}\right), \tag{5.9a}$$

$$\mathbf{u} = \frac{1}{2}\left(\mathbf{R}_{15} + \mathbf{R}_{16}\right), \tag{5.9b}$$

Equation (5.8) is rephrased as

$$P\left(\mathbf{R}_{12},\mathbf{R}_{13},\mathbf{R}_{14}\right)=\frac{2}{\pi a^{2}}\int\int W_{n_{15}}^{\mathrm{C}}\left(|\mathbf{v}+\mathbf{u}|\right)W_{n_{52}}^{\mathrm{C}}\left(|\mathbf{R}_{12}-\mathbf{v}-\mathbf{u}|\right)$$
$$\times W_{n_{63}}^{\mathrm{C}}\left(|\mathbf{R}_{13}+\mathbf{v}-\mathbf{u}|\right)W_{n_{46}}^{\mathrm{C}}\left(|\mathbf{R}_{14}+\mathbf{v}-\mathbf{u}|\right)\delta(2|\mathbf{v}|-a)\mathrm{d}\mathbf{u}\mathrm{d}\mathbf{v}. \tag{5.10}$$

Utilizing $\delta\left(2|\mathbf{v}|-a\right)=\frac{1}{2}\delta\left(|\mathbf{v}|-\frac{a}{2}\right)$, and applying the sifting property of the Dirac delta function, one layer of integration is eliminated, resulting in

$$P\left(\mathbf{R}_{12},\mathbf{R}_{13},\mathbf{R}_{14}\right)=\frac{1}{4\pi}\int\left[\int_{\phi=0}^{\pi}\int_{\theta=0}^{2\pi}W_{n_{15}}^{\mathrm{C}}\left(|\mathbf{v}+\mathbf{u}|\right)W_{n_{52}}^{\mathrm{C}}\left(|\mathbf{R}_{12}-\mathbf{v}-\mathbf{u}|\right)\right.$$
$$\left.\times W_{n_{63}}^{\mathrm{C}}\left(|\mathbf{R}_{13}+\mathbf{v}-\mathbf{u}|\right)W_{n_{46}}^{\mathrm{C}}\left(|\mathbf{R}_{14}+\mathbf{v}-\mathbf{u}|\right)\sin\phi\,\mathrm{d}\phi\,\mathrm{d}\theta\right]\mathrm{d}\mathbf{u}, \tag{5.11}$$

where $\mathbf{v}$ is given in spherical coordinate as

$$\mathbf{v}=\frac{a}{2}\left(\sin\phi\cos\theta,\sin\phi\sin\theta,\cos\phi\right). \tag{5.12}$$

The schematics of the above variables are illustrated in Fig. 5.2. It should be recalled that in freely-jointed chain models, coils cannot extend beyond their fully extended state, where the associated probability is zero. Analogously, the maximum value of $|\mathbf{u}|$ is the fully extended length of chain 15 plus half of the rod length, $n_{15}b+a/2$. Any probability larger than this critical value is zero. However, constraints from other ends can impose stricter conditions on the probability, leading to smaller critical values of $|\mathbf{u}|$, which may not be immediately apparent. This critical value helps us in performing numerical integration without encountering infinity in the bounds of integrals.

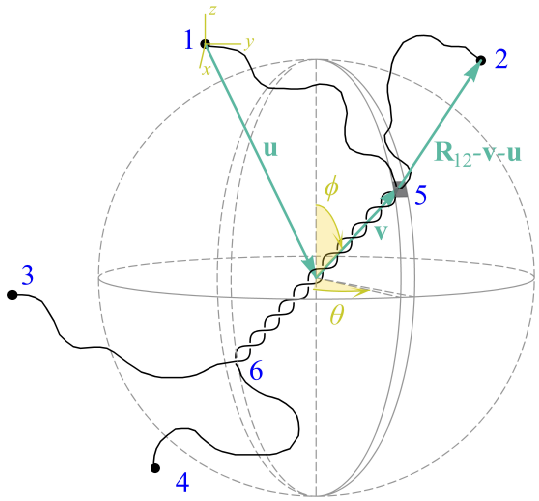

Figure 5.2: The five layers of integration in Equation (5.11) include three-dimensional integration over all possible vectors $\mathbf{u}$ and the surface integral with variable ϕ and θ over the sphere with position center $\mathbf{u}$ and radius $a/2$.

In the context of more complicated system of coils and rods, the number of integration layers is given by $3n_f - n_r$, where n_f represents the count of free nodes (in this case, two nodes 5 and 6), and n_r denotes the number of rigid rods. In the scenario shown in Fig. 5.2, the number of integration layers is $3 \times 2 - 1 = 5$.

5.2.3 Fourier space representation of the probability

Fourier space representation sometimes offers a simpler approach to calculating the probability distribution. Since nodes 1 to 4 are attached to the macroscopic element, the following constraints between the end-to-end vectors hold:

$$\mathbf{R}_{12} = \mathbf{R}_{15} + \mathbf{R}_{52}, \tag{5.13a}$$

$$\mathbf{R}_{13} = \mathbf{R}_{15} + \mathbf{R}_{56} + \mathbf{R}_{63}, \tag{5.13b}$$

$$\mathbf{R}_{14} = \mathbf{R}_{15} + \mathbf{R}_{56} + \mathbf{R}_{64}. \tag{5.13c}$$

Now, the probability (5.8) is restated as follows:

$$P\left(\mathbf{R}_{12},\mathbf{R}_{13},\mathbf{R}_{14}\right)=\int W_{n_{15}}^{\mathrm{C}}(|\mathbf{R}_{15}|)W_{n_{52}}^{\mathrm{C}}(|\mathbf{R}_{52}|)W^{\mathrm{R}}(|\mathbf{R}_{56}|)W_{n_{63}}^{\mathrm{C}}(|\mathbf{R}_{63}|)W_{n_{64}}^{\mathrm{C}}(|\mathbf{R}_{64}|)$$
$$\times\,\delta(\mathbf{R}_{12}-\mathbf{R}_{15}-\mathbf{R}_{52})\delta(\mathbf{R}_{13}-\mathbf{R}_{15}-\mathbf{R}_{56}-\mathbf{R}_{63})\delta(\mathbf{R}_{14}-\mathbf{R}_{15}-\mathbf{R}_{56}-\mathbf{R}_{64})$$
$$\times\,\mathrm{d}\mathbf{R}_{15}\,\mathrm{d}\mathbf{R}_{52}\,\mathrm{d}\mathbf{R}_{56}\,\mathrm{d}\mathbf{R}_{63}\,\mathrm{d}\mathbf{R}_{64},\tag{5.14}$$

where the constraints (5.13) are enforced through three-dimensional Dirac delta functions $\delta(\mathbf{r})$. It can be readily verified that the above integration can be transformed back into Equation (5.8) by applying the sifting property of the three-dimensional Dirac delta function, together with a change of variables. By utilizing the following property of the three-dimensional Dirac delta function,

$$\delta(\mathbf{r})=(2\pi)^{-3}\int\exp\left[-\boldsymbol{i}\mathbf{k}\cdot\mathbf{r}\right]\mathrm{d}\mathbf{k},\tag{5.15}$$

where $\boldsymbol{i}=\sqrt{-1}$ is the imaginary unit, and rearranging the integration in (5.14), we obtain the following expression:

$$P\left(\mathbf{R}_{12},\mathbf{R}_{13},\mathbf{R}_{14}\right)=$$
$$(2\pi)^{-9}\int\overline{W_{n_{15}}^{\mathrm{C}}}(|\mathbf{k}_{12}+\mathbf{k}_{13}+\mathbf{k}_{14}|)\overline{W_{n_{52}}^{\mathrm{C}}}(|\mathbf{k}_{12}|)\overline{W^{\mathrm{R}}}(|\mathbf{k}_{13}+\mathbf{k}_{14}|)\overline{W_{n_{63}}^{\mathrm{C}}}(|\mathbf{k}_{13}|)\overline{W_{n_{64}}^{\mathrm{C}}}(|\mathbf{k}_{14}|)$$
$$\times\exp\left[-\boldsymbol{i}\mathbf{k}_{12}\cdot\mathbf{R}_{12}\right]\exp\left[-\boldsymbol{i}\mathbf{k}_{13}\cdot\mathbf{R}_{13}\right]\exp\left[-\boldsymbol{i}\mathbf{k}_{14}\cdot\mathbf{R}_{14}\right]\mathrm{d}\mathbf{k}_{12}\mathrm{d}\mathbf{k}_{13}\mathrm{d}\mathbf{k}_{14}.\tag{5.16}$$

In the above formulation, the bar over a symbol denotes the Fourier transform of the function defined as:

$$\overline{W}(\mathbf{k})=\int W(\mathbf{r})\exp\left(\boldsymbol{i}\mathbf{k}\cdot\mathbf{r}\right)\mathrm{d}\mathbf{r}.\tag{5.17}$$

For the rigid rod with length a, the Fourier transform of Equation (5.2) gives rise to

$$\overline{W^{\mathrm{R}}}(|\mathbf{k}|)=\frac{\sin|\mathbf{k}|a}{|\mathbf{k}|a},\tag{5.18}$$

and $|\mathbf{k}|=\sqrt{\mathbf{k}\cdot\mathbf{k}}$.

5.2.4 Gaussian coil approximation

Thus far, the probability distribution has been expressed in the form of five layers of integration, involving a substantial numerical burden. In this section, it will be shown that Gaussian approximation of coils can significantly simplify the calculations.

The probability distribution function of the Gaussian phantom network (with no rods) has been obtained by Flory [9] using real space representation. In Appendix D.1, the same network is formulated with the aid of Fourier transform and it is shown that the result has an analytical closed form. Likewise, the integration described in (5.16) can be simplified by assuming a Gaussian distribution for coils 15, 52, 63, and 46. Suppose that $W_n^{\mathrm{C}}(r)$ follows a Gaussian distribution (5.1). Then, the Fourier transform of Equation (5.1) is given as

$$\overline{W_n^{\mathrm{C}}}(|\mathbf{k}|) = \exp\left[\frac{-nb^2\,|\mathbf{k}|^2}{6}\right]. \tag{5.19}$$

Let us represent the vectors $\mathbf{R}_{ij}$ and $\mathbf{k}_{ij}$ in the Cartesian coordinate system respectively with unit vectors $(\hat{\mathbf{i}}, \hat{\mathbf{j}}, \hat{\mathbf{k}})$ and $(\hat{\mathbf{e}}_x, \hat{\mathbf{e}}_y, \hat{\mathbf{e}}_z)$ as

$$\mathbf{R}_{ij} = (R_{ij})_x\,\hat{\mathbf{i}} + (R_{ij})_y\hat{\mathbf{j}} + (R_{ij})_z\,\hat{\mathbf{k}}, \tag{5.20a}$$

$$\mathbf{k}_{ij} = (k_{ij})_x\,\hat{\mathbf{e}}_x + (k_{ij})_y\,\hat{\mathbf{e}}_y + (k_{ij})_z\,\hat{\mathbf{e}}_z. \tag{5.20b}$$

Now, by defining the matrices

$$\mathbf{K}^{\mathrm{T}} = \{(k_{12})_x \quad (k_{12})_y \quad (k_{12})_z \quad (k_{13})_x \quad (k_{13})_y \quad (k_{13})_z \quad (k_{14})_x \quad (k_{14})_y \quad (k_{14})_z\}, \tag{5.21a}$$

$$\mathbf{R}^{\mathrm{T}} = \{(R_{12})_x \quad (R_{12})_y \quad (R_{12})_z \quad (R_{13})_x \quad (R_{13})_y \quad (R_{13})_z \quad (R_{14})_x \quad (R_{14})_y \quad (R_{14})_z\}, \tag{5.21b}$$

with label T denotes the transpose of the matrix, the integration (5.16) is simplified to the following compact form:

$$P\,(\mathbf{R}_{12}, \mathbf{R}_{13}, \mathbf{R}_{14}) = (2\pi)^{-9} \int \overline{W^{\mathrm{R}}}(\sqrt{\mathbf{K}^{\mathrm{T}}\boldsymbol{\Lambda}\mathbf{K}})\exp\Big[-\frac{1}{2}\mathbf{K}^{\mathrm{T}}\boldsymbol{\Gamma}\mathbf{K} - \boldsymbol{i}\mathbf{R}^{\mathrm{T}}\mathbf{K}\Big]\mathrm{d}\mathbf{K}, \tag{5.22}$$

where

$$\mathbf{\Gamma} = \frac{b^2}{3}\begin{pmatrix} (n_{15}+n_{52})\,[\mathbf{I}]_{3\times3} & n_{15}\,[\mathbf{I}]_{3\times3} & n_{15}\,[\mathbf{I}]_{3\times3} \\ n_{15}\,[\mathbf{I}]_{3\times3} & (n_{15}+n_{63})\,[\mathbf{I}]_{3\times3} & n_{15}\,[\mathbf{I}]_{3\times3} \\ n_{15}\,[\mathbf{I}]_{3\times3} & n_{15}\,[\mathbf{I}]_{3\times3} & (n_{15}+n_{64})\,[\mathbf{I}]_{3\times3} \end{pmatrix}, \tag{5.23}$$

and

$$\mathbf{\Lambda} = \begin{pmatrix} [\mathbf{0}]_{3\times3} & [\mathbf{0}]_{3\times3} & [\mathbf{0}]_{3\times3} \\ [\mathbf{0}]_{3\times3} & [\mathbf{I}]_{3\times3} & [\mathbf{I}]_{3\times3} \\ [\mathbf{0}]_{3\times3} & [\mathbf{I}]_{3\times3} & [\mathbf{I}]_{3\times3} \end{pmatrix}. \tag{5.24}$$

In the above relations, $[\mathbf{I}]_{3\times3}$ and $[\mathbf{0}]_{3\times3}$ respectively denote the 3×3 identity and zero matrices. Furthermore, let us define the change of variable

$$\mathbf{Y} = \mathbf{A}\mathbf{K} \tag{5.25}$$

where

$$\mathbf{Y}^{\mathrm{T}} = \{(k_{12})_x \quad (k_{12})_y \quad (k_{12})_z \quad (k_{13})_x \quad (k_{13})_y \quad (k_{13})_z \quad w_x \quad w_y \quad w_z\}, \tag{5.26}$$

$$\mathbf{w} = w_x\hat{\mathbf{e}}_x + w_y\hat{\mathbf{e}}_y + w_z\hat{\mathbf{e}}_z, \tag{5.27}$$

and

$$\mathbf{A} = \begin{pmatrix} [\mathbf{I}]_{3\times3} & [\mathbf{0}]_{3\times3} & [\mathbf{0}]_{3\times3} \\ [\mathbf{0}]_{3\times3} & [\mathbf{I}]_{3\times3} & [\mathbf{0}]_{3\times3} \\ [\mathbf{0}]_{3\times3} & [\mathbf{I}]_{3\times3} & [\mathbf{I}]_{3\times3} \end{pmatrix}. \tag{5.28}$$

Since $\det\mathbf{A} = 1$, the integration (5.22) is rewritten as:

$$P\left(\mathbf{R}_{12},\mathbf{R}_{13},\mathbf{R}_{14}\right) = (2\pi)^{-9}\int \frac{\sin(\sqrt{\mathbf{w}^{\mathrm{T}}\mathbf{w}}\,a)}{\sqrt{\mathbf{w}^{\mathrm{T}}\mathbf{w}}\,a}\exp\Big[-\frac{1}{2}\mathbf{Y}^{\mathrm{T}}\tilde{\mathbf{\Gamma}}\mathbf{Y} - \boldsymbol{i}\tilde{\mathbf{R}}^{\mathrm{T}}\mathbf{Y}\Big]\mathrm{d}\mathbf{Y}, \tag{5.29}$$

where

$$\tilde{\mathbf{\Gamma}} = \mathbf{A}^{-\mathrm{T}}\mathbf{\Gamma}\mathbf{A}^{-1} = \frac{b^2}{3}\begin{pmatrix} (n_{15}+n_{52})\,[\mathbf{I}]_{3\times3} & [\mathbf{0}]_{3\times3} & n_{15}\,[\mathbf{I}]_{3\times3} \\ [\mathbf{0}]_{3\times3} & (n_{63}+n_{64})\,[\mathbf{I}]_{3\times3} & -n_{64}\,[\mathbf{I}]_{3\times3} \\ n_{15}\,[\mathbf{I}]_{3\times3} & -n_{64}\,[\mathbf{I}]_{3\times3} & (n_{15}+n_{64})\,[\mathbf{I}]_{3\times3} \end{pmatrix}, \tag{5.30}$$

and $\tilde{\mathbf{R}} = \mathbf{A}^{-\mathrm{T}}\mathbf{R}$, i.e.,

$$\tilde{\mathbf{R}}^{\mathrm{T}} = \{(R_{12})_x \quad (R_{12})_y \quad (R_{12})_z \quad (R_{43})_x \quad (R_{43})_y \quad (R_{43})_z \quad (R_{14})_x \quad (R_{14})_y \quad (R_{14})_z\}. \tag{5.31}$$

Label -T in the superscript represents the inverse transpose of the matrix. Based on the results provided in Appendix D.2 (Equation (D.16) with $p = 3$), Equation (5.29) can be written in a closed form:

$$P(\mathbf{R}_{12}, \mathbf{R}_{13}, \mathbf{R}_{14}) = \sqrt{\frac{\tilde{\zeta}_{33}}{(2\pi)^9 \det\tilde{\mathbf{\Gamma}}_{\mathrm{aa}}}} \frac{1}{a\left|\tilde{\mathbf{L}}\right|} \exp\left[-\frac{1}{2}\left(\tilde{\mathbf{R}}_{\mathrm{a}}^{\mathrm{T}}\tilde{\mathbf{\Gamma}}_{\mathrm{aa}}^{-1}\tilde{\mathbf{R}}_{\mathrm{a}}\right) - \frac{\tilde{\zeta}_{33}}{2}\left(a^2 + \left|\tilde{\mathbf{L}}\right|^2\right)\right] \sinh\left[a\left|\tilde{\mathbf{L}}\right|\tilde{\zeta}_{33}\right], \tag{5.32}$$

in which

$$\tilde{\mathbf{\Gamma}}_{\mathrm{aa}}^{-1} = \frac{3}{b^2}\begin{pmatrix} (n_{15}+n_{52})^{-1}[\mathbf{I}]_{3\times3} & [\mathbf{0}]_{3\times3} \\ [\mathbf{0}]_{3\times3} & (n_{63}+n_{64})^{-1}[\mathbf{I}]_{3\times3} \end{pmatrix}, \tag{5.33a}$$

$$\tilde{\mathbf{R}}_{\mathrm{a}}^{\mathrm{T}} = \{(R_{12})_x \quad (R_{12})_y \quad (R_{12})_z \quad (R_{43})_x \quad (R_{43})_y \quad (R_{43})_z\}, \tag{5.33b}$$

$$\tilde{\mathbf{L}} = \frac{n_{63}}{n_{63}+n_{64}}\mathbf{R}_{14} + \frac{n_{64}}{n_{63}+n_{64}}\mathbf{R}_{13} - \frac{n_{15}}{n_{15}+n_{52}}\mathbf{R}_{12}, \tag{5.33c}$$

$$\tilde{\zeta}_{33} = \frac{3}{b^2}\frac{(n_{15}+n_{52})(n_{63}+n_{64})}{n_{52}n_{63}n_{64} + n_{15}(n_{63}n_{64} + n_{52}(n_{63}+n_{64}))}, \tag{5.33d}$$

$$\det\tilde{\mathbf{\Gamma}}_{\mathrm{aa}} = \frac{b^{12}}{3^6}(n_{15}+n_{52})^3(n_{63}+n_{64})^3. \tag{5.33e}$$

The position vectors $\mathbf{R}_{12}$, $\mathbf{R}_{13}$, and $\mathbf{R}_{14}$ along with the geometric interpretation of $\tilde{\mathbf{L}}$ are shown in Figs. 5.3a and 5.3b.

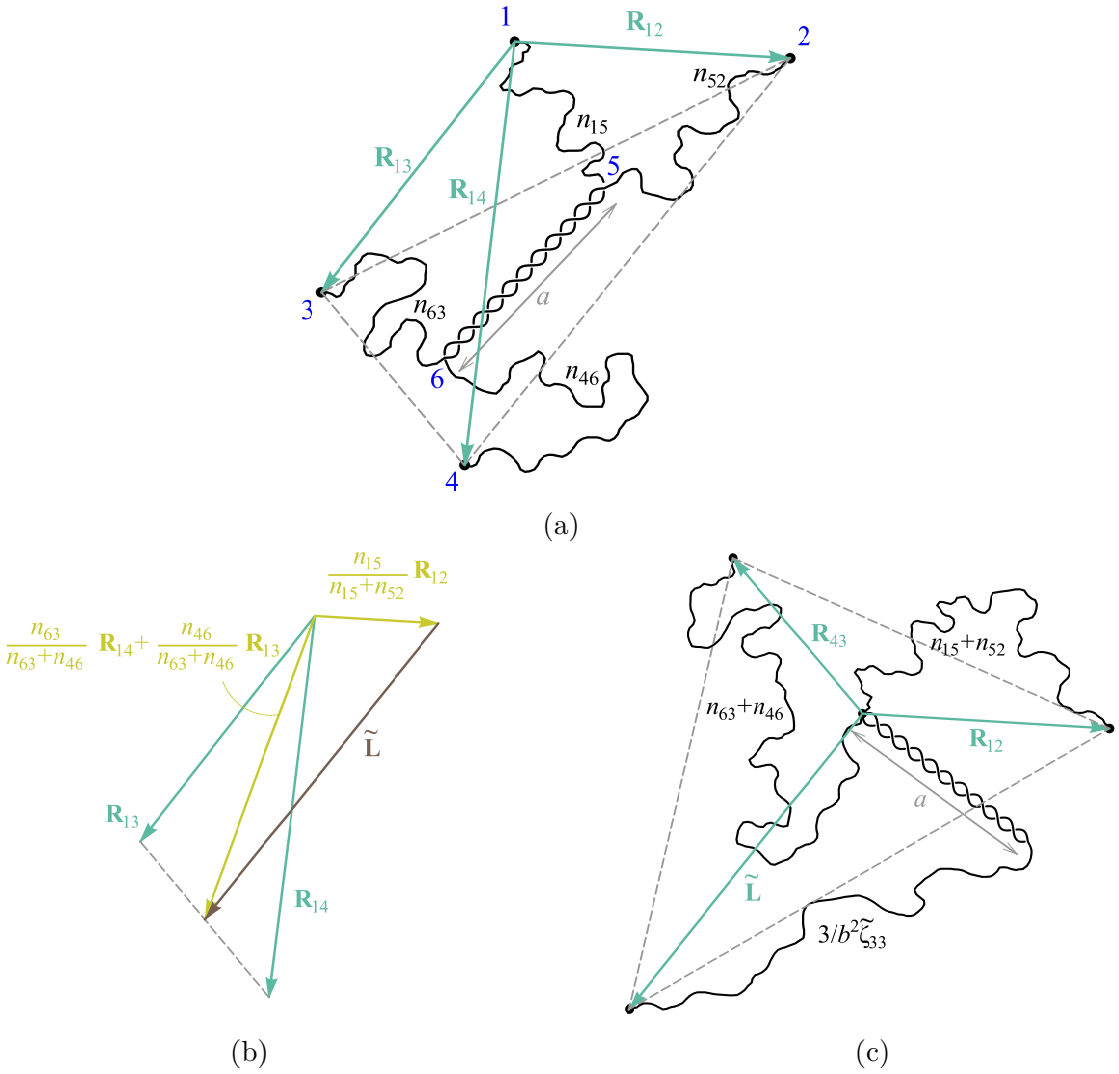

Figure 5.3: (a) The topology of the four-node coil-rod structure with rod length a and corresponding end-to-end vectors $\mathbf{R}_{12}$, $\mathbf{R}_{13}$, and $\mathbf{R}_{14}$. (b) The Geometric interpretation of $\tilde{\mathbf{L}}$ in (5.33c). (c) The equivalent network model with three chains: one two-node coil-rod and two pure coils based on Equation (5.34).

The probability distribution of the four-node coil-rod structure can be generalized to p-node structure with one rod as shown in Appendix D.3. Based on the interpretation given in Appendix D.3, p-node structure with one rod can be decomposed to $p-1$ coils and one two-node coil-rod structure fixated between $p+1$ nodes. For the simple case of four-node coil-rod structure, as shown in Fig. 5.3c, the associated probability distribution can be decomposed to three chains: one two-node coil-rod

structure with rod length a, $\dfrac{3}{b^2\tilde{\zeta}_{33}}$ Kuhn segments in the coil and end-to-end vector $\tilde{\mathbf{L}}$; one Gaussian coil with $n_{15}+n_{52}$ Kuhn segments and end-to-end vector $\mathbf{R}_{12}$; and the other Gaussian coil with $n_{63}+n_{64}$ Kuhn segments and end-to-end vector $\mathbf{R}_{43}$. With the aid of (5.3) and (5.1), the probability distribution function (5.32) is rewritten as:

$$P\left(\mathbf{R}_{12},\mathbf{R}_{13},\mathbf{R}_{14}\right)=W^{\mathrm{C}}_{n_{15}+n_{52}}\left(|\mathbf{R}_{12}|\right)W^{\mathrm{C}}_{n_{63}+n_{64}}\left(|\mathbf{R}_{43}|\right)W^{\mathrm{CR}}_{3b^{-2}\tilde{\zeta}_{33}^{-1}}\left(\left|\tilde{\mathbf{L}}\right|\right). \tag{5.34}$$

The above representation not only makes the notation simpler but also lays the solid base for comparing the present models with models in the literature based on two-node coil-rod structure and pure coils. Now suppose that the chains 15 and 52, as well as chains 63 and 46 are identical such that $n_{15}=n_{52}=n$ and $n_{63}=n_{46}=n+2m^*$, where n is the number of Kuhn segments in chains 15 and 52, while $2m^*$ indicates the extra number of segments 46 and 63 compared to 15 and 52. Then, Equations (5.33c) and (5.33d) can be further simplified to

$$\tilde{\mathbf{L}}=\frac{1}{2}\left(\mathbf{R}_{14}+\mathbf{R}_{13}-\mathbf{R}_{12}\right), \tag{5.35a}$$

$$\tilde{\zeta}_{33}=\frac{3}{\left(n+m^*\right)b^2}. \tag{5.35b}$$

Therefore, Equation (5.34) is rewritten as

$$P\left(\mathbf{R}_{12},\mathbf{R}_{13},\mathbf{R}_{14}\right)=W^{\mathrm{C}}_{2n}\left(|\mathbf{R}_{12}|\right)W^{\mathrm{C}}_{2n+4m^*}\left(|\mathbf{R}_{43}|\right)W^{\mathrm{CR}}_{n+m^*}\left(\frac{1}{2}\left|\mathbf{R}_{14}+\mathbf{R}_{13}-\mathbf{R}_{12}\right|\right). \tag{5.36}$$

5.3 Application: in-plane placement of four nodes

As mentioned earlier, once the probability distribution is established, the mechanical response of the gel can be determined by placing the four-node coil-rod structure within a macroscopic network with specific geometry. In this manner, the macroscopic deformation can be properly translated to the constituent structure. To examine the features of the four-node coil-rod structure, a simple scenario is considered where the four nodes are placed in the same plane in the form of a rectangular cell as seen in

Fig. 5.4a. It should be noted that while the nodes form a two-dimensional cell, the chains can occupy the three-dimensional space.

Referring to Fig. 5.4a, suppose the nodes 1 to 4 are initially positioned at the vertices of a rectangle with edge lengths of l_1 and l_2. To avoid any unnecessary complexity, the number of Kuhn segments of all coils is set to be equal to n. Deformations are assumed to be applied such that the principal stretches λ_1 and λ_2 align with the horizontal and vertical edges of the rectangle. By setting the Cartesian coordinate system at node 1 with coordinate axes along the rectangle edges, the position vectors of the nodes of the deformed cell can be expressed as:

$$\mathbf{R}_1 = (0,0,0), \qquad \mathbf{R}_2 = (\lambda_1 l_1, 0, 0), \qquad \mathbf{R}_3 = (\lambda_1 l_1, \lambda_2 l_2, 0), \qquad \mathbf{R}_4 = (0, \lambda_2 l_2, 0), \tag{5.37}$$

where setting $\lambda_1 = \lambda_2 = 1$ reverts the cell to its undeformed state. Such representation is capable of capturing any in-plane deformations including shear and extension within the plane $x_1 x_2$. By replacing (5.37) in Equation (5.36), and considering an equal number of Kuhn segments n for the coils ($m^* = 0$), one can conclude that

$$P(\mathbf{R}_{13}, \mathbf{R}_{13}, \mathbf{R}_{14}) = W_n^{\mathrm{CR}}(\lambda_2 l_2) W_{2n}^{\mathrm{C}}(\lambda_1 l_1) W_{2n}^{\mathrm{C}}(\lambda_1 l_1). \tag{5.38}$$

Now, by substitution of Equation (5.38) into Equations (5.4) and (5.5), the Helmholtz free energy can be calculated as follows:

$$\Psi + \Psi_0 = -G \ln \left[l_1^2 \lambda_1^2 l_2 \lambda_2 \right] - G \ln \left[\sinh \left(\frac{3a \lambda_2 l_2}{n b^2} \right) \right] + \frac{3G}{2nb^2} \left(l_1^2 \lambda_1^2 + l_2^2 \lambda_2^2 \right), \tag{5.39}$$

in which $G = \varrho k_B T$. Ψ_0 is the Helmholtz free energy where $\lambda_1 = \lambda_2 = 1$ so that the condition $\Psi(\lambda_1 = \lambda_2 = 1) = 0$ is imposed. For coil-rod structure with $n = 25$ and $a = 5\,b$, the contour of $(\Psi + \Psi_0)/G$ is depicted in Fig. 5.4b as a function of $\lambda_1 l_1 / b$ and $\lambda_2 l_2 / b$. The minimum value of Helmholtz free energy is indicated by the red point on the contour. By setting $\lambda_1 = \lambda_2 = 1$ in the reference state, this point signifies the initial stress-free state.

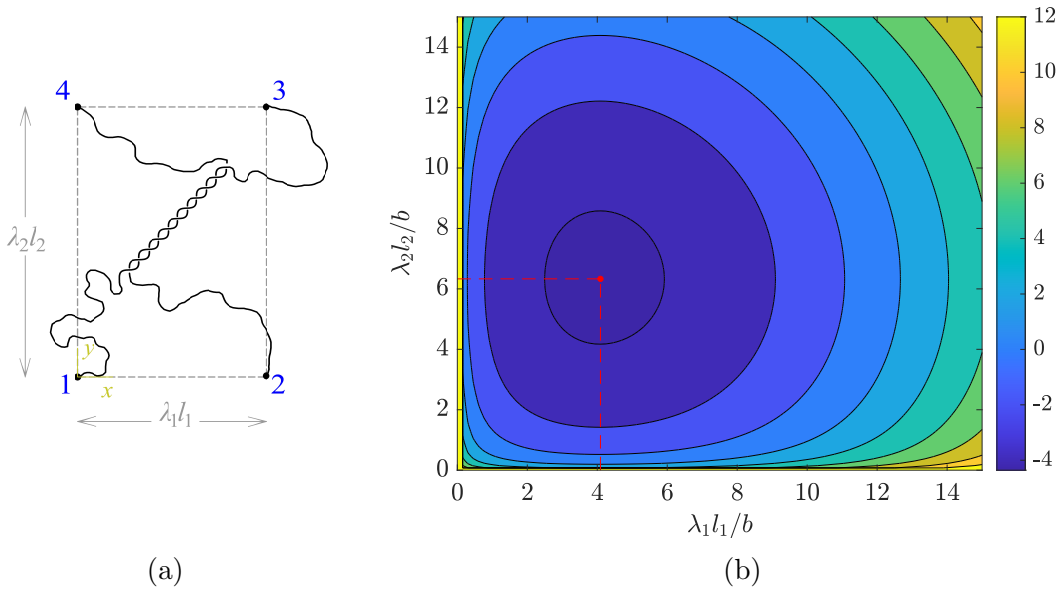

(a) (b)

Figure 5.4: (a) The four-node coil-rod structure with the four nodes placed in the same plane in a rectangular manner with dimensions $\lambda_1 l_1$ and $\lambda_2 l_2$. (b) The Helmholtz free energy contour $(\Psi + \Psi_0)/G$ of the four-node structure with $n = 25$, $a = 5\,b$, showing the minimum at $l_1\lambda_1 = 4.09\,b$ and $l_2\lambda_2 = 6.33\,b$.

Based on the free energy (5.39), Equation (5.6) is simplified to

$$P_1 = \frac{\partial \Psi}{\partial \lambda_1} = G\left(\frac{3l_1^2\lambda_1}{nb^2} - \frac{2}{\lambda_1}\right), \tag{5.40}$$

$$P_2 = \frac{\partial \Psi}{\partial \lambda_2} = G\left(\frac{3l_2^2\lambda_2}{nb^2} - \frac{1}{\lambda_2} - \frac{3al_2}{nb^2}\coth\left[\frac{3al_2\lambda_2}{nb^2}\right]\right). \tag{5.41}$$

Clearly, the Gaussian coils decouple the behavior of the system along the two principal directions, such that P_1 and P_2 depend solely on λ_1 and λ_2, respectively. This is due to the fact that the Gaussian probability function always gives nonzero values even for large extensions. In reality, approaching the fully extended state in one principal direction triggers the deformation along other principal directions and this cannot be achieved through Gaussian distribution. By the same token, the formulation highlights that P_1 remains unaffected by the values of a because the average position of the rod aligns with the vertical axis. The above stress components can be set to

zero for $\lambda_1 = \lambda_2 = 1$ to ensure that the initial state is stress-free. Hence,

$$l_1 = \sqrt{\frac{2}{3}}nb, \tag{5.42a}$$

$$\frac{3l_2^2}{nb^2} - \frac{3al_2}{nb^2}\coth\left[\frac{3al_2}{nb^2}\right] = 1. \tag{5.42b}$$

Equation (5.42b) is an implicit function of a and typically requires numerical computations. However, for $a > \sqrt{nb^2}$, the following approximation can be utilized:

$$l_2 = \frac{a}{2} + \frac{\sqrt{3a^2 + 4nb^2}}{\sqrt{12}}. \tag{5.43}$$

In this case, as $n \to 0$, $l_2 \to a$ verifying that the pure rod with no coil forms a rectangle with dimension $l_1 = 0$ and $l_2 = a$. Additionally, by applying Padé approximation about $a = 0$ to the second order for $\coth(x)$, one can show that

$$l_2 = \sqrt{\frac{nb^2}{6a^2}}\sqrt{7a^2 - 5nb^2 + \sqrt{25n^2b^4 - 30a^2nb^2 + 49a^4}} \tag{5.44}$$

holds for $a < 0.5\sqrt{nb^2}$. For $a \ll \sqrt{nb^2}$, $l_2 \to l_1$, in this case the stress-free state of the rectangular cell becomes a square for the four-node structure with a junction point rather than a junction zone. For $a = 5\,b$ and $n = 25$, $l_2 = 1.27\sqrt{nb^2}$ and $l_1 = 0.82\sqrt{nb^2}$, corresponding to the values that minimize the Helmholtz free energy in Fig. 5.4b for $\lambda_1 = \lambda_2 = 1$.

5.3.1 Applicability of Gaussian approximation

As it was alluded to, the applicability of Gaussian coils in the freely-jointed chain model is constrained to small extensions of the coils and a large number of Kuhn segments. To assess the validity of such approximation in determining l_1 and l_2, the exact Helmholtz free energy of the system is minimized based on Equation (5.11) combined with (5.4) and (5.5). To obtain the exact result, all chains 15, 52, 63, and 46 in Equation (5.11) with the same number of Kuhn segments n, are assumed to obey the following non-Gaussian probability distribution (see Chapter 2)

$$W^{\mathrm{C}}_{n_{15}}(r) = W^{\mathrm{C}}_{n_{52}}(r) = W^{\mathrm{C}}_{n_{63}}(r) = W^{\mathrm{C}}_{n_{46}}(r) = \frac{A_0\beta}{r}\left(\frac{\sinh\beta}{\beta}\right)^n \exp\left[-\frac{\beta r}{b}\right], \tag{5.45}$$

with

$$\beta = \mathscr{L}^{-1}\left(\frac{r}{nb}\right), \tag{5.46}$$

and A_0 being the normalization factor. $\mathscr{L}(x) = \coth x - 1/x$ denotes the Langevin function and to calculate its inverse, the Padé approximation [14] is utilized. The five-tuple integration (5.11) in our analysis is performed by employing the adaptive quadrature techniques [15]. To obtain l_1 and l_2 associated with the minimum free energy, the differential evolution algorithm [16] is adopted, with a convergence tolerance of 0.01. The initial length l_1 and l_2 are depicted vs. n for $a = 5\,b$ in Figs. 5.5a and 5.5b, respectively where the results are compared with the Gaussian approximation (5.42a) and (5.42b). It can be inferred that the Gaussian approximation can be satisfactorily applied to determine l_1 and l_2.

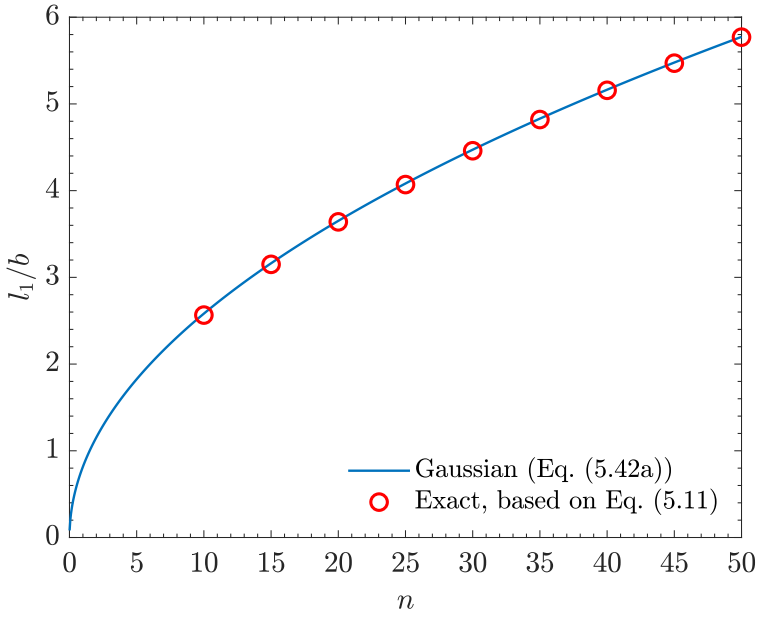

(a)

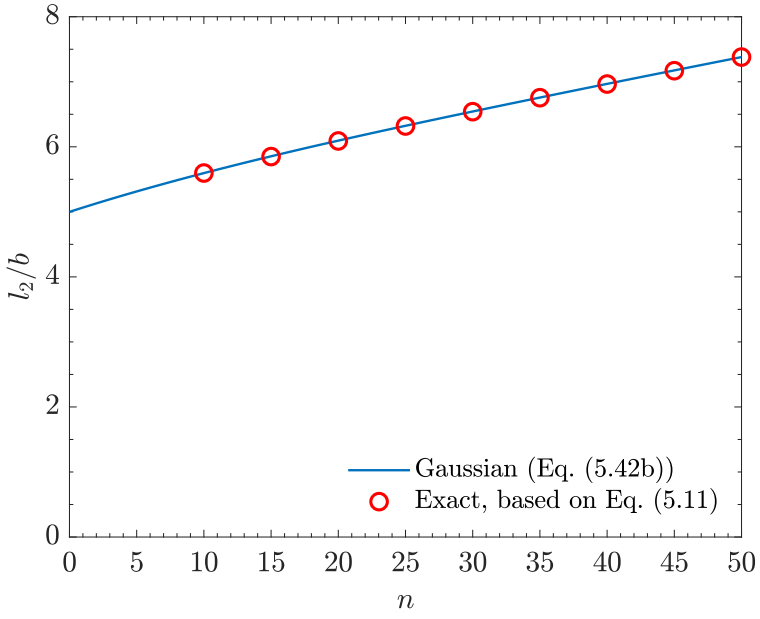

(b)

Figure 5.5: (a) l_1 vs. n, (b) l_2 vs. n for $a = 5\,b$. Comparison is made between the Gaussian appproximations (5.42a) and (5.42b) and exact result based on Equation (5.11).

Now, the performance of the constitutive relations (5.40) and (5.41) should be compared with the exact result. As mentioned earlier, after calculation of the exact Helmholtz free energy via Equations (5.11), (5.4), (5.5), and (5.45), the stress components can be determined through Equation (5.6). These results serve as the basis for evaluation. Since the numerical calculation burden of (5.11) is heavy, the biaxial test is preferred over the uniaxial test. In the biaxial test, P_1 and P_2 are directly given by known λ_1 and λ_2, unlike the uniaxial test, which requires solving for unknown stretches to achieve zero stress in the direction perpendicular to the loading axis. The values of P_1/G against λ_1 is illustrated for $\lambda_2 = 1$, $n = 25$ and $a = 5\,b$ in Fig. 5.6a. Acknowledging the solid blue curve as the exact representation, the Gaussian result from distribution (5.38) (Equation (5.40)) shows minimal error and reliability in compression ($\lambda_1 < 1$). This holds true in tension as well, up to the extension of $\lambda_1 = 3$. Beyond this point, due to significant elongation of the coils within the cell, the Gaussian approximation diverges from the blue curve. The performance of Gaussian approximation is similar in the other direction, as demonstrated in Fig. 5.6b for the biaxial test along direction 2 with $\lambda_1 = 1$, $n = 25$ and $a = 5\,b$. In this experiment, the rod effect is more dominant, resulting in higher stiffness under both tension ($\lambda_2 > 1$) and compression ($\lambda_2 < 1$) compared to direction 1. Similar to direction 1, Gaussian approximations in (5.38) hold true in compression. However, the results deviate from the solid blue curve at $\lambda_2 > 2$.

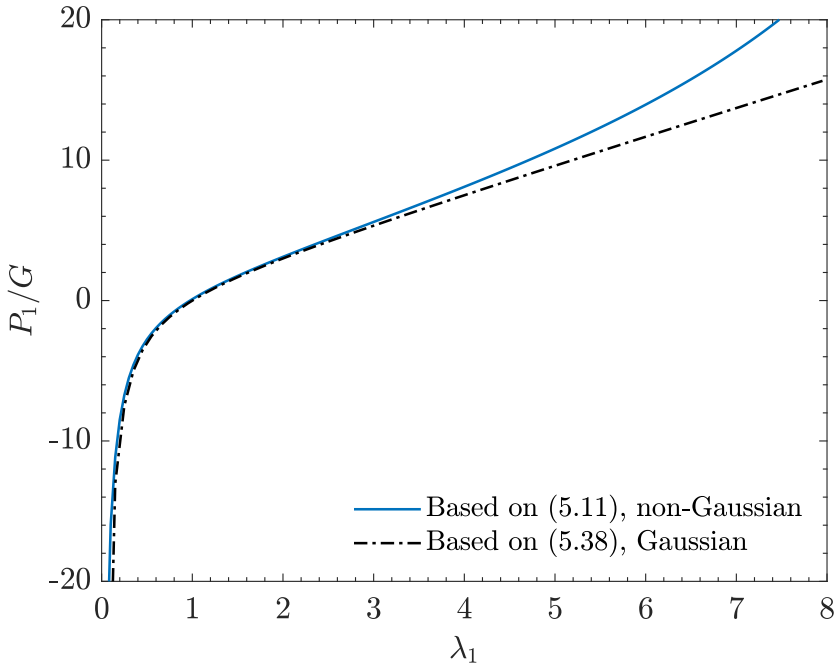

(a)

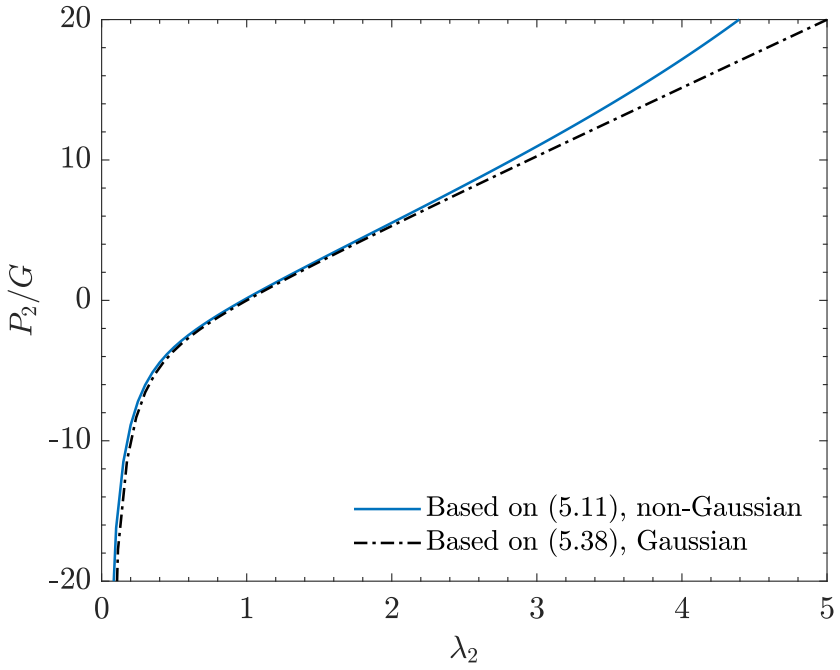

(b)

Figure 5.6: The normalized principal stress vs. the principal stretch for biaxial test and $a = 5\,b$, $l_2 = 6.33\,b$, $l_1 = 4.09\,b$ with and without Gaussian approximation, (a) P_1/G vs. λ_1 with $\lambda_2 = 1$ (b) P_2/G vs. λ_2 with $\lambda_1 = 1$.

5.3.2 Inclusion of unzipping

So far, the four-node coil-rod structure has been developed based on the assumption of a fixed number of Kuhn segments in the coils (denoted as n if all four coils are identical) and a fixed rod length a. However, studies have shown that the junction zones in disordered biopolymer gels may shrink when the gel is subjected to loading. To account for this phenomenon, known as unzipping, the conditions of fixed n and a are relaxed, allowing segments in the rod to be transferred to the coils while conserving the total number of segments in the entire system. The grand canonical ensemble is used to enable segment exchange, and the partition function in this ensemble is formulated. Based on Chapter 3, this partition function is expressed as a summation of different configurations with fixed n (or fixed a), with the Boltzmann weight. Once the partition function is established, the determination of entropy, free energy, and stress-stretch relations follows the same procedure as in the previous sections.

Let us focus on the configuration in Fig. 5.4a, where all coils in the four-node coil-rod structure have the same number of Kuhn segments n and the rod length is a. If the fully dissociated state of the four-node coil-rod structure contains two coils, each having N Kuhn segments, then the conservation of segments for the structure implies that there are $N - 2n$ Kuhn segments in the rod. It is further postulated that each Kuhn segment, which has a length of b in the coil, changes to a new length of αb when it becomes part of the rod structure. In this case, the rod length can be represented as $a = (N - 2n)\alpha b$. Now, let ε denote the energy needed to liberate one Kuhn segment from the rod into the coil. The energy of a four-node coil-rod structure with n Kuhn segments in the coil and rod length $(N - 2n)\alpha b$ can then be written as $-(N - 2n)\varepsilon$. For this specific configuration, the designation of energy enables us to recognize the value of Boltzmann factor as $\exp\left[\dfrac{(N - 2n)\varepsilon}{k_B T}\right]$. On the other hand, the probability distribution function of this configuration can be given by Equation (5.38) using Gaussian statistics. Thus, the probability distribution of

this configuration weighted by the Boltzmann factor is given by

$$W_n^{\mathrm{CR}}(\lambda_2 l_2) W_{2n}^{\mathrm{C}}(\lambda_1 l_1) W_{2n}^{\mathrm{C}}(\lambda_1 l_1) \exp\left[\frac{(N-2n)\,\varepsilon}{k_B T}\right]. \tag{5.47}$$

If the available configurations of four-node coil-rod structure are restricted to those with equal Kuhn segments for all coils, then varying the variable n allows for the exploration of all possible configurations. In other words, segment exchange between the coils and the rod is only permitted simultaneously from both ends of the rod, ensuring that the coils remain identical. Under this assumption, n is supposed to start from a minimum allowable Kuhn segment $n_{\min}$ in each of the four coils. Furthermore, n can take a maximum value of $N/2-1$, in which case the rod with two Kuhn segments maintains a minimum length of $2\alpha b$. Further symmetric migration of segments from the rod ends to the coils results in a fully dissociated state, where the two pure coils, each with N Kuhn segments, are no longer connected through the rod and thus behave independently. For this dissociated configuration, the distribution function weighted by Boltzmann factor is given by

$$\left[W_N^{\mathrm{C}}(\lambda_2 l_2)\right]^2, \tag{5.48}$$

where the associated Boltzmann factor is one due to the vanishing rod. Moreover, the power of two arises from the presence of two independent pure coils.

Summing the expressions (5.47) from $n_{\min}$ to $N/2-1$ and (5.48) yields the grand canonical partition function as

$$\Omega(\lambda_1, \lambda_2) = \left[W_N^{\mathrm{C}}(\lambda_2 l_2)\right]^2 + \sum_{n=n_{\min}}^{N/2-1} W_n^{\mathrm{CR}}(\lambda_2 l_2) W_{2n}^{\mathrm{C}}(\lambda_1 l_1) W_{2n}^{\mathrm{C}}(\lambda_1 l_1) \exp\left[\frac{(N-2n)\,\varepsilon}{k_B T}\right]. \tag{5.49}$$

The above formulation not only models the unzipping of the system due to the rod shrinkage but also considers the transition from the four-node coil-rod structure to the two fully dissociated pure coils. After obtaining the grand canonical ensemble, the entropy per unit reference volume is obtained as

$$S = c + \varrho k_B \ln\left[\mathrm{d}\mathbf{R}_{12}\,\mathrm{d}\mathbf{R}_{13}\,\mathrm{d}\mathbf{R}_{14}\right] + \varrho k_B \ln \Omega(\lambda_1, \lambda_2). \tag{5.50}$$

Applying (5.5) together with (5.37) results in

$$\Psi + \Psi_0 = -G \ln \left[l_1^2 \lambda_1^2 l_2^2 \lambda_2^2 \right] - G \ln \Omega \left(\lambda_1, \lambda_2 \right). \tag{5.51}$$

The first term on the right-hand side represents the free energy associated with the change in the area of the rectangular cell. Now, the stress-stretch relation can be obtained from (5.6). Unlike (5.39), it can be seen that P_1 and P_2 during unzipping are functions of both λ_1 and λ_2.

Fig. 5.7 illustrates the unzipping phenomenon under a uniaxial test for the four-node coil-rod structure with $n_{\min} = 25$, $N = 60$, $\alpha = 0.5$, and $\varepsilon = 5k_BT$ (solid curves), along with the fully dissociated state with no rod, $N = 60$ (dotted-dashed curves), and the fixed four-node coil-rod structure with $n = 25$ (dashed curves). The reference state is set as $l_1 = 4.09\,b$ and $l_2 = 55.15\,b$, corresponding to $n_{\min} = 25$ and $a = (N-2n)\alpha b = 55\,b$. Plot 5.7a shows the normalized values of P_1/G vs. λ_1. The solid curve follows the dashed curve up to $\lambda_1 = 23.21$, indicating that the rod length remains fixed with $n = 25$. Beyond this point, the solid curve diverges, signaling the onset of unzipping. The decreasing trend in the stress continues up to $\lambda_1 = 27.87$. After this point, the plot experiences a sharp drop toward zero stress, indicating the transition from the four-node structure to the fully dissociated state. This phenomenon is more clearly illustrated in Plot 5.7b, where the number n that contributed most to the sum in Equation (5.49), denoted by n_0, is plotted against λ_1. $n_0 = 80$ designates the fully dissociated chains and is equivalent to $N = 160$. The fixed n_0 from $\lambda_1 = 1$ to 23.21 indicates that the structure's configuration remains unchanged. Beyond this point, the increase in n_0 from 25 to 28 shows that unzipping occurs and the rod shrinks accordingly up to $\lambda_1 = 27.87$. The sudden increase to $n_0 = 80$ indicates that the contribution from the dissociated state becomes predominant, leading to full dissociation of the junction zone. Further extension shows that the system follows the dotted-dashed curve, where the two pure coils extend independently. In Plot 5.7c, the stretch λ_2 is depicted against the prescribed λ_1 by solving $P_2 = 0$. As shown

in Equations (5.40) and (5.41), the stress versus stretch of the four-node coil-rod structure with fixed n is decoupled. Hence, the stretch λ_2 is not affected by stretching along λ_1. This is demonstrated by the horizontal dashed curve and dash-dotted curve, where $\lambda_2 = 1$ for the four-node coil-rod structure with fixed $n = 25$, and $\lambda_2 = 0.13$ for the fully dissociated two-node coil-rod structure. By activating unzipping, the solid curve experiences a smooth transition from $\lambda_2 = 1$ at $\lambda_1 = 23.21$ to $\lambda_2 = 0.85$ at $\lambda_1 = 27.87$. During full dissociation, this transition becomes sharper, approaching $\lambda_2 = 0.13$. While the example in Fig. 5.7 shows a gradual unzipping process prior to full dissociation, this can change with different parameter values. For example, Fig. 5.8 depicts the same plots for the same variables, but with N decreased from 160 to 60 ($a = 5$). The initial state is set as $l_1 = 4.09\,b$ and $l_2 = 6.33\,b$. In this case, as shown in Plot 5.8a, full dissociation occurs in a sudden fashion, without any gradual unzipping behavior is observed. Compared to Fig. 5.7a, the sudden drop occurs at a smaller stretch, $\lambda_1 = 6.7$. Plot 5.8b also confirms that the transition from $n = 25$ to $n = 30$ leads the system to prefer the fully dissociated state, bypassing the intermediate unzipping states with a finite rod. The same interpretation applies to λ_2 vs. λ_1 in Plot. 5.8c where the sharp decrease is observed due to full dissociation.

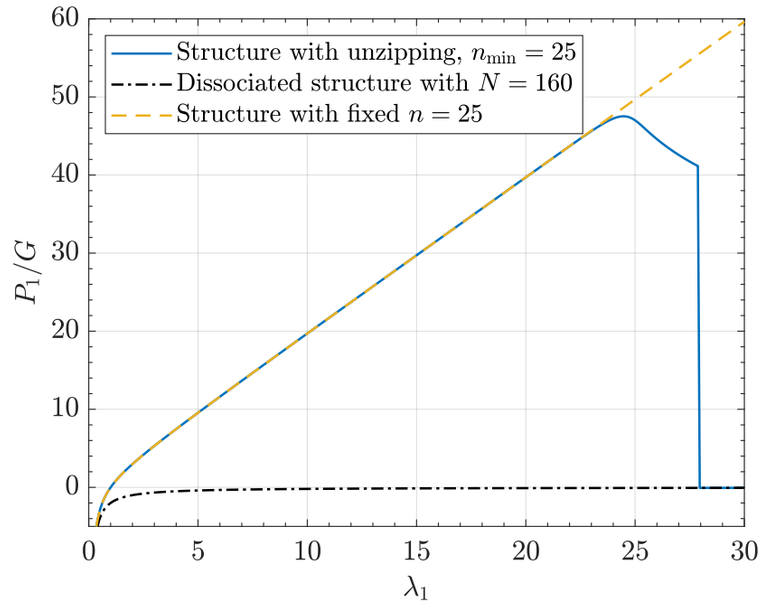

(a)

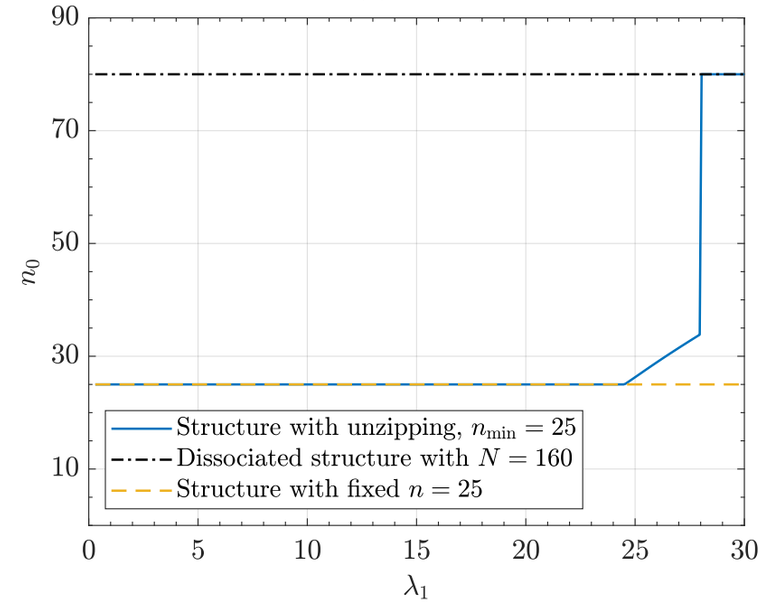

(b)

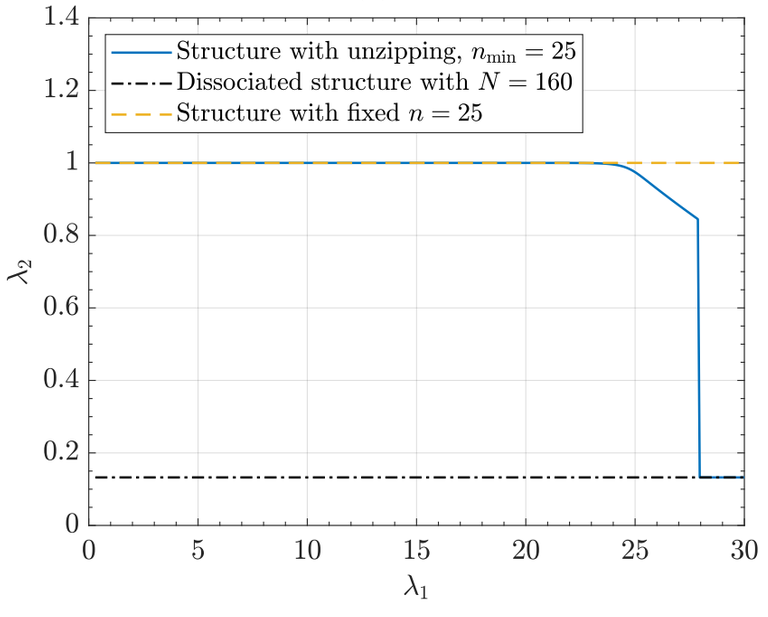

(c)

Figure 5.7: Uniaxial test allowing unzipping with $n_{\min} = 25$, $N = 160$, $\alpha = 0.5$, $\varepsilon = 5k_BT$: (a) The normalized principal stress P_1/G vs. λ_1, (b) the number n that contributes most to the sum in Equation (5.49), n_0, vs. λ_1, (c) the principal stretch λ_2 vs. λ_1.

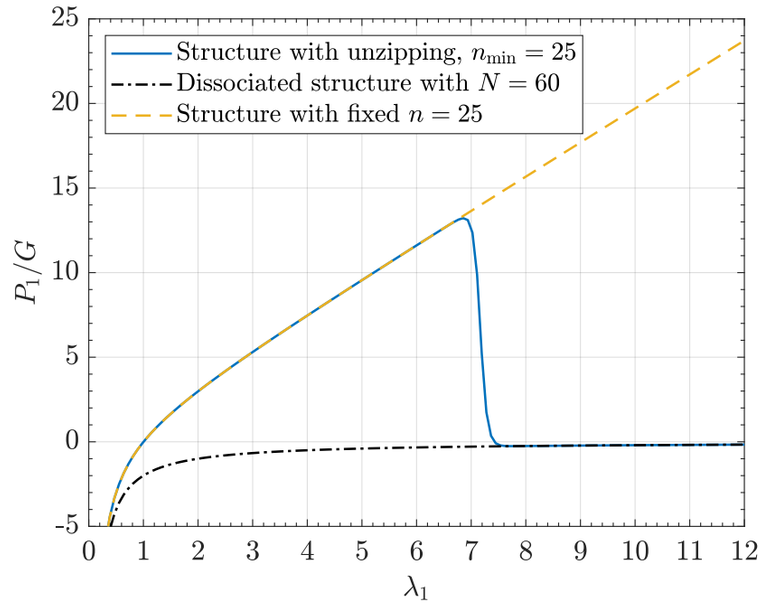

(a)

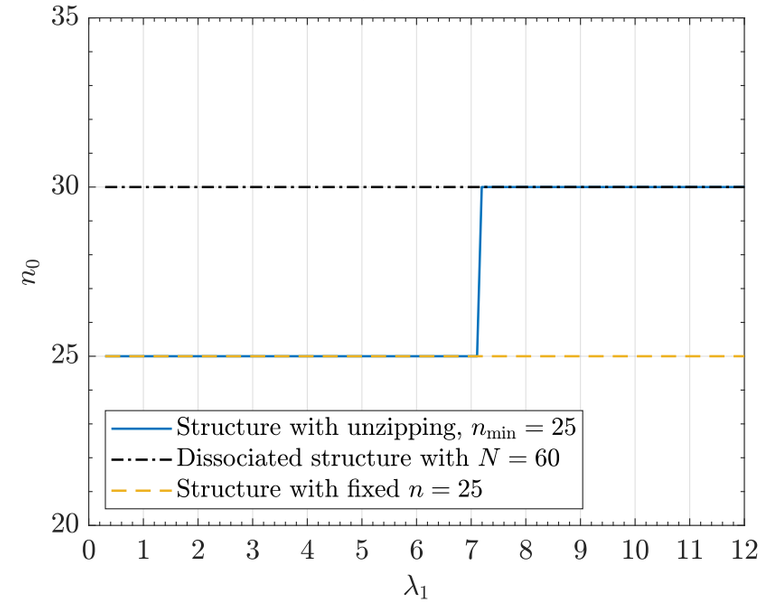

(b)

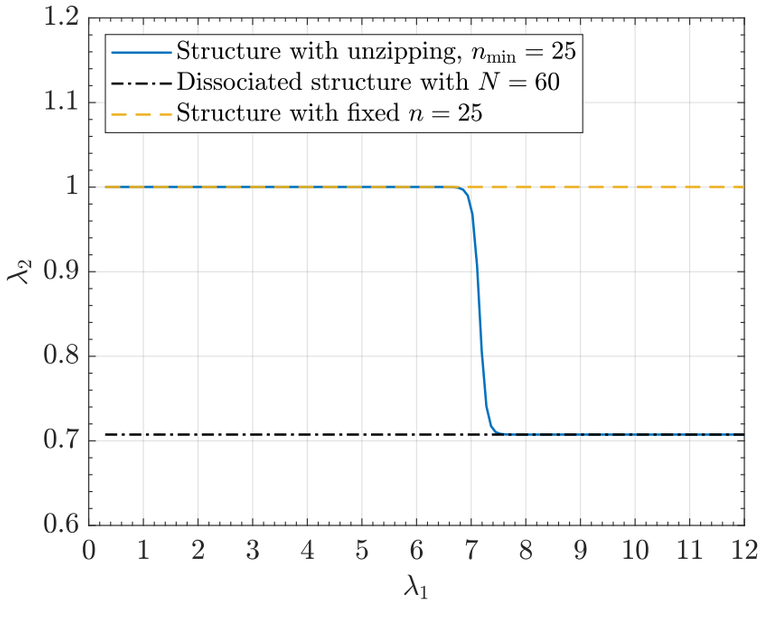

(c)

Figure 5.8: Uniaxial test allowing unzipping with $n_{\min} = 25$, $N = 60$, $\alpha = 0.5$, $\varepsilon = 5k_BT$: (a) The normalized principal stress P_1/G vs. λ_1, (b) the number n that contributes most to the sum in Equation (5.49), n_0, vs. λ_1, (c) the principal stretch λ_2 vs. λ_1.

5.4 Discussion

Based on the formulation in Section 5.3, the four-node coil-rod structure shown in Fig. 5.4a can be incorporated into the three-dimensional network to account for more general deformation states. One example is shown in Fig. 5.9, where identical four-node coil-rod structures are placed, with different orientations, on three faces of the rectangular prism: 1234, 1256, and 1458. Suppose that the principal stretches are aligned with the prism edges. The arrangement of the four-node coil-rod structures is such that the length of the cell for $\lambda_1 = \lambda_2 = \lambda_3 = 1$ has a cube shape in the stress-free state. In the Cartesian coordinate system fixed at the centre of the cell, the positions of $\mathbf{R}_i$ are specified as follows:

$$\begin{aligned}
\mathbf{R}_1 &= \left(-\frac{h\lambda_1}{2}, -\frac{h\lambda_2}{2}, -\frac{h\lambda_3}{2}\right), & \mathbf{R}_2 &= \left(\frac{h\lambda_1}{2}, -\frac{h\lambda_2}{2}, -\frac{h\lambda_3}{2}\right), \\
\mathbf{R}_3 &= \left(\frac{h\lambda_1}{2}, \frac{h\lambda_2}{2}, -\frac{h\lambda_3}{2}\right), & \mathbf{R}_4 &= \left(-\frac{h\lambda_1}{2}, \frac{h\lambda_2}{2}, -\frac{h\lambda_3}{2}\right), \\
\mathbf{R}_5 &= \left(-\frac{h\lambda_1}{2}, -\frac{h\lambda_2}{2}, \frac{h\lambda_3}{2}\right), & \mathbf{R}_6 &= \left(\frac{h\lambda_1}{2}, -\frac{h\lambda_2}{2}, \frac{h\lambda_3}{2}\right), \\
\mathbf{R}_7 &= \left(\frac{h\lambda_1}{2}, \frac{h\lambda_2}{2}, \frac{h\lambda_3}{2}\right), & \mathbf{R}_8 &= \left(-\frac{h\lambda_1}{2}, \frac{h\lambda_2}{2}, \frac{h\lambda_3}{2}\right).
\end{aligned} \tag{5.52}$$

Similar to (5.4), the entropy of the deformed cell per unit reference volume can be written as

$$\begin{aligned}
S = c &+ \varrho k_B \ln \left[(\mathrm{d}\mathbf{R}_{12})^2 \, \mathrm{d}\mathbf{R}_{13} \, (\mathrm{d}\mathbf{R}_{14})^2 \, (\mathrm{d}\mathbf{R}_{15})^2 \, \mathrm{d}\mathbf{R}_{16} \, \mathrm{d}\mathbf{R}_{18}\right] \\
&+ \varrho k_B \ln \left[P(\mathbf{R}_{12}, \mathbf{R}_{15}, \mathbf{R}_{16}) P(\mathbf{R}_{15}, \mathbf{R}_{14}, \mathbf{R}_{18}) P(\mathbf{R}_{14}, \mathbf{R}_{12}, \mathbf{R}_{13})\right].
\end{aligned} \tag{5.53}$$

By setting $\Psi(\lambda_1 = \lambda_2 = \lambda_3 = 1) = 0$ and using (5.5), it can be shown that

$$\begin{aligned}
\Psi = -\Psi_0 - G \ln \left[h^3 \lambda_1 \lambda_2 \lambda_3\right] - \frac{G}{3} \ln \left[\sinh\left(\frac{3ah\lambda_1}{nb^2}\right) \sinh\left(\frac{3ah\lambda_2}{nb^2}\right) \sinh\left(\frac{3ah\lambda_3}{nb^2}\right)\right] \\
+ \frac{Gh^2}{nb^2}\left(\lambda_1^2 + \lambda_2^2 + \lambda_3^2\right),
\end{aligned} \tag{5.54}$$

and Ψ_0 is the free energy of the stress-free state. Now by using (5.6), the principal components of stress are

$$P_i = G\left(\frac{-1}{\lambda_i} + \frac{2h^2\lambda_i}{nb^2} - \frac{ah}{nb^2}\coth\left[\frac{3ah\lambda_i}{nb^2}\right]\right), \qquad i = 1, 2, 3. \tag{5.55}$$

Analogous to the treatment in Section 5.3, the stress-free state at $\lambda_1 = \lambda_2 = \lambda_3 = 1$ can provide the value of h obtained by solving the following equation:

$$\frac{2h^2}{nb^2} - \frac{ah}{nb^2}\coth\left[\frac{3ah}{nb^2}\right] = 1. \tag{5.56}$$

By decomposing the four-node coil-rod structure positioned at each prism face into one coil-rod and two coil structures, one can conclude that the three-dimensional network model is equivalent to the summation of three three-chain networks (Fig. 5.9): one containing three two-node coil-rod structures on the prism edges, each having rod length a and n Kuhn segments in the coil; and two identical networks each containing three Gaussian coils with $2n$ Kuhn segments. The overall interaction of these three networks yields the Helmholtz free energy (5.54).

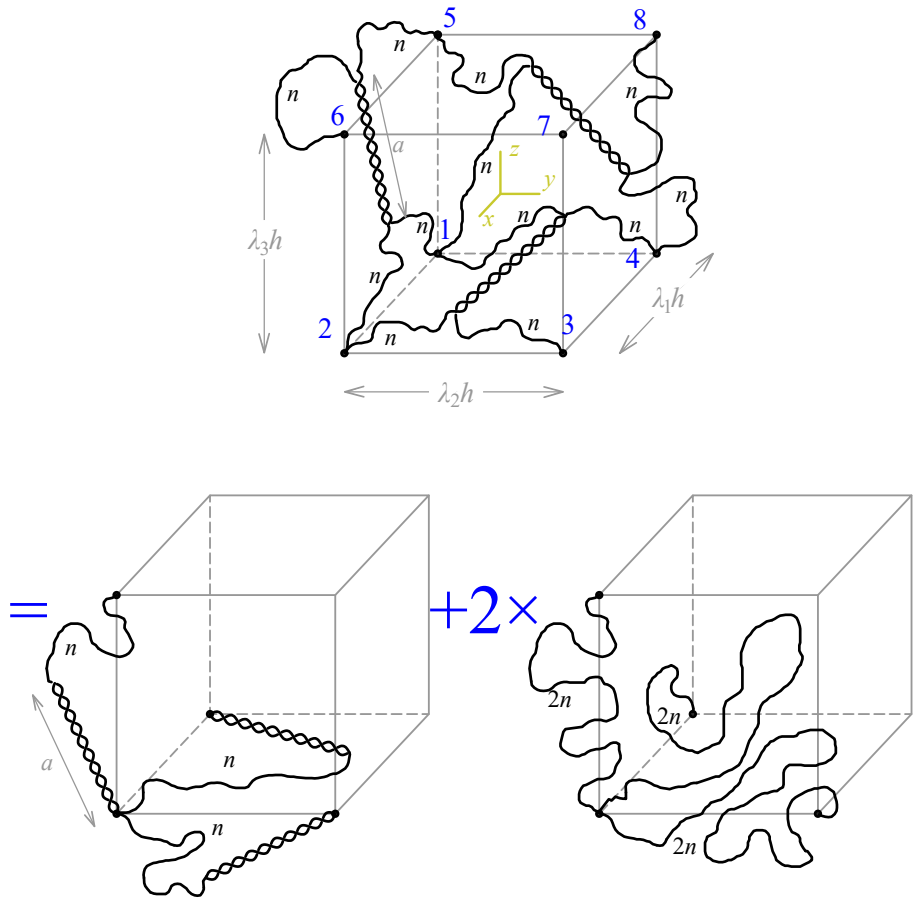

Figure 5.9: The topology of the four-chain coil-rod structure in the faces of the rectangular prism which is equivalent to combination of three three-chain networks.

In the literature, there is a correspondence between three-chain network models and a well-known type of material referred to as Valanis-Landel [17], where the strain energy is written as the sum of three scalar functions, each evaluated independently for three principal stretches. Due to the simplicity of this model, there are some generalizations for such network models, as shown by Ehret and Stracuzzi [18]. However, more involved network models, such as the eight-chain model, demonstrate superior performance in handling different types of experiments [6]. The comparison and relationship between the three-chain model and the eight-chain model are provided by Carroll [19] for pure coils without the presence of a junction zone. To examine the performance of the proposed chain network model (Fig. 5.9), first we formulate

the eight-chain network model of the Gaussian coil-rod structure based on Chapter 3. Following the original model of Arruda and Boyce [6], eight two-node coil-rod structures are placed inside a diagonals of the cell with edges $\lambda_1 h$, $\lambda_2 h$, and $\lambda_3 h$. The probability of finding a two-node coil-rod with one end fixed at the center and the other inside the volume element $\mathrm{d}\mathbf{R}_7$ is given by $W_n^{\mathrm{CR}}\left(|\mathbf{R}_7|\right)\mathrm{d}\mathbf{R}_7$. Likewise, the probability of the other seven chains is established. Therefore, the entropy of the deformed state per unit volume is given by:

$$S = c + \varrho k_B \ln\left[\mathrm{d}\mathbf{R}_7\right] + \varrho k_B \ln W_n^{\mathrm{CR}}\left(|\mathbf{R}_7|\right). \tag{5.57}$$

Now by applying (5.5), and relation (5.52), one can conclude that

$$\begin{aligned}&\Psi + \Psi_0 = \\ &- G\ln[h^3\lambda_1\lambda_2\lambda_3] - G\ln\left[\frac{\sinh\left(\dfrac{3ah}{2nb^2}\sqrt{\lambda_1^2+\lambda_2^2+\lambda_3^2}\right)}{\sqrt{\lambda_1^2+\lambda_2^2+\lambda_3^2}}\right] + \frac{3Gh^2}{8nb^2}\left(\lambda_1^2+\lambda_2^2+\lambda_3^2\right),\end{aligned} \tag{5.58}$$

where Ψ_0 is the Helmholtz free energy at $\lambda_1 = \lambda_2 = \lambda_3 = 1$ yielding $\Psi(\lambda_1 = \lambda_2 = \lambda_3 = 1) = 0$. By employing (5.6), the principal components of stress are written as

$$\begin{aligned}&P_i = G\left(-\frac{1}{\lambda_i} + \frac{3h^2\lambda_i}{4nb^2} + \frac{\lambda_i}{\lambda_1^2+\lambda_2^2+\lambda_3^2} - \frac{3ah\lambda_i}{2nb^2}\frac{\coth\left[\dfrac{3ah}{2nb^2}\sqrt{\lambda_1^2+\lambda_2^2+\lambda_3^2}\right]}{\sqrt{\lambda_1^2+\lambda_2^2+\lambda_3^2}}\right),\\ &i = 1,2,3.\end{aligned} \tag{5.59}$$

Setting $P_1 = P_2 = P_3 = 0$ for $\lambda_1 = \lambda_2 = \lambda_3 = 1$ gives rise to the following relation between h, a, and $\sqrt{n}\,b$:

$$\frac{2}{3} = \frac{3h^2}{4nb^2} - \frac{\sqrt{3}ah}{2nb^2}\coth\left(\frac{3\sqrt{3}ah}{2nb^2}\right). \tag{5.60}$$

Using the above relation, the initial stress-free state of the network with cube edge length h can be determined for given values of a and n.

Fig. 5.10 illustrates the difference between P_1 vs. λ_1 in the uniaxial test for Equations (5.55) and (5.59) with $a = 5\,b$ and $n = 25$. To ensure a fair comparison, for

Equation (5.55), $G = 0.73$ kPa, while for (5.59), $G = 1$ kPa, such that the shear modulus (curve slope) of the biopolymer networks is identical at $\lambda_1 = \lambda_2 = 1$. Furthermore, the values of h are obtained by solving Equations (5.56) and (5.60) as $h = 5.00\,b$ and $h = 8.40\,b$, respectively. Although, in compression the results show indistinguishable behavior, in tension the eight-chain two-node coil-rod structure exhibits larger stress for $\lambda_1 > 1.9$. The results are also compared with the eight-chain non-Gaussian coil-rod structure proposed in Chapter 4, as shown by the dotted curve. Non-Gaussian effects emerge when the sample is stretched beyond $\lambda_1 = 2.0$, while the results remain consistent under compression. Based on these results, it can be observed that the overall behavior of the proposed network model is similar to that of the eight-chain network model when Gaussian statistics are assumed for the coils. Based on the current framework, it is also possible to construct other three-dimensional network models, such as the symmetric eight-node structure with a rod, as elaborated in Appendix D.3. However, a more detailed comparison between different networks requires testing them on real disordered biopolymer gels, where various mechanical tests are conducted on the samples.

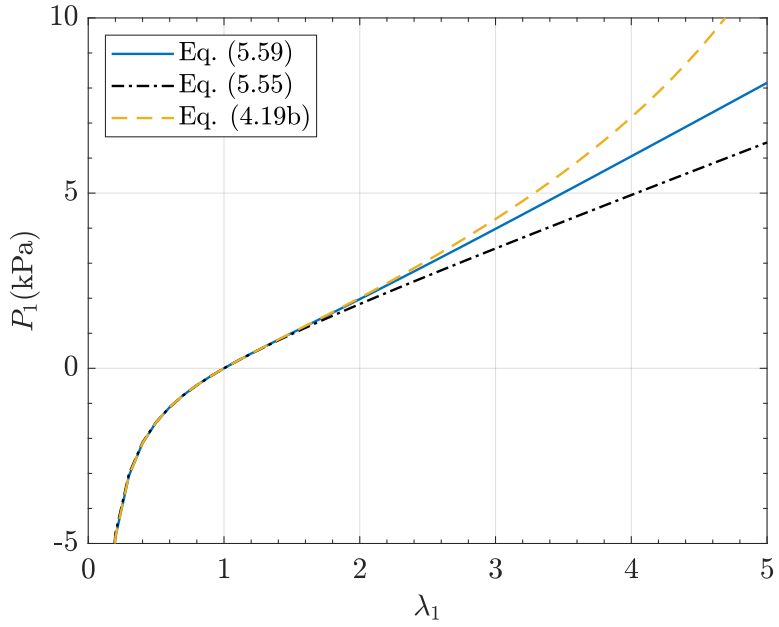

Figure 5.10: P_1 vs. λ_1 in the uniaxial test with $a = 5\,b$ and $n = 25$. For Equation (5.55), $G = 0.73$ kPa and $h = 5.00\,b$, while for the eight-chain network (Equation (5.59) and Equation (4.19b)), $G = 1$ kPa and $h = 8.40\,b$.

As shown in Section 5.3, the promising formulation of unzipping can also be extended to the three-dimensional network in Fig. 5.9. This extension can account for unzipping in different principal directions, leading to anisotropic effects – a property still unaddressed in the developed eight-chain network models in Chapter 4. The sharp drop during dissociation observed in Fig. 5.8 can also be related to the failure point of the macroscopic sample and will be examined in future studies.

The current study aimed to provide explicit modeling of interactions within junction zones, and it can be concluded that under the Gaussian statistics assumption, the two-node coil-rod structure network can be effectively applied. It should be recalled that the phantom network model assumes that components can easily pass through each other. Therefore, the interaction between coils and rods can be extended by considering long-range interaction effects, such as excluded volume effects or entanglement between components [20–22], which would render the governing for-

mulation more realistic but also computationally more challenging. Additionally, the current results are based on the presence of a single rod within the system. For a more comprehensive generalization, the inclusion of multiple rods and their associated configurations needs to be considered. In the latter case, the unzipping behavior of different rods is another intriguing subject that warrants future investigation.

5.5 Conclusion

The present work provides preliminary insight into modeling junction zones and their explicit interactions with the amorphous regions in disordered biopolymer gels. The previous model of a two-node coil-rod structure is generalized to a four-node coil-rod structure, where two chains intertwine to form a common rod as a junction zone. The probability distribution function in the context of a phantom network is developed, which is mathematically more involved than the two-node coil-rod structure. Nevertheless, within the Gaussian statistics of the coils, the analytical probability distribution function can be derived with the aid of Fourier transform. It is demonstrated that, under this assumption, the four-node coil-rod structure is equivalent to a collection of two coils and one two-node coil-rod structure situated inside an affine network. This argument can also be generalized to multiple Gaussian coils sharing a single rod. To examine the characteristics of this structure, the four nodes are placed on the same plane to form a rectangular cell. The stress-stretch relationship of this network is derived, and the applicability of the Gaussian distribution is evaluated through comparison with the exact distribution. Additionally, by introducing the grand canonical ensemble, the unzipping of the junction zone is incorporated into the constitutive relation. Lastly, a three-dimensional network model is developed by arranging the four-node coil-rod structures on the faces of a rectangular prism. Results from this model is compared with the eight-chain network model combined with two-node coil-rod structure developed in Chapter 3, which confirms that the network model with the two-node coil-rod structure is suitable for investigating the

effects of more explicit interactions between coils and rods, as long as the Gaussian approximation for the coils remains valid. Moreover, the proposed model provides a systematic framework for developing more complex networks that involve collections of coils connected by multiple rods.

Acknowledgements

TT acknowledges financial support from the Natural Sciences and Engineering Research Council of Canada (NSERC; Grant numbers: RGPIN-2018-04281, RGPAS-2018-522655) and Canada Research Chairs Program (Grant number: TIER1 2021-00023). HM acknowledges scholarship support from Alberta Innovates.

References

[1] M. Zhong, R. Wang, K. Kawamoto, B. D. Olsen, and J. A. Johnson, "Quantifying the impact of molecular defects on polymer network elasticity," *Science*, vol. 353, no. 6305, pp. 1264–1268, 2016. DOI: 10.1126/science.aag0184. eprint: https://www.science.org/doi/pdf/10.1126/science.aag0184.

[2] H. M. James and E. Guth, "Theory of the increase in rigidity of rubber during cure," *The Journal of Chemical Physics*, vol. 15, no. 9, pp. 669–683, 1947. DOI: 10.1063/1.1746626. eprint: https://doi.org/10.1063/1.1746626.

[3] M. C. Wang and E. Guth, "Statistical theory of networks of non-gaussian flexible chains," *The Journal of Chemical Physics*, vol. 20, no. 7, pp. 1144–1157, 1952. DOI: 10.1063/1.1700682. eprint: https://doi.org/10.1063/1.1700682.

[4] P. Wu and E. Van Der Giessen, "On improved network models for rubber elasticity and their applications to orientation hardening in glassy polymers," *Journal of the Mechanics and Physics of Solids*, vol. 41, no. 3, pp. 427–456, 1993, ISSN: 0022-5096. DOI: https://doi.org/10.1016/0022-5096(93)90043-F.

[5] M. Itskov, A. E. Ehret, and R. Dargazany, "A full-network rubber elasticity model based on analytical integration," *Mathematics and Mechanics of Solids*, vol. 15, no. 6, pp. 655–671, 2010. DOI: 10.1177/1081286509106441.

[6] E. M. Arruda and M. C. Boyce, "A three-dimensional constitutive model for the large stretch behavior of rubber elastic materials," *Journal of the Mechanics and Physics of Solids*, vol. 41, no. 2, pp. 389–412, 1993, ISSN: 0022-5096. DOI: https://doi.org/10.1016/0022-5096(93)90013-6.

[7] M. C. Boyce and E. M. Arruda, "Swelling and mechanical stretching of elastomeric materials," *Mathematics and Mechanics of Solids*, vol. 6, no. 6, pp. 641–659, 2001. DOI: 10.1177/108128650100600605. eprint: https://doi.org/10.1177/108128650100600605.

[8] C. Miehe, S. Göktepe, and F. Lulei, "A micro-macro approach to rubber-like materials—part I: The non-affine micro-sphere model of rubber elasticity," *Journal of the Mechanics and Physics of Solids*, vol. 52, no. 11, pp. 2617–2660, 2004, ISSN: 0022-5096. DOI: https://doi.org/10.1016/j.jmps.2004.03.011.

[9] P. J. Flory, "Statistical thermodynamics of random networks," *Proceedings of the Royal Society of London. A. Mathematical and Physical Sciences*, vol. 351, no. 1666, pp. 351–380, 1976. DOI: 10.1098/rspa.1976.0146. eprint: https://royalsocietypublishing.org/doi/pdf/10.1098/rspa.1976.0146.

[10] S. B. Ross-Murphy, "Physical gelation of biopolymers," *Food Hydrocolloids*, vol. 1, no. 5, pp. 485–495, 1987, Special issue: 2nd International Workshop on Plant Polysaccharides, ISSN: 0268-005X. DOI: https://doi.org/10.1016/S0268-005X(87)80047-4.

[11] A. H. Clark and S. B. Ross-Murphy, "Structural and mechanical properties of biopolymer gels," in *Biopolymers*, Berlin, Heidelberg: Springer Berlin Heidelberg, 1987, pp. 57–192, ISBN: 978-3-540-47827-0.

[12] P. G. Higgs and R. C. Ball, "Some ideas concerning the elasticity of biopolymer networks," *Macromolecules*, vol. 22, no. 5, pp. 2432–2437, 1989. DOI: 10.1021/ma00195a073. eprint: https://doi.org/10.1021/ma00195a073.

[13] R. Ogden, *Non-linear Elastic Deformations* (Dover Civil and Mechanical Engineering). Dover Publications, 1997, ISBN: 9780486696485.

[14] A. Cohen, "A padé approximant to the inverse langevin function," *Rheologica acta*, vol. 30, pp. 270–273, 1991.

[15] W. H. Press, S. A. Teukolsky, W. T. Vetterling, and B. P. Flannery, *Numerical Recipes: The Art of Scientific Computing*, 3rd. Cambridge University Press, 2007.

[16] S. Das and P. N. Suganthan, "Differential evolution: A survey of the state-of-the-art," *IEEE Transactions on Evolutionary Computation*, vol. 15, no. 1, pp. 4–31, 2011. DOI: 10.1109/TEVC.2010.2059031.

[17] K. C. Valanis and R. F. Landel, "The Strain-Energy Function of a Hyperelastic Material in Terms of the Extension Ratios," *Journal of Applied Physics*, vol. 38, no. 7, pp. 2997–3002, Jun. 1967, ISSN: 0021-8979. DOI: 10.1063/1.1710039. eprint: https://pubs.aip.org/aip/jap/article-pdf/38/7/2997/18342417/2997_1_online.pdf.

[18] A. E. Ehret and A. Stracuzzi, "Variations on ogden's model: Close and distant relatives," *Philosophical Transactions of the Royal Society A: Mathematical, Physical and Engineering Sciences*, vol. 380, no. 2234, p. 20 210 322, 2022. DOI: 10.1098/rsta.2021.0322. eprint: https://royalsocietypublishing.org/doi/pdf/10.1098/rsta.2021.0322.

[19] M. M. Carroll, "Molecular chain networks and strain energy functions in rubber elasticity," *Philosophical Transactions of the Royal Society A: Mathematical, Physical and Engineering Sciences*, vol. 377, no. 2144, p. 20 180 067, 2019. DOI: 10.1098/rsta.2018.0067. eprint: https://royalsocietypublishing.org/doi/pdf/10.1098/rsta.2018.0067.

[20] R. J. Gaylord, "Entanglement and excluded volume effects in rubber elasticity," *Polymer Engineering & Science*, vol. 19, no. 4, pp. 263–266, 1979. DOI: https://doi.org/10.1002/pen.760190407. eprint: https://4spepublications.onlinelibrary.wiley.com/doi/pdf/10.1002/pen.760190407.

[21] M. Doi and N. Y. Kuzuu, "Nonlinear elasticity of rodlike macromolecules in condensed state," *Journal of Polymer Science: Polymer Physics Edition*, vol. 18, no. 3, pp. 409–419, 1980. DOI: https://doi.org/10.1002/pol.1980.180180301. eprint: https://onlinelibrary.wiley.com/doi/pdf/10.1002/pol.1980.180180301.

[22] R. Ball, M. Doi, S. Edwards, and M. Warner, "Elasticity of entangled networks," *Polymer*, vol. 22, no. 8, pp. 1010–1018, 1981, ISSN: 0032-3861. DOI: https://doi.org/10.1016/0032-3861(81)90284-6.

Chapter 6

Conclusions and Future Work

6.1 Conclusions

The present study aimed to provide a framework for modeling disordered bipolymer gels by considering, at the microscopic level, statistical mechanics of the constituting elements and, at the macroscopic level, the implementation of network models. In these gels, amorphous coils are interconnected through ordered regions known as junction zones. The behavior of junction zones is notably more intricate than that of cross-links in rubber-like materials, and they constitute significant portions of the network. Under applied loading, junction zones can change in length, leading to zipping/unzipping phenomena. Chapter 2 targets the modeling of the coils where a critical gap in the traditional development of the force-extension relationship for freely-jointed chain (FJC) is identified. A widely neglected error, although pointed out by Flory [1], is corrected by examining the different ensembles and their associated probability distributions. Subsequently, the significance of the accurate treatment is highlighted for the two-node coil-rod structure as a building block for the biopolymer gels. In Chapter 3, this consideration is applied to derive the partition function of the coil-rod structure without assuming the coil to be Gaussian. To address the zipping/unzipping phenomena within coil-rod structures, the grand canonical ensemble is used to allow for segment exchange between the coil and rod components. It is demonstrated that this approach predicts a force-extension relationship that captures

unzipping-induced relaxation, which successfully models the unwinding of a double-stranded DNA under force. In Chapter 4, the force-extension relationship of the coil-rod structure is utilized to establish the Helmholtz free energy for the eight-chain network model [2]. The end-to-end distance of the coil-rod structure in a stress-free network is thoroughly examined. It is demonstrated that to accurately determine the stress-free state, it is necessary to relax the assumption of incompressibility and allow for changes in volume. Subsequently, the statistical mechanics of solvent introduction and the effects of mixing are developed based on the Flory-Huggins theory [3, 4]. Using these considerations, the resulting stress-stretch relationship illustrates how unzipping within the coil-rod structure contribute to dissipation in disordered biopolymer gels and the presence of a permanent set after complete unloading. Experimental evidence is also validated for alginate gels, with material parameters within the model derived based on chemical structure combined with fitting. Formulations up to this point are based on the two-node coil-rod structure and the affinity assumption. To take a step closer to explicitly modeling the formation of junction zone from association of multiple coils, Chapter 5 extends the statistical mechanics of a four-node coil-rod structure, where two coils share the same rod. Compared to the two-node coil-rod structure, the governing partition function in this case is more complex and can only be simplified to a five-tuple integration. However, through the application of Gaussian coil statistics in conjunction with Fourier transform, the closed-form partition function was derived and generalized to any p-node structure sharing the same rod. Under these circumstances, it is demonstrated that the structure can be equivalently represented as a collection comprising one coil-rod and multiple coils in the affine network model. Finally, the four-node coil-rod structure is implemented into a network model to demonstrate its capability to describe bulk material behavior.

6.2 Future work

There exists substantial potential for further development of the framework explored in this study. In Chapter 3, the coil component of the coil-rod structure was modeled using the FJC model. However, more sophisticated approaches, such as employing freely-rotating chains [1], chain models with extensible links [5, 6], or deformable active bonds [6], could be employed. Furthermore, the rod was assumed to be rigid, yet literature suggests that utilizing the worm-like chain model [7] may offer a more precise representation [8]. Such considerations warrant scrutiny; however, as the mathematical complexity may compromise their efficacy. Other considerations on the chain scale, such as long-range interactions between the chain segments (excluded volume effect)[9, 10] and polydispersity[11], remain undeveloped for coil-rod. In particular, some biopolymer chains, such as alginate, consist of guluronic residues β-D-mannuronic acid (M) and α-L-guluronic acid (G). The order of such units can significantly affect the behavior of the junction zone as well as the coils [12, 13]. Another important issue is related to the kinetics [14, 15] of zipping/unzipping, where the effects of loading rate are taken into account. The coil-rod structures can also be equppied with the full dissociation of the chain as a result of unwinding or bond scission [16, 17].

All such considerations are also extensible to the network models in Chapter 4 for capturing phenomena on a macro-scale and developing stress-stretch relations. For instance, including kinetic theory enables us to incorporate viscoelastic effects in the constitutive relations of disordered biopolymer gels. The formulation of non-affine network models [18, 19], such as the micro-sphere model [20], is another path worth exploring for future studies. The entanglement effects between the coil-rod structures can also be accounted for through the introduction of well-known models such as the tube model [21, 22]. Parallel to such augmentation, it is also necessary to investigate the application of the proposed model in inhomogeneous deformation

where zipping/unzipping occurs locally in the sample. Regarding the network/solvent interaction, there is room for modeling phenomena such as diffusion [23] or the introduction of a sequence of solvents [24], as is customary in the gelation of biopolymer gels. Moreover, studying ion concentration, such as Ca^{2+}, on the mechanical properties of gels, such as alginate, is also possible if detailed experimental data are available.

In Chapter 5, the phantom network can be extended to more involved models where coils and rods are not allowed to pass through each other. In this regard, it can be generalized from long-range interactions, such as excluded-volume effects, to account for rod interactions and possible rod bending [25, 26]. Moreover, the influence of loops and other imperfections in the network topology [27] on the proposed formulation deserves further investigation. Lastly, the model can be examined for more complex networks with multiple rods where unzipping/zipping can occur in different rods.

References

[1] P. Flory, *Statistical Mechanics of Chain Molecules*. Interscience Publishers, 1969.

[2] E. M. Arruda and M. C. Boyce, "A three-dimensional constitutive model for the large stretch behavior of rubber elastic materials," *Journal of the Mechanics and Physics of Solids*, vol. 41, no. 2, pp. 389–412, 1993, ISSN: 0022-5096. DOI: https://doi.org/10.1016/0022-5096(93)90013-6.

[3] P. J. Flory, "Thermodynamics of high polymer solutions," *The Journal of Chemical Physics*, vol. 10, no. 1, pp. 51–61, 1942. DOI: 10.1063/1.1723621. eprint: https://doi.org/10.1063/1.1723621.

[4] M. L. Huggins, "Solutions of Long Chain Compounds," *The Journal of Chemical Physics*, vol. 9, no. 5, pp. 440–440, 1941, ISSN: 0021-9606. DOI: 10.1063/1.1750930. eprint: https://pubs.aip.org/aip/jcp/article-pdf/9/5/440/8138635/440_1_online.pdf.

[5] M. R. Buche, M. N. Silberstein, and S. J. Grutzik, "Freely jointed chain models with extensible links," *Phys. Rev. E*, vol. 106, p. 024 502, 2 2022. DOI: 10.1103/PhysRevE.106.024502.

[6] S. R. Lavoie, R. Long, and T. Tang, "Modeling the mechanics of polymer chains with deformable and active bonds," *The Journal of Physical Chemistry B*, vol. 124, no. 1, pp. 253–265, 2020, PMID: 31790253. DOI: 10.1021/acs.jpcb.9b09068. eprint: https://doi.org/10.1021/acs.jpcb.9b09068.

[7] J. F. Marko and E. D. Siggia, "Stretching dna," *Macromolecules*, vol. 28, no. 26, pp. 8759–8770, 1995. DOI: 10.1021/ma00130a008. eprint: https://doi.org/10.1021/ma00130a008.

[8] A. Buhot and A. Halperin, "Extension behavior of helicogenic polypeptides," *Macromolecules*, vol. 35, no. 8, pp. 3238–3252, 2002, ISSN: 00249297. DOI: 10.1021/ma011631w.

[9] T. Norisuye, A. Tsuboi, and A. Teramoto, "Remarks on excluded-volume effects in semiflexible polymer solutions," *Polymer journal*, vol. 28, no. 4, pp. 357–361, 1996.

[10] M. Rubinstein and R. Colby, *Polymer Physics*. OUP Oxford, 2003, ISBN: 9780198520597.

[11] X. Xu and S. A. Safran, "Compressive elasticity of polydisperse biopolymer gels," *Phys. Rev. E*, vol. 95, p. 052 415, 5 2017. DOI: 10.1103/PhysRevE.95.052415.

[12] H. Hecht and S. Srebnik, "Structural characterization of sodium alginate and calcium alginate," *Biomacromolecules*, vol. 17, no. 6, pp. 2160–2167, 2016. DOI: 10.1021/acs.biomac.6b00378. eprint: https://doi.org/10.1021/acs.biomac.6b00378.

[13] M. Mancini, M. Moresi, and R. Rancini, "Mechanical properties of alginate gels: Empirical characterisation," *Journal of Food Engineering*, vol. 39, no. 4, pp. 369–378, 1999, ISSN: 0260-8774. DOI: https://doi.org/10.1016/S0260-8774(99)00022-9.

[14] K. W. Scott and R. S. Stein, "A Molecular Theory of Stress Relaxation in Polymeric Media," *The Journal of Chemical Physics*, vol. 21, no. 7, pp. 1281–1286, Jul. 1953, ISSN: 0021-9606. DOI: 10.1063/1.1699181. eprint: https://pubs.aip.org/aip/jcp/article-pdf/21/7/1281/18803234/1281_1_online.pdf.

[15] F. J. Vernerey, "Transient response of nonlinear polymer networks: A kinetic theory," *Journal of the Mechanics and Physics of Solids*, vol. 115, pp. 230–247, 2018, ISSN: 0022-5096. DOI: https://doi.org/10.1016/j.jmps.2018.02.018.

[16] Y. Mao, B. Talamini, and L. Anand, "Rupture of polymers by chain scission," *Extreme Mechanics Letters*, vol. 13, pp. 17–24, 2017, ISSN: 2352-4316. DOI: https://doi.org/10.1016/j.eml.2017.01.003.

[17] Q. Guo and F. Zaïri, "A micromechanics-based model for deformation-induced damage and failure in elastomeric media," *International Journal of Plasticity*, vol. 140, p. 102 976, 2021, ISSN: 0749-6419. DOI: https://doi.org/10.1016/j.ijplas.2021.102976.

[18] Q. Wen, A. Basu, P. A. Janmey, and A. G. Yodh, "Non-affine deformations in polymer hydrogels," *Soft Matter*, vol. 8, pp. 8039–8049, 31 2012. DOI: 10.1039/C2SM25364J.

[19] A. R. Cioroianu, E. M. Spiesz, and C. Storm, "Disorder, pre-stress and non-affinity in polymer 8-chain models," *Journal of the Mechanics and Physics of Solids*, vol. 89, pp. 110–125, 2016, ISSN: 0022-5096. DOI: https://doi.org/10.1016/j.jmps.2016.01.014.

[20] C. Miehe, S. Göktepe, and F. Lulei, "A micro-macro approach to rubber-like materials—part I: The non-affine micro-sphere model of rubber elasticity," *Journal of the Mechanics and Physics of Solids*, vol. 52, no. 11, pp. 2617–2660, 2004, ISSN: 0022-5096. DOI: https://doi.org/10.1016/j.jmps.2004.03.011.

[21] R. T. Deam and S. F. Edwards, "The theory of rubber elasticity," *Philosophical Transactions of the Royal Society of London. Series A, Mathematical and Physical Sciences*, vol. 280, no. 1296, pp. 317–353, 1976. DOI: 10.1098/rsta.1976.0001. eprint: https://royalsocietypublishing.org/doi/pdf/10.1098/rsta.1976.0001.

[22] S. F. Edwards and T. A. Vilgis, "The tube model theory of rubber elasticity," *Reports on Progress in Physics*, vol. 51, no. 2, p. 243, 1988. DOI: 10.1088/0034-4885/51/2/003.

[23] W. Hong, X. Zhao, J. Zhou, and Z. Suo, "A theory of coupled diffusion and large deformation in polymeric gels," *Journal of the Mechanics and Physics of Solids*, vol. 56, no. 5, pp. 1779–1793, 2008, ISSN: 0022-5096. DOI: https://doi.org/10.1016/j.jmps.2007.11.010.

[24] A. H. Clark and S. B. Ross-Murphy, "Structural and mechanical properties of biopolymer gels," in *Biopolymers*, Berlin, Heidelberg: Springer Berlin Heidelberg, 1987, pp. 57–192, ISBN: 978-3-540-47827-0.

[25] R. Ball, M. Doi, S. Edwards, and M. Warner, "Elasticity of entangled networks," *Polymer*, vol. 22, no. 8, pp. 1010–1018, 1981, ISSN: 0032-3861. DOI: https://doi.org/10.1016/0032-3861(81)90284-6.

[26] M. Doi and N. Y. Kuzuu, "Nonlinear elasticity of rodlike macromolecules in condensed state," *Journal of Polymer Science: Polymer Physics Edition*, vol. 18, no. 3, pp. 409–419, 1980. DOI: https://doi.org/10.1002/pol.1980.180180301. eprint: https://onlinelibrary.wiley.com/doi/pdf/10.1002/pol.1980.180180301.

[27] M. Zhong, R. Wang, K. Kawamoto, B. D. Olsen, and J. A. Johnson, "Quantifying the impact of molecular defects on polymer network elasticity," *Science*, vol. 353, no. 6305, pp. 1264–1268, 2016. DOI: 10.1126/science.aag0184. eprint: https://www.science.org/doi/pdf/10.1126/science.aag0184.

Global Bibliography

[1-1] J. L. Drury and D. J. Mooney, "Hydrogels for tissue engineering: Scaffold design variables and applications," *Biomaterials*, vol. 24, no. 24, pp. 4337–4351, 2003, Synthesis of Biomimetic Polymers, ISSN: 0142-9612. DOI: https://doi.org/10.1016/S0142-9612(03)00340-5.

[1-2] N. Peppas, P. Bures, W. Leobandung, and H. Ichikawa, "Hydrogels in pharmaceutical formulations," *European Journal of Pharmaceutics and Biopharmaceutics*, vol. 50, no. 1, pp. 27–46, 2000, ISSN: 0939-6411. DOI: https://doi.org/10.1016/S0939-6411(00)00090-4.

[1-3] J. S. Boateng, K. H. Matthews, H. N. Stevens, and G. M. Eccleston, "Wound healing dressings and drug delivery systems: A review," *Journal of Pharmaceutical Sciences*, vol. 97, no. 8, pp. 2892–2923, 2008, ISSN: 0022-3549. DOI: https://doi.org/10.1002/jps.21210.

[1-4] N. A. Ibrahim, A. A. Nada, and B. M. Eid, "Polysaccharide-based polymer gels and their potential applications," in *Polymer Gels: Synthesis and Characterization*, V. K. Thakur and M. K. Thakur, Eds. Singapore: Springer Singapore, 2018, pp. 97–126.

[1-5] A. Imeson, *Food stabilisers, thickeners and gelling agents*. John Wiley & Sons, 2011.

[1-6] T. Bourtoom, "Edible films and coatings: Characteristics and properties," *International food research journal*, vol. 15, no. 3, pp. 237–248, 2008.

[1-7] R. K. Sivamani, J. Goodman, N. V. Gitis, and H. I. Maibach, "Coefficient of friction: Tribological studies in man – an overview," *Skin Research and Technology*, vol. 9, no. 3, pp. 227–234, 2003. DOI: https://doi.org/10.1034/j.1600-0846.2003.02366.x. eprint: https://onlinelibrary.wiley.com/doi/pdf/10.1034/j.1600-0846.2003.02366.x.

[1-8] J. Koehler, F. P. Brandl, and A. M. Goepferich, "Hydrogel wound dressings for bioactive treatment of acute and chronic wounds," *European Polymer Journal*, vol. 100, pp. 1–11, 2018, ISSN: 0014-3057. DOI: https://doi.org/10.1016/j.eurpolymj.2017.12.046.

[1-9] K. Kabiri, H. Omidian, M. J. Zohuriaan-Mehr, and S. Doroudiani, "Superabsorbent hydrogel composites and nanocomposites: A review," *Polymer Composites*, vol. 32, no. 2, pp. 277–289, 2011. DOI: https://doi.org/10.1002/pc.21046. eprint: https://4spepublications.onlinelibrary.wiley.com/doi/pdf/10.1002/pc.21046.

[1-10] T. Someya, Z. Bao, and G. G. Malliaras, "The rise of plastic bioelectronics," *Nature*, vol. 540, no. 7633, pp. 379–385, 2016.

[1-11] R. S. Dassanayake, S. Acharya, and N. Abidi, "Biopolymer-based materials from polysaccharides: Properties, processing, characterization and sorption applications," in *Advanced Sorption Process Applications*, S. Edebali, Ed., Rijeka: IntechOpen, 2019, ch. 1. DOI: 10.5772/intechopen.80898.

[1-12] J. OLIVEIRA and R. REIS, "18 - hydrogels from polysaccharide-based materials: Fundamentals and applications in regenerative medicine," in *Natural-Based Polymers for Biomedical Applications*, ser. Woodhead Publishing Series in Biomaterials, R. L. Reis, N. M. Neves, J. F. Mano, M. E. Gomes, A. P. Marques, and H. S. Azevedo, Eds., Woodhead Publishing, 2008, pp. 485–514, ISBN: 978-1-84569-264-3. DOI: https://doi.org/10.1533/9781845694814.4.485.

[1-13] A. H. Clark and S. B. Ross-Murphy, "Structural and mechanical properties of biopolymer gels," in *Biopolymers*, Berlin, Heidelberg: Springer Berlin Heidelberg, 1987, pp. 57–192, ISBN: 978-3-540-47827-0.

[1-14] J.-Y. Sun *et al.*, "Highly stretchable and tough hydrogels," *Nature*, vol. 489, no. 7414, pp. 133–136, 2012.

[1-15] A. Clark, "Structural and mechanical properties of biopolymer gels," in *Food Polymers, Gels and Colloids*, E. Dickinson, Ed., Woodhead Publishing, 1991, pp. 322–338, ISBN: 978-1-85573-787-7. DOI: https://doi.org/10.1533/9781845698331.322.

[1-16] S. Kasapis, I. Norton, and U. Johan B, *Modern Biopolymer Science: Bridging the Divide between Fundamental Treatise and Industrial Application*. Elsevier Science, 2009, ISBN: 9780080921143.

[1-17] R. W. Ogden, G. Saccomandi, and I. Sgura, "Fitting hyperelastic models to experimental data," *Computational Mechanics*, vol. 34, pp. 484–502, 2004.

[1-18] H. McEvoy, S. Ross-Murphy, and A. Clark, "Large deformation and ultimate properties of biopolymer gels: 1. single biopolymer component systems," *Polymer*, vol. 26, no. 10, pp. 1483–1492, 1985, ISSN: 0032-3861. DOI: https://doi.org/10.1016/0032-3861(85)90081-3.

[1-19] J. Tang, M. A. Tung, J. Lelievre, and Y. Zeng, "Stress-strain relationships for gellan gels in tension, compression and torsion," *Journal of Food Engineering*, vol. 31, no. 4, pp. 511–529, 1997, ISSN: 0260-8774. DOI: https://doi.org/10.1016/S0260-8774(96)00087-8.

[1-20] J. Zhang, C. R. Daubert, and E. Allen Foegeding, "A proposed strain-hardening mechanism for alginate gels," *Journal of Food Engineering*, vol. 80, no. 1, pp. 157–165, 2007, ISSN: 0260-8774. DOI: https://doi.org/10.1016/j.jfoodeng.2006.04.057.

[1-21] V. Magnenet, J. Schiavi-Tritz, C. Huselstein, and R. Rahouadj, "Constitutive equations for Ca2+ -alginate gels," *Journal of the Mechanical Behavior of Biomedical Materials*, vol. 5, no. 1, pp. 90–98, 2012, ISSN: 1751-6161. DOI: https://doi.org/10.1016/j.jmbbm.2011.08.009.

[1-22] X. Xu and S. A. Safran, "Nonlinearities of biopolymer gels increase the range of force transmission," *Phys. Rev. E*, vol. 92, p. 032 728, 3 2015. DOI: 10.1103/PhysRevE.92.032728.

[1-23] C. Wex, S. Arndt, A. Stoll, C. Bruns, and Y. Kupriyanova, "Isotropic incompressible hyperelastic models for modelling the mechanical behaviour of biological tissues: A review," *Biomedical Engineering / Biomedizinische Technik*, vol. 60, no. 6, pp. 577–592, 2015. DOI: doi:10.1515/bmt-2014-0146.

[1-24] H. Wang and X. Xu, "Continuum elastic models for force transmission in biopolymer gels," *Soft Matter*, vol. 16, pp. 10 781–10 808, 48 2020. DOI: 10.1039/D0SM01451F.

[1-25] K. Upadhyay, G. Subhash, and D. Spearot, "Hyperelastic constitutive modeling of hydrogels based on primary deformation modes and validation under 3d stress states," *International Journal of Engineering Science*, vol. 154, p. 103 314, 2020, ISSN: 0020-7225. DOI: https://doi.org/10.1016/j.ijengsci.2020.103314.

[2-1] M. Rubinstein and R. Colby, *Polymer Physics*. OUP Oxford, 2003, ISBN: 9780198520597.

[2-2] W. Kuhn, "Beziehungen zwischen Molekülgröße, statistischer Molekülgestalt und elastischen Eigenschaften hochpolymerer Stoffe," *Kolloid-Zeitschrift*, vol. 76, no. 3, pp. 258–271, 1936.

[2-3] W. Kuhn and F. Grün, "Beziehungen zwischen elastischen Konstanten und Dehnungsdoppelbrechung hochelastischer Stoffe," *Kolloid-Zeitschrift*, vol. 101, no. 3, pp. 248–271, 1942.

[2-4] L. R. G. Treloar, "The statistical length of long-chain molecules," *Trans. Faraday Soc.*, vol. 42, pp. 77–82, 0 1946. DOI: 10.1039/TF9464200077.

[2-5] M. Volkenshteĭn, S. Timasheff, and M. Timasheff, *Configurational Statistics of Polymeric Chains* (High polymers). Interscience Publishers, 1963.

[2-6] L. Treloar, *The Physics of Rubber Elasticity* (Oxford Classic Texts in the Physical Sciences). Oxford University Press, USA, 1975, ISBN: 9780191523304.

[2-7] S. B. Smith, L. Finzi, and C. Bustamante, "Direct mechanical measurements of the elasticity of single dna molecules by using magnetic beads," *Science*, vol. 258, no. 5085, pp. 1122–1126, 1992. DOI: 10.1126/science.1439819. eprint: https://www.science.org/doi/pdf/10.1126/science.1439819.

[2-8] J. Weiner, *Statistical Mechanics of Elasticity* (Dover Books on Physics). Dover Publications, 2002, ISBN: 9780486422602.

[2-9] S. B. Smith, Y. Cui, and C. Bustamante, "Overstretching b-dna: The elastic response of individual double-stranded and single-stranded dna molecules," *Science*, vol. 271, no. 5250, pp. 795–799, 1996. DOI: 10.1126/science.271.5250.795. eprint: https://www.science.org/doi/pdf/10.1126/science.271.5250.795.

[2-10] A. Fiasconaro and F. Falo, "Analytical results of the extensible freely jointed chain model," *Physica A: Statistical Mechanics and its Applications*, vol. 532, p. 121 929, 2019, ISSN: 0378-4371. DOI: https://doi.org/10.1016/j.physa.2019.121929.

[2-11] M. R. Buche, M. N. Silberstein, and S. J. Grutzik, "Freely jointed chain models with extensible links," *Phys. Rev. E*, vol. 106, p. 024 502, 2 2022. DOI: 10.1103/PhysRevE.106.024502.

[2-12] P. G. Higgs and R. C. Ball, "Some ideas concerning the elasticity of biopolymer networks," *Macromolecules*, vol. 22, no. 5, pp. 2432–2437, 1989. DOI: 10.1021/ma00195a073. eprint: https://doi.org/10.1021/ma00195a073.

[2-13] M. C. Wang and E. Guth, "Statistical theory of networks of non-gaussian flexible chains," *The Journal of Chemical Physics*, vol. 20, no. 7, pp. 1144–1157, 1952. DOI: 10.1063/1.1700682. eprint: https://doi.org/10.1063/1.1700682.

[2-14] L. R. G. Treloar, "The photoelastic properties of short-chain molecular networks," *Trans. Faraday Soc.*, vol. 50, pp. 881–896, 0 1954. DOI: 10.1039/TF9545000881.

[2-15] L. R. G. Treloar, G. Riding, and G. Gee, "A non-gaussian theory for rubber in biaxial strain. i. mechanical properties," *Proceedings of the Royal Society of London. A. Mathematical and Physical Sciences*, vol. 369, no. 1737, pp. 261–280, 1979. DOI: 10.1098/rspa.1979.0163. eprint: https://royalsocietypublishing.org/doi/pdf/10.1098/rspa.1979.0163.

[2-16] E. M. Arruda and M. C. Boyce, "A three-dimensional constitutive model for the large stretch behavior of rubber elastic materials," *Journal of the Mechanics and Physics of Solids*, vol. 41, no. 2, pp. 389–412, 1993, ISSN: 0022-5096. DOI: https://doi.org/10.1016/0022-5096(93)90013-6.

[2-17] P. Wu and E. Van Der Giessen, "On improved network models for rubber elasticity and their applications to orientation hardening in glassy polymers," *Journal of the Mechanics and Physics of Solids*, vol. 41, no. 3, pp. 427–456, 1993, ISSN: 0022-5096. DOI: https://doi.org/10.1016/0022-5096(93)90043-F.

[2-18] M. C. Boyce and E. M. Arruda, "Constitutive models of rubber elasticity: A review," *Rubber chemistry and technology*, vol. 73, no. 3, pp. 504–523, 2000.

[2-19] C. O. Horgan and G. Saccomandi, "A molecular-statistical basis for the gent constitutive model of rubber elasticity," *Journal of Elasticity*, vol. 68, no. 1, pp. 167–176, 2002.

[2-20] C. Miehe, S. Göktepe, and F. Lulei, "A micro-macro approach to rubber-like materials—part I: The non-affine micro-sphere model of rubber elasticity," *Journal of the Mechanics and Physics of Solids*, vol. 52, no. 11, pp. 2617–2660, 2004, ISSN: 0022-5096. DOI: https://doi.org/10.1016/j.jmps.2004.03.011.

[2-21] A. Bahrololoumi, V. Morovati, E. A. Poshtan, and R. Dargazany, "A multi-physics constitutive model to predict hydrolytic aging in quasi-static behaviour of thin cross-linked polymers," *International Journal of Plasticity*, vol. 130, p. 102 676, 2020, ISSN: 0749-6419. DOI: https://doi.org/10.1016/j.ijplas.2020.102676.

[2-22] T. Zhao, J. Cao, X. Li, M. Xia, B. Xue, and H. Yuan, "A network-based visco-hyperelastic constitutive model for optically clear adhesives," *Extreme Mechanics Letters*, vol. 51, p. 101 594, 2022, ISSN: 2352-4316. DOI: https://doi.org/10.1016/j.eml.2021.101594.

[2-23] R. Dargazany, V. N. Khiêm, and M. Itskov, "A generalized network decomposition model for the quasi-static inelastic behavior of filled elastomers," *International Journal of Plasticity*, vol. 63, pp. 94–109, 2014, Deformation Tensors in Material Modeling in Honor of Prof. Otto T. Bruhns, ISSN: 0749-6419. DOI: https://doi.org/10.1016/j.ijplas.2013.12.004.

[2-24] X. Zhao, "A theory for large deformation and damage of interpenetrating polymer networks," *Journal of the Mechanics and Physics of Solids*, vol. 60, no. 2, pp. 319–332, 2012, ISSN: 0022-5096. DOI: https://doi.org/10.1016/j.jmps.2011.10.005.

[2-25] Y. Liu, H. Zhang, and Y. Zheng, "A Micromechanically Based Constitutive Model for the Inelastic and Swelling Behaviors in Double Network Hydrogels," *Journal of Applied Mechanics*, vol. 83, no. 2, Nov. 2015, 021008, ISSN: 0021-8936. DOI: 10.1115/1.4031897.

[2-26] D. Zhong *et al.*, "A constitutive model for multi network elastomers pre-stretched by swelling," *Extreme Mechanics Letters*, vol. 40, p. 100 926, 2020, ISSN: 2352-4316. DOI: https://doi.org/10.1016/j.eml.2020.100926.

[2-27] Q. Wang and Z. Gao, "A constitutive model of nanocomposite hydrogels with nanoparticle crosslinkers," *Journal of the Mechanics and Physics of Solids*, vol. 94, pp. 127–147, 2016, ISSN: 0022-5096. DOI: https://doi.org/10.1016/j.jmps.2016.04.011.

[2-28] Q. Wang, G. R. Gossweiler, S. L. Craig, and X. Zhao, "Mechanics of mechanochemically responsive elastomers," *Journal of the Mechanics and Physics of Solids*, vol. 82, pp. 320–344, 2015, ISSN: 0022-5096. DOI: https://doi.org/10.1016/j.jmps.2015.05.007.

[2-29] D. Sun, T. Lu, and T. Wang, "Nonlinear photoelasticity of rubber-like soft materials: Comparison between theory and experiment," *Soft Matter*, vol. 17, pp. 4998–5005, 19 2021. DOI: 10.1039/D1SM00267H.

[2-30] S. R. Lavoie, R. Long, and T. Tang, "A rate-dependent damage model for elastomers at large strain," *Extreme Mechanics Letters*, vol. 8, pp. 114–124, 2016, Nanomechanics: Bridging Spatial and Temporal Scales, ISSN: 2352-4316. DOI: https://doi.org/10.1016/j.eml.2016.05.016.

[2-31] Y. Mao, B. Talamini, and L. Anand, "Rupture of polymers by chain scission," *Extreme Mechanics Letters*, vol. 13, pp. 17–24, 2017, ISSN: 2352-4316. DOI: https://doi.org/10.1016/j.eml.2017.01.003.

[2-32] F. J. Vernerey, R. Brighenti, R. Long, and T. Shen, "Statistical damage mechanics of polymer networks," *Macromolecules*, vol. 51, no. 17, pp. 6609–6622, 2018. DOI: 10.1021/acs.macromol.8b01052. eprint: https://doi.org/10.1021/acs.macromol.8b01052.

[2-33] S. C. Lamont, J. Mulderrig, N. Bouklas, and F. J. Vernerey, "Rate-dependent damage mechanics of polymer networks with reversible bonds," *Macromolecules*, vol. 54, no. 23, pp. 10 801–10 813, 2021. DOI: 10.1021/acs.macromol.1c01943. eprint: https://doi.org/10.1021/acs.macromol.1c01943.

[2-34] J. Lei, Z. Li, S. Xu, and Z. Liu, "A mesoscopic network mechanics method to reproduce the large deformation and fracture process of cross-linked elastomers," *Journal of the Mechanics and Physics of Solids*, vol. 156, p. 104 599, 2021, ISSN: 0022-5096. DOI: https://doi.org/10.1016/j.jmps.2021.104599.

[2-35] P. K. Arunachala, R. Rastak, and C. Linder, "Energy based fracture initiation criterion for strain-crystallizing rubber-like materials with pre-existing cracks," *Journal of the Mechanics and Physics of Solids*, vol. 157, p. 104 617, 2021, ISSN: 0022-5096. DOI: https://doi.org/10.1016/j.jmps.2021.104617.

[2-36] P. Flory, *Statistical Mechanics of Chain Molecules*. Interscience Publishers, 1969.

[2-37] A. Ghatak, K. Vorvolakos, H. She, D. L. Malotky, and M. K. Chaudhury, "Interfacial rate processes in adhesion and friction," *The Journal of Physical Chemistry B*, vol. 104, no. 17, pp. 4018–4030, 2000. DOI: 10.1021/jp9942973. eprint: https://doi.org/10.1021/jp9942973.

[2-38] P. Bažant and B. H. Oh, "Efficient numerical integration on the surface of a sphere," *ZAMM - Journal of Applied Mathematics and Mechanics / Zeitschrift für Angewandte Mathematik und Mechanik*, vol. 66, no. 1, pp. 37–49, 1986. DOI: https://doi.org/10.1002/zamm.19860660108. eprint: https://onlinelibrary.wiley.com/doi/pdf/10.1002/zamm.19860660108.

[2-39] K. Nishinari, S. Koide, and K. Ogino, "On the temperature dependence of elasticity of thermo-reversible gels," *Journal de Physique*, vol. 46, no. 5, pp. 793–797, 1985. DOI: 10.1051/jphys:01985004605079300.

[2-40] H. McEvoy, S. Ross-Murphy, and A. Clark, "Large deformation and ultimate properties of biopolymer gels: 1. single biopolymer component systems," *Polymer*, vol. 26, no. 10, pp. 1483–1492, 1985, ISSN: 0032-3861. DOI: https://doi.org/10.1016/0032-3861(85)90081-3.

[3-1] L. Treloar, *The Physics of Rubber Elasticity* (Oxford Classic Texts in the Physical Sciences). Oxford University Press, USA, 1975, ISBN: 9780191523304.

[3-2] A. H. Clark and S. B. Ross-Murphy, "The concentration dependence of biopolymer gel modulus," *British Polymer Journal*, vol. 17, no. 2, pp. 164–168, 1985. DOI: https://doi.org/10.1002/pi.4980170214. eprint: https://onlinelibrary.wiley.com/doi/pdf/10.1002/pi.4980170214.

[3-3] W. Wang, Y. Zhang, and W. Liu, "Bioinspired fabrication of high strength hydrogels from non-covalent interactions," *Progress in Polymer Science*, vol. 71, pp. 1–25, 2017, ISSN: 00796700. DOI: 10.1016/j.progpolymsci.2017.04.001.

[3-4] S. T. Moe, K. I. Draget, G. Skjåk-Bræk, and O. Simdsrød, "Temperature dependence of the elastic modulus of alginate gels," *Carbohydrate Polymers*, vol. 19, no. 4, pp. 279–284, 1992, ISSN: 0144-8617. DOI: https://doi.org/10.1016/0144-8617(92)90081-Z.

[3-5] M. Moresi and M. Bruno, "Characterisation of alginate gels using quasi-static and dynamic methods," *Journal of Food Engineering*, vol. 82, no. 3, pp. 298–309, 2007, ISSN: 0260-8774. DOI: https://doi.org/10.1016/j.jfoodeng.2007.02.040.

[3-6] A. H. Clark and S. B. Ross-Murphy, "Structural and mechanical properties of biopolymer gels," in *Biopolymers*, Berlin, Heidelberg: Springer Berlin Heidelberg, 1987, pp. 57–192, ISBN: 978-3-540-47827-0.

[3-7] A. Clark, "Structural and mechanical properties of biopolymer gels," in *Food Polymers, Gels and Colloids*, E. Dickinson, Ed., Woodhead Publishing, 1991, pp. 322–338, ISBN: 978-1-85573-787-7. DOI: https://doi.org/10.1533/9781845698331.322.

[3-8] H. McEvoy, S. Ross-Murphy, and A. Clark, "Large deformation and ultimate properties of biopolymer gels: 1. single biopolymer component systems," *Polymer*, vol. 26, no. 10, pp. 1483–1492, 1985, ISSN: 0032-3861. DOI: https://doi.org/10.1016/0032-3861(85)90081-3.

[3-9] J. Zhang, C. R. Daubert, and E. Allen Foegeding, "A proposed strain-hardening mechanism for alginate gels," *Journal of Food Engineering*, vol. 80, no. 1, pp. 157–165, 2007, ISSN: 0260-8774. DOI: https://doi.org/10.1016/j.jfoodeng.2006.04.057.

[3-10] A. H. Clark and S. B. Ross-Murphy, "Chapter 1 - biopolymer network assembly: Measurement and theory," in *Modern Biopolymer Science*, S. Kasapis, I. T. Norton, and J. B. Ubbink, Eds., San Diego: Academic Press, 2009, pp. 1–27, ISBN: 978-0-12-374195-0. DOI: https://doi.org/10.1016/B978-0-12-374195-0.00001-X.

[3-11] V. Magnenet, J. Schiavi-Tritz, C. Huselstein, and R. Rahouadj, "Constitutive equations for Ca2+ -alginate gels," *Journal of the Mechanical Behavior of Biomedical Materials*, vol. 5, no. 1, pp. 90–98, 2012, ISSN: 1751-6161. DOI: https://doi.org/10.1016/j.jmbbm.2011.08.009.

[3-12] X. Xu and S. A. Safran, "Nonlinearities of biopolymer gels increase the range of force transmission," *Phys. Rev. E*, vol. 92, p. 032 728, 3 2015. DOI: 10.1103/PhysRevE.92.032728.

[3-13] H. Wang and X. Xu, "Continuum elastic models for force transmission in biopolymer gels," *Soft Matter*, vol. 16, pp. 10 781–10 808, 48 2020. DOI: 10.1039/D0SM01451F.

[3-14] M. Doi and N. Y. Kuzuu, "Nonlinear elasticity of rodlike macromolecules in condensed state," *Journal of Polymer Science: Polymer Physics Edition*, vol. 18, no. 3, pp. 409–419, 1980. DOI: https://doi.org/10.1002/pol.1980.180180301. eprint: https://onlinelibrary.wiley.com/doi/pdf/10.1002/pol.1980.180180301.

[3-15] A. V. Dobrynin and J. M. Y. Carrillo, "Universality in nonlinear elasticity of biological and polymeric networks and gels," *Macromolecules*, vol. 44, no. 1, pp. 140–146, 2011, ISSN: 00249297. DOI: 10.1021/ma102154u.

[3-16] D. De Tommasi, G. Puglisi, and G. Saccomandi, "Multiscale mechanics of macromolecular materials with unfolding domains," *Journal of the Mechanics and Physics of Solids*, vol. 78, pp. 154–172, 2015, ISSN: 0022-5096. DOI: https://doi.org/10.1016/j.jmps.2015.02.002.

[3-17] K. Nishinari, S. Koide, and K. Ogino, "On the temperature dependence of elasticity of thermo-reversible gels," *Journal de Physique*, vol. 46, no. 5, pp. 793–797, 1985. DOI: 10.1051/jphys:01985004605079300.

[3-18] K. Nishinari, "Rheological and related studies on industrially important polysaccharides and proteins," *Journal of Central South University of Technology*, vol. 14, no. 1, pp. 498–504, 2007.

[3-19] P. G. Higgs and R. C. Ball, "Some ideas concerning the elasticity of biopolymer networks," *Macromolecules*, vol. 22, no. 5, pp. 2432–2437, 1989. DOI: 10.1021/ma00195a073. eprint: https://doi.org/10.1021/ma00195a073.

[3-20] P. Flory, *Statistical Mechanics of Chain Molecules*. Interscience Publishers, 1969.

[3-21] T. Hill, *An Introduction to Statistical Thermodynamics* (Addison-Wesley series in chemistry). Dover Publications, 1986, ISBN: 9780486652429.

[3-22] J. T. Titantah, C. Pierleoni, and J.-P. Ryckaert, "Different statistical mechanical ensembles for a stretched polymer," *Phys. Rev. E*, vol. 60, pp. 7010–7021, 6 1999. DOI: 10.1103/PhysRevE.60.7010.

[3-23] R. G. Winkler, "Equivalence of statistical ensembles in stretching single flexible polymers," *Soft Matter*, vol. 6, pp. 6183–6191, 24 2010. DOI: 10.1039/C0SM00488J.

[3-24] S. Giordano, "Helmholtz and Gibbs ensembles, thermodynamic limit and bistability in polymer lattice models," *Continuum Mechanics and Thermodynamics*, vol. 30, no. 3, pp. 459–483, 2018, ISSN: 09351175. DOI: 10.1007/s00161-017-0615-5.

[3-25] J. M. Y. Carrillo, F. C. MacKintosh, and A. V. Dobrynin, "Nonlinear elasticity: From single chain to networks and gels," *Macromolecules*, vol. 46, no. 9, pp. 3679–3692, 2013, ISSN: 00249297. DOI: 10.1021/ma400478f.

[3-26] J. F. Marko and E. D. Siggia, "Stretching dna," *Macromolecules*, vol. 28, no. 26, pp. 8759–8770, 1995. DOI: 10.1021/ma00130a008. eprint: https://doi.org/10.1021/ma00130a008.

[3-27] A. Buhot and A. Halperin, "Extension behavior of helicogenic polypeptides," *Macromolecules*, vol. 35, no. 8, pp. 3238–3252, 2002, ISSN: 00249297. DOI: 10.1021/ma011631w.

[3-28] J. H. Weiner, "Use of s = k log p for stretched polymers," *Macromolecules*, vol. 15, no. 2, pp. 542–544, 1982. DOI: 10.1021/ma00230a064. eprint: https://doi.org/10.1021/ma00230a064.

[3-29] L. R. G. Treloar, "The statistical length of long-chain molecules," *Trans. Faraday Soc.*, vol. 42, pp. 77–82, 0 1946. DOI: 10.1039/TF9464200077.

[3-30] H. Yamakawa, *Modern theory of polymer solutions*. Harper & Row, 1971.

[3-31] E. M. Arruda and M. C. Boyce, "A three-dimensional constitutive model for the large stretch behavior of rubber elastic materials," *Journal of the Mechanics and Physics of Solids*, vol. 41, no. 2, pp. 389–412, 1993, ISSN: 0022-5096. DOI: https://doi.org/10.1016/0022-5096(93)90013-6.

[3-32] H. Clausen-Schaumann, M. Rief, C. Tolksdorf, and H. E. Gaub, "Mechanical stability of single dna molecules," *Biophysical journal*, vol. 78, no. 4, pp. 1997–2007, 2000.

[3-33] K. Liebl and M. Zacharias, "Unwinding induced melting of double-stranded dna studied by free energy simulations," *The Journal of Physical Chemistry B*, vol. 121, no. 49, pp. 11 019–11 030, 2017, PMID: 29064703. DOI: 10.1021/acs.jpcb.7b07701. eprint: https://doi.org/10.1021/acs.jpcb.7b07701.

[3-34] C. Dong, N. Zahir, and K. Konstantopoulos, *Biomechanics in Oncology* (Advances in Experimental Medicine and Biology). Springer International Publishing, 2018, ISBN: 9783319952949.

[3-35] S. B. Smith, Y. Cui, and C. Bustamante, "Overstretching B-DNA: the elastic response of individual double-stranded and single-stranded DNA molecules," *Science*, vol. 271, no. 5250, pp. 795–799, 1996.

[3-36] W. Zhang and X. Zhang, "Single molecule mechanochemistry of macromolecules," *Progress in Polymer Science (Oxford)*, vol. 28, no. 8, pp. 1271–1295, 2003, ISSN: 00796700. DOI: 10.1016/S0079-6700(03)00046-7.

[3-37] G. Florio and G. Puglisi, "Unveiling the influence of device stiffness in single macromolecule unfolding," *Scientific Reports*, vol. 9, no. 1, pp. 1–11, 2019, ISSN: 20452322. DOI: 10.1038/s41598-019-41330-x.

[3-38] L. Bellino, G. Florio, and G. Puglisi, "The influence of device handles in single-molecule experiments," *Soft Matter*, vol. 15, no. 43, pp. 8680–8690, 2019, ISSN: 17446848. DOI: 10.1039/c9sm01376h.

[3-39] F. Manca, S. Giordano, P. L. Palla, F. Cleri, and L. Colombo, "Two-state theory of single-molecule stretching experiments," *Physical Review E - Statistical, Nonlinear, and Soft Matter Physics*, vol. 87, no. 3, pp. 1–6, 2013, ISSN: 15393755. DOI: 10.1103/PhysRevE.87.032705.

[3-40] N. Theodorakopoulos, M. Peyrard, and R. S. MacKay, "Nonlinear structures and thermodynamic instabilities in a one-dimensional lattice system," *Physical Review Letters*, vol. 93, no. 25, pp. 1–4, 2004, ISSN: 00319007. DOI: 10.1103/PhysRevLett.93.258101.

[3-41] M. Peyrard, "Nonlinear dynamics and statistical physics of DNA," *Nonlinearity*, vol. 17, no. 2, 2004, ISSN: 09517715. DOI: 10.1088/0951-7715/17/2/R01.

[3-42] M. Rief, M. Gautel, F. Oesterhelt, J. M. Fernandez, and H. E. Gaub, "Reversible unfolding of individual titin immunoglobulin domains by AFM," *Science*, vol. 276, no. 5315, pp. 1109–1112, 1997, ISSN: 00368075. DOI: 10.1126/science.276.5315.1109.

[3-43] H. J. Qi, C. Ortiz, and M. C. Boyce, "Mechanics of biomacromolecular networks containing folded domains," *Journal of Engineering Materials and Technology*, vol. 128, no. 4, pp. 509–518, 2006, ISSN: 00944289. DOI: 10.1115/1.2345442.

[3-44] F. Manca, S. Giordano, P. L. Palla, R. Zucca, F. Cleri, and L. Colombo, "Elasticity of flexible and semiflexible polymers with extensible bonds in the Gibbs and Helmholtz ensembles," *Journal of Chemical Physics*, vol. 136, no. 15, p. 154 906, 2012, ISSN: 00219606. DOI: 10.1063/1.4801656.

[3-45] A. Cannizzo, L. Bellino, G. Florio, G. Puglisi, and S. Giordano, "Thermal control of nucleation and propagation transition stresses in discrete lattices with non-local interactions and non-convex energy," *European Physical Journal Plus*, vol. 137, no. 5, 2022, ISSN: 21905444. DOI: 10.1140/epjp/s13360-022-02790-9.

[3-46] D. De Tommasi, G. Puglisi, and G. Saccomandi, "Damage, self-healing, and hysteresis in spider silks," *Biophysical Journal*, vol. 98, no. 9, pp. 1941–1948, 2010, ISSN: 15420086. DOI: 10.1016/j.bpj.2010.01.021.

[3-47] D. De Tommasi, G. Puglisi, and G. Saccomandi, "Localized versus diffuse damage in amorphous materials," *Physical Review Letters*, vol. 100, no. 8, pp. 1–4, 2008, ISSN: 00319007. DOI: 10.1103/PhysRevLett.100.085502.

[3-48] D. De Tommasi, N. Millardi, G. Puglisi, and G. Saccomandi, "An energetic model for macromolecules unfolding in stretching experiments," *Journal of the Royal Society Interface*, vol. 10, no. 88, 2013, ISSN: 17425662. DOI: 10.1098/rsif.2013.0651.

[4-1] K. Y. Lee and D. J. Mooney, "Hydrogels for tissue engineering," *Chemical Reviews*, vol. 101, no. 7, pp. 1869–1880, 2001, PMID: 11710233. DOI: 10.1021/cr000108x. eprint: https://doi.org/10.1021/cr000108x.

[4-2] A. S. Hoffman, "Hydrogels for biomedical applications," *Advanced Drug Delivery Reviews*, vol. 64, pp. 18–23, 2012, MOST CITED PAPERS IN THE HISTORY OF ADVANCED DRUG DELIVERY REVIEWS: A TRIBUTE TO THE 25TH ANNIVERSARY OF THE JOURNAL, ISSN: 0169-409X. DOI: https://doi.org/10.1016/j.addr.2012.09.010.

[4-3] S. Mohan, O. S. Oluwafemi, N. Kalarikkal, S. Thomas, and S. P. Songca, "Biopolymers – application in nanoscience and nanotechnology," in *Recent Advances in Biopolymers*, F. K. Perveen, Ed., Rijeka: IntechOpen, 2016, ch. 3. DOI: 10.5772/62225.

[4-4] J. L. Drury and D. J. Mooney, "Hydrogels for tissue engineering: Scaffold design variables and applications," *Biomaterials*, vol. 24, no. 24, pp. 4337–4351, 2003, Synthesis of Biomimetic Polymers, ISSN: 0142-9612. DOI: https://doi.org/10.1016/S0142-9612(03)00340-5.

[4-5] J.-Y. Sun *et al.*, "Highly stretchable and tough hydrogels," *Nature*, vol. 489, no. 7414, pp. 133–136, 2012.

[4-6] T. L. Sun *et al.*, "Physical hydrogels composed of polyampholytes demonstrate high toughness and viscoelasticity," *Nature materials*, vol. 12, no. 10, pp. 932–937, 2013.

[4-7] J. Wang, J. Wei, S. Su, J. Qiu, and S. Wang, "Ion-linked double-network hydrogel with high toughness and stiffness," *Journal of Materials Science*, vol. 50, pp. 5458–5465, 2015.

[4-8] A. B. Ihsan *et al.*, "Self-healing behaviors of tough polyampholyte hydrogels," *Macromolecules*, vol. 49, no. 11, pp. 4245–4252, 2016. DOI: 10.1021/acs.macromol.6b00437. eprint: https://doi.org/10.1021/acs.macromol.6b00437.

[4-9] A. H. Clark and S. B. Ross-Murphy, "Structural and mechanical properties of biopolymer gels," in *Biopolymers*, Berlin, Heidelberg: Springer Berlin Heidelberg, 1987, pp. 57–192, ISBN: 978-3-540-47827-0.

[4-10] C. Joly-Duhamel, D. Hellio, A. Ajdari, and M. Djabourov, "All gelatin networks: 2. the master curve for elasticity," *Langmuir*, vol. 18, no. 19, pp. 7158–7166, 2002. DOI: 10.1021/la020190m. eprint: https://doi.org/10.1021/la020190m.

[4-11] H. Hecht and S. Srebnik, "Structural characterization of sodium alginate and calcium alginate," *Biomacromolecules*, vol. 17, no. 6, pp. 2160–2167, 2016. DOI: 10.1021/acs.biomac.6b00378. eprint: https://doi.org/10.1021/acs.biomac.6b00378.

[4-12] D. Dhar and Y. Singh, "Linear and branched polymers on fractals," in *Statistics of Linear Polymers in Disordered Media*, B. K. Chakrabarti, Ed., Amsterdam: Elsevier Science, 2005, pp. 149–194, ISBN: 978-0-444-51709-8. DOI: https://doi.org/10.1016/B978-044451709-8/50005-0.

[4-13] S. B. Ross-Murphy, "Physical gelation of biopolymers," *Food Hydrocolloids*, vol. 1, no. 5, pp. 485–495, 1987, Special issue: 2nd International Workshop on Plant Polysaccharides, ISSN: 0268-005X. DOI: https://doi.org/10.1016/S0268-005X(87)80047-4.

[4-14] T. Baumberger and O. Ronsin, "Cooperative effect of stress and ion displacement on the dynamics of cross-link unzipping and rupture of alginate gels," *Biomacromolecules*, vol. 11, no. 6, pp. 1571–1578, 2010, PMID: 20499914. DOI: 10.1021/bm1002015. eprint: https://doi.org/10.1021/bm1002015.

[4-15] K. Nishinari, S. Koide, and K. Ogino, "On the temperature dependence of elasticity of thermo-reversible gels," *Journal de Physique*, vol. 46, no. 5, pp. 793–797, 1985. DOI: 10.1051/jphys:01985004605079300.

[4-16] P. G. Higgs and R. C. Ball, "Some ideas concerning the elasticity of biopolymer networks," *Macromolecules*, vol. 22, no. 5, pp. 2432–2437, 1989. DOI: 10.1021/ma00195a073. eprint: https://doi.org/10.1021/ma00195a073.

[4-17] S. Cocco, J. F. Marko, and R. Monasson, "Theoretical models for single-molecule DNA and RNA experiments: From elasticity to unzipping," *Comptes Rendus Physique*, vol. 3, no. 5, pp. 569–584, 2002, ISSN: 1631-0705. DOI: https://doi.org/10.1016/S1631-0705(02)01345-2.

[4-18] N. Singh and Y. Singh, "Statistical theory of force-induced unzipping of dna," *The European Physical Journal E*, vol. 17, no. 1, pp. 7–19, 2005.

[4-19] S. Kutter and E. M. Terentjev, "Networks of helix-forming polymers," *The European Physical Journal E*, vol. 8, pp. 539–547, 2002.

[4-20] S. Courty, J. L. Gornall, and E. M. Terentjev, "Mechanically induced helix-coil transition in biopolymer networks," *Biophysical Journal*, vol. 90, no. 3, pp. 1019–1027, 2006, ISSN: 0006-3495. DOI: https://doi.org/10.1529/biophysj.105.067090.

[4-21] J. Zhang, C. R. Daubert, and E. Allen Foegeding, "A proposed strain-hardening mechanism for alginate gels," *Journal of Food Engineering*, vol. 80, no. 1, pp. 157–165, 2007, ISSN: 0260-8774. DOI: https://doi.org/10.1016/j.jfoodeng.2006.04.057.

[4-22] V. Magnenet, J. Schiavi-Tritz, C. Huselstein, and R. Rahouadj, "Constitutive equations for Ca2+ -alginate gels," *Journal of the Mechanical Behavior of Biomedical Materials*, vol. 5, no. 1, pp. 90–98, 2012, ISSN: 1751-6161. DOI: https://doi.org/10.1016/j.jmbbm.2011.08.009.

[4-23] E. M. Arruda and M. C. Boyce, "A three-dimensional constitutive model for the large stretch behavior of rubber elastic materials," *Journal of the Mechanics and Physics of Solids*, vol. 41, no. 2, pp. 389–412, 1993, ISSN: 0022-5096. DOI: https://doi.org/10.1016/0022-5096(93)90013-6.

[4-24] T. Distler, E. Schaller, P. Steinmann, A. Boccaccini, and S. Budday, "Alginate-based hydrogels show the same complex mechanical behavior as brain tissue," *Journal of the Mechanical Behavior of Biomedical Materials*, vol. 111, p. 103 979, 2020, ISSN: 1751-6161. DOI: https://doi.org/10.1016/j.jmbbm.2020.103979.

[4-25] Z. Clapacs *et al.*, "Biocompatible and enzymatically degradable gels for 3d cellular encapsulation under extreme compressive strain," *Gels*, vol. 7, no. 3, 2021, ISSN: 2310-2861. DOI: 10.3390/gels7030101.

[4-26] L. Treloar, *The Physics of Rubber Elasticity* (Oxford Classic Texts in the Physical Sciences). Oxford University Press, USA, 1975, ISBN: 9780191523304.

[4-27] S. M. Bhattacharjee, A. Giacometti, and A. Maritan, "Flory theory for polymers," *Journal of Physics: Condensed Matter*, vol. 25, no. 50, p. 503 101, 2013. DOI: 10.1088/0953-8984/25/50/503101.

[4-28] A. R. Cioroianu, E. M. Spiesz, and C. Storm, "Disorder, pre-stress and non-affinity in polymer 8-chain models," *Journal of the Mechanics and Physics of Solids*, vol. 89, pp. 110–125, 2016, ISSN: 0022-5096. DOI: https://doi.org/10.1016/j.jmps.2016.01.014.

[4-29] J. E. Bischoff, E. M. Arruda, and K. Grosh, "A new constitutive model for the compressibility of elastomers at finite deformations," *Rubber chemistry and technology*, vol. 74, no. 4, pp. 541–559, 2001.

[4-30] R. Ogden, *Non-linear Elastic Deformations* (Dover Civil and Mechanical Engineering). Dover Publications, 1997, ISBN: 9780486696485.

[4-31] R. W. Ogden and D. G. Roxburgh, "A pseudo-elastic model for the Mullins effect in filled rubber," *Proceedings of the Royal Society of London. Series A: Mathematical, Physical and Engineering Sciences*, vol. 455, no. 1988, pp. 2861–2877, 1999. DOI: 10.1098/rspa.1999.0431.

[4-32] A. Dorfmann and R. Ogden, "A constitutive model for the mullins effect with permanent set in particle-reinforced rubber," *International Journal of Solids and Structures*, vol. 41, no. 7, pp. 1855–1878, 2004, ISSN: 0020-7683. DOI: https://doi.org/10.1016/j.ijsolstr.2003.11.014.

[4-33] H. Sund and K. Markau, "Association-dissociation phenomena in biopolymers," *International Journal of Polymeric Materials and Polymeric Biomaterials*, vol. 4, no. 3-4, pp. 251–292, 1976. DOI: 10.1080/00914037608072382. eprint: https://doi.org/10.1080/00914037608072382.

[4-34] M. C. Boyce and E. M. Arruda, "Swelling and mechanical stretching of elastomeric materials," *Mathematics and Mechanics of Solids*, vol. 6, no. 6, pp. 641–659, 2001. DOI: 10.1177/108128650100600605. eprint: https://doi.org/10.1177/108128650100600605.

[4-35] S. R. Lavoie, P. Millereau, C. Creton, R. Long, and T. Tang, "A continuum model for progressive damage in tough multinetwork elastomers," *Journal of the Mechanics and Physics of Solids*, vol. 125, pp. 523–549, 2019, ISSN: 0022-5096. DOI: https://doi.org/10.1016/j.jmps.2019.01.001.

[4-36] P. J. Flory, "Thermodynamics of high polymer solutions," *The Journal of Chemical Physics*, vol. 10, no. 1, pp. 51–61, 1942. DOI: 10.1063/1.1723621. eprint: https://doi.org/10.1063/1.1723621.

[4-37] M. L. Huggins, "Solutions of Long Chain Compounds," *The Journal of Chemical Physics*, vol. 9, no. 5, pp. 440–440, 1941, ISSN: 0021-9606. DOI: 10.1063/1.1750930. eprint: https://pubs.aip.org/aip/jcp/article-pdf/9/5/440/8138635/440_1_online.pdf.

[4-38] G. T. Grant, E. R. Morris, D. A. Rees, P. J. Smith, and D. Thom, "Biological interactions between polysaccharides and divalent cations: The egg-box model," *FEBS Letters*, vol. 32, no. 1, pp. 195–198, 1973, ISSN: 0014-5793. DOI: https://doi.org/10.1016/0014-5793(73)80770-7.

[4-39] T. Baumberger and O. Ronsin, "From thermally activated to viscosity controlled fracture of biopolymer hydrogels," *The Journal of Chemical Physics*, vol. 130, no. 6, p. 061 102, 2009. DOI: 10.1063/1.3078267. eprint: https://doi.org/10.1063/1.3078267.

[4-40] I. M. N. Vold, K. A. Kristiansen, and B. E. Christensen, "A study of the chain stiffness and extension of alginates, in vitro epimerized alginates, and periodate-oxidized alginates using size-exclusion chromatography combined with light scattering and viscosity detectors," *Biomacromolecules*, vol. 7, no. 7, pp. 2136–2146, 2006, PMID: 16827580. DOI: 10.1021/bm060099n. eprint: https://doi.org/10.1021/bm060099n.

[4-41] O. Smidsrød, R. Glover, and S. G. Whittington, "The relative extension of alginates having different chemical composition," *Carbohydrate Research*, vol. 27, no. 1, pp. 107–118, 1973, ISSN: 0008-6215. DOI: https://doi.org/10.1016/S0008-6215(00)82430-1.

[4-42] D. R. Rottach, J. G. Curro, J. Budzien, G. S. Grest, C. Svaneborg, and R. Everaers, "Permanent set of cross-linking networks: Comparison of theory with molecular dynamics simulations," *Macromolecules*, vol. 39, no. 16, pp. 5521–5530, 2006. DOI: 10.1021/ma060767x. eprint: https://doi.org/10.1021/ma060767x.

[4-43] F. Trentadue, D. De Tommasi, and G. Puglisi, "A predictive micromechanically-based model for damage and permanent deformations in copolymer sutures," *Journal of the Mechanical Behavior of Biomedical Materials*, vol. 115, p. 104 277, 2021, ISSN: 1751-6161. DOI: https://doi.org/10.1016/j.jmbbm.2020.104277.

[4-44] V. Fazio, D. De Tommasi, N. M. Pugno, and G. Puglisi, "Spider silks mechanics: Predicting humidity and temperature effects," *Journal of the Mechanics and Physics of Solids*, vol. 164, p. 104 857, 2022, ISSN: 0022-5096. DOI: https://doi.org/10.1016/j.jmps.2022.104857.

[4-45] D. De Tommasi, G. Puglisi, and G. Saccomandi, "Multiscale mechanics of macromolecular materials with unfolding domains," *Journal of the Mechanics and Physics of Solids*, vol. 78, pp. 154–172, 2015, ISSN: 0022-5096. DOI: https://doi.org/10.1016/j.jmps.2015.02.002.

[4-46] A. Hajikhani, P. Wriggers, and M. Marino, "Chemo-mechanical modelling of swelling and crosslinking reaction kinetics in alginate hydrogels: A novel theory and its numerical implementation," *Journal of the Mechanics and Physics of Solids*, vol. 153, p. 104 476, 2021, ISSN: 0022-5096. DOI: https://doi.org/10.1016/j.jmps.2021.104476.

[4-47] G. Puglisi, D. De Tommasi, M. F. Pantano, N. M. Pugno, and G. Saccomandi, "Micromechanical model for protein materials: From macromolecules to macroscopic fibers," *Phys. Rev. E*, vol. 96, p. 042 407, 4 2017. DOI: 10.1103/PhysRevE.96.042407.

[4-48] G. Vitucci, D. De Tommasi, G. Puglisi, and F. Trentadue, "A predictive microstructure inspired approach for anisotropic damage, residual stretches and hysteresis in biodegradable sutures," *International Journal of Solids and Structures*, vol. 270, p. 112 232, 2023, ISSN: 0020-7683. DOI: https://doi.org/10.1016/j.ijsolstr.2023.112232.

[5-1] M. Zhong, R. Wang, K. Kawamoto, B. D. Olsen, and J. A. Johnson, "Quantifying the impact of molecular defects on polymer network elasticity," *Science*, vol. 353, no. 6305, pp. 1264–1268, 2016. DOI: 10.1126/science.aag0184. eprint: https://www.science.org/doi/pdf/10.1126/science.aag0184.

[5-2] H. M. James and E. Guth, "Theory of the increase in rigidity of rubber during cure," *The Journal of Chemical Physics*, vol. 15, no. 9, pp. 669–683, 1947. DOI: 10.1063/1.1746626. eprint: https://doi.org/10.1063/1.1746626.

[5-3] M. C. Wang and E. Guth, "Statistical theory of networks of non-gaussian flexible chains," *The Journal of Chemical Physics*, vol. 20, no. 7, pp. 1144–1157, 1952. DOI: 10.1063/1.1700682. eprint: https://doi.org/10.1063/1.1700682.

[5-4] P. Wu and E. Van Der Giessen, "On improved network models for rubber elasticity and their applications to orientation hardening in glassy polymers," *Journal of the Mechanics and Physics of Solids*, vol. 41, no. 3, pp. 427–456, 1993, ISSN: 0022-5096. DOI: https://doi.org/10.1016/0022-5096(93)90043-F.

[5-5] M. Itskov, A. E. Ehret, and R. Dargazany, "A full-network rubber elasticity model based on analytical integration," *Mathematics and Mechanics of Solids*, vol. 15, no. 6, pp. 655–671, 2010. DOI: 10.1177/1081286509106441.

[5-6] E. M. Arruda and M. C. Boyce, "A three-dimensional constitutive model for the large stretch behavior of rubber elastic materials," *Journal of the Mechanics and Physics of Solids*, vol. 41, no. 2, pp. 389–412, 1993, ISSN: 0022-5096. DOI: https://doi.org/10.1016/0022-5096(93)90013-6.

[5-7] M. C. Boyce and E. M. Arruda, "Swelling and mechanical stretching of elastomeric materials," *Mathematics and Mechanics of Solids*, vol. 6, no. 6, pp. 641–659, 2001. DOI: 10.1177/108128650100600605. eprint: https://doi.org/10.1177/108128650100600605.

[5-8] C. Miehe, S. Göktepe, and F. Lulei, "A micro-macro approach to rubber-like materials—part I: The non-affine micro-sphere model of rubber elasticity," *Journal of the Mechanics and Physics of Solids*, vol. 52, no. 11, pp. 2617–2660, 2004, ISSN: 0022-5096. DOI: https://doi.org/10.1016/j.jmps.2004.03.011.

[5-9] P. J. Flory, "Statistical thermodynamics of random networks," *Proceedings of the Royal Society of London. A. Mathematical and Physical Sciences*, vol. 351, no. 1666, pp. 351–380, 1976. DOI: 10.1098/rspa.1976.0146. eprint: https://royalsocietypublishing.org/doi/pdf/10.1098/rspa.1976.0146.

[5-10] S. B. Ross-Murphy, "Physical gelation of biopolymers," *Food Hydrocolloids*, vol. 1, no. 5, pp. 485–495, 1987, Special issue: 2nd International Workshop on Plant Polysaccharides, ISSN: 0268-005X. DOI: https://doi.org/10.1016/S0268-005X(87)80047-4.

[5-11] A. H. Clark and S. B. Ross-Murphy, "Structural and mechanical properties of biopolymer gels," in *Biopolymers*, Berlin, Heidelberg: Springer Berlin Heidelberg, 1987, pp. 57–192, ISBN: 978-3-540-47827-0.

[5-12] P. G. Higgs and R. C. Ball, "Some ideas concerning the elasticity of biopolymer networks," *Macromolecules*, vol. 22, no. 5, pp. 2432–2437, 1989. DOI: 10.1021/ma00195a073. eprint: https://doi.org/10.1021/ma00195a073.

[5-13] R. Ogden, *Non-linear Elastic Deformations* (Dover Civil and Mechanical Engineering). Dover Publications, 1997, ISBN: 9780486696485.

[5-14] A. Cohen, "A padé approximant to the inverse langevin function," *Rheologica acta*, vol. 30, pp. 270–273, 1991.

[5-15] W. H. Press, S. A. Teukolsky, W. T. Vetterling, and B. P. Flannery, *Numerical Recipes: The Art of Scientific Computing*, 3rd. Cambridge University Press, 2007.

[5-16] S. Das and P. N. Suganthan, "Differential evolution: A survey of the state-of-the-art," *IEEE Transactions on Evolutionary Computation*, vol. 15, no. 1, pp. 4–31, 2011. DOI: 10.1109/TEVC.2010.2059031.

[5-17] K. C. Valanis and R. F. Landel, "The Strain-Energy Function of a Hyperelastic Material in Terms of the Extension Ratios," *Journal of Applied Physics*, vol. 38, no. 7, pp. 2997–3002, Jun. 1967, ISSN: 0021-8979. DOI: 10.1063/1.1710039. eprint: https://pubs.aip.org/aip/jap/article-pdf/38/7/2997/18342417/2997_1_online.pdf.

[5-18] A. E. Ehret and A. Stracuzzi, "Variations on ogden's model: Close and distant relatives," *Philosophical Transactions of the Royal Society A: Mathematical, Physical and Engineering Sciences*, vol. 380, no. 2234, p. 20 210 322, 2022. DOI: 10.1098/rsta.2021.0322. eprint: https://royalsocietypublishing.org/doi/pdf/10.1098/rsta.2021.0322.

[5-19] M. M. Carroll, "Molecular chain networks and strain energy functions in rubber elasticity," *Philosophical Transactions of the Royal Society A: Mathematical, Physical and Engineering Sciences*, vol. 377, no. 2144, p. 20 180 067, 2019. DOI: 10.1098/rsta.2018.0067. eprint: https://royalsocietypublishing.org/doi/pdf/10.1098/rsta.2018.0067.

[5-20] R. J. Gaylord, "Entanglement and excluded volume effects in rubber elasticity," *Polymer Engineering & Science*, vol. 19, no. 4, pp. 263–266, 1979. DOI: https://doi.org/10.1002/pen.760190407. eprint: https://4spepublications.onlinelibrary.wiley.com/doi/pdf/10.1002/pen.760190407.

[5-21] M. Doi and N. Y. Kuzuu, "Nonlinear elasticity of rodlike macromolecules in condensed state," *Journal of Polymer Science: Polymer Physics Edition*, vol. 18, no. 3, pp. 409–419, 1980. DOI: https://doi.org/10.1002/pol.1980.180180301. eprint: https://onlinelibrary.wiley.com/doi/pdf/10.1002/pol.1980.180180301.

[5-22] R. Ball, M. Doi, S. Edwards, and M. Warner, "Elasticity of entangled networks," *Polymer*, vol. 22, no. 8, pp. 1010–1018, 1981, ISSN: 0032-3861. DOI: https://doi.org/10.1016/0032-3861(81)90284-6.

[6-1] P. Flory, *Statistical Mechanics of Chain Molecules*. Interscience Publishers, 1969.

[6-2] E. M. Arruda and M. C. Boyce, "A three-dimensional constitutive model for the large stretch behavior of rubber elastic materials," *Journal of the Mechanics and Physics of Solids*, vol. 41, no. 2, pp. 389–412, 1993, ISSN: 0022-5096. DOI: https://doi.org/10.1016/0022-5096(93)90013-6.

[6-3] P. J. Flory, "Thermodynamics of high polymer solutions," *The Journal of Chemical Physics*, vol. 10, no. 1, pp. 51–61, 1942. DOI: 10.1063/1.1723621. eprint: https://doi.org/10.1063/1.1723621.

[6-4] M. L. Huggins, "Solutions of Long Chain Compounds," *The Journal of Chemical Physics*, vol. 9, no. 5, pp. 440–440, 1941, ISSN: 0021-9606. DOI: 10.1063/1.1750930. eprint: https://pubs.aip.org/aip/jcp/article-pdf/9/5/440/8138635/440_1_online.pdf.

[6-5] M. R. Buche, M. N. Silberstein, and S. J. Grutzik, "Freely jointed chain models with extensible links," *Phys. Rev. E*, vol. 106, p. 024 502, 2 2022. DOI: 10.1103/PhysRevE.106.024502.

[6-6] S. R. Lavoie, R. Long, and T. Tang, "Modeling the mechanics of polymer chains with deformable and active bonds," *The Journal of Physical Chemistry B*, vol. 124, no. 1, pp. 253–265, 2020, PMID: 31790253. DOI: 10.1021/acs.jpcb.9b09068. eprint: https://doi.org/10.1021/acs.jpcb.9b09068.

[6-7] J. F. Marko and E. D. Siggia, "Stretching dna," *Macromolecules*, vol. 28, no. 26, pp. 8759–8770, 1995. DOI: 10.1021/ma00130a008. eprint: https://doi.org/10.1021/ma00130a008.

[6-8] A. Buhot and A. Halperin, "Extension behavior of helicogenic polypeptides," *Macromolecules*, vol. 35, no. 8, pp. 3238–3252, 2002, ISSN: 00249297. DOI: 10.1021/ma011631w.

[6-9] T. Norisuye, A. Tsuboi, and A. Teramoto, "Remarks on excluded-volume effects in semiflexible polymer solutions," *Polymer journal*, vol. 28, no. 4, pp. 357–361, 1996.

[6-10] M. Rubinstein and R. Colby, *Polymer Physics*. OUP Oxford, 2003, ISBN: 9780198520597.

[6-11] X. Xu and S. A. Safran, "Compressive elasticity of polydisperse biopolymer gels," *Phys. Rev. E*, vol. 95, p. 052 415, 5 2017. DOI: 10.1103/PhysRevE.95.052415.

[6-12] H. Hecht and S. Srebnik, "Structural characterization of sodium alginate and calcium alginate," *Biomacromolecules*, vol. 17, no. 6, pp. 2160–2167, 2016. DOI: 10.1021/acs.biomac.6b00378. eprint: https://doi.org/10.1021/acs.biomac.6b00378.

[6-13] M. Mancini, M. Moresi, and R. Rancini, "Mechanical properties of alginate gels: Empirical characterisation," *Journal of Food Engineering*, vol. 39, no. 4, pp. 369–378, 1999, ISSN: 0260-8774. DOI: https://doi.org/10.1016/S0260-8774(99)00022-9.

[6-14] K. W. Scott and R. S. Stein, "A Molecular Theory of Stress Relaxation in Polymeric Media," *The Journal of Chemical Physics*, vol. 21, no. 7, pp. 1281–1286, Jul. 1953, ISSN: 0021-9606. DOI: 10.1063/1.1699181. eprint: https://pubs.aip.org/aip/jcp/article-pdf/21/7/1281/18803234/1281_1_online.pdf.

[6-15] F. J. Vernerey, "Transient response of nonlinear polymer networks: A kinetic theory," *Journal of the Mechanics and Physics of Solids*, vol. 115, pp. 230–247, 2018, ISSN: 0022-5096. DOI: https://doi.org/10.1016/j.jmps.2018.02.018.

[6-16] Y. Mao, B. Talamini, and L. Anand, "Rupture of polymers by chain scission," *Extreme Mechanics Letters*, vol. 13, pp. 17–24, 2017, ISSN: 2352-4316. DOI: https://doi.org/10.1016/j.eml.2017.01.003.

[6-17] Q. Guo and F. Zaïri, "A micromechanics-based model for deformation-induced damage and failure in elastomeric media," *International Journal of Plasticity*, vol. 140, p. 102 976, 2021, ISSN: 0749-6419. DOI: https://doi.org/10.1016/j.ijplas.2021.102976.

[6-18] Q. Wen, A. Basu, P. A. Janmey, and A. G. Yodh, "Non-affine deformations in polymer hydrogels," *Soft Matter*, vol. 8, pp. 8039–8049, 31 2012. DOI: 10.1039/C2SM25364J.

[6-19] A. R. Cioroianu, E. M. Spiesz, and C. Storm, "Disorder, pre-stress and non-affinity in polymer 8-chain models," *Journal of the Mechanics and Physics of Solids*, vol. 89, pp. 110–125, 2016, ISSN: 0022-5096. DOI: https://doi.org/10.1016/j.jmps.2016.01.014.

[6-20] C. Miehe, S. Göktepe, and F. Lulei, "A micro-macro approach to rubber-like materials—part I: The non-affine micro-sphere model of rubber elasticity," *Journal of the Mechanics and Physics of Solids*, vol. 52, no. 11, pp. 2617–2660, 2004, ISSN: 0022-5096. DOI: https://doi.org/10.1016/j.jmps.2004.03.011.

[6-21] R. T. Deam and S. F. Edwards, "The theory of rubber elasticity," *Philosophical Transactions of the Royal Society of London. Series A, Mathematical and Physical Sciences*, vol. 280, no. 1296, pp. 317–353, 1976. DOI: 10.1098/rsta.1976.0001. eprint: https://royalsocietypublishing.org/doi/pdf/10.1098/rsta.1976.0001.

[6-22] S. F. Edwards and T. A. Vilgis, "The tube model theory of rubber elasticity," *Reports on Progress in Physics*, vol. 51, no. 2, p. 243, 1988. DOI: 10.1088/0034-4885/51/2/003.

[6-23] W. Hong, X. Zhao, J. Zhou, and Z. Suo, "A theory of coupled diffusion and large deformation in polymeric gels," *Journal of the Mechanics and Physics of Solids*, vol. 56, no. 5, pp. 1779–1793, 2008, ISSN: 0022-5096. DOI: https://doi.org/10.1016/j.jmps.2007.11.010.

[6-24] A. H. Clark and S. B. Ross-Murphy, "Structural and mechanical properties of biopolymer gels," in *Biopolymers*, Berlin, Heidelberg: Springer Berlin Heidelberg, 1987, pp. 57–192, ISBN: 978-3-540-47827-0.

[6-25] R. Ball, M. Doi, S. Edwards, and M. Warner, "Elasticity of entangled networks," *Polymer*, vol. 22, no. 8, pp. 1010–1018, 1981, ISSN: 0032-3861. DOI: https://doi.org/10.1016/0032-3861(81)90284-6.

[6-26] M. Doi and N. Y. Kuzuu, "Nonlinear elasticity of rodlike macromolecules in condensed state," *Journal of Polymer Science: Polymer Physics Edition*, vol. 18, no. 3, pp. 409–419, 1980. DOI: https://doi.org/10.1002/pol.1980.180180301. eprint: https://onlinelibrary.wiley.com/doi/pdf/10.1002/pol.1980.180180301.

[6-27] M. Zhong, R. Wang, K. Kawamoto, B. D. Olsen, and J. A. Johnson, "Quantifying the impact of molecular defects on polymer network elasticity," *Science*, vol. 353, no. 6305, pp. 1264–1268, 2016. DOI: 10.1126/science.aag0184. eprint: https://www.science.org/doi/pdf/10.1126/science.aag0184.

Appendix A: Supporting Information for Chapter 2

A.1 Proof of Equation (2.30)

Let us consider an ensemble of the chain such that the projection of end-to-end vector along an arbitrary direction is fixed. With no loss of generality, this arbitrary direction is chosen along x axis of the coordinate system. Next, segments of the chain are divided into subgroups. If $\tilde{n}_j$ is the number of segments possessing a projection between l_{xj} and $l_{xj} + \delta l_{xj}$ on the x axis, then the set $\{\tilde{n}_1, \tilde{n}_2, \cdots\}$ subjected to the following conditions

$$\sum_j \tilde{n}_j = n, \tag{A.1}$$

$$\sum_j \tilde{n}_j l_{xj} = x \tag{A.2}$$

provides a distribution for the conformations in the above-mentioned ensemble. The first condition specifies the fixed number of segments, while the second ensures that the projection of the chain onto the x axis remains fixed. It is worthwhile to mention that there is no constraint on the displacements along y or z axes and accordingly the end-to-end vector $\mathbf{r}$ of the chain is allowed to change. The projection of each rigid segment can vary in the range of $-b < l_{xj} < b$. For a FJC not subjected to any external forces, the probability distribution for l_{xj} is uniform in this range. Therefore, the probability that the projection of a segment is within any interval l_{xj} to $l_{xj} + \delta l_{xj}$ is $\frac{\delta l_{xj}}{2b}$. Considering the number of ways to assign l_{xj} to the n segments, the total

number of conformations for a free chain is calculated as

$$\bar{\Omega} = \sum_{\{n_1, n_2, \cdots\}} n! \prod_j \frac{1}{\tilde{n}_j!} \left(\frac{\delta l_{xj}}{2b} \right)^{\tilde{n}_j}, \tag{A.3}$$

in which $\{\tilde{n}_1, \tilde{n}_2, \cdots\}$ must satisfy the constraints (A.1) and (A.2). The simplification of (A.3) is a formidable task. However, for sufficiently large n, it is possible to approximate the entire sum by its largest term. In this regard, the expression in (A.3) is replaced by

$$\bar{\Omega} = n! \prod_j \frac{1}{\tilde{n}_j!} \left(\frac{\delta l_{xj}}{2b} \right)^{\tilde{n}_j}, \tag{A.4}$$

where $\tilde{n}_j$'s are to be determined by maximizing $\bar{\Omega}$. To facilitate the calculation, factorials are replaced by Stirling's approximation, which is only justified for $\tilde{n}_j \gg 1$. With this simplification and keeping only the leading order terms,

$$\ln \bar{\Omega}(x) = n \ln n - n + \sum_j \tilde{n}_j \left(\ln \left[\frac{\delta l_{xj}}{2b} \right] - \ln \tilde{n}_j + 1 \right). \tag{A.5}$$

The above function can be maximized subject to (A.1) and (A.2). For this purpose, α and ξ/b are introduced as Lagrange multipliers to define the following function that needs to be maximized with respect to $\tilde{n}_j$'s.

$$\ln \bar{\Omega}(x) + \alpha \left(\sum_j \tilde{n}_j - n \right) + \xi \left(\sum_{i=1}^{j} \tilde{n}_j \frac{l_{xj}}{b} - \frac{x}{b} \right). \tag{A.6}$$

Setting the derivatives of the above expression with respect to $\tilde{n}_j$ to zero yields

$$\frac{\partial \ln \bar{\Omega}}{\partial \tilde{n}_j} + \alpha + \xi \frac{l_{xj}}{b} = 0. \tag{A.7}$$

Differentiation of Equation (A.5) yields

$$\frac{\partial \ln \bar{\Omega}}{\partial \tilde{n}_i} = \ln \left[\frac{\delta l_{xj}}{2b} \right] - \ln \tilde{n}_j. \tag{A.8}$$

Substitution of Equation (A.8) into Equation (A.7) results in

$$\ln \tilde{n}_j = \ln \left[\frac{\delta l_{xj}}{2b} \right] + \alpha + \frac{\xi l_{xj}}{b}, \tag{A.9}$$

leading to

$$\tilde{n}_j = \exp\alpha \exp\left[\frac{\xi l_{xj}}{b}\right] \frac{\delta l_{xj}}{2b}. \tag{A.10}$$

By substituting the above expression into Equation (A.1) and rewriting the summation into integration, the following relation is obtained:

$$n = \exp\alpha \int_{l_{xj}=-b}^{b} \exp\left[\frac{\xi l_{xj}}{b}\right] \frac{\mathrm{d}l_{xj}}{2b} = \exp\alpha \frac{\sinh\xi}{\xi}. \tag{A.11}$$

Hence, α is determined as

$$\alpha = \ln\left[\frac{n\xi}{\sinh\xi}\right]. \tag{A.12}$$

Now, Equation (A.10) becomes

$$\tilde{n}_j = \frac{n\xi}{\sinh\xi} \exp\left[\frac{\xi l_{xj}}{b}\right] \frac{\delta l_{xj}}{2b}. \tag{A.13}$$

Similarly by substitution of (A.13) and replacing summation with integration, one can convert Equation (A.2) to

$$x = \frac{n\xi}{\sinh\xi} \int_{l_{xj}=-b}^{b} l_{xj} \exp\left[\frac{\xi l_{xj}}{b}\right] \frac{\mathrm{d}l_{xj}}{2b} = nb\mathscr{L}(\xi). \tag{A.14}$$

To this end, let us rewrite Equation (A.5) as

$$\begin{aligned}
\ln\bar{\Omega}(x) &= n\ln n - n + \sum_j \tilde{n}_j \left(\ln\left[\frac{\delta l_{xj}}{2b}\right] - \ln\left[\tilde{n}_j\right]\right) + \sum_j \tilde{n}_j \\
&= \ln n \sum_j \tilde{n}_j + \sum_j \tilde{n}_j \left(\ln\left[\frac{\delta l_{xj}}{2b}\right] - \ln\left[\tilde{n}_j\right]\right) \\
&= \sum_j \tilde{n}_j \left(\ln\left[\frac{\delta l_{xj}}{2b}\right] - \ln\left[\frac{\tilde{n}_j}{n}\right]\right).
\end{aligned} \tag{A.15}$$

On the other hand, by taking the natural logarithm of both sides of (A.13) and rearranging the terms,

$$\ln\left[\frac{\delta l_{xj}}{2b}\right] - \ln\left[\frac{\tilde{n}_j}{n}\right] = -\ln\left[\frac{\xi}{\sinh\xi}\right] - \frac{\xi l_{xj}}{b}. \tag{A.16}$$

With the aid of (A.16), one can simplify Equation (A.15) to

$$\ln \bar{\Omega}(x) = \sum_j \tilde{n}_j \left(\ln \left[\frac{\sinh\xi}{\xi} \right] - \frac{\xi l_{xj}}{b} \right). \tag{A.17}$$

Since ξ is a Lagrange multiplier and by definition independent of $\tilde{n}_j$, by utilizing Equations (A.1) and (A.2) the above relation can be finally written as

$$\ln \bar{\Omega}(x) = n \ln \left[\frac{\sinh\xi}{\xi} \right] - \frac{\xi\, x}{b}. \tag{A.18}$$

The probability $p_n^{\mathrm{C}}(x)\mathrm{d}x$ is proportional to the number of chain conformations at given x, i.e., $p_n^{\mathrm{C}}(x) \propto \bar{\Omega}(x)$. Let

$$p_n^{\mathrm{C}}(x) = \frac{A_0}{\sqrt{n}} \left(\frac{\sinh\xi}{\xi} \right)^n \exp\left[-\frac{\xi x}{b} \right], \tag{A.19}$$

with

$$\xi = \mathscr{L}^{-1}\left(\frac{x}{nb} \right) \tag{A.20}$$

obtained from (A.14), Equation (2.30) is thus proved.

A.2 Proof of Equation (2.32)

By setting $\mathbf{f} = \mathbf{0}$ in Equation (2.23), it is seen that

$$p_n(x) = \int_{y=-\infty}^{+\infty} \int_{z=-\infty}^{+\infty} W_n(\mathbf{r})\, \mathrm{d}y\mathrm{d}z. \tag{A.21}$$

If $W_n(\mathbf{r})$ is insensitive to the chain orientation, it can be replaced by $W_n(r)$. By applying the polar coordinates $\rho - \varphi$ in the $y - z$ plane ($y = \rho\cos\varphi$, $z = \rho\sin\varphi$), and using $r = \sqrt{x^2 + \rho^2}$, the above integration is converted to

$$p_n(x) = 2\pi \int_{\rho=0}^{+\infty} W_n\left(\sqrt{x^2+\rho^2} \right) \rho \mathrm{d}\rho = 2\pi \int_{u=|x|}^{+\infty} W_n(u)\, u\mathrm{d}u, \tag{A.22}$$

where the last identity is arrived at by using the change of variable $u = \sqrt{x^2 + \rho^2}$. Now, the Leibniz integral rule implies that

$$-\left(\frac{\mathrm{d}p_n(x)}{\mathrm{d}x} \right)_{x=r} = 2\pi r W_n(r). \tag{A.23}$$

Appendix B: Supporting Information for Chapter 3

B.1 Proof of Equation (3.9)

Based on the definitions given in Equations (3.5) and (3.8), it is straightforward to verify that

$$p(x) = \int_{y=-\infty}^{+\infty} \int_{z=-\infty}^{+\infty} W(r)\, \mathrm{d}y\mathrm{d}z. \tag{B.1}$$

By applying the polar coordinates $\rho - \phi$ in $y - z$ plane ($y = \rho\cos\phi$, $z = \rho\sin\phi$), and using $r = \sqrt{x^2 + \rho^2}$, the above integration is converted to

$$p(x) = 2\pi \int_{\rho=0}^{+\infty} W\left(\sqrt{x^2+\rho^2}\right) \rho \mathrm{d}\rho = 2\pi \int_{u=|x|}^{+\infty} W(u)\, u\mathrm{d}u, \tag{B.2}$$

where the last identity is arrived at by using the change of variable $u = \sqrt{x^2 + \rho^2}$. Now, the Leibniz integral rule implies that

$$-\left(\frac{\mathrm{d}p(x)}{\mathrm{d}x}\right)_{x=r} = 2\pi r W(r). \tag{B.3}$$

B.2 Weiner's rigid model for a single rod

In this part, the rigid model of Weiner and Perchak [1] is expounded and the differences from the flexible model in the limit of infinite stiffness are explored.

Suppose that a rigid rod with fixed length a is placed between two fixed walls separated by a distance x under a fixed temperature T as shown in Figure B.1a. If one end of the rod is fixed at A, the other end is allowed to move along the circle with

radius $\sqrt{a^2 - x^2}$, which is interpreted as a single degree of freedom. To describe such a system, it is necessary to introduce the generalized coordinate φ and its conjugate variable, angular momentum L about $x-$axis. It is further assumed that the intrinsic energy within the rod structure is E_0 and remains fixed for different conformations. Hence, the Hamiltonian of such a system reads as

$$\mathscr{H} = E_0 + \frac{L^2}{2I^*}, \tag{B.4}$$

where I^* stands for the moment of inertia of the rod around the $x-$axis. It can be shown that I^* is proportional to $a^2 - x^2$ regardless of the mass distribution along the rod:

$$I^* = c_0 m(a^2 - x^2), \tag{B.5}$$

in which m is the total mass of the rigid rod. The factor c_0 depends on the rod's mass distribution and equals 1 for concentrated masses at the two ends. In the forthcoming derivations, it will be seen that c_0 does not affect the final result. By utilizing Equations (B.4) and (B.5), the canonical partition function for fixed x and T is written as

$$Z^{\mathrm{W}}(x,T) = \\ \frac{1}{h}\int_{L=-\infty}^{+\infty}\int_{\varphi=0}^{2\pi} \exp\left[-\frac{\mathscr{H}}{k_B T}\right] \mathrm{d}L\,\mathrm{d}\varphi = \exp\left[-\frac{E_0}{k_B T}\right]\sqrt{\frac{8k_B T\pi^3 m a^2}{h^2}}\sqrt{1-\left(\frac{x}{a}\right)^2}, |x| < a. \tag{B.6}$$

The superscript W indicates Weiner's rigid model. Although the primary goal of both Weiner's rigid model and flexible model with large stiffness is to impose the constraint of rigidity on the formulation of the partition function, the results of (3.17) and (B.6) are different. In the flexible model, the position and momentum vectors are treated independently and the constraints of fixed length are only applied on the position vectors, while in the rigid model, the constraint of fixed length implies extra constraints on the momentum vector. In other words, the Hamiltonian of Weiner's

rigid model can be rewritten in the same way as Equation (3.15) under the following constraints:

$$x^2 + q_y^2 + q_z^2 = a^2, \tag{B.7a}$$

$$q_y p_y + q_z p_z = 0, \tag{B.7b}$$

where the second relation is the time derivative of the first one. As a result of the second constraint, the kinetic and potential energy parts in (3.15) become coupled together in Weiner's rigid model, yielding the reduction of the accessible conformations of the system in the phase space. Accordingly, the degree of freedom reduces from two in the flexible model to one in Weiner's rigid model, and Equation (3.15) collapses to Equation (B.6). Hence, the rigid model cannot be derived through the decomposition of the kinetic and configurational parts of the partition function as in the flexible model.

Next, the isothermal-isotension partition function of the rigid rod is formulated considering Figure B.1b. One end (A) of the rigid rod is fixed at the origin and a fixed force f_x is applied on the other end B. The internal energy of the rod is E_0 independent of the conformations. For simplicity, it is assumed that the mass m is concentrated at point B. The system has two degrees of freedom such that the end B is allowed to move on the surface of a sphere centered at A with radius a. By using spherical coordinate, one can establish the position of the mass as follows

$$\begin{aligned} q_x &= a \sin\varphi \cos\theta, \\ q_z &= a \sin\varphi \sin\theta, \\ q_y &= a \cos\varphi. \end{aligned} \tag{B.8}$$

Taking time derivatives, the components of velocity are given as

$$\begin{aligned} p_x &= ma\,\dot{\varphi} \cos\varphi \cos\theta \; - ma\,\dot{\theta} \sin\varphi \sin\theta, \\ p_z &= ma\,\dot{\varphi} \cos\varphi \sin\theta \; + ma\,\dot{\theta} \sin\varphi \cos\theta, \\ p_y &= -ma\,\dot{\varphi} \sin\varphi. \end{aligned} \tag{B.9}$$

An overdot indicates the time derivative of the variable. The kinetic energy is written as

$$\frac{1}{2m}\left(p_x^2+p_y^2+p_z^2\right)=\frac{1}{2}ma^2\left(\dot{\varphi}^2+\dot{\theta}^2\sin^2\varphi\right). \tag{B.10}$$

Now, by defining generalized momentum L_θ and L_φ as

$$\begin{aligned} L_\varphi &= ma^2\dot{\varphi}, \\ L_\theta &= ma^2\sin^2\varphi\,\dot{\theta}, \end{aligned} \tag{B.11}$$

the Hamiltonian can be obtained

$$\mathscr{H}=E_0+\frac{L_\varphi}{2ma^2}+\frac{L_\theta}{2ma^2\sin^2\varphi}-f_x a\cos\varphi. \tag{B.12}$$

The isothermal-isotension partition function is therefore

$$\begin{aligned} Q^{\mathrm{W}}(f_x,T) &= \frac{1}{h^2}\int_{L_\varphi=-\infty}^{+\infty}\int_{L_\theta=-\infty}^{+\infty}\int_{\varphi=0}^{\pi}\int_{\theta=0}^{2\pi}\exp\left[-\frac{\mathscr{H}}{k_BT}\right]\mathrm{d}L_\varphi\,\mathrm{d}L_\theta\,\mathrm{d}\varphi\,\mathrm{d}\theta \\ &= \exp\left[-\frac{E_0}{k_BT}\right]\frac{8k_BT\pi^2ma^2}{h^2}\frac{k_BT}{f_xa}\sinh\left(\frac{f_xa}{k_BT}\right). \end{aligned} \tag{B.13}$$

Interestingly, the above result is in the same form as Equation (3.20) with the difference being the coefficient. It is worthwhile to mention that the above result cannot be recovered through substitution of Equation (B.6) in (3.10). Consequently, the formulations of (3.10) (or equivalently (3.11)) no longer hold for Weiner's rigid model.

After calculation of partition functions (B.6), the average force $\langle f_x\rangle$ can be obtained in terms of displacement x by using Equations (3.3) and (3.4). The result is

$$\frac{\langle f_x\rangle a}{k_BT}=\frac{x}{a\left[1-\left(\frac{x}{a}\right)^2\right]}=\frac{x}{a}+\mathscr{O}\left(\left(\frac{x}{a}\right)^3\right). \tag{B.14}$$

As a consequence of the stronger constraint imposed by the rigid model, it predicts stiffer behaviour compared to the flexible model with infinite stiffness, see Figure B.2 and comparison with Figure 3.3. In a similar fashion, substitution of (B.13) in Equations (3.12) and (3.13) leads to

$$\frac{\langle x\rangle}{a}=\mathscr{L}\left(\frac{f_xa}{k_BT}\right)=\frac{1}{3}\frac{f_xa}{k_BT}+\mathscr{O}\left(\left(\frac{f_xa}{k_BT}\right)^3\right). \tag{B.15}$$

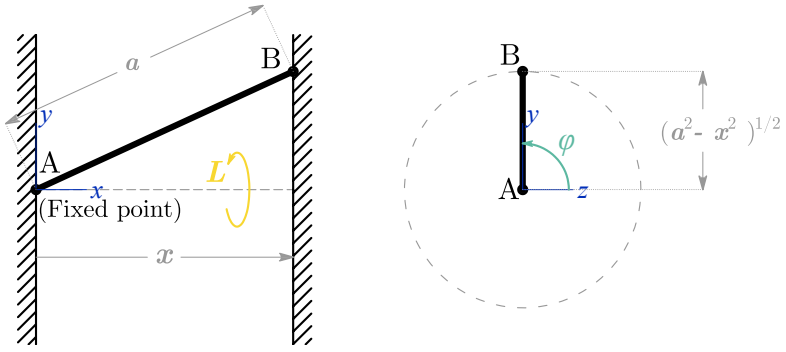

(a) Canonical ensemble with fixed x

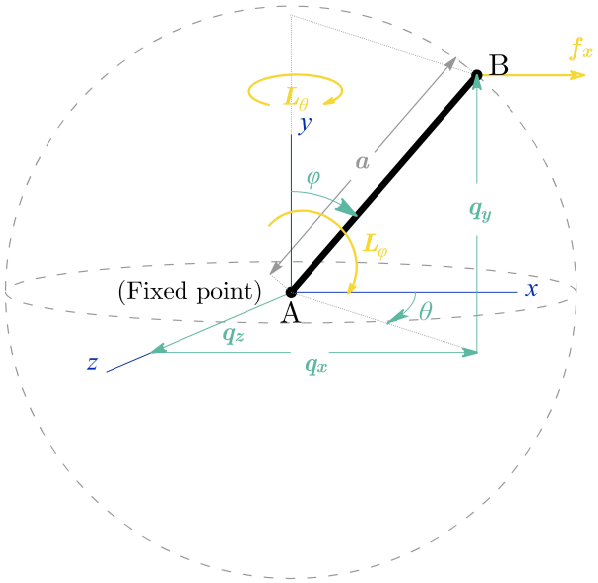

(b) Isothermal-isotension ensemble with fixed f_x

Figure B.1: Weiner's rigid model of a single rod: (a) Canonical ensemble in which the rod is constrained between two fixed walls with distance x. The projection of the rigid rod on the right wall shows that there is only one degree of freedom and the end B is confined to the circumference of the circle with radius $\sqrt{a^2 - x^2}$. (b) Isothermal-isotension ensemble in which the rod is subjected to the force f_x and the end B with two degrees of freedom can be located on the surface of a sphere with radius a.

The latter result is identical to Equation (3.23) for the flexible model with infinite stiffness. In both Weiner's rigid model and flexible model with infinite stiffness, the isothermal-isotension ensemble predicts stiffer behaviour compared to the canonical ensemble.

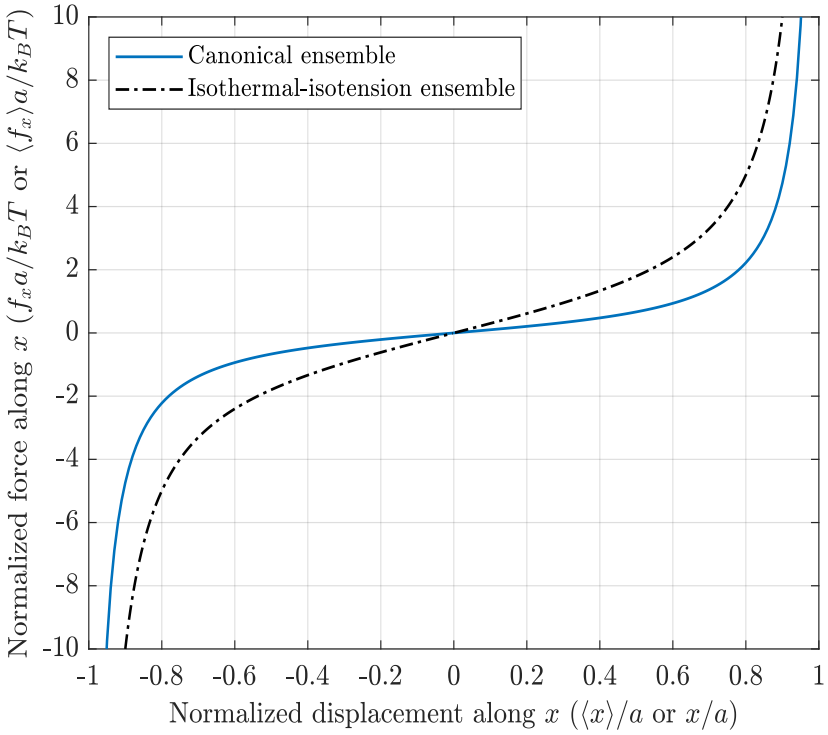

Figure B.2: Normalized force vs. normalized displacement along the $x-$axis for Weiner's rigid model. For the isothermal-isotension ensemble $f_x a/k_B T$ is plotted against $\langle x \rangle/a$, while for the canonical ensemble $\langle f_x \rangle a/k_B T$ is plotted against x/a.

So far, two different approaches for modelling a rigid rod have been briefly outlined. In the original work of Weiner and Perchak [1], a similar analysis was proposed for a structure consisting of two rigid rods connected together with fixed end-to-end distance through the analogy with Frenkel's governor model Frenkel [2]. It was concluded that the results are radically distinctive such that by increasing the end-to-end distance, the average force in the flexible model with infinite stiffness decreases while that in the Weiner's rigid model increases.

The same discrepancy between the rigid and flexible models was reported in the modelling of the angles between consecutive segments in the freely rotating chain structure. It is a highly controversial issue which method can describe the chain properties more realistically. For example, Gō and Scheraga [3] showed that although both methods have errors when compared to the quantum statistical mechanics, the results driven from the flexible model with infinite stiffness are more accurate. Furthermore, as shown by Weiner [4] the entropy change of the flexible model is proportional to the logarithm of the probability density based on the random walk model. In the current study, for the sake of consistency with other works in the literature, we focused on the flexible model in the limiting case of $\kappa \to +\infty$. For further information, readers are referred to chapter 6 of the book by Weiner [5].

B.3 Derivation of the probability distribution of the coil-rod structure along x- direction

Let us reconsider Equation (3.24),

$$p_n^{\mathrm{CR}}(x) = \frac{1}{2a}\int_{x-a}^{x+a} p_n^{\mathrm{C}}(x')\mathrm{d}x', \tag{B.16}$$

where $p_n^{\mathrm{C}}(x)$ is given by Equation (3.31). Now define the following function

$$\mathscr{F}(x,k) = \sum_{s=0}^{k} \frac{(-1)^s}{s!(n-s)!}\left[\frac{1}{2}\left(n-\frac{x}{b}\right)-s\right]^n, \quad \text{if } -(2k+2-n)b \le x \le (n-2k)b \tag{B.17}$$

where $|x| \le nb$ and zero otherwise. Then, it can be verified that

$$\int_{-nb}^{x} p_n^{\mathrm{C}}(x')\mathrm{d}x' = 1 - \mathscr{F}(x,k). \tag{B.18}$$

Using Equations (B.16) and (B.18) leads to

$$p_n^{\mathrm{CR}}(x) = \frac{1}{2a}\left[\mathscr{F}(x-a,k') - \mathscr{F}(x+a,k''-1)\right]. \tag{B.19}$$

in which k' and k'' hold in the following relations:

$$\frac{nb+a-x}{2b}-1\leq k'\leq\frac{nb+a-x}{2b}, \tag{B.20a}$$

$$\frac{nb-a-x}{2b}\leq k''\leq\frac{nb-a-x}{2b}+1. \tag{B.20b}$$

Special case: $a=b$

Since Equation (B.19) is valid for any $a>0$, we can check the result for the special case of $a=b$. In this case, by comparing Equations (B.20a) and (B.20b), it can be concluded that $k'=k''$. With the aid of Equation (B.17), the first term in (B.19) is simply

$$\mathscr{F}(x-b,k')=\sum_{s=0}^{k'}\frac{(-1)^s(n-s+1)}{s!(n-s+1)!}\left[\frac{1}{2}\left(n-\frac{x}{b}+1\right)-s\right]^n. \tag{B.21}$$

On the other hand, by using Equation (B.17) the second term in (B.19) is rewritten as

$$\mathscr{F}(x+b,k'-1)=\sum_{s=0}^{k'-1}\frac{(-1)^s}{s!(n-s)!}\left[\frac{1}{2}\left(n-\frac{x}{b}-1\right)-s\right]^n. \tag{B.22}$$

Now, applying $s'=s+1$, we have

$$\begin{aligned}\mathscr{F}(x+b,k'-1)&=\sum_{s'=1}^{k'}\frac{(-1)^{s'-1}}{(s'-1)!(n-s'+1)!}\left[\frac{1}{2}\left(n-\frac{x}{b}+1\right)-s'\right]^n\\&=\sum_{s=0}^{k'}\frac{-(-1)^s s}{s!(n-s+1)!}\left[\frac{1}{2}\left(n-\frac{x}{b}+1\right)-s\right]^n.\end{aligned} \tag{B.23}$$

In the latter step, we replaced $s'=1$ by $s'=0$ and change the notation to s with no loss of generality. By combining the results of (B.21) and (B.23),

$$\begin{aligned}p_n^{\mathrm{CR}}(x)=&\frac{1}{2b}\left[\mathscr{F}(x-b,k')-\mathscr{F}(x+b,k'-1)\right]\\=&\frac{1}{2b}\sum_{s=0}^{k'}\frac{(-1)^s(n+1)}{s!(n-s+1)!}\left[\frac{1}{2}\left(n-\frac{x}{b}+1\right)-s\right]^n.\end{aligned} \tag{B.24}$$

This equation is true for condition (B.20a),

$$\frac{nb-b-x}{2b}\leq k'\leq\frac{nb+b-x}{2b}, \tag{B.25}$$

or equivalently,

$$(n-1-2k')b \leq x \leq (n+1-2k)b. \tag{B.26}$$

Equation (B.24) together with (B.26) recovers the probability density in Equation (3.31), with the number of Kuhn segments being increased from n to $n+1$. This is expected since when $a = b$, the rod can be treated as a Kuhn segment added to the coil, rendering a new coil structure with $n+1$ Kuhn segment.

References

[1] J. Weiner and D. Perchak, "Frenkel's governor model for stretched polymers," *Macromolecules*, vol. 14, no. 5, pp. 1590–1591, 1981.

[2] J. Frenkel, *Kinetic Theory of Liquids*. Dover, 1955.

[3] N. Gō and H. A. Scheraga, "On the use of classical statistical mechanics in the treatment of polymer chain conformation," *Macromolecules*, vol. 9, no. 4, pp. 535–542, 1976. DOI: 10.1021/ma60052a001. eprint: https://doi.org/10.1021/ma60052a001.

[4] J. H. Weiner, "Use of s = k log p for stretched polymers," *Macromolecules*, vol. 15, no. 2, pp. 542–544, 1982. DOI: 10.1021/ma00230a064. eprint: https://doi.org/10.1021/ma00230a064.

[5] J. Weiner, *Statistical Mechanics of Elasticity* (Dover Books on Physics). Dover Publications, 2002, ISBN: 9780486422602.

Appendix C: Supporting Information for Chapter 4

C.1 Analytical expressions for C_n

To determine C_n, one can refer to the work in Chapter 3 in which $W_n(r)$ is given by

$$W_n^{\mathrm{CR}}(r) = \frac{1}{4\pi a r}\left[p_n(r-a) - p_n(r+a)\right], \tag{C.1}$$

and for large n

$$p_n(r) = C_n \left[\frac{\sinh\beta}{\beta}\right]^n \exp\left[-\frac{\beta r}{b}\right], \tag{C.2}$$

where

$$\beta = \mathscr{L}^{-1}\left[\frac{r}{nb}\right]. \tag{C.3}$$

Now, the normalization condition

$$\int_0^{+\infty} W_n^{\mathrm{CR}}(r)\, 4\pi r^2 \mathrm{d}r = 1 \tag{C.4}$$

can be rephrased as

$$\int_0^{+\infty} p_n(r-a) r \mathrm{d}r - \int_0^{+\infty} p_n(r+a) r \mathrm{d}r = a. \tag{C.5}$$

By change of variables $y = r - a$ and $z = -r - a$ in the first and second integrations respectively, Equation (C.5) reads

$$\int_{-a}^{+\infty} p_n(y)(y+a)\mathrm{d}y + \int_{-\infty}^{-a} p_n(-z)(z+a)\mathrm{d}z = a. \tag{C.6}$$

Since $p_n(x)$ is an even function, one can simply deduce that

$$\int_{-\infty}^{+\infty} p_n(r)\mathrm{d}r = 1. \tag{C.7}$$

Substitution of Equation (C.2) into the above normalization condition implies that

$$C_n \int_{-\infty}^{+\infty} \exp\left\{-\frac{\beta r}{b} + n\ln\left[\frac{\sinh\beta}{\beta}\right]\right\}\mathrm{d}r = 1. \tag{C.8}$$

For large n, β can be asymptotically approximated by $\dfrac{3r}{nb}$, and the argument of the exponential function can be expanded using the series expansion:

$$-\frac{\beta r}{b} + n\ln\left[\frac{\sinh\beta}{\beta}\right] = -n\left(\frac{3}{2}\left(\frac{r}{nb}\right)^2 + \frac{9}{20}\left(\frac{r}{nb}\right)^4 + \cdots\right). \tag{C.9}$$

By keeping only the lowest order term, one can solve Equation (C.8) analytically leading to

$$C_n^{(1)} = \sqrt{\frac{3}{2\pi n b^2}}, \tag{C.10}$$

which corresponds to the normalization factor in the Gaussian coil distribution [1]. However, by applying the expansion of (C.9) up to the second term, one can compute the normalization factor as

$$C_n^{(2)} = \sqrt{\frac{6}{5b^2n^2}}\,\frac{\exp\left(-5n/8\right)}{K_{\frac{1}{4}}\left(5n/8\right)}, \tag{C.11}$$

where $K_{\frac{1}{4}}(x)$ is the (1/4)th order modified Bessel function of the second kind. For large values of n [2]

$$K_\rho(\rho x) \sim \sqrt{\frac{\pi}{2\rho}}\frac{\exp\left(-\rho x\right)}{\sqrt{x}}, \tag{C.12}$$

and consequently $C_n^{(2)}$ converges to $C_n^{(1)}$. To probe into the validity range of $C_n^{(1)}$ and $C_n^{(2)}$, C_n is computed through numerical evaluation of the integral in (C.8). The ratios of estimated values to the exact value, $C_n^{(i)}/C_n$, $(i = 1, 2)$ are shown in Figure C.1. As can be seen $C_n^{(1)}$ and $C_n^{(2)}$ can predict C_n with an error of less than 2% for $n \geq 10$. Therefore, the application of $C_n^{(1)}$ in the current study is deemed reliable.

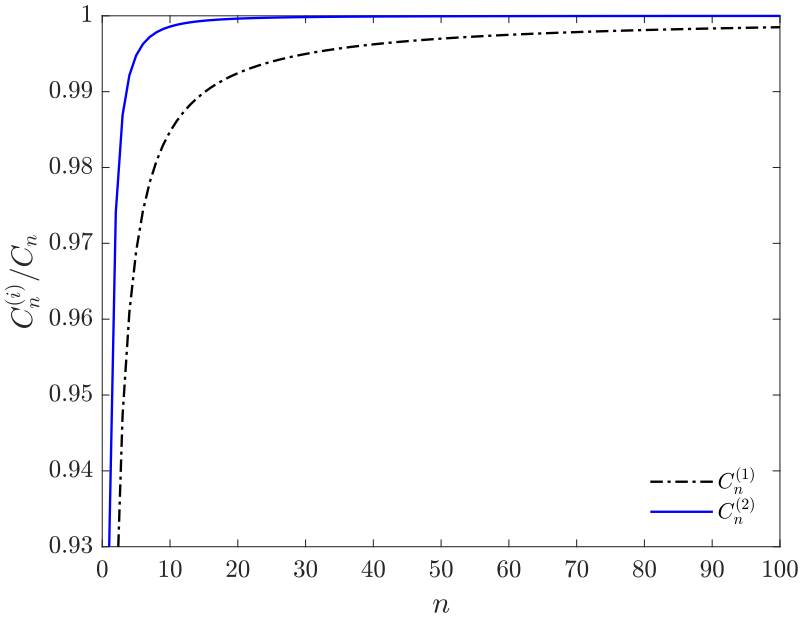

Figure C.1: The ratio of $C_n^{(i)}/C_n$ as a function of n for two different approximations.

C.2 Simplification of Equation (3.37) for $a \to 0$

By taking $a \to 0$, Equations (3.36a) and (3.36b) convert to

$$\lim_{a\to 0} \xi_1 = \lim_{a\to 0} \xi_2 = \mathscr{L}^{-1}\left[\frac{r}{nb}\right] = \beta. \tag{C.13}$$

Thus, the second term in Equation (3.37) encounters the indeterminate form of $0/0$. To evaluate this expression, L'Hospital's rule is applied. Let us rewrite Equation (3.37) as

$$\frac{b\langle f_r\rangle}{k_B T} = \frac{b}{r} + \frac{\xi_1 \mathscr{I}_1 - \xi_2 \mathscr{I}_2}{\mathscr{I}_1 - \mathscr{I}_2}. \tag{C.14}$$

where

$$\mathscr{I}_1 = \left[\frac{\sinh\xi_1}{\xi_1}\right]^n \exp\left[-\xi_1\left(\frac{r-a}{b}\right)\right], \tag{C.15a}$$

$$\mathscr{I}_2 = \left[\frac{\sinh\xi_2}{\xi_2}\right]^n \exp\left[-\xi_2\left(\frac{r+a}{b}\right)\right]. \tag{C.15b}$$

By adopting the chain rule,

$$\frac{\mathrm{d}\mathscr{I}_1}{\mathrm{d}a} = \left(\frac{\partial \mathscr{I}_1}{\partial \xi_1}\right)_a \frac{\mathrm{d}\xi_1}{\mathrm{d}a} + \left(\frac{\partial \mathscr{I}_1}{\partial a}\right)_{\xi_1}. \tag{C.16}$$

While from Equation (C.15a):

$$\left(\frac{\partial \mathscr{I}_1}{\partial \xi_1}\right)_a = n\left[\frac{\sinh\xi_1}{\xi_1}\right]^n \exp\left[-\xi_1\left(\frac{r-a}{b}\right)\right]\left(\coth\xi_1 - \frac{1}{\xi_1} - \frac{r-a}{nb}\right) = 0. \quad \text{(C.17)}$$

Now, Equation (C.16) is simplified to

$$\frac{\mathrm{d}\mathscr{I}_1}{\mathrm{d}a} = \left(\frac{\partial \mathscr{I}_1}{\partial a}\right)_{\xi_1} = \frac{\xi_1}{b}\mathscr{I}_1. \quad \text{(C.18)}$$

Similarly,

$$\frac{\mathrm{d}\mathscr{I}_2}{\mathrm{d}a} = \left(\frac{\partial \mathscr{I}_2}{\partial a}\right)_{\xi_2} = -\frac{\xi_2}{b}\mathscr{I}_2. \quad \text{(C.19)}$$

Consequently, by defining

$$\mathscr{I} = \lim_{a\to 0}\mathscr{I}_1 = \lim_{a\to 0}\mathscr{I}_2 = \left[\frac{\sinh\beta}{\beta}\right]^n \exp\left[-\frac{\beta r}{b}\right], \quad \text{(C.20)}$$

and using Equations (C.13), (C.18), and (C.19) one can write

$$\lim_{a\to 0}\frac{\mathrm{d}\mathscr{I}_1}{\mathrm{d}a} = -\lim_{a\to 0}\frac{\mathrm{d}\mathscr{I}_2}{\mathrm{d}a} = \frac{\beta}{b}\mathscr{I}. \quad \text{(C.21)}$$

On the other hand, if $a \to 0$, Equations (3.36a) and (3.36b) lead to

$$\lim_{a\to 0}\frac{\mathrm{d}\xi_1}{\mathrm{d}a} = -\lim_{a\to 0}\frac{\mathrm{d}\xi_2}{\mathrm{d}a} = \frac{-1}{nb}\left(\mathscr{L}^{-1}\right)'(x)\Big|_{x=\frac{r}{nb}} = \frac{-1}{nb}\frac{1}{\mathscr{L}'\left(\mathscr{L}^{-1}\left[\frac{r}{nb}\right]\right)}, \quad \text{(C.22)}$$

where the inverse function rule has been applied for the last identity. Now adopting (C.13) and using the fact that $\mathscr{L}(x) = \coth(x) - 1/x$ yield the following result

$$\lim_{a\to 0}\frac{\mathrm{d}\xi_1}{\mathrm{d}a} = -\lim_{a\to 0}\frac{\mathrm{d}\xi_2}{\mathrm{d}a} = \frac{-1}{nb}\frac{\beta^2}{1-\beta^2\,\mathrm{csch}^2\beta}. \quad \text{(C.23)}$$

With the aid of Equations (C.20), (C.21) and (C.23), Equation (C.14) in the limit of $a \to 0$ is given by

$$\begin{aligned}\lim_{a\to 0}\frac{b\langle f_r\rangle}{k_BT} &= \frac{b}{r} + \lim_{a\to 0}\frac{\xi_1\dfrac{\mathrm{d}\mathscr{I}_1}{\mathrm{d}a} - \xi_2\dfrac{\mathrm{d}\mathscr{I}_2}{\mathrm{d}a}}{\dfrac{\mathrm{d}\mathscr{I}_1}{\mathrm{d}a} - \dfrac{\mathrm{d}\mathscr{I}_2}{\mathrm{d}a}} + \lim_{a\to 0}\frac{\mathscr{I}_1\dfrac{\mathrm{d}\xi_1}{\mathrm{d}a} - \mathscr{I}_2\dfrac{\mathrm{d}\xi_2}{\mathrm{d}a}}{\dfrac{\mathrm{d}\mathscr{I}_1}{\mathrm{d}a} - \dfrac{\mathrm{d}\mathscr{I}_2}{\mathrm{d}a}} \\ &= \beta + \left(\frac{b}{r} - \frac{\beta}{n\left(1-\beta^2\mathrm{csch}^2\beta\right)}\right). \end{aligned} \quad \text{(C.24)}$$

This result corresponds to the force-extension relationship for a pure coil as shown in Chapter 2. It should be noted that for $n \to \infty$ the term in the parenthesis is negligible and the following well-known result is recovered:

$$\lim_{a\to 0} \langle f_r \rangle = \frac{k_B T}{b}\beta. \tag{C.25}$$

With the same approach, by employing L'Hospital's rule and using Equations (C.18) and (C.19), one can simplify Equation (3.35) for $a \to 0$ to

$$\lim_{a\to 0} W_n^{\mathrm{CR}}(r) = \frac{C_n \beta}{2\pi b\, r}\left[\frac{\sinh\beta}{\beta}\right]^n \exp\left[-\frac{\beta r}{b}\right]. \tag{C.26}$$

C.3 Derivation of Equation (4.8) and simplification for $a \to 0$

Let us rewrite Equation (3.35) as

$$W_n^{\mathrm{CR}}(r) = \frac{C_n\,(\mathscr{I}_1 - \mathscr{I}_2)}{4\pi a r}, \tag{C.27}$$

where $\mathscr{I}_1$ and $\mathscr{I}_2$ have been introduced in (C.15a) and (C.15b), respectively. By applying the chain rule, one can write

$$\frac{\mathrm{d}\mathscr{I}_1}{\mathrm{d}n} = \left(\frac{\partial \mathscr{I}_1}{\partial \xi_1}\right)_n \frac{\mathrm{d}\xi_1}{\mathrm{d}n} + \left(\frac{\partial \mathscr{I}_1}{\partial n}\right)_{\xi_1} = \left(\frac{\partial \mathscr{I}_1}{\partial n}\right)_{\xi_1} = \ln\left[\frac{\sinh\,\xi_1}{\xi_1}\right]\mathscr{I}_1. \tag{C.28}$$

in which the partial derivative of $\mathscr{I}_1$ with respect to ξ_1 vanishes according to (C.17). It can be similarly concluded that

$$\frac{\mathrm{d}\mathscr{I}_2}{\mathrm{d}n} = \left(\frac{\partial \mathscr{I}_2}{\partial \xi_2}\right)_n \frac{\mathrm{d}\xi_2}{\mathrm{d}n} + \left(\frac{\partial \mathscr{I}_1}{\partial n}\right)_{\xi_2} = \left(\frac{\partial \mathscr{I}_1}{\partial n}\right)_{\xi_2} = \ln\left[\frac{\sinh\,\xi_2}{\xi_2}\right]\mathscr{I}_2. \tag{C.29}$$

Now, the partial derivative of (C.27) with respect to n is carried out by utilizing Equations (C.28) and (C.29) as

$$\frac{\partial W_n^{\mathrm{CR}}}{\partial n} = \frac{1}{4\pi a r}\left\{\frac{\partial C_n}{\partial n}(\mathscr{I}_1 - \mathscr{I}_2) + C_n\left(\ln\left[\frac{\sinh\,\xi_1}{\xi_1}\right]\mathscr{I}_1 - \ln\left[\frac{\sinh\,\xi_2}{\xi_2}\right]\mathscr{I}_2\right) - \frac{C_n(\mathscr{I}_1 - \mathscr{I}_2)}{a}\frac{\partial a}{\partial n}\right\} \tag{C.30}$$

Carrying Equation (C.30) into Equation (4.7) and setting $a = (N-n)\alpha$ yields

$$\left.\frac{\frac{\partial C_n}{\partial n}}{C_n}\right|_{n=n_0} + \left.\frac{\ln\left[\frac{\sinh\,\xi_1}{\xi_1}\right]\mathscr{I}_1 - \ln\left[\frac{\sinh\,\xi_2}{\xi_2}\right]\mathscr{I}_2}{\mathscr{I}_1 - \mathscr{I}_2}\right|_{n=n_0} + \frac{1}{N-n} = \frac{\varepsilon}{k_B T}. \tag{C.31}$$

For $n > 10$, C_n can be approximated by Equation (C.10). Thus,

$$\frac{\partial C_n}{\partial n} = \frac{-C_n}{2n}, \tag{C.32}$$

and Equation (C.31) collapses to Equation (4.8).

For $a \to 0$, it is required to substitute Equation (C.26) into (4.7). After some mathematical manipulation, it can be shown that Equation (4.8) reduces to

$$\frac{-1}{2n} + \ln\left[\frac{\sinh\,\beta}{\beta}\right] - \frac{r}{n^2 b}\frac{\beta}{1-\beta^2\mathrm{csch}^2\beta} = \frac{\varepsilon}{k_B T}. \tag{C.33}$$

If $n \to \infty$, the first and third terms on the left hand side are negligible, hence

$$\ln\left[\frac{\sinh\,\beta}{\beta}\right] = \frac{\varepsilon}{k_B T}, \tag{C.34}$$

which is a relationship presented by Higgs and Ball [3].

C.4 Another example of uniaxial loading-unloading with different material parameters

Parallel to Figure 2.2 in the main text, Figure C.2 shows another example of unaxial loading-unloading for a different set of parameters: $N = 50$, $\alpha = 0.1$, $\varepsilon = 5k_BT$. The loading curve is generated for $n_{\min} = 10$, while the unloading curve is provided for $n_{\min} = 30$. Fig C.2(a) shows the normalized first Piola Kirchhoff stress P_1/G against λ_1 with a permanent set 1.1 as shown in the inset. The curve exhibits fluctuations during unzipping, where each drop indicates, on average, the release of one Kuhn segment from the rod to the coil. As stretching continues, the curve maintains a plateau-like behavior, but the magnitude of fluctuations diminishes as the rod shrinks. Upon reaching state (III), the load is gradually removed, and the unloading curve

converges to the curve with a fixed $n = 30$. Fig C.2(b) shows the change of n_0 as a function of λ_1, and different from Figure 2.2, the deviation of n_0 from 10 starts at state (II). Finally, Figures C.2(c) and (d) illustrate the variations of λ_2 and J with respect to λ_1, which also contain fluctuation regions corresponding to the occurrence of unzipping.

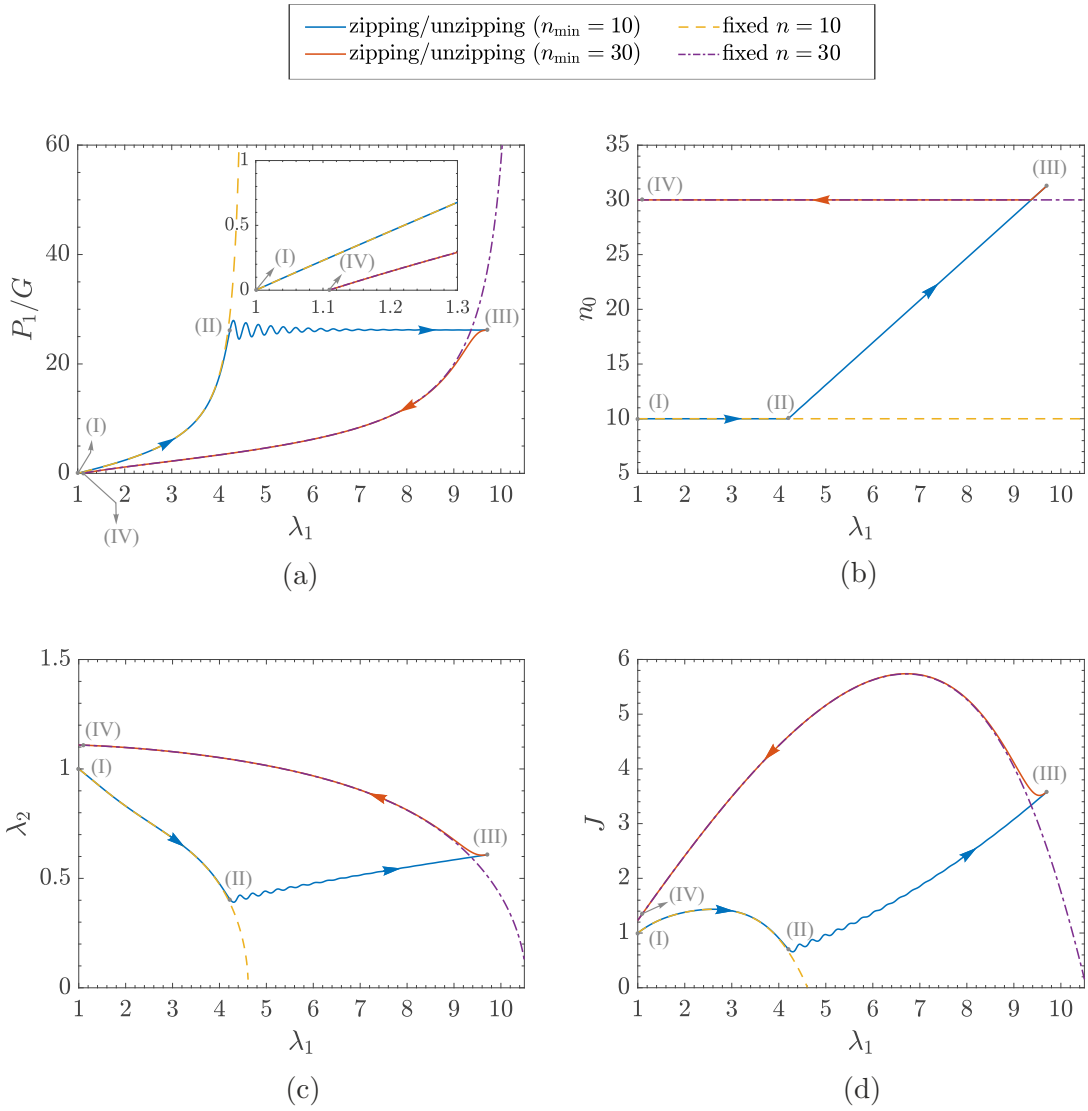

Figure C.2: Different parameters vs. stretch λ_1 for a uniaxial loading-unloading cycle along direction 1; $N = 50$, $\alpha = 0.1$, $\varepsilon = 5k_BT$. Dashed yellow and dash-dotted purple curves assume fixed $n = 10$ and 30, respectively. Blue and red curves depict the presence of zipping/unzipping with $n_{\min} = 10$ and 30, respectively. (a) Normalized Piola-Kirchhoff stress P_1, (b) Number of Kuhn segments n_0 in the coil with maximum contribution to the grand canonical partition function, (c) Stretch ratio λ_2, (d) Volume ratio J.

C.5 Derivation of (4.23) and (4.27)

Let us suppose that the unswollen state $(0')$ comprises ϱ free chains per unit unswollen volume. As shown in Figure C.3, the volume of the body is denoted as V_0 and assumed

to be the summation of the volume occupied by each chain. State (I′) is the swollen state resulting from the addition of M solvent molecules (per unit unswollen volume in 0′) to state (0′). The total volume of the swollen body (I′) is assumed to be $V_p + V_s$ where V_s and V_p are the volumes occupied by solvent and polymer chains, respectively. The entropy change per unit unswollen volume from state (0′) to (I′) is written based on the Flory-Huggins model as [4, 5]:

$$\Delta S_{0'\to \mathrm{I}'} = -k_B \left(M \ln \left[\frac{V_s}{V_s + V_p} \right] + \varrho \ln \left[\frac{V_p}{V_s + V_p} \right] \right). \tag{C.35}$$

Due to gelation, coil-rod structures with n Kuhn segments in the coil are formed in state (I) on the diagonals of the cubes in Figure 4.6. If it is assumed that the volume change from state (I′) to (I) is zero, the entropy change per unit unswollen volume from state (I′) to (I) is given by

$$\Delta S_{\mathrm{I}'\to \mathrm{I}} = \varrho k_B \ln \left[W_n^{\mathrm{CR}} \left(\lambda_v r_0 \right) \lambda_v^3 \mathrm{d}V_0 \right], \tag{C.36}$$

where the stretch λ_v^3 represents the ratio of volume in (I′) (or (I)) to the volume in (0′), and is equal to

$$\lambda_v^3 = \frac{V_s + V_p}{V_0}. \tag{C.37}$$

If we consider that each solvent molecule occupies one lattice cell in the Flory-Huggins theory, while each chain in the unswollen state (0′) occupies τ cells, then $V_0/V_s = \varrho\tau/M$. Consequently, Equation (C.37) can be rewritten as

$$V_p = \left(\mu^{-1} \tau \lambda_v^3 - 1 \right) V_s, \tag{C.38}$$

where μ is defined in (4.22). The combination of (C.35) and (C.36), along with Equation (C.38), results in

$$\Delta S_{0'\to \mathrm{I}} = -M k_B \ln \left[\mu \tau^{-1} \lambda_v^{-3} \right] - \varrho k_B \ln \left[1 - \mu \tau^{-1} \lambda_v^{-3} \right] + \varrho k_B \ln \left[W_n^{\mathrm{CR}} \left(\lambda_v r_0 \right) \lambda_v^3 \mathrm{d}V_0 \right]. \tag{C.39}$$

Now, let us define state (0) with the same volume as (0′), in which the unswollen network is formed by constructing coil-rod structures along the diagonals of the cubes in

Figure 4.6. In a manner similar to the change from (I′) to (I) but without introducing any solvents, the entropy change from state (0′) to (0) is simply obtained by setting $\lambda_v = 1$ and $M = 0$ ($\mu = 0$) in Equation (C.39):

$$\Delta S_{0'\to 0} = \varrho k_B \, \ln \left[W_n^{\mathrm{CR}} \left(r_0 \right) \mathrm{d}V_0 \right] . \tag{C.40}$$

By utilizing (C.39) and (C.40), one can conclude that

$$\Delta S_{0\to \mathrm{I}} = - \, M k_B \ln \left[\mu \tau^{-1} \lambda_v^{-3} \right] - \varrho k_B \, \ln \left[\frac{\lambda_v^3 - \mu \tau^{-1}}{\lambda_v^6} \right] + \varrho k_B \, \ln \left[\frac{W_n^{\mathrm{CR}} \left(\lambda_v r_0 \right)}{W_n^{\mathrm{CR}} \left(r_0 \right)} \right] . \tag{C.41}$$

Equation (C.41) presents the change of entropy due to the addition of the solvents to the unwollen network as given by (4.23). By simply replacing λ_v with λ_s in the above relations, it is emphasized that the states (I) and (I′) are stress-free.

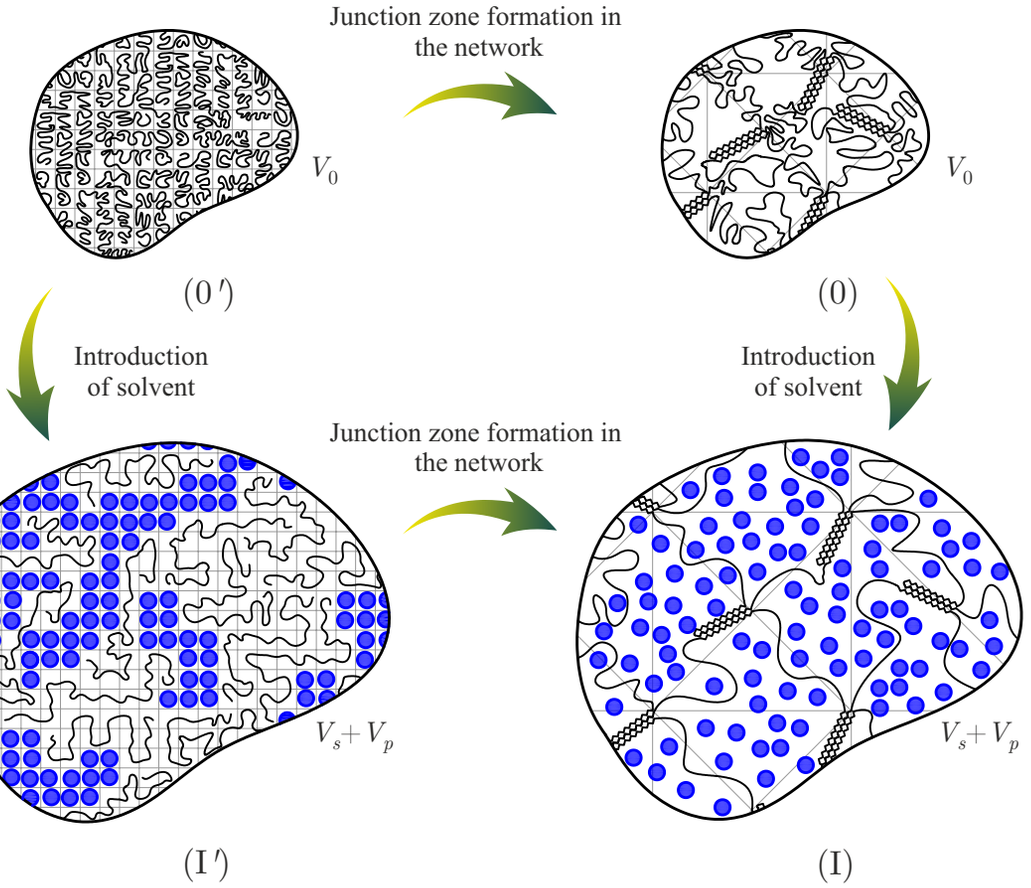

Figure C.3: Different states of the body during gelation in a schematic two-dimensional representation: State (0′) illustrates free chains inside the body with volume V_0. The lattice in the context of Flory-Huggins theory is also shown. Each chain occupies a certain number x of lattice cells (in this specific schematic, $\tau = 8$). State (0) shows the formation of junction zones in the network with the same volume V_0. State (I′) is achieved through the mixing of solvents with the chains in state (0′), resulting in isotropic expansion of the body with a new volume $V_s + V_p$. Each solvent molecule occupies one cell in the swollen state (I′), while each chain undergoing extension occupies more cells compared to state (0′) (in this schematic, it is 15 cells). State (I) with volume $V_s + V_p$ represents the formation of junction zones in the network in the presence of the solvent molecules.

Now consider the swollen stress-free state (I) deforming to a new state (II), in which the number of solvents remains fixed, but the sample undergoes stretches of λ_1, λ_2, and λ_3 with a volume expansion $J = \lambda_1\lambda_2\lambda_3$ measured with respect to state (I). Likewise, an intermediate state (II$'$) can be constructed through isotropic expansion of state (I$'$) by J with respect to (I$'$), while the number of solvents does not change. By defining V_p' as the volume occupied by the polymers in state (II) (or (II$'$)) and considering fixed M, the entropy of mixing per unit unswollen volume between (0$'$) and (II$'$) is given by

$$\Delta S_{0'\to \mathrm{II}'} = -k_B \left(M \ln \left[\frac{V_s}{V_s + V_p'} \right] + \varrho \ln \left[\frac{V_p'}{V_s + V_p'} \right] \right). \tag{C.42}$$

Additionally, the volume ratio J can also be expressed as

$$J = \frac{V_p' + V_s}{V_p + V_s}. \tag{C.43}$$

By employing (C.37) in the above relation, it can be shown that

$$V_p' = \left(\mu^{-1} \tau J \lambda_s^3 - 1 \right) V_s. \tag{C.44}$$

Substitution of (C.44) into (C.42) yields

$$\Delta S_{0'\to \mathrm{II}'} = -k_B \left(M \ln \left[\mu \tau^{-1} \lambda_s^{-3} J^{-1} \right] + \varrho \ln \left[1 - \mu \tau^{-1} \lambda_s^{-3} J^{-1} \right] \right). \tag{C.45}$$

On the other hand, the entropy change per unit unswollen volume between states (II$'$) and (II) is constructed in a manner similar to Equation (C.36):

$$\Delta S_{\mathrm{II}'\to \mathrm{II}} = \varrho k_B \, \ln \left[W_n^{\mathrm{CR}} \left(\lambda_s \lambda_{\mathrm{chain}} r_0 \right) J \lambda_s^3 \mathrm{d}V_0 \right], \tag{C.46}$$

where it is assumed that the number of Kuhn segments in the coil is n, the same as that of state (I). Summation of (C.45) and (C.46) gives rise to

$$\begin{aligned} &\Delta S_{0'\to \mathrm{II}} \\ &= -M k_B \ln \left[\mu \tau^{-1} \lambda_s^{-3} J^{-1} \right] - \varrho k_B \ln \left[\frac{1 - \mu \tau^{-1} \lambda_s^{-3} J^{-1}}{J \lambda_s^3} \right] + \varrho k_B \, \ln \left[W_n^{\mathrm{CR}} \left(\lambda_s \lambda_{\mathrm{chain}} r_0 \right) \mathrm{d}V_0 \right]. \end{aligned} \tag{C.47}$$

To this end, the entropy change per unit unswollen volume from state (0) to (II) is given by subtracting (C.40) from (C.47) as

$$\Delta S_{0\to \mathrm{II}} = -Mk_B \ln\left[\mu\tau^{-1}\lambda_s^{-3}J^{-1}\right] - \varrho k_B \ln\left[\frac{\lambda_s^3 J - \mu\tau^{-1}}{J^2\lambda_s^6}\right] + \varrho k_B \ln\left[\frac{W_n^{\mathrm{CR}}\left(\lambda_s\lambda_{\mathrm{chain}}r_0\right)}{W_n^{\mathrm{CR}}\left(r_0\right)}\right], \tag{C.48}$$

which is equivalent to Equation (4.27).

C.6 Thermodynamics consideration of the constitutive relation

In this section, the second law of thermodynamics as applied to the constitutive relation developed in this work is discussed. For a spontaneous process, in the absence of heat transfer, the Clausius-Duhem inequality implies that [6]

$$\mathbf{P} : \dot{\mathbf{F}} - \dot{\Psi} - S\dot{T} \geq 0, \tag{C.49}$$

where overdot denotes the material time derivative, $\mathbf{A} : \mathbf{B} = \mathrm{tr}\left(\mathbf{A}\mathbf{B}^{\mathrm{T}}\right)$ and superscript T is the transpose. $\mathbf{P}$ and $\mathbf{F}$ are respectively the first Piola-Kirchhoff stress tensor and the deformation gradient tensor. Since our formulation involves dissipation mechanism represented by change in $n_{\min}$, $n_{\min}$ can be considered as an internal variable for the Helmholtz free energy, in addition to $\mathbf{F}$ and T. The elastic and plastic deformations can be stated using the multiplicative decomposition of [7]:

$$\mathbf{F} = \mathbf{F}^e\mathbf{F}^p, \tag{C.50}$$

where the plastic deformation $\mathbf{F}^p$ is expressed in terms of λ_p introduced in section 4.4

$$\mathbf{F}^p = \lambda_p\mathbf{I}, \tag{C.51}$$

and $\mathbf{I}$ is the identity tensor. By applying Equation (4.26), one can find a relationship between λ_p and $n_{\min}$ as below:

$$\frac{\lambda_p r_0}{b}\frac{b\langle f_r\rangle\Big|_{r_0\lambda_p}}{k_BT} = 3\left(1+\mu\right), \tag{C.52}$$

where $\langle f_r \rangle$ is given by Equation (3.37) with n is replaced by $n_{\min}$. This relation is analogous to Equation (4.18) but with the consideration of swelling. Since $\mathbf{F}^p$ is given in terms of $n_{\min}$, the Helmholtz free energy can be written as

$$\Psi = \Psi(\mathbf{F}^e, T, n_{\min}). \tag{C.53}$$

Using (C.50) and (C.53), Equation (C.49) is rewritten as [8]

$$\left(\mathbf{F}^p\mathbf{P} - \frac{\partial \Psi}{\partial \mathbf{F}^e}\right) : \dot{\mathbf{F}}^e + \mathbf{P}\mathbf{F}^e : \dot{\mathbf{F}}^p - \frac{\partial \Psi}{\partial n_{\min}}\dot{n}_{\min} \geq 0. \tag{C.54}$$

The partial differentiation with respect to each variable, $\mathbf{F}^e$, T, or $n_{\min}$, implicitly implies that the other two are kept fixed. By applying the definition

$$\mathbf{P} = \frac{\partial \Psi}{\partial \mathbf{F}}, \tag{C.55}$$

the first term in (C.54) automatically vanishes. Furthermore, by applying the chain rule

$$\frac{\partial \Psi}{\partial n_{\min}} = \left(\frac{\partial \Psi}{\partial \mathbf{F}^p}\right)_{n_{\min}} \frac{\partial \mathbf{F}^p}{\partial n_{\min}} + \left(\frac{\partial \Psi}{\partial n_{\min}}\right)_{\mathbf{F}}, \tag{C.56}$$

and (C.55), the inequality (C.54) is simplified to

$$-\left(\frac{\partial \Psi}{\partial n_{\min}}\right)_{\mathbf{F}} \dot{n}_{\min} \geq 0. \tag{C.57}$$

In the above relation, the subscript $\mathbf{F}$ emphasizes that the partial differentiation is conducted while not only $\mathbf{F}^e$ but also $\mathbf{F}^p$ are treated as fixed. To derive a more explicit expression for the inequality (C.57), one should generalize Equation (4.28) in the presence of zipping/unzipping. For this purpose, in Equation (4.28), the canonical partition functions W_n is replaced by the grand canonical partition function Ω. Under general deformation $\mathbf{F}$, the Helmholtz free energy can be stated as:

$$\Psi = \Psi_{\mathrm{I}} + G\left\{-\ln\left[\frac{\Omega(\lambda_s \lambda_{\text{chain}} r_0, T, \varepsilon)}{\Omega(\lambda_s r_0, T, \varepsilon)}\right] - (\mu + 1)\ \ln J\right\}, \tag{C.58}$$

where the large τ approximation has been used,

$$\lambda_{\text{chain}} = \sqrt{\frac{\mathbf{F} : \mathbf{F}}{3}}, \tag{C.59}$$

and $J = \det\mathbf{F}$. It should be noted that using Equation (C.58) together with Equation (4.14) recovers the constitutive relation (4.30) presented earlier. By treating $n_{\min}$ as a continuous variable, Ω in Equation (3.43) can be rewritten into the following integral form:

$$\Omega(r, T, \varepsilon) \propto \int_{n=n_{\min}}^{N} \exp\left(\ln\left[W_n^{\mathrm{CR}}(r)\right] - \frac{n\varepsilon}{k_B T}\right) \mathrm{d}n. \tag{C.60}$$

Applying the above result in (C.57) leads to

$$G \exp\left[\frac{-n_{\min}\varepsilon}{k_B T}\right] \left(\frac{W_{n_{\min}}^{\mathrm{CR}}(\lambda_s r_0)}{\Omega(\lambda_s r_0)} - \frac{W_{n_{\min}}^{\mathrm{CR}}(\lambda_s \lambda_{\mathrm{chain}} r_0)}{\Omega(\lambda_s \lambda_{\mathrm{chain}} r_0)}\right) \dot{n}_{\min} \geq 0. \tag{C.61}$$

Since G and $\exp\left[\frac{-n_{\min}\varepsilon}{k_B T}\right]$ are positive, the second law of thermodynamics leads to

$$\left(\frac{W_{n_{\min}}^{\mathrm{CR}}(\lambda_s r_0)}{\Omega(\lambda_s r_0)} - \frac{W_{n_{\min}}^{\mathrm{CR}}(\lambda_s \lambda_{\mathrm{chain}} r_0)}{\Omega(\lambda_s \lambda_{\mathrm{chain}} r_0)}\right) \dot{n}_{\min} \geq 0. \tag{C.62}$$

Physically, (C.62) can be understood in the context of zipping/unzipping. Specifically, $\frac{W_{n_{\min}}^{\mathrm{CR}}(\lambda_s r_0)}{\Omega(\lambda_s r_0)}$ and $\frac{W_{n_{\min}}^{\mathrm{CR}}(\lambda_s \lambda_{\mathrm{chain}} r_0)}{\Omega(\lambda_s \lambda_{\mathrm{chain}} r_0)}$ represent, respectively, the contributions of $n_{\min}$ to the grand canonical partition function Ω when the chains are in a stress-free bulk and when the chains are subjected to λ_{chain}. Although Figure 4.5 is generated for the case without swelling and a common factor of $\exp\left[\frac{-n\varepsilon}{k_B T}\right]$ is included in the plot (which is inconsequential for this discussion), it can be used as an example to assess the contribution of $n_{\min}$ to Ω. By looking at the data along the vertical axis where $n = n_{\min} = 10$, it can be seen that as λ_1 and hence λ_{chain} increases, the contribution of $n_{\min}$ to Ω decreases, i.e., $\frac{W_{n_{\min}}^{\mathrm{CR}}(\lambda_s r_0)}{\Omega(\lambda_s r_0)} > \frac{W_{n_{\min}}^{\mathrm{CR}}(\lambda_s \lambda_{\mathrm{chain}} r_0)}{\Omega(\lambda_s \lambda_{\mathrm{chain}} r_0)}$. Meanwhile, unzipping occurs indicating $\dot{n}_{\min} > 0$. Together the inequality (C.62) is satisfied. Likewise, if $\dot{n}_{\min} < 0$ i.e., the chains tend to zip and form longer rods, the contribution of $n_{\min}$ to Ω is expected to increase causing the term inside the parenthesis of (C.62) to be negative. The second law of thermodynamics is again satisfied under the scenario of zipping.

References

[1] L. Treloar, *The Physics of Rubber Elasticity* (Oxford Classic Texts in the Physical Sciences). Oxford University Press, USA, 1975, ISBN: 9780191523304.

[2] F. Olver, *Asymptotics and Special Functions*, W. Rheinbolt, Ed. Elsevier Science, 1974, ISBN: 9781483267449.

[3] P. G. Higgs and R. C. Ball, "Some ideas concerning the elasticity of biopolymer networks," *Macromolecules*, vol. 22, no. 5, pp. 2432–2437, 1989. DOI: 10.1021/ma00195a073. eprint: https://doi.org/10.1021/ma00195a073.

[4] P. J. Flory, "Thermodynamics of high polymer solutions," *The Journal of Chemical Physics*, vol. 10, no. 1, pp. 51–61, 1942. DOI: 10.1063/1.1723621. eprint: https://doi.org/10.1063/1.1723621.

[5] M. L. Huggins, "Solutions of Long Chain Compounds," *The Journal of Chemical Physics*, vol. 9, no. 5, pp. 440–440, 1941, ISSN: 0021-9606. DOI: 10.1063/1.1750930. eprint: https://pubs.aip.org/aip/jcp/article-pdf/9/5/440/8138635/440_1_online.pdf.

[6] G. Holzapfel, *Nonlinear Solid Mechanics: A Continuum Approach for Engineering*. Wiley, 2000, ISBN: 9780471823049.

[7] E. H. Lee, "Elastic-Plastic Deformation at Finite Strains," *Journal of Applied Mechanics*, vol. 36, no. 1, pp. 1–6, Mar. 1969, ISSN: 0021-8936. DOI: 10.1115/1.3564580.

[8] G. A. Maugin, "Eshelby stress in elastoplasticity and ductile fracture," *International Journal of Plasticity*, vol. 10, no. 4, pp. 393–408, 1994, ISSN: 0749-6419. DOI: https://doi.org/10.1016/0749-6419(94)90040-X.

Appendix D: Supporting Information for Chapter 5

D.1 Formulation for a phantom network of Gaussian coils

Suppose there is a collection of ν Gaussian chains forming a network structure, with no independent cyclic paths [1]. The total number of nodes in this structure is $\nu + 1$, out of which $p + 1$ nodes (labelled as s_1, s_2, $\cdots$, s_{p+1}) are fixed while the rest are free to fluctuate. These fixed nodes may later be transformed under macroscopic deformation. However, for the time being, they are called as fixed. With $p + 1$ fixed nodes, there are p constraints. Following the same approach presented in Section 5.2.3, all constraints are formulated using the three-dimensional Dirac delta function defined in Equation (5.15). Now, the probability distribution can be expressed using Fourier space representation:

$$P\left(\mathbf{R}_{s_1 s_2}, \cdots, \mathbf{R}_{s_1 s_{p+1}}\right) = (2\pi)^{-3p} \int \exp\Big[-\frac{1}{2}\mathbf{K}^{\mathrm{T}}\boldsymbol{\Gamma}\mathbf{K} - \boldsymbol{i}\mathbf{R}^{\mathrm{T}}\mathbf{K}\Big]\mathrm{d}\mathbf{K}, \tag{D.1}$$

where $\mathbf{K}$ is a $3p \times 1$ vector, and $\boldsymbol{\Gamma}$ is a $3p \times 3p$ symmetric matrix. Herein, it will be shown that Equation (D.1) can be envisioned as the probability distribution function of the $p + 1$ Gaussian chains with different orientation.

Theorem 1 *If* $\mathbf{K}$ *is a* $3p \times 1$ *variable vector,* $\mathbf{R}$ *is an arbitrary* $3p \times 1$ *parametric vector, and* $\boldsymbol{\Gamma}^T = \boldsymbol{\Gamma}$ *is a symmetric* $3p \times 3p$ *matrix. Then it can be shown that the*

[1] In graph theory, such a structure is referred to as a "tree".

following 3p-layer integration satisfies:

$$\int \exp\Big[-\frac{1}{2}\mathbf{K}^{\mathrm{T}}\boldsymbol{\Gamma}\mathbf{K}-\boldsymbol{i}\mathbf{R}^{\mathrm{T}}\mathbf{K}\Big]\mathrm{d}\mathbf{K}=\sqrt{\frac{(2\pi)^{3p}}{\det\boldsymbol{\Gamma}}}\exp\Big[-\frac{1}{2}\mathbf{R}^{\mathrm{T}}\boldsymbol{\Gamma}^{-1}\mathbf{R}\Big]. \tag{D.2}$$

Proof. By change of variable $\mathbf{K}=\mathbf{Y}-\boldsymbol{i}\boldsymbol{\Gamma}^{-1}\mathbf{R}$, the left hand side of Equation (D.2) is converted to

$$\exp\Big[-\frac{1}{2}\mathbf{R}^{\mathrm{T}}\boldsymbol{\Gamma}^{-1}\mathbf{R}\Big]\int \exp\Big[-\frac{1}{2}\mathbf{Y}^{\mathrm{T}}\boldsymbol{\Gamma}\mathbf{Y}\Big]\mathrm{d}\mathbf{Y}. \tag{D.3}$$

Since $\boldsymbol{\Gamma}$ is symmetric, it can be orthogonally diagonalized. Then determination of the above integration is simply achieved through introduction of orthogonal matrix $\mathbf{M}$:

$$\mathbf{M}^{\mathrm{T}}\boldsymbol{\Gamma}\mathbf{M}=\begin{pmatrix}\eta_1 & 0 & \cdots & 0\\ 0 & \eta_2 & \cdots & 0\\ \vdots & \vdots & \ddots & \vdots\\ 0 & 0 & \cdots & \eta_{3p}\end{pmatrix}, \tag{D.4}$$

such that $\eta_i,\ i=1,2,\cdots,3p$ are the eigenvalues of the matrix $\boldsymbol{\Gamma}$. Applying the following change of variables

$$\mathbf{X}=\mathbf{M}^{\mathrm{T}}\mathbf{Y} \tag{D.5}$$

leads to

$$\int \exp\Big[-\frac{1}{2}\mathbf{Y}^{\mathrm{T}}\boldsymbol{\Gamma}\mathbf{Y}\Big]\mathrm{d}\mathbf{Y}=\prod_{k=1}^{3p}\int \exp\Big[-\frac{1}{2}\eta_k X_k^2\Big]\mathrm{d}X_k=\prod_{k=1}^{3p}\sqrt{\frac{2\pi}{\eta_k}}=\sqrt{\frac{(2\pi)^{3p}}{\det\boldsymbol{\Gamma}}}, \tag{D.6}$$

where X_k is the kth element of vector $\mathbf{X}$. The last identity in the above relation is given based on the fact that

$$\det\boldsymbol{\Gamma}=\prod_{k=1}^{3p}\eta_k. \tag{D.7}$$

Substitution of Equation (D.6) in (D.3) completes the proof. ■

By applying (D.2), one can show that

$$P\left(\mathbf{R}_{s_1s_2},\cdots,\mathbf{R}_{s_1s_{p+1}}\right)=\sqrt{\frac{1}{(2\pi)^{3p}\det\boldsymbol{\Gamma}}}\exp\Big[-\frac{1}{2}\mathbf{R}^{\mathrm{T}}\boldsymbol{\Gamma}^{-1}\mathbf{R}\Big]. \tag{D.8}$$

Since $\mathbf{\Gamma}^{-1}$ is symmetric, the orthogonal matrix $\mathbf{M}$ ($\mathbf{M}^{-1} = \mathbf{M}^{\mathrm{T}}$) diagonalizes $\mathbf{\Gamma}^{-1}$ as

$$\mathbf{D} = \mathbf{M}^{\mathrm{T}}\mathbf{\Gamma}^{-1}\mathbf{M}, \tag{D.9}$$

and $\mathbf{D}$ is the diagonal matrix with eigenvalues entities. By defining

$$\bar{\mathbf{R}} = \mathbf{M}^{\mathrm{T}}\mathbf{R}, \tag{D.10}$$

and knowing the fact that $\mathbf{\Gamma}^{-1}$ contains the components of $[\mathbf{I}]_{3\times 3}$, one can conclude that there are p eigenvalues in the form of $\frac{3}{\bar{n}_i b^2}$, $i = 1, 2, \cdots, p$, with each eigenvalue having a triple degeneracy. Hence,

$$\det\mathbf{\Gamma} = \prod_{i=1}^{p} \left(\frac{\bar{n}_i b^2}{3}\right)^3. \tag{D.11}$$

Then,

$$P\left(\mathbf{R}_{s_1 s_2}, \cdots, \mathbf{R}_{s_1 s_{p+1}}\right) = \prod_{i=1}^{p} \left(\frac{3}{2\pi\bar{n}_i b^2}\right)^{3/2} \exp\left[-\frac{3\left(\bar{R}_i\right)_x^2}{2\bar{n}_i b^2} - \frac{3\left(\bar{R}_i\right)_y^2}{2\bar{n}_i b^2} - \frac{3\left(\bar{R}_i\right)_z^2}{2\bar{n}_i b^2}\right], \tag{D.12}$$

This result shows that any Gaussian phantom network with no cyclic paths can be modelled by equivalent p Gaussian chains where $\bar{n}_i$ is the number of Kuhn segments of the equivalent ith chain with end-to-end vector $\bar{\mathbf{R}}_i$ obtained from eigensystem $\mathbf{\Gamma}$ or $\mathbf{\Gamma}^{-1}$.

D.2 Calculation of integration (5.29)

Theorem 2 *If* $\mathbf{K}$ *is a* $3p \times 1$ *vector, consisting of a* $(3p-3) \times 1$ *vector* $\mathbf{K}_{\mathrm{a}}$ *and a* 3×1 *vector* $\mathbf{K}_{\mathrm{b}}$*, where* p *is an arbitrary positive integer:*

$$\mathbf{K} = \begin{pmatrix} \mathbf{K}_{\mathrm{a}} \\ \mathbf{K}_{\mathrm{b}} \end{pmatrix}, \tag{D.13}$$

$\mathbf{R}$ *is a* $3p \times 1$ *vector as*

$$\mathbf{R} = \begin{pmatrix} \mathbf{R}_{\mathrm{a}} \\ \mathbf{R}_{\mathrm{b}} \end{pmatrix}, \tag{D.14}$$

and $\mathbf{\Gamma}$ *is a* $3p \times 3p$ *symmetric matrix in the form of*

$$\mathbf{\Gamma} = \begin{pmatrix} \gamma_{11}\left[\mathbf{I}\right]_{3\times3} & \cdots & \gamma_{1p}\left[\mathbf{I}\right]_{3\times3} \\ \vdots & \ddots & \vdots \\ \gamma_{1p}\left[\mathbf{I}\right]_{3\times3} & \cdots & \gamma_{pp}\left[\mathbf{I}\right]_{3\times3} \end{pmatrix}, \tag{D.15}$$

then it can be shown

$$\begin{aligned} &\int \frac{1}{\mathbf{K}_{\mathrm{b}}^{\mathrm{T}}\mathbf{K}_{\mathrm{b}}\, a} \sin\left(\sqrt{\mathbf{K}_{\mathrm{b}}^{\mathrm{T}}\mathbf{K}_{\mathrm{b}}}\, a\right) \exp\Big[-\frac{1}{2}\mathbf{K}^{\mathrm{T}}\mathbf{\Gamma}\mathbf{K} - \boldsymbol{i}\mathbf{R}^{\mathrm{T}}\mathbf{K}\Big]\mathrm{d}\mathbf{K} \\ &= \sqrt{\frac{(2\pi)^{3p}\zeta_{pp}}{\det\mathbf{\Gamma}_{\mathrm{aa}}}}\, \frac{1}{a|\mathbf{L}|}\exp\left[-\frac{1}{2}\left(\mathbf{R}_{\mathrm{a}}^{\mathrm{T}}\mathbf{\Gamma}_{\mathrm{aa}}^{-1}\mathbf{R}_{\mathrm{a}}\right) - \frac{\zeta_{pp}}{2}\left(a^2 + |\mathbf{L}|^2\right)\right]\sinh\left[a|\mathbf{L}|\zeta_{pp}\right], \end{aligned} \tag{D.16}$$

where

$$\mathbf{L} = \mathbf{R}_b + \begin{pmatrix} \dfrac{\zeta_{1p}}{\zeta_{pp}}\left[\mathbf{I}\right]_{3\times3} & \dfrac{\zeta_{2p}}{\zeta_{pp}}\left[\mathbf{I}\right]_{3\times3} & \cdots & \dfrac{\zeta_{(p-1)p}}{\zeta_{pp}}\left[\mathbf{I}\right]_{3\times3} \end{pmatrix}\mathbf{R}_{\mathrm{a}}, \tag{D.17}$$

$$\mathbf{\Gamma}_{\mathrm{aa}} = \begin{pmatrix} \gamma_{11}\left[\mathbf{I}\right]_{3\times3} & \cdots & \gamma_{1(p-1)}\left[\mathbf{I}\right]_{3\times3} \\ \vdots & \ddots & \vdots \\ \gamma_{1(p-1)}\left[\mathbf{I}\right]_{3\times3} & \cdots & \gamma_{(p-1)(p-1)}\left[\mathbf{I}\right]_{3\times3} \end{pmatrix}, \tag{D.18}$$

and ζ_{ij}*,* $i, j = 1, 2, \cdots, p$ *are defined based on the inverse of* $\mathbf{\Gamma}$*:*

$$\mathbf{\Gamma}^{-1} = \left(\begin{array}{ccc:c} \zeta_{11}\left[\mathbf{I}\right]_{3\times3} & \cdots & \zeta_{1(p-1)}\left[\mathbf{I}\right]_{3\times3} & \zeta_{1p}\left[\mathbf{I}\right]_{3\times3} \\ \vdots & \vdots & \ddots & \vdots \\ \zeta_{1(p-1)}\left[\mathbf{I}\right]_{3\times3} & \cdots & \zeta_{(p-1)(p-1)}\left[\mathbf{I}\right]_{3\times3} & \zeta_{p(p-1)}\left[\mathbf{I}\right]_{3\times3} \\ \hdashline \zeta_{1p}\left[\mathbf{I}\right]_{3\times3} & \cdots & \zeta_{p(p-1)}\left[\mathbf{I}\right]_{3\times3} & \zeta_{pp}\left[\mathbf{I}\right]_{3\times3} \end{array}\right). \tag{D.19}$$

Proof. Let us define

$$I_0 = \int \frac{1}{\mathbf{K}_{\mathrm{b}}^{\mathrm{T}}\mathbf{K}_{\mathrm{b}}\, a} \sin\left(\sqrt{\mathbf{K}_{\mathrm{b}}^{\mathrm{T}}\mathbf{K}_{\mathrm{b}}}\, a\right) \exp\Big[-\frac{1}{2}\mathbf{K}^{\mathrm{T}}\mathbf{\Gamma}\mathbf{K} - \boldsymbol{i}\mathbf{R}^{\mathrm{T}}\mathbf{K}\Big]\mathrm{d}\mathbf{K}_{\mathrm{a}}\mathrm{d}\mathbf{K}_{\mathrm{b}}. \tag{D.20}$$

By rewriting Equation (D.15) in the form of block matrix:

$$\mathbf{\Gamma} = \begin{pmatrix} \mathbf{\Gamma}_{\mathrm{aa}} & \mathbf{\Gamma}_{\mathrm{ab}} \\ \mathbf{\Gamma}_{\mathrm{ab}}^{\mathrm{T}} & \mathbf{\Gamma}_{\mathrm{bb}} \end{pmatrix}, \tag{D.21}$$

where $\mathbf{\Gamma}_{\mathrm{bb}} = \gamma_{pp}\,[\mathbf{I}]_{3\times 3}$, one can expand the left hand side of Equation (D.20) in the block matrix form

$$I_0 = \int \frac{1}{\mathbf{K}_{\mathrm{b}}^{\mathrm{T}}\mathbf{K}_{\mathrm{b}}\,a}\sin\left(\sqrt{\mathbf{K}_{\mathrm{b}}^{\mathrm{T}}\mathbf{K}_{\mathrm{b}}}\,a\right)\exp\Big[-\frac{1}{2}\mathbf{K}_b^{\mathrm{T}}\mathbf{\Gamma}_{\mathrm{bb}}\mathbf{K}_{\mathrm{b}} - \boldsymbol{i}\mathbf{R}_{\mathrm{b}}^{\mathrm{T}}\mathbf{K}_{\mathrm{b}}\Big]$$
$$\times\left(\int \exp\Big[-\frac{1}{2}\mathbf{K}_a^{\mathrm{T}}\mathbf{\Gamma}_{\mathrm{aa}}\mathbf{K}_{\mathrm{a}} - \boldsymbol{i}\left(\mathbf{R}_{\mathrm{a}}^{\mathrm{T}} - \boldsymbol{i}\mathbf{K}_{\mathrm{b}}^{\mathrm{T}}\mathbf{\Gamma}_{\mathrm{ab}}^{\mathrm{T}}\right)\mathbf{K}_{\mathrm{a}}\Big]\mathrm{d}\mathbf{K}_{\mathrm{a}}\right)\mathrm{d}\mathbf{K}_{\mathrm{b}}. \tag{D.22}$$

With the aid of Theorem 1, the integration in the parenthesis of Equation (D.22) can be obtained as

$$\int \exp\Big[-\frac{1}{2}\mathbf{K}_a^{\mathrm{T}}\mathbf{\Gamma}_{\mathrm{aa}}\mathbf{K}_{\mathrm{a}} - \boldsymbol{i}\left(\mathbf{R}_{\mathrm{a}}^{\mathrm{T}} - \boldsymbol{i}\mathbf{K}_{\mathrm{b}}^{\mathrm{T}}\mathbf{\Gamma}_{\mathrm{ab}}^{\mathrm{T}}\right)\mathbf{K}_{\mathrm{a}}\Big]\mathrm{d}\mathbf{K}_{\mathrm{a}}$$
$$= \sqrt{\frac{(2\pi)^{3p-3}}{\det\mathbf{\Gamma}_{\mathrm{aa}}}}\exp\Big[-\frac{1}{2}\left(\mathbf{R}_{\mathrm{a}}^{\mathrm{T}} - \boldsymbol{i}\mathbf{K}_{\mathrm{b}}^{\mathrm{T}}\mathbf{\Gamma}_{\mathrm{ab}}^{\mathrm{T}}\right)\mathbf{\Gamma}_{\mathrm{aa}}^{-1}\left(\mathbf{R}_{\mathrm{a}} - \boldsymbol{i}\mathbf{\Gamma}_{\mathrm{ab}}\mathbf{K}_{\mathrm{b}}\right)\Big]. \tag{D.23}$$

Carrying Equation (D.23) into (D.22) and rearranging the expanded terms yields

$$I_0 = \sqrt{\frac{(2\pi)^{3p-3}}{\det\mathbf{\Gamma}_{\mathrm{aa}}}}\exp\Big[-\frac{1}{2}\left(\mathbf{R}_{\mathrm{a}}^{\mathrm{T}}\mathbf{\Gamma}_{\mathrm{aa}}^{-1}\mathbf{R}_{\mathrm{a}}\right)\Big]\int \frac{1}{\mathbf{K}_{\mathrm{b}}^{\mathrm{T}}\mathbf{K}_{\mathrm{b}}\,a}\sin\left(\sqrt{\mathbf{K}_{\mathrm{b}}^{\mathrm{T}}\mathbf{K}_{\mathrm{b}}}\,a\right)$$
$$\times\exp\Big[-\frac{1}{2}\mathbf{K}_b^{\mathrm{T}}\left(\mathbf{\Gamma}_{\mathrm{bb}} - \mathbf{\Gamma}_{\mathrm{ab}}^{\mathrm{T}}\mathbf{\Gamma}_{\mathrm{aa}}^{-1}\mathbf{\Gamma}_{\mathrm{ab}}\right)\mathbf{K}_{\mathrm{b}}\Big]\left(\exp\Big[-\boldsymbol{i}\left(\mathbf{R}_{\mathrm{b}}^{\mathrm{T}} - \mathbf{R}_{\mathrm{a}}^{\mathrm{T}}\mathbf{\Gamma}_{\mathrm{aa}}^{-1}\mathbf{\Gamma}_{\mathrm{ab}}\right)\mathbf{K}_{\mathrm{b}}\Big]\right)\mathrm{d}\mathbf{K}_{\mathrm{b}}. \tag{D.24}$$

Now, based on the definition (D.21), the inverse of symmetric matrix $\mathbf{\Gamma}$ is:

$$\mathbf{\Gamma}^{-1} = \left(\begin{array}{c|c} \mathbf{\Gamma}_{\mathrm{aa}}^{-1} + \mathbf{\Gamma}_{\mathrm{aa}}^{-1}\mathbf{\Gamma}_{\mathrm{ab}}\left(\mathbf{\Gamma}_{\mathrm{bb}} - \mathbf{\Gamma}_{\mathrm{ab}}^{\mathrm{T}}\mathbf{\Gamma}_{\mathrm{aa}}^{-1}\mathbf{\Gamma}_{\mathrm{ab}}\right)^{-1}\mathbf{\Gamma}_{\mathrm{ab}}^{\mathrm{T}}\mathbf{\Gamma}_{\mathrm{aa}}^{-1} & -\mathbf{\Gamma}_{\mathrm{aa}}^{-1}\mathbf{\Gamma}_{\mathrm{ab}}\left(\mathbf{\Gamma}_{\mathrm{bb}} - \mathbf{\Gamma}_{\mathrm{ab}}^{\mathrm{T}}\mathbf{\Gamma}_{\mathrm{aa}}^{-1}\mathbf{\Gamma}_{\mathrm{ab}}\right)^{-1} \\ \hline -\left(\mathbf{\Gamma}_{\mathrm{bb}} - \mathbf{\Gamma}_{\mathrm{ab}}^{\mathrm{T}}\mathbf{\Gamma}_{\mathrm{aa}}^{-1}\mathbf{\Gamma}_{\mathrm{ab}}\right)^{-1}\mathbf{\Gamma}_{\mathrm{ab}}^{\mathrm{T}}\mathbf{\Gamma}_{\mathrm{aa}}^{-1} & \left(\mathbf{\Gamma}_{\mathrm{bb}} - \mathbf{\Gamma}_{\mathrm{ab}}^{\mathrm{T}}\mathbf{\Gamma}_{\mathrm{aa}}^{-1}\mathbf{\Gamma}_{\mathrm{ab}}\right)^{-1} \end{array}\right). \tag{D.25}$$

By comparing Equations (D.25) and (D.19), one can easily conclude that

$$\mathbf{\Gamma}_{\mathrm{bb}} - \mathbf{\Gamma}_{\mathrm{ab}}^{\mathrm{T}}\mathbf{\Gamma}_{\mathrm{aa}}^{-1}\mathbf{\Gamma}_{\mathrm{ab}} = \frac{1}{\zeta_{pp}}\,[\mathbf{I}]_{3\times 3}\,. \tag{D.26}$$

Likewise, by defining

$$\mathbf{L} = \left(\mathbf{R}_b^{\mathrm{T}} - \mathbf{R}_{\mathrm{a}}^{\mathrm{T}}\mathbf{\Gamma}_{\mathrm{aa}}^{-1}\mathbf{\Gamma}_{\mathrm{ab}}\right)^{\mathrm{T}} \tag{D.27}$$

and analogy between the block matrices in (D.25) and (D.19), one can verify Equation (D.17). Substitution of Equations (D.26) and (D.17) in (D.24) gives rise to

$$I_0 = \sqrt{\frac{(2\pi)^{3p-3}}{\det\boldsymbol{\Gamma}_{\rm aa}}}\exp\Big[-\frac{1}{2}\left(\mathbf{R}_{\rm a}^{\rm T}\boldsymbol{\Gamma}_{\rm aa}^{-1}\mathbf{R}_{\rm a}\right)\Big] \int \frac{1}{\mathbf{K}_{\rm b}^{\rm T}\mathbf{K}_{\rm b}\,a}\sin\left(\sqrt{\mathbf{K}_{\rm b}^{\rm T}\mathbf{K}_{\rm b}}\,a\right)\exp\Big[-\frac{1}{2\zeta_{pp}}\mathbf{K}_b^{\rm T}\mathbf{K}_{\rm b}\Big]\exp\Big[-\boldsymbol{i}\mathbf{L}\cdot\mathbf{K}_{\rm b}\Big]\mathrm{d}\mathbf{K}_{\rm b}. \tag{D.28}$$

The integration on the right hand side is simplified by utilizing Equation (5.18), and $\mathrm{d}\mathbf{K}_{\rm b} = \mathrm{d}\mathbf{w}$ as

$$\begin{aligned}\int_{\theta=0}^{2\pi}\int_{w=0}^{+\infty}\int_{\phi=0}^{\pi}\frac{\sin(wa)}{wa}\exp\Big[-\frac{w^2}{2\zeta_{pp}}\Big]\exp\Big[-\boldsymbol{i}\,|\mathbf{L}|\,w\cos\phi\Big]w^2\sin\phi\,\mathrm{d}\phi\,\mathrm{d}w\,\mathrm{d}\theta&\\ =\frac{4\pi}{a\,|\mathbf{L}|}\int_{w=0}^{+\infty}\sin(wa)\,\sin(|\mathbf{L}|\,w)\,\exp\Big[-\frac{w^2}{2\zeta_{pp}}\Big]\,\mathrm{d}w&\\ =\frac{\sqrt{(2\pi)^3\,\zeta_{pp}}}{a\,|\mathbf{L}|}\exp\left[-\frac{\zeta_{pp}}{2}\left(a^2+|\mathbf{L}|^2\right)\right]\sinh\left[a\,|\mathbf{L}|\,\zeta_{pp}\right],&\end{aligned} \tag{D.29}$$

where spherical coordinates were used and $w = |\mathbf{w}|$. Finally, replacement of (D.29) in (D.28) completes the proof. ■

D.3 General formulation for one rod shared by multiple coils

Consider nodes s_1, s_2, $\cdots$, and s_t are located on one side of the rod, and the nodes s_{t+1} to s_{p+1} are located on the other side as seen in Fig. D.1a. The follwoing constraints hold

$$\mathbf{R}_{s_1 s_j} = \mathbf{R}_{s_1 f_1} + \mathbf{R}_{f_1 s_j}, \quad j = 2, 3, \cdots, t, \tag{D.30}$$

and the second set of constraints are

$$\mathbf{R}_{s_1 s_j} = \mathbf{R}_{s_1 f_1} + \mathbf{R}_{f_1 f_2} + \mathbf{R}_{f_2 s_j}, \quad j = t+1, \cdots, p+1. \tag{D.31}$$

In total, there are $3p$ constraints.

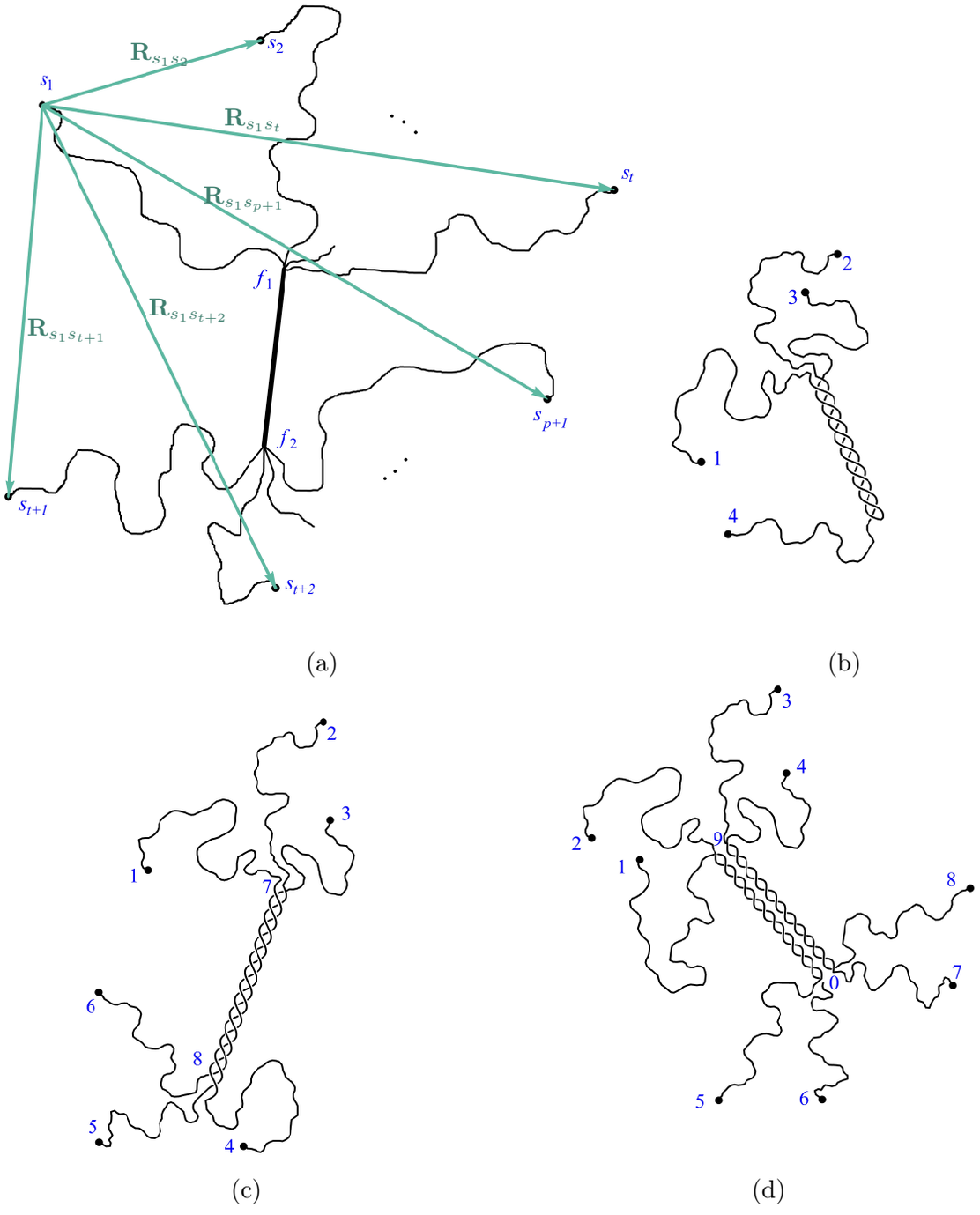

Figure D.1: (a) The topology of $(p+1)$-node coil-rod structure with one rod, (b) asymmetric four-node coil-rod structure, (c) symmetric six-node coil-rod structure, (d) symmetric eight-node coil-rod structure.

Similar to the four-node coil-rod structure, the probability density functioncan be written in the Fourier space as

$$
\begin{aligned}
&P\left(\mathbf{R}_{s_1s_2},\cdots,\mathbf{R}_{s_1s_p}\right)=(2\pi)^{-3p}\\
&\int\overline{W^{\mathrm{C}}}_{s_1f_1}\left(\left|\sum_{j=2}^{p+1}\mathbf{k}_{s_1s_j}\right|\right)\prod_{j=2}^{t}\overline{W^{\mathrm{C}}}_{s_jf_1}\left(\left|\mathbf{k}_{s_1s_j}\right|\right)\prod_{j=t+1}^{p+1}\overline{W^{\mathrm{C}}}_{s_jf_2}\left(\left|\mathbf{k}_{s_1s_j}\right|\right)\\
&\times\overline{W^{\mathrm{R}}}\left(\left|\sum_{j=t+1}^{p+1}\mathbf{k}_{s_1s_j}\right|\right)\exp\left[-\boldsymbol{i}\sum_{j=2}^{p+1}\mathbf{k}_{1j}\cdot\mathbf{R}_{1j}\right]\prod_{j=2}^{p+1}\mathrm{d}\mathbf{k}_{1j}.
\end{aligned}
\tag{D.32}
$$

The integration given by (D.32) is now expressed in the following compact form:

$$
P\left(\mathbf{R}_{s_1s_2},\cdots,\mathbf{R}_{s_1s_{p+1}}\right)=(2\pi)^{-3p}\int\overline{W^{\mathrm{R}}}(\sqrt{\mathbf{K}^{\mathrm{T}}\boldsymbol{\Lambda}\mathbf{K}})\exp\Big[-\frac{1}{2}\mathbf{K}^{\mathrm{T}}\boldsymbol{\Gamma}\mathbf{K}-\boldsymbol{i}\mathbf{R}^{\mathrm{T}}\mathbf{K}\Big]\mathrm{d}\mathbf{K},
\tag{D.33}
$$

where $\boldsymbol{\Gamma}$ is a $3p\times 3p$ matrix given as below

$$
\boldsymbol{\Gamma}=\frac{b^2}{3}\times
\begin{pmatrix}
(n_{s_1f_1}+n_{s_2f_1})[\mathbf{I}]_{3\times3} & \cdots & n_{s_1f_1}[\mathbf{I}]_{3\times3} & n_{s_1f_1}[\mathbf{I}]_{3\times3} & \cdots & n_{s_1f_1}[\mathbf{I}]_{3\times3}\\
\vdots & \ddots & \vdots & \vdots & \ddots & \vdots\\
n_{s_1f_1}[\mathbf{I}]_{3\times3} & \cdots & (n_{s_1f_1}+n_{s_tf_1})[\mathbf{I}]_{3\times3} & n_{s_1f_1}[\mathbf{I}]_{3\times3} & \cdots & n_{s_1f_1}[\mathbf{I}]_{3\times3}\\
n_{s_1f_1}[\mathbf{I}]_{3\times3} & \cdots & n_{s_1f_1}[\mathbf{I}]_{3\times3} & (n_{s_1f_1}+n_{s_{t+1}f_2})[\mathbf{I}]_{3\times3} & \cdots & n_{s_1f_1}[\mathbf{I}]_{3\times3}\\
\vdots & \ddots & \vdots & \vdots & \ddots & \vdots\\
n_{s_1f_1}[\mathbf{I}]_{3\times3} & \cdots & n_{s_1f_1}[\mathbf{I}]_{3\times3} & n_{s_1f_1}[\mathbf{I}]_{3\times3} & \cdots & (n_{s_1f_1}+n_{s_{p+1}f_2})[\mathbf{I}]_{3\times3}
\end{pmatrix},
\tag{D.34}
$$

and $\boldsymbol{\Lambda}$ is a $3p\times 3p$ written as

$$
\boldsymbol{\Lambda}=\left(\begin{array}{c|ccc}
\mathbf{0}_{(3t-3)\times(3t-3)} & \mathbf{0}_{(3t-3)\times3} & \cdots & \mathbf{0}_{(3t-3)\times3}\\
\hline
\mathbf{0}_{3\times(3t-3)} & [\mathbf{I}]_{3\times3} & \cdots & [\mathbf{I}]_{3\times3}\\
\vdots & \vdots & \ddots & \vdots\\
\mathbf{0}_{3\times(3t-3)} & [\mathbf{I}]_{3\times3} & \cdots & [\mathbf{I}]_{3\times3}
\end{array}\right).
\tag{D.35}
$$

and

$$\mathbf{K}^{\mathrm{T}} =$$

$$\{(k_{s_1s_2})_x \quad (k_{s_1s_2})_y \quad (k_{s_1s_2})_z \quad (k_{s_1s_3})_x \quad (k_{s_1s_3})_y \quad (k_{s_1s_3})_z \cdots (k_{s_1s_{p+1}})_x \quad (k_{s_1s_{p+1}})_y \quad (k_{s_1s_{p+1}})_z\}, \tag{D.36a}$$

$$\mathbf{R}^{\mathrm{T}} =$$

$$\{(R_{s_1s_2})_x \quad (R_{s_1s_2})_y \quad (R_{s_1s_2})_z \quad (R_{s_1s_3})_x \quad (R_{s_1s_3})_y \quad (R_{s_1s_3})_z \cdots (R_{s_1s_{p+1}})_x \quad (R_{s_1s_{p+1}})_y \quad (R_{s_1s_{p+1}})_z\}. \tag{D.36b}$$

Analogous to the method given for integration (5.22), one can employ the follwoing change of variable

$$\mathbf{Y} = \mathbf{A}\mathbf{K} \tag{D.37}$$

where

$$\mathbf{Y}^{\mathrm{T}} = \{(k_{s_1s_2})_x \quad (k_{s_1s_2})_y \quad (k_{s_1s_2})_z \quad \cdots \quad (k_{s_1s_p})_x \quad (k_{s_1s_p})_y \quad (k_{s_1s_p})_z \quad w_x \quad w_y \quad w_z\}, \tag{D.38}$$

and $\mathbf{A}$ is a $3p \times 3p$ matrix defined as

$$\mathbf{A} = \left(\begin{array}{ccc:ccc:c} \overbrace{\begin{matrix}[\mathbf{I}]_{3\times3} & \cdots & [\mathbf{0}]_{3\times3} \\ \vdots & \ddots & \vdots \\ [\mathbf{0}]_{3\times3} & \cdots & [\mathbf{I}]_{3\times3}\end{matrix}}^{3t-3 \text{ columns}} & \begin{matrix}[\mathbf{0}]_{3\times3} \\ \vdots \\ [\mathbf{0}]_{3\times3}\end{matrix} & \cdots & \begin{matrix}[\mathbf{0}]_{3\times3} \\ \vdots \\ [\mathbf{0}]_{3\times3}\end{matrix} & \begin{matrix}[\mathbf{0}]_{3\times3} \\ \vdots \\ [\mathbf{0}]_{3\times3}\end{matrix} \\ \hdashline \begin{matrix}[\mathbf{0}]_{3\times3} & \cdots & [\mathbf{0}]_{3\times3} \\ \vdots & \ddots & \vdots \\ [\mathbf{0}]_{3\times3} & \cdots & [\mathbf{0}]_{3\times3}\end{matrix} & \begin{matrix}[\mathbf{I}]_{3\times3} \\ \vdots \\ [\mathbf{0}]_{3\times3}\end{matrix} & \cdots & \begin{matrix}[\mathbf{0}]_{3\times3} \\ \vdots \\ [\mathbf{I}]_{3\times3}\end{matrix} & \begin{matrix}[\mathbf{0}]_{3\times3} \\ \vdots \\ [\mathbf{0}]_{3\times3}\end{matrix} \\ \hdashline \begin{matrix}[\mathbf{0}]_{3\times3} & \cdots & [\mathbf{0}]_{3\times3}\end{matrix} & \begin{matrix}[\mathbf{I}]_{3\times3}\end{matrix} & \cdots & \begin{matrix}[\mathbf{I}]_{3\times3}\end{matrix} & \begin{matrix}[\mathbf{I}]_{3\times3}\end{matrix} \end{array}\right), \tag{D.39}$$

with $\det\mathbf{A} = 1$. Now Equation (D.33) is rewritten as

$$P\left(\mathbf{R}_{s_1s_2}, \cdots, \mathbf{R}_{s_1s_{p+1}}\right) = (2\pi)^{-3p} \int \frac{1}{\sqrt{\mathbf{w}^{\mathrm{T}}\mathbf{w}}\, a} \sin\left(\sqrt{\mathbf{w}^{\mathrm{T}}\mathbf{w}}\, a\right) \exp\Big[-\frac{1}{2}\mathbf{Y}^{\mathrm{T}}\tilde{\mathbf{\Gamma}}\mathbf{Y} - \boldsymbol{i}\tilde{\mathbf{R}}^{\mathrm{T}}\mathbf{Y}\Big] \mathrm{d}\mathbf{Y}, \tag{D.40}$$

where

$$\tilde{\boldsymbol{\Gamma}} = \mathbf{A}^{-\mathrm{T}} \boldsymbol{\Gamma} \mathbf{A}^{-1}, \tag{D.41}$$

and

$$\tilde{\mathbf{R}} = \mathbf{A}^{-\mathrm{T}} \mathbf{R}. \tag{D.42}$$

Using (D.16), the result is simplified to

$$P\left(\mathbf{R}_{s_1 s_2}, \cdots, \mathbf{R}_{s_1 s_{p+1}}\right) = \sqrt{\frac{\tilde{\zeta}_{pp}}{(2\pi)^{3p} \det \tilde{\boldsymbol{\Gamma}}_{\mathrm{aa}}}} \frac{1}{a\tilde{L}} \exp\left[-\frac{1}{2}\left(\tilde{\mathbf{R}}_{\mathrm{a}}^{\mathrm{T}} \tilde{\boldsymbol{\Gamma}}_{\mathrm{aa}}^{-1} \tilde{\mathbf{R}}_{\mathrm{a}}\right) - \frac{\tilde{\zeta}_{pp}}{2}\left(a^2 + \tilde{L}^2\right)\right] \sinh\left[a\tilde{L}\tilde{\zeta}_{pp}\right], \tag{D.43}$$

in which

$$\tilde{\boldsymbol{\Gamma}} = \begin{pmatrix} \tilde{\boldsymbol{\Gamma}}_{\mathrm{aa}} & \tilde{\boldsymbol{\Gamma}}_{\mathrm{ab}} \\ \tilde{\boldsymbol{\Gamma}}_{\mathrm{ab}}^{\mathrm{T}} & \tilde{\boldsymbol{\Gamma}}_{\mathrm{bb}} \end{pmatrix}, \tag{D.44}$$

and

$$\tilde{\mathbf{L}} = \tilde{\mathbf{R}}_{\mathrm{b}} + \begin{pmatrix} \frac{\tilde{\zeta}_{1p}}{\tilde{\zeta}_{pp}} [\mathbf{I}]_{3\times 3} & \frac{\tilde{\zeta}_{2p}}{\tilde{\zeta}_{pp}} [\mathbf{I}]_{3\times 3} & \cdots & \frac{\tilde{\zeta}_{(p-1)p}}{\tilde{\zeta}_{pp}} [\mathbf{I}]_{3\times 3} \end{pmatrix} \tilde{\mathbf{R}}_{\mathrm{a}}. \tag{D.45}$$

Now, Equation (D.43) can be rewritten as

$$P\left(\mathbf{R}_{s_1 s_2}, \cdots, \mathbf{R}_{s_1 s_{p+1}}\right) = \sqrt{\frac{\tilde{\zeta}_{pp}}{(2\pi)^3}} \frac{1}{a\tilde{L}} \exp\left[-\frac{\tilde{\zeta}_{pp}\left(a^2 + \tilde{L}^2\right)}{2}\right] \sinh\left[a\tilde{L}\tilde{\zeta}_{pp}\right] \times \sqrt{\frac{1}{(2\pi)^{3p-3} \det \tilde{\boldsymbol{\Gamma}}_{\mathrm{aa}}}} \exp\left[-\frac{1}{2}\left(\tilde{\mathbf{R}}_{\mathrm{a}}^{\mathrm{T}} \tilde{\boldsymbol{\Gamma}}_{\mathrm{aa}}^{-1} \tilde{\mathbf{R}}_{\mathrm{a}}\right)\right]. \tag{D.46}$$

The above relation shows that the probability distribution of the any structure with one rod can be equivalent to the probability distribution of a coil-rod structure with rod length a and number of Kuhn segments $\dfrac{3}{\tilde{\zeta}_{pp} b^2}$ in coil with end-to-end vector $\tilde{\mathbf{L}}$, and the $p-1$ coils which is obtained from the eigenvector $\tilde{\boldsymbol{\Gamma}}_{\mathrm{aa}}^{-1}$ following the provided approach in D.1.

In the rest of this appendix, the proposed probability distribution function is further simplified for the special cases.

The extreme case $a \to 0$

Setting $a \to 0$ in Equation (D.46) leads to

$$P\left(\mathbf{R}_{s_1 s_2}, \cdots, \mathbf{R}_{s_1 s_{p+1}}\right) = \sqrt{\frac{\tilde{\zeta}_{pp}^3}{(2\pi)^{3p}\det\tilde{\mathbf{\Gamma}}_{\mathrm{aa}}}}\exp\left[-\frac{1}{2}\left(\tilde{\mathbf{R}}_{\mathrm{a}}^{\mathrm{T}}\tilde{\mathbf{\Gamma}}_{\mathrm{aa}}^{-1}\tilde{\mathbf{R}}_{\mathrm{a}} - \tilde{\zeta}_{pp}\tilde{L}^2\right)\right]. \quad \text{(D.47)}$$

By applying Equations (D.13), (D.25), (D.26), and (D.27) the identity

$$\mathbf{R}^{\mathrm{T}}\mathbf{\Gamma}^{-1}\mathbf{R} = \mathbf{R}_{\mathrm{a}}^{\mathrm{T}}\mathbf{\Gamma}_{\mathrm{aa}}^{-1}\mathbf{R}_{\mathrm{a}} + \zeta_{pp}L^2 \quad \text{(D.48)}$$

holds. The analogous conclusion can be drawn for the same variables with overtilde:

$$\tilde{\mathbf{R}}^{\mathrm{T}}\tilde{\mathbf{\Gamma}}^{-1}\tilde{\mathbf{R}} = \tilde{\mathbf{R}}_{\mathrm{a}}^{\mathrm{T}}\tilde{\mathbf{\Gamma}}_{\mathrm{aa}}^{-1}\tilde{\mathbf{R}}_{\mathrm{a}} + \tilde{\zeta}_{pp}\tilde{L}^2. \quad \text{(D.49)}$$

On the other hand, by applying the properties of the block matrix, from Equation (D.44),

$$\det\tilde{\mathbf{\Gamma}} = \det\tilde{\mathbf{\Gamma}}_{\mathrm{aa}}\det\left(\tilde{\mathbf{\Gamma}}_{\mathrm{bb}} - \tilde{\mathbf{\Gamma}}_{\mathrm{ab}}^{\mathrm{T}}\tilde{\mathbf{\Gamma}}_{\mathrm{aa}}^{-1}\tilde{\mathbf{\Gamma}}_{\mathrm{ab}}\right) = \frac{1}{\tilde{\zeta}_{pp}^3}\det\tilde{\mathbf{\Gamma}}_{\mathrm{aa}}, \quad \text{(D.50)}$$

where for the latter identity the similar properties of (D.26) is adopted. In the extreme case of $a \to 0$, it can be readily seen that

$$P\left(\mathbf{R}_{s_1 s_2}, \cdots, \mathbf{R}_{s_1 s_{p+1}}\right) = \sqrt{\frac{1}{(2\pi)^{3p}\det\tilde{\mathbf{\Gamma}}}}\exp\left[-\frac{1}{2}\left(\tilde{\mathbf{R}}^{\mathrm{T}}\tilde{\mathbf{\Gamma}}^{-1}\tilde{\mathbf{R}}\right)\right]. \quad \text{(D.51)}$$

The relation (D.51) was already provided by Flory [1] for a general phantom network containing only coils.

Asymmetric four-node structure with a rod

Using Equation (D.46) for $p = t = 3$ (see Fig. D.1b) yields

$$\begin{aligned} P\left(\mathbf{R}_{12}, \mathbf{R}_{13}, \mathbf{R}_{14}\right) =& \sqrt{\frac{\tilde{\zeta}_{33}}{(2\pi)^9\det\tilde{\mathbf{\Gamma}}_{\mathrm{aa}}}}\frac{1}{a\tilde{L}}\exp\left[-\frac{\tilde{\zeta}_{33}\left(a^2 + \tilde{L}^2\right)}{2}\right]\sinh\left[a\tilde{L}\tilde{\zeta}_{33}\right] \\ & \times \exp\left[-\frac{1}{2}\left(\tilde{\mathbf{R}}_{\mathrm{a}}^{\mathrm{T}}\tilde{\mathbf{\Gamma}}_{\mathrm{aa}}^{-1}\tilde{\mathbf{R}}_{\mathrm{a}}\right)\right], \end{aligned} \quad \text{(D.52)}$$

where

$$\tilde{\mathbf{\Gamma}}_{\mathrm{aa}} = \frac{b^2}{3}\begin{pmatrix} (n_{15}+n_{52})\,[\mathbf{I}]_{3\times3} & n_{15}\,[\mathbf{I}]_{3\times3} \\ n_{15}\,[\mathbf{I}]_{3\times3} & (n_{15}+n_{53})\,[\mathbf{I}]_{3\times3} \end{pmatrix}, \tag{D.53a}$$

$$\det\tilde{\mathbf{\Gamma}}_{\mathrm{aa}} = \frac{b^{12}}{3^6}\left(n_{15}n_{52}+n_{52}n_{53}+n_{15}n_{53}\right)^3, \tag{D.53b}$$

and

$$\tilde{\mathbf{R}}_{\mathrm{a}}^{\mathrm{T}} = \{(R_{12})_x \quad (R_{12})_y \quad (R_{12})_z \quad (R_{13})_x \quad (R_{13})_y \quad (R_{13})_z\}. \tag{D.54}$$

Moreover, $\tilde{\zeta}_{33}$ is defined according to Equation (D.19) for $\tilde{\mathbf{\Gamma}}^{-1}$, i.e.,:

$$\tilde{\zeta}_{33} = \frac{3}{b^2}\frac{n_{52}n_{53}+n_{15}\left(n_{52}+n_{53}\right)}{n_{52}n_{53}n_{64}+n_{15}\left(n_{53}n_{64}+n_{52}\left(n_{53}+n_{64}\right)\right)}. \tag{D.55}$$

Lastly, by using (D.17), and definition (D.13) one can show that

$$\tilde{\mathbf{L}} = \mathbf{R}_{14} - \frac{n_{15}n_{53}}{n_{15}n_{52}+n_{15}n_{53}+n_{52}n_{53}}\mathbf{R}_{12} - \frac{n_{15}n_{52}}{n_{15}n_{52}+n_{15}n_{53}+n_{52}n_{53}}\mathbf{R}_{13}. \tag{D.56}$$

For $n_{15}=n_{52}=n_{53}=n_{64}=n$, It can be concluded that $\tilde{\zeta}_{33} = 9/\left(4nb^2\right)$ and

$$\tilde{\mathbf{L}} = \mathbf{R}_{14} - \frac{1}{3}\mathbf{R}_{12} - \frac{1}{3}\mathbf{R}_{13}. \tag{D.57}$$

Symmetric six-node structure with a rod

Using Equation (D.46) for $t=3$, and $p=5$ (see Fig. D.1c) results in

$$P\left(\mathbf{R}_{12},\mathbf{R}_{13},\mathbf{R}_{14},\mathbf{R}_{15},\mathbf{R}_{16}\right) = \sqrt{\frac{\tilde{\zeta}_{55}}{(2\pi)^{15}\det\tilde{\mathbf{\Gamma}}_{\mathrm{aa}}}}\frac{1}{a\tilde{L}}\exp\left[-\frac{\tilde{\zeta}_{55}\left(a^2+\tilde{L}^2\right)}{2}\right]\sinh\left[a\tilde{L}\tilde{\zeta}_{55}\right]$$
$$\times\exp\left[-\frac{1}{2}\left(\tilde{\mathbf{R}}_{\mathrm{a}}^{\mathrm{T}}\tilde{\mathbf{\Gamma}}_{\mathrm{aa}}^{-1}\tilde{\mathbf{R}}_{\mathrm{a}}\right)\right]. \tag{D.58}$$

where

$$\tilde{\mathbf{\Gamma}}_{\mathrm{aa}} = \frac{b^2}{3}\begin{pmatrix} (n_{17}+n_{72})\,[\mathbf{I}]_{3\times3} & n_{17}\,[\mathbf{I}]_{3\times3} & [\mathbf{0}]_{3\times3} & [\mathbf{0}]_{3\times3} \\ n_{17}\,[\mathbf{I}]_{3\times3} & (n_{17}+n_{73})\,[\mathbf{I}]_{3\times3} & [\mathbf{0}]_{3\times3} & [\mathbf{0}]_{3\times3} \\ [\mathbf{0}]_{3\times3} & [\mathbf{0}]_{3\times3} & (n_{84}+n_{86})\,[\mathbf{I}]_{3\times3} & n_{86}\,[\mathbf{I}]_{3\times3} \\ [\mathbf{0}]_{3\times3} & [\mathbf{0}]_{3\times3} & n_{86}\,[\mathbf{I}]_{3\times3} & (n_{85}+n_{86})\,[\mathbf{I}]_{3\times3} \end{pmatrix}, \tag{D.59a}$$

$$\det\tilde{\mathbf{\Gamma}}_{\mathrm{aa}} = \frac{b^{24}}{3^{12}}\left(n_{17}n_{72}+n_{72}n_{73}+n_{17}n_{73}\right)^3\left(n_{84}n_{85}+n_{85}n_{86}+n_{85}n_{86}\right)^3, \tag{D.59b}$$

$$\tilde{\mathbf{R}}_{\mathrm{a}}^{\mathrm{T}} = \{(R_{12})_x \quad (R_{12})_y \quad (R_{12})_z \quad (R_{13})_x \quad (R_{13})_y \quad (R_{13})_z \quad (R_{64})_x \quad (R_{64})_y \quad (R_{64})_z$$
$$(R_{65})_x \quad (R_{65})_y \quad (R_{65})_z\}, \tag{D.60}$$

and

$$\tilde{\zeta}_{55} = \frac{3}{b^2}$$
$$\times \frac{(n_{72}n_{73} + n_{17}(n_{72}+n_{73}))(n_{85}n_{86} + n_{84}(n_{85}+n_{86}))}{n_{17}n_{73}n_{84}n_{85}n_{86} + n_{72}n_{73}n_{84}n_{85}n_{86} + n_{17}n_{72}(n_{73}n_{85}n_{86} + n_{84}n_{85}n_{86} + n_{73}n_{84}(n_{85}+n_{86}))}. \tag{D.61}$$

Lastly, by using (D.17), (5.31) and definition (D.13).

$$\begin{aligned}\tilde{\mathbf{L}} = &-\frac{n_{17}n_{73}}{n_{17}n_{72}+n_{17}n_{73}+n_{72}n_{73}}\mathbf{R}_{12} - \frac{n_{17}n_{72}}{n_{17}n_{72}+n_{17}n_{73}+n_{72}n_{73}}\mathbf{R}_{13} \\ &+\frac{n_{85}n_{86}}{n_{85}n_{86}+n_{84}n_{85}+n_{84}n_{86}}\mathbf{R}_{14} + \frac{n_{84}n_{85}}{n_{85}n_{86}+n_{84}n_{85}+n_{84}n_{86}}\mathbf{R}_{15} \\ &+\frac{n_{84}n_{85}}{n_{85}n_{86}+n_{84}n_{85}+n_{84}n_{86}}\mathbf{R}_{16}.\end{aligned} \tag{D.62}$$

For $n_{17} = n_{72} = n_{73} = n$ and $= n_{84} = n_{85} = n_{86} = n + 2m$, It can be concluded that $\tilde{\zeta}_{55} = 9/\left(2(n+m)b^2\right)$ and

$$\tilde{\mathbf{L}} = \frac{1}{3}\left(\mathbf{R}_{14} + \mathbf{R}_{15} + \mathbf{R}_{16} - \mathbf{R}_{12} - \mathbf{R}_{13}\right). \tag{D.63}$$

For $n_{17} = n_{72} = n_{73} = n_{84} = n_{85} = n_{86} = n$, It can be concluded that $\tilde{\zeta}_{55} = 9/\left(2nb^2\right)$.

Symmetric eight-node structure with a rod

Using Equation (D.46) for $t = 4$, and $p = 7$ (see Fig. D.1d) leads to

$$\begin{aligned}P\left(\mathbf{R}_{12}, \mathbf{R}_{13}, \cdots, \mathbf{R}_{18}\right) = &\sqrt{\frac{\tilde{\zeta}_{77}}{(2\pi)^{21}\det\tilde{\mathbf{\Gamma}}_{\mathrm{aa}}}}\frac{1}{a\tilde{L}}\exp\left[-\frac{\tilde{\zeta}_{77}\left(a^2+\tilde{L}^2\right)}{2}\right]\sinh\left[a\tilde{L}\tilde{\zeta}_{77}\right] \\ &\times\exp\left[-\frac{1}{2}\left(\tilde{\mathbf{R}}_{\mathrm{a}}^{\mathrm{T}}\tilde{\mathbf{\Gamma}}_{\mathrm{aa}}^{-1}\tilde{\mathbf{R}}_{\mathrm{a}}\right)\right],\end{aligned} \tag{D.64}$$

where

$$\tilde{\mathbf{\Gamma}}_{\rm aa} = \frac{b^2}{3}\times$$
$$\begin{pmatrix} (n_{19}+n_{92})[\mathbf{I}]_{3\times3} & n_{19}[\mathbf{I}]_{3\times3} & n_{19}[\mathbf{I}]_{3\times3} & [\mathbf{0}]_{3\times3} & [\mathbf{0}]_{3\times3} & [\mathbf{0}]_{3\times3} \\ n_{19}[\mathbf{I}]_{3\times3} & (n_{19}+n_{93})[\mathbf{I}]_{3\times3} & n_{19}[\mathbf{I}]_{3\times3} & [\mathbf{0}]_{3\times3} & [\mathbf{0}]_{3\times3} & [\mathbf{0}]_{3\times3} \\ n_{19}[\mathbf{I}]_{3\times3} & n_{19}[\mathbf{I}]_{3\times3} & (n_{19}+n_{94})[\mathbf{I}]_{3\times3} & [\mathbf{0}]_{3\times3} & [\mathbf{0}]_{3\times3} & [\mathbf{0}]_{3\times3} \\ [\mathbf{0}]_{3\times3} & [\mathbf{0}]_{3\times3} & [\mathbf{0}]_{3\times3} & (n_{05}+n_{08})[\mathbf{I}]_{3\times3} & n_{08}[\mathbf{I}]_{3\times3} & n_{08}[\mathbf{I}]_{3\times3} \\ [\mathbf{0}]_{3\times3} & [\mathbf{0}]_{3\times3} & [\mathbf{0}]_{3\times3} & n_{08}[\mathbf{I}]_{3\times3} & (n_{06}+n_{08})[\mathbf{I}]_{3\times3} & n_{08}[\mathbf{I}]_{3\times3} \\ [\mathbf{0}]_{3\times3} & [\mathbf{0}]_{3\times3} & [\mathbf{0}]_{3\times3} & n_{08}[\mathbf{I}]_{3\times3} & n_{08}[\mathbf{I}]_{3\times3} & (n_{07}+n_{08})[\mathbf{I}]_{3\times3} \end{pmatrix}, \tag{D.65}$$

$$\begin{aligned} \det\tilde{\mathbf{\Gamma}}_{\rm aa} = \frac{b^{36}}{3^{18}} &\left(n_{05}n_{07}n_{08} + n_{06}n_{07}n_{08} + n_{05}n_{06}(n_{07}+n_{08})\right)^3 \\ &\times \left(n_{19}n_{93}n_{94} + n_{92}n_{93}n_{94} + n_{19}n_{92}(n_{93}+n_{94})\right)^3, \end{aligned} \tag{D.66}$$

$$\begin{aligned} \tilde{\mathbf{R}}_{\rm a}^{\rm T} = \{&(R_{12})_x \quad (R_{12})_y \quad (R_{12})_z \quad (R_{13})_x \quad (R_{13})_y \quad (R_{13})_z \quad (R_{14})_x \quad (R_{14})_y \quad (R_{14})_z \\ &(R_{85})_x \quad (R_{85})_y \quad (R_{85})_z \quad (R_{86})_x \quad (R_{86})_y \quad (R_{86})_z \quad (R_{87})_x \quad (R_{87})_y \quad (R_{87})_z\}, \end{aligned} \tag{D.67}$$

and

$$\begin{aligned} \tilde{\zeta}_{77} = &\frac{3}{b^2}\left(n_{05}n_{07}n_{08} + n_{06}n_{07}n_{08} + n_{05}n_{06}\left(n_{07}+n_{08}\right)\right) \\ &\times \left(n_{19}n_{93}n_{94} + n_{92}n_{93}n_{94} + n_{19}n_{92}\left(n_{93}+n_{94}\right)\right) \\ &\times \Big[n_{05}n_{07}n_{08}n_{19}n_{92}n_{93}n_{94} + n_{06}n_{07}n_{08}n_{19}n_{92}n_{93}n_{94} + n_{05}n_{06}(n_{07}n_{19}n_{92}n_{93}n_{94} \\ &+ n_{08}n_{19}n_{92}n_{93}n_{94} + n_{07}n_{08}(n_{19}n_{93}n_{94} + n_{92}n_{93}n_{94} + n_{19}n_{92}(n_{93}+n_{94})))\Big]^{-1}. \end{aligned} \tag{D.68}$$

Lastly, by using (D.17), (5.31) and definition (D.13).

$$\begin{aligned}\widetilde{\mathbf{L}} = &- \frac{n_{19}n_{93}n_{94}\mathbf{R}_{12}}{n_{19}n_{93}n_{94}+n_{92}n_{93}n_{94}+n_{19}n_{92}(n_{93}+n_{94})} \\ &- \frac{n_{19}n_{92}n_{94}\mathbf{R}_{13}}{n_{19}n_{93}n_{94}+n_{92}n_{93}n_{94}+n_{19}n_{92}(n_{93}+n_{94})} \\ &- \frac{n_{19}n_{92}n_{93}\mathbf{R}_{14}}{n_{19}n_{93}n_{94}+n_{92}n_{93}n_{94}+n_{19}n_{92}(n_{93}+n_{94})} \\ &+ \frac{n_{06}n_{07}n_{08}\mathbf{R}_{15}}{n_{05}n_{07}n_{08}+n_{06}n_{07}n_{08}+n_{05}n_{06}(n_{07}+n_{08})} \\ &+ \frac{n_{05}n_{07}n_{08}\mathbf{R}_{16}}{n_{05}n_{07}n_{08}+n_{06}n_{07}n_{08}+n_{05}n_{06}(n_{07}+n_{08})} \\ &+ \frac{n_{05}n_{06}n_{08}\mathbf{R}_{17}}{n_{05}n_{07}n_{08}+n_{06}n_{07}n_{08}+n_{05}n_{06}(n_{07}+n_{08})} \\ &+ \frac{n_{05}n_{06}n_{07}\mathbf{R}_{18}}{n_{05}n_{07}n_{08}+n_{06}n_{07}n_{08}+n_{05}n_{06}(n_{07}+n_{08})}. \end{aligned} \tag{D.69}$$

For $n_{19} = n_{92} = n_{93} = n_{94} = n$ and $n_{05} = n_{06} = n_{07} = n_{08} = n + 2m^*$, It can be concluded that $\tilde{\zeta}_{77} = 6/\left((n+m^*)b^2\right)$.

$$\widetilde{\mathbf{L}} = \frac{1}{4}\left(\mathbf{R}_{15}+\mathbf{R}_{16}+\mathbf{R}_{17}+\mathbf{R}_{18}-\mathbf{R}_{12}-\mathbf{R}_{13}-\mathbf{R}_{14}\right). \tag{D.70}$$

By finding the eigenvalues of $\widetilde{\mathbf{\Gamma}}_{\mathrm{aa}}$, one can write the expression (D.64) in terms of the probability distribution function of the system of one coil-rod and six coil structures as follows:

$$\begin{aligned} P\left(\mathbf{R}_{12},\mathbf{R}_{13},\cdots,\mathbf{R}_{18}\right) &= W^{\mathrm{CR}}_{(n+m^*)/2}\left(\widetilde{\mathbf{L}}\right) W^{\mathrm{C}}_{n}\left(\frac{1}{\sqrt{2}}\mathbf{R}_{23}\right) W^{\mathrm{C}}_{n+2m^*}\left(\frac{1}{\sqrt{2}}\mathbf{R}_{56}\right) \\ &\times W^{\mathrm{C}}_{n}\left(\frac{1}{\sqrt{6}}\mathbf{R}_{12}+\frac{1}{\sqrt{6}}\mathbf{R}_{13}-\sqrt{\frac{2}{3}}\mathbf{R}_{14}\right) W^{\mathrm{C}}_{n+2m^*}\left(\frac{1}{\sqrt{6}}\mathbf{R}_{85}+\frac{1}{\sqrt{6}}\mathbf{R}_{86}-\sqrt{\frac{2}{3}}\mathbf{R}_{87}\right) \\ &\times W^{\mathrm{C}}_{4n}\left(\frac{1}{\sqrt{3}}\left(\mathbf{R}_{12}+\mathbf{R}_{13}+\mathbf{R}_{14}\right)\right) W^{\mathrm{C}}_{4n+8m^*}\left(\frac{1}{\sqrt{3}}\left(\mathbf{R}_{85}+\mathbf{R}_{86}+\mathbf{R}_{87}\right)\right). \end{aligned} \tag{D.71}$$

References

[1] P. J. Flory, "Statistical thermodynamics of random networks," *Proceedings of the Royal Society of London. A. Mathematical and Physical Sciences*, vol. 351, no. 1666, pp. 351–380, 1976. DOI: 10.1098/rspa.1976.0146. eprint: https://royalsocietypublishing.org/doi/pdf/10.1098/rspa.1976.0146.